Pyroclastic density currents at Ruapehu volcano; New Zealand

A thesis submitted in partial fulfilment of the requirements for the degree of

Doctor of Philosophy

in the Department of Geological Sciences *at the*

University of Canterbury

James Daniel Cowlyn

2016

Figure 1: A newly rediscovered image appears to show a pyroclastic density current descending Ruapehu's eastern flank in 1945 (N. Mosen, Lansdown Collection; In Johnston and Neall, 1995).

Acknowledgements

This PhD thesis would not have been possible without the help of many amazing people who contributed to this study through their guidance and support. Firstly, I would like to acknowledge my undergraduate volcanology teachers Dr. Mark Davies and Dr. Jenni Barclay, who gave me the opportunity to visit volcanoes in Guatemala and Montserrat, and who first made me realise that people really can study volcanoes as a career. Thanks too to Professor Mike Branney, who by coincidence lives on the same street as my home in the UK, and who helped me in my initial decision to pursue a volcanological career. I am supremely grateful to the staff at the Seismic Research Unit of the University of the West Indies (Trinidad), the Centre for Exchange & Research in Volcanology at the University of Colima (Mexico), the Instituto Geofísico del Escuela Politécnica Nacional (Ecuador), and the Rabaul Volcano Observatory (Papua New Guinea); all of whom generously allowed me to volunteer at their institutions and gain experience at their countries' amazing volcanoes. In particular Dr. Nico Fournier, Dr. Nick Varley, Patricio Ramón, and Steve Saunders all went out of their way to host me and pass on their tremendous volcanological knowledge and experience.

I am indebted to my supervisors for having faith in me and for helping me find a project that so closely matched my interests. In particular Dr. Ben Kennedy, Dr. Darren Gravley, Prof. Shane Cronin and Dr. Thomas Wilson spent countless hours discussing the research and providing valuable feedback. These supervisors, as well as Dr. Graham Leonard and Dr. Dougal Townsend, spent valuable time at Ruapehu with me discussing the deposits in the field, which greatly improved my understanding and hugely benefited my broader volcanological experience. I extend special thanks to Dr. Natalia Pardo, whose previous work on Ruapehu's ring plain tephras directly set the context for this study. The time spent with Natalia in the field introduced me to the stratigraphic framework on which the timings of all of the PDC deposits described here are based. Chris Conway, who was simultaneously working on his PhD looking at the petrological evolution and ice-contact features of Ruapehu's lavas, also provided valuable insight into Ruapehu's glacial history.

Spending several months at a time in an isolated part of Ruapehu was only made possible thanks to the extremely generous support of members of the Tukino Alpine Sports

Club and Tukino Skifield, who made their wonderful ski lodge available to me over the summer months. I enjoyed watching the lodge develop over the course of numerous 'working bees' from its leaking walls, freezing showers and tiny generator that characterised the first field season, to the luxurious lodge it is today. In particular Don French went out of his way time after time to facilitate my use of the lodge, and to encourage me to feel like it was my home. None of this research would have been possible without Don. I also particularly thank Dave Spicer, Thomas Wilson, and a very special thanks to Bruce McGregor who drove 2 hours from Taupo to rescue my supervisors and I when a 'key-related incident' left us not only locked out of the lodge but also unable to leave the mountain through the locked access gate.

My time at Ruapehu was made much more enjoyable by visits and help from several people in the field. In particular, I am forever grateful to Emma Rhodes who spent 2 months as my field assistant during the first field season, and then willingly returned on multiple occasions during the second field season to provide me with encouragement and further help. Thanks too to Paula Burgi, Zarah Heyworth, Matt Edwards, Doug Spicer, Amaya Menéndez Gamella, Paul Ashwell, Felix Von Aulock and Dr. Josef Dufek; all of whom visited me in the field and assisted with fieldwork. I also extend special thanks to Dr. Harry Keys and Karen Williams, who maintained an active interest in my research and invited me to join them on an aerial survey of Ruapehu that resulted in photographs that form the basis of key figures in this thesis.

Laboratory processing of the Ruapehu samples was made far less tedious thanks to the generous help of Brigitt White, Regine Morgenstern, Rebecca Fitzgerald, Kaylon Higginbotham and Anne Fulton. I am also extremely grateful to all of the U.C. technical staff, including Rob Spiers for making beautiful thin sections, Stephen Brown for running the XRF chemical analyses, Chris Grimshaw for help in the sedimentology laboratory, and Sacha Baldwin-Cunningham and Cathy Higgins for help arranging my field equipment. Thanks also to the staff at the Australian Synchrotron for use of their world-leading facility, and to Dr. Ian Schipper, Matt Edwards, Anton Maksimenko and Darren Thompson for help with processing the 3D microtomography data.

Central to many of the interpretetaions in this thesis are estimated magma storage pressures and temperatures (Chapter 5), modelled using a modified version of the rhyolite-MELTS geobarometer (Bégué et al., 2014; Gualda and Ghiorso, 2014). This geobarometer has never previously been used for andesitic compositions, but Associate Professor Guilherme Gualda and Lydia Harmon worked tirelessly to update the geobarometer to accommodate the Ruapehu samples. They also provided unlimited access to Vanderbilt University's Scanning Electron Microscope during my visit in 2014. Similarly, I am indebted to Dr. Josef Dufek and Julian McAdams for hosting me at the Georgia Institute of Technology in 2014 and helping me perform microphysical pyroclast-ice contact experiments that form the basis of Chapter 6. Dr. Dufek's world-leading multiphase numerical simulations, using the data from the microphysical experiments and Ruapehu deposits, are already producing exciting results that in future may help to better constrain PDC hazards at ice-covered volcanoes (Chapter 6).

Finally I would like to acknowledge the support of all staff in the University of Canterbury Geological Sciences department, and thank my friends and family in NZ and around the world who have encouraged, supported, and motivated me throughout this thesis. Thanks in particular to Zarah, Emma, Grace, Brigitt, Ryan, Abe, Sam, Paula, Anne, Carlos, Anthea, Amber, Kirsty and Kathy. A very special thanks also to the staff at The Astro Lounge and the Antigua Boat Sheds & Cafe, who adopted me as their 'resident' volcanologist and supplied me with near-continuous coffees and banter during the thesis write-up. Above all, thanks to my amazing parents, Martin and Trudy, who have supported, encouraged and inspired me throughout every step of my university studies and travels around the world to pursue my interest in volcanoes. I would never have thought a career in volcanology was even possible had it not been for their unwaivering support.

Funding for this PhD research was provided by a University of Canterbury Doctoral Scholarship, the University of Canterbury Mason Trust Fund, a Project Tongariro Memorial Award and a Royal Society of New Zealand International Mobility Fund grant. Very special thanks to Dr. Harry Keys and the New Zealand Department of Conservation, Ngati Tuwharetoa and Ngati Rangi for providing access and sampling at Ruapehu and maintaining an interest in this research.

Pyroclastic density currents at Ruapehu volcano; New Zealand

James Cowlyn

Abstract

Pyroclastic density currents (PDCs) are hazardous mixtures of volcanic particles and gas that travel along the flanks of a volcano due to a higher bulk density than the surrounding atmosphere. Understanding the frequencies, magnitudes, and different PDC generation and transport processes is essential for understanding the PDC hazard. At Mount Ruapehu, a much-visited active volcano in the North Island of New Zealand, future PDCs represent a significant threat to life and infrastructure. However no extensive historical PDCs and very few prehistoric deposits have been studied at this volcano. Here, we develop a new confidence-based system for identifying and distinguishing small-volume PDC deposits from other proximal volcaniclastic deposits in the field, and use this to identify 12 young (<13.6 ka) PDC units exposed on Ruapehu's eastern flanks. Field investigations of deposit morphologies and textures show that Ruapehu's PDCs were generated by a variety of eruption styles. These ranged from (1) collapsing plinian eruption columns that emplaced massive pumice-rich PDC deposits (Units 1-5, ~13.6 - 11.6 ka), through to (2) welded scoriaceous deposits that resulted from periodic collapses of spatter/cinders that first accumulated on steep proximal slopes (Units 6, ~11.6 ka, and 7, unknown age). Additionally, (3) several small-volume deposits containing denser pyroclasts (Units 8-10, <11.6 ka, and 11-12, ~13.6-11.6 ka) are interpreted to result from smaller eruptions not dissimilar to Ruapehu's historical activity. Detailed studies of (a) bulk and glass pyroclast chemistries, (b) pyroclast density distributions, (c) vesicle textures, and (d) rhyolite-MELTS modelled storage conditions provide further insight into the underlying magmatic processes that led to generation of these PDCs. These show that magma storage depths and temperatures, magma mingling between new and relict magmas, and open vs. closed systems strongly influenced the amounts of pre-eruptive degassing and bulk pyroclast densities. This in turn affected the buoyancy of the erupting mixture, and hence the tendency to generate PDCs. In most cases, heterogeneous storage and ascent pathways at Ruapehu appear to have favoured PDC generation, and this may be an important consid-

eration when assessing the future PDC hazard. Furthermore, the deposit ages, textures, and distributions indicate that many of Ruapehu's PDCs encountered glacial ice during transport, and this is interpreted to have affected the PDC dynamics and preservation of the deposits. By combining results from microphysical pyroclast-ice contact experiments with high-resolution mutiphase numerical simulations, we here model the large-scale effects of PDC transport over ice for the first time. Simulations based on interpreted prehistoric ice extents at Ruapehu suggest that transport over ~2km of ice strongly affects the PDC dynamics, increasing the runout distance of the hazardous high-particle concentration bedload and generating meltwater quantities equivalent to ~25% of the PDC bedload volume. This may then generate secondary debris flows which, following flow bulking, have volumes equivalent to at least 50% of the bedload volume of the primary PDC. These results have implications for assessing the PDC and associated hazards at Ruapehu and other glaciated volcanoes worldwide.

Contents

List of Figures

List of Tables

1

Introduction

Introduction

Pyroclastic density currents (PDCs) are hazardous mixtures of volcanic particles and gas that travel along the flanks of a volcano due to gravity and have killed nearly 60,000 people since 1783 (Tanguy et al., 1998). At Mount Ruapehu in the North Island of New Zealand, future PDCs represent a major threat to life and important ski field, transportation and power infrastructure. However no historical granular fluid-based PDCs and very few prehistoric PDC deposits have been studied at this volcano. This represents a significant gap in the knowledge required to properly understand the nature of the pyroclastic density current hazard at Ruapehu.

The **Primary Objective** (Figure 1.1) of this research is to investigate prehistoric pyroclastic density current deposits at Ruapehu, in order to improve current understanding of the nature of PDCs and associated hazards at Ruapehu and similar volcanoes worldwide.

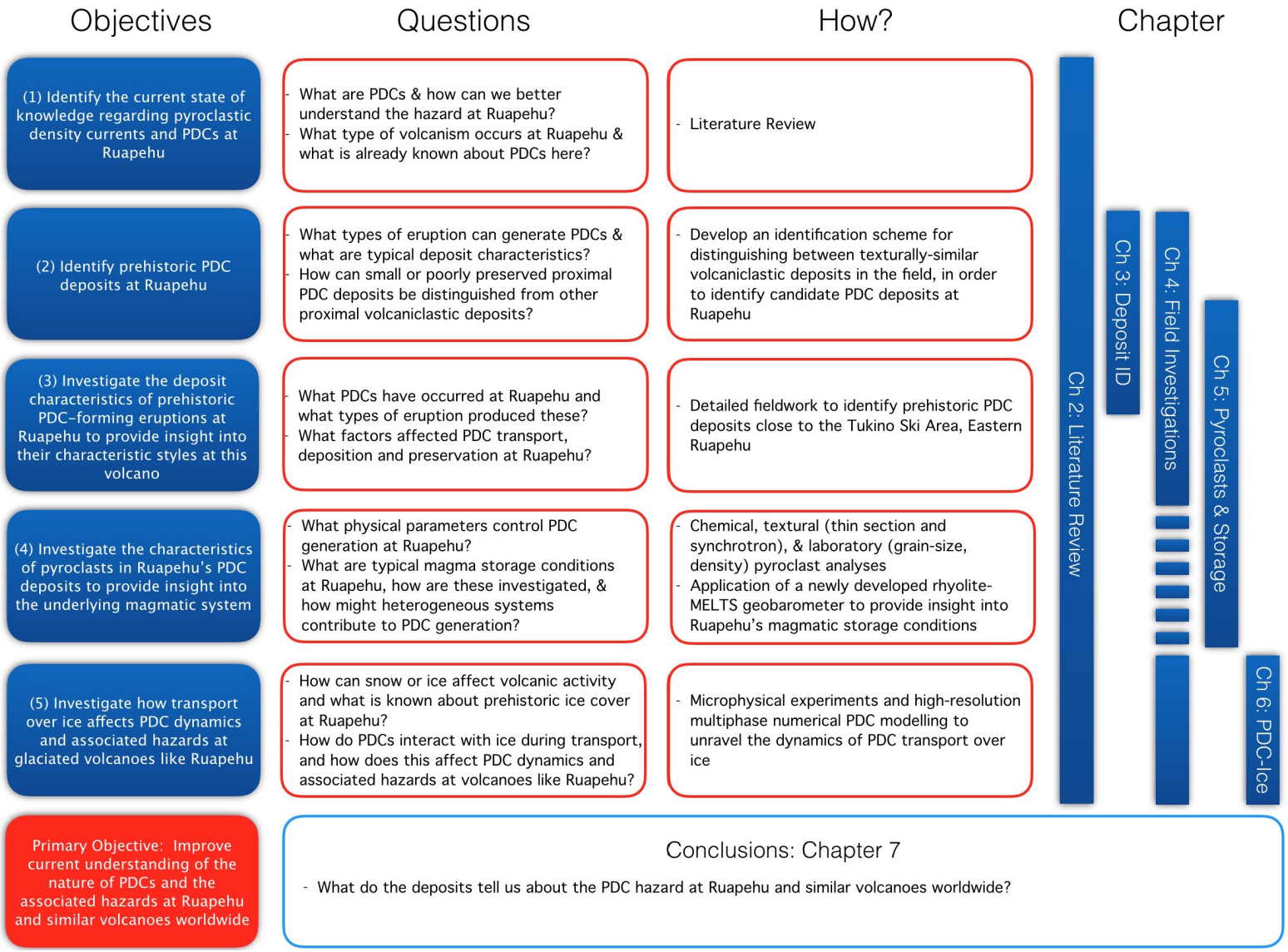

Figure 1.1: Thesis objectives, research questions, and outline.

1.1 Overview of this study and detailed objectives

An essential component to understanding the nature of pyroclastic density currents at any volcano is to first understand the PDCs that have occurred there before. At volcanoes like Ruapehu where significant PDCs have not been historically described, this relies on identifying and studying deposits in the geological record (**Objective 2**, Figure 1.1). However, unconsolidated PDC deposits have poor preservation potential, and can be difficult to distinguish from other near-source volcaniclastic deposits. This issue is addressed in **Chapter 3**, which presents a new confidence-based identification method that permits assessment of volcaniclastic deposits in the field. The method differs from traditional identification charts in that it considers the confidence levels by which observed deposit textures can be attributed to a wide variety of volcaniclastic processes, including but not limited to PDCs. This provides a rapid field method for identifying candidate PDC deposits as targets for further investigation.

Using the system developed in **Chapter 3**, 12 young (<13.6 k.a.) PDC deposits are identified near to the Tukino Ski Area in Eastern Ruapehu. **Chapter 4** outlines the major field characteristics of these deposits, together with broad interpretations of their associated eruptive styles (**Objective 3**, Figure 1.1). The deposits are interpreted to reflect PDCs from eruptions spanning a wide range of eruption styles and magnitudes; including Ruapehu's largest known plinian eruptions, as well as PDCs generated by smaller eruptions that have similarities to Ruapehu's modern activity. The observation that 4 of these previously undescribed deposits occur within 100m of Tukino Village emphasises how easily small and poorly exposed PDC deposits can be overlooked.

Chapter 5 extends the field based interpretations of Chapter 4 to consider the underlying magmatic and eruptive conditions that have led to PDC generation at Ruapehu (**Objective 4**, Figure 1.1). Central to this is application of an innovative new rhyolite-MELTS geobarometer being developed at Vanderbilt University. The results presented here are the first time the geobarometer has been used for andesitic rocks, and this has provided new insight into the pre-eruptive storage conditions that led to Ruapehu's PDC-generating eruptions. These observations, together with detailed textural observations of

clasts within the PDC deposits, support the notion that Ruapehu's hetrogeneous shallow magma system may increase the likelihood of PDC-forming eruptions by promoting the eruption of denser pyroclasts.

The ages of Ruapehu's PDC deposits, which coincide with periods of significant ice cover (Conway et al., 2015), suggest that many of the PDCs must have encountered snow or ice during transport. In the field (**Chapter 4**), this is interpreted to have affected the deposit distributions, preservation, and in rare cases the deposit textures. However, understanding the impact of snow and ice on the PDC dynamics is not directly possible from the deposits alone. Therefore, **Chapter 6** combines microphysical experments of pyroclast-ice interactions with high resolution multiphase numerical simulations to investigate the effects that transport over ice has on PDC flow dynamics, including runout distances and steam and meltwater generation (**Objective 5**, Figure 1.1). This has never previously been investigated, and provides insight not only into the Ruapehu deposits, but also PDC dynamics and the associated hazards at other glaciated volcanoes worldwide.

Figure 1.1 details the objectives and key questions addressed in this study, and Box 1.1 outlines the scope of the study. The thesis is presented in chapter form, though each chapter is structured in a format similar to an expanded academic publication with the intention of submitting condensed versions of all four science chapters (Chapters 3 - 6) to academic journals after thesis submission.

Box 1.1: Scope of the project and Terminology

Pyroclastic density currents (PDCs) form a continuous spectrum (Branney and Kokelaar, 2002) from highly mobile, fully dilute pyroclastic density currents dominated by fluid turbulence (historically referred to as pyroclastic 'surges'), to highly concentrated granular fluid-based currents dominated by particle collisions near the lower flow boundary (historically referred to as pyroclastic 'flows'). In practice the same PDC can exhibit both flow-like and surge-like characteristics at different points throughout the flow, and as such the term pyroclastic density current (PDC) is now usually preferred. However, the end-member types remain important in terms of their resulting deposits. Fully dilute ('surge') PDC deposits are interpreted to result from particles carried by dilute turbulent suspensions, resulting in deposits that can mantle topography and that commonly have traction bedforms. In contrast, granular fluid-based ('flow') PDC deposits are interpreted to result from highly concentrated currents or the concentrated bases of density-stratified currents, and result in massive, poorly sorted deposits that are mostly confined by topography (Druitt, 1998). At Ruapehu, small fully dilute PDCs ('surges') have frequently impacted the summit area during historical phreatic and phreatomagmatic eruptions, producing volumetrically small deposits of limited extent. However, larger granular fluid-based PDCs (pyroclastic 'flows') have not been historically described at this volcano. **This study is therefore restricted to studying deposits from the granular fluid-based PDC end member (Branney and Kokelaar, 2002) preserved on Ruapehu's eastern flank.**

In this thesis, we refer extensively to *deposit textures*. This is intended in a sedimentological sense, and refers to outcrop-scale deposit features. This fits within the broader concepts of deposit *structure* (large scale geometry, often across multiple outcrops or the whole deposit), *texture*, and *composition* (the chemical and mineralogical characteristics of the deposits). Hence in this thesis, the *deposit texture* refers to all outcrop-scale field observations that characterise the deposit, including outcrop and pyroclast colours, componentry, clast sizes, shapes, sorting, and any outcrop scale grading or bedforms.

2

Literature Review

Introduction to Chapter 2

In this chapter, I briefly summarise the relevant literature on the hazard from pyroclastic density currents, as well as the diverse processes that lead to their generation and emplacement at andesitic cone volcanoes. This provides the broad justification for investigating prehistoric PDC deposits at any volcano, and the relevant theoretical background for identifying and interpreting PDC deposits at Ruapehu.

The key outcomes are:

1. Recognition that PDCs are the deadliest co-eruptive hazard in historical time; but deposits from a volcano's prehistoric PDCs can provide insight into the possible future hazard.

2. Recognition that Ruapehu is a high-risk volcano, but absence of historical granular fluid-based PDCs and challenges in identifying small volume prehistoric PDC deposits means Ruapehu's PDC hazard has been under-represented.

3. Recognition that PDCs can be formed by any process that results in gravitational collapse of erupted material, and that deposit and pyroclast textures can provide insight into the volcanic and magmatic processes that lead to PDC generation.

4. Recognition that Ruapehu had extensive prehistoric ice cover, which may have affected the dynamics and associated hazards of Ruapehu's prehistoric PDCs.

Each section of this literature review addresses specific questions, outlined in a box at the beginning of the section. These questions align with the **thesis objectives** outlined in **Chapter 1**, and provide context for the topics addressed in research **Chapters 3 to 6**. The concepts that are most relevant to this study are summarised at the end of each section.

It is most likely that an eruption similar to previous eruptions will occur in the future. A comprehensive understanding of eruption phenomena and frequency is therefore needed for hazard mitigation. Areas impacted by pyroclastic flows previously are likely to be affected again in future eruptions.

- Nakada (2000)

2.1 Pyroclastic density currents and the associated hazard

Key Questions:

- *What are pyroclastic density currents (PDCs) and how hazardous are they?*
- *How can we better understand the likely future PDC hazard at stratovolcanoes like Ruapehu?*

These concepts outline the broad justification for this PhD research studying PDC deposits at Ruapehu (**all Chapters**).

Long-lived andesitic volcanoes produce frequent, often violent eruptions that represent a significant threat to human populations. As such, the processes driving volcanism and the likely extents of associated hazards are a major focus of current volcanological research. Of all direct volcanic hazards, pyroclastic density currents (PDCs) have caused the most fatalities in historical time; accounting for ~27% of volcanic deaths (direct and indirect) since 1783 and 49% (44,928 deaths) of all recorded volcanic deaths in the 20th century (Tanguy et al., 1998; Witham, 2005). These mobile currents are fast-moving mass flows of pyroclastic particles and gas that travel along the flanks of a volcano in response to gravity and their higher density than the surrounding atmosphere (Branney and Kokelaar, 2002; Yamamoto et al., 2005). They can reach velocities of tens to hundreds of meters per second and cause near-complete destruction over widespread areas (Sheridan, 1979; Druitt, 1998). PDC deposits range in scale over several orders of magnitude from extensive pumiceous ignimbrites (10^2 to $>10^3$ km^3) emplaced during caldera-forming eruptions (e.g. Cole and Spinks, 2009), through to small-volume deposits ($<10^{-2}$ km^3) from smaller events that represent a frequent proximal-medial hazard at many stratovolcanoes (Figure 2.1; Stinton and Sheridan, 2008). These smaller, more frequent PDCs and their associated deposits are characteristic of subduction-related andesitic volcanoes like Ruapehu, and are the focus of this thesis.

Despite advances in volcano monitoring and better understanding of PDC dynamics,

Figure 2.1: A pyroclastic density current descends from the summit of Mount St. Helens during an eruption on August 7, 1980 (Photo courtesy of USGS).

fatalities continue to result from PDCs (Charbonnier et al., 2013). Eruptions including Mt St Helens (USA, 1980; 57 deaths), El Chichon (Mexico, 1982; >2000 deaths), Unzen (Japan, 1991; 43 deaths), and Soufrière Hills (Montserrat, 1997; 19 deaths) have highlighted the devastating immediate and longer-term effects that pyroclastic density currents can have on nearby populations and infrastructure. The risk posed by PDCs is frequently underestimated, as demonstrated by the 2010 eruption of Merapi volcano, Indonesia, where >200 people died and 2200 buildings were damaged despite a long history of deadly PDCs at this volcano (Boudon et al., 1993; Jenkins et al., 2013). Here, many of the casualties occurred more than a week after the onset of the eruption, during which time over 120 PDCs had already been emplaced (Cronin et al., 2013). The increasingly mobile currents impacted earlier unaffected areas, eventually reaching 15.5 km from source and devastating 22 km^2 of the volcano's densely populated southern flank. This example highlights not only the need for recognising the existence of the PDC hazard, but also for thoroughly understanding its likely extent and relative timing. This is no easy task, since every volcano and every eruption is unique (Cashman and Biggs, 2014). However at any given volcano, the areas previously impacted and the kinds of PDCs previously produced provide strong indications of the kind of activity that can be reasonably expected in future (Nakada, 2000). This is the primary justifcation for identifying and studying prehistoric PDC deposits at Ruapehu and any volcano where PDCs represent a threat to life or infrastructure.

Key Points:

- ✓ Pyroclastic density currents are the deadliest co-eruptive volcanic hazard in historical time.
- ✓ The best way to understand the possible future PDC hazard at any volcano is to understand the characteristic nature of previous PDCs at that volcano. This can be through direct observation of historical PDCs, or by investigating the deposits from prehistoric PDCs.

2.2 Ruapehu volcano, New Zealand

Key Questions:

- *What type of volcanism occurs at Ruapehu and what styles of activity have occurred there before?*
- *What is already known about pyroclastic density currents at this volcano?*
- *What is already known about the risks and hazards at this volcano?*
- *Why is it important to investigate PDC deposits at Ruapehu?*

These concepts provide background for **Chapters 3 and 4**, in which we identify and investigate Ruapehu's PDC deposits in the field.

Mount Ruapehu (Rua "pit", pehu "to explode"; in Te Reo Māori) is one of New Zealand's most frequently active volcanoes. It is also one of the most visited, with ~800,000 people visiting Tongariro National Park (comprising Ruapehu and Tongariro volcanoes) annually for hiking and snowsports (H. Keys, Dept. of Conservation, pers. comm). In winter, Ruapehu hosts NZ's largest commercial ski fields, with several thousand skiers coming to the mountain each day in peak season. Therefore, a thorough understanding of the volcanic hazards at Ruapehu is essential.

2.2.1 Geological setting

Volcanism in New Zealand is focused in the Taupo Volcanic Zone (TVZ); an active continental arc/back-arc system resulting from oblique westward subduction of the Pacific plate beneath NZ's North Island (Cole, 1990; Wilson et al., 1995). The central TVZ is the most active rhyolite system on earth (Houghton et al., 1995), and has been the focus of frequent prehistoric caldera-forming eruptions with large associated ignimbrites, air-fall tephras and post-caldera domes (e.g. Cole and Spinks, 2009). In contrast, the southern and northern TVZ is dominated by cone-forming andesitic volcanism, with frequent historical activity at Ruapehu and Tongariro volcanoes in the south and White Island volcano in the north (Cole, 1990).

Mount Ruapehu is a large (~150 km^3) stratovolcano located at the southern end of the Taupo Volcanic Zone (Hackett and Houghton, 1989; Conway et al., 2015). The 2797m high composite cone has been constructed over the past ~250 ka (Figure 2.2) by episodes of voluminous lava production from multiple vents (Graham and Hackett, 1987; Waight et al., 1999; Gamble et al., 2003), and is surrounded by an equally voluminous ring plain comprising extensive laharic, fluvial and pyroclastic fall deposits (Palmer, 1991; Palmer et al., 1993; Cronin et al., 1996b; Lecointre et al., 1998; Donoghue and Neall, 2001). Periods of more intense activity occurred at 200, 134,45, 22, and <15ka (Gamble et al., 2003), punctuated by periods of erosion and sector collapse (Palmer and Neall, 1989; McClelland and Erwin, 2003). The oldest parts of the edifice comprise low-K basaltic andesite lavas emplaced between ~250 and 60 ka. These are now only exposed in the south-east and north (Figure 2.3), while the majority of the modern edifice comprises younger basaltic-andesite to dacite lavas, autoclastic breccias, glacial deposits and reworked volcaniclastic deposits emplaced during the past 60 ka (Gamble et al., 2003; Conway et al., 2015).

2.2.2 Explosive volcanism at Ruapehu

Large explosive eruptions frequently occurred at Ruapehu throughout the late Pleistocene (~60-10 ka BP cal; Topping, 1973; Donoghue et al., 1995b, 1999; Pardo et al., 2011, 2012). The largest of these produced extensive plinian and sub-plinian tephras now exposed on Ruapehu's eastern ring plain in the 27,097 ±957 (see Box 1) to ~10,000 cal. years BP Bullot Formation (Figure 2.2; Donoghue, 1991; Donoghue et al., 1995b; Pardo et al., 2011; Pardo Villaveces, 2012). During this time, explosive activity appears to have been mostly focused in Northern Ruapehu; however Pardo et al. (2012) interpreted Ruapehu's final known plinian eruption (Okupata-Pourahu eruptive unit, ~11.6 ka BP cal) to have excavated a new vent near to the now-active South Crater (Figure 2.4). Subsequent explosive activity has been an order of magnitude smaller, with only limited deposits preserved in the volcanic record (Donoghue et al., 1995b). At least 19 small, mostly phreatomagmatic eruptions are recorded in the <~2 ka Tufa Trig tephras (Figure 2.2), and these have been interpreted by Donoghue et al. (1997) to represent eruptions through an ancestral crater lake similar to the one present at Ruapehu today. A further 20 small eruptions during this

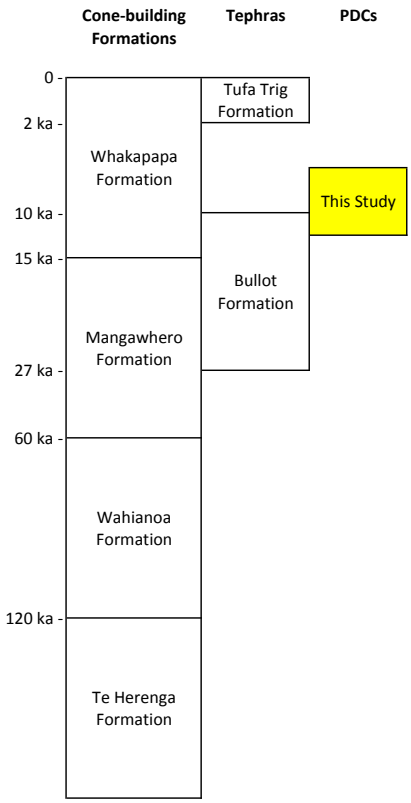

Figure 2.2: Simplified stratigraphy of Ruapehu. Hackett (1985) and Hackett and Houghton (1989) identified four cone-building phases at Ruapehu on the basis of lithologic/petrologic differences in the eruptive products and conspicuous unconformities that separate deposits from each cone. Tephras from explosive eruptions at Ruapehu have been relatively little studied, with most studies focusing on deposits from plinian eruptions from the 27,097 ±957 to ~10,000 cal. years BP Bullot Formation (Donoghue, 1991; Donoghue et al., 1995b; Pardo et al., 2011; Pardo Villaveces, 2012). Smaller eruptions, not significantly dissimilar to Ruapehu's modern activity, produced tephras of the <~2 ka Tufa Trig Formation (Donoghue et al., 1997; Moebis et al., 2011). The PDC deposits described in this thesis are all <13.6 ka and fall within the time periods of the Whakapapa and Bullot Formations.

time have also been inferred on the basis of detailed chemical analyses of glasses within the broader tephra deposits (Moebis et al., 2011).

Box 2.1: Age constraints and unit names:

This thesis uses the calibrated radiocarbon ages (presented in years before present) and stratigraphic names detailed in Pardo et al. (2011) to describe the relative stratigraphy of Ruapheu's Bullot Formation tephras and young PDC deposits. These are the most up-to-date ages and names available, and replace any used in earlier studies.

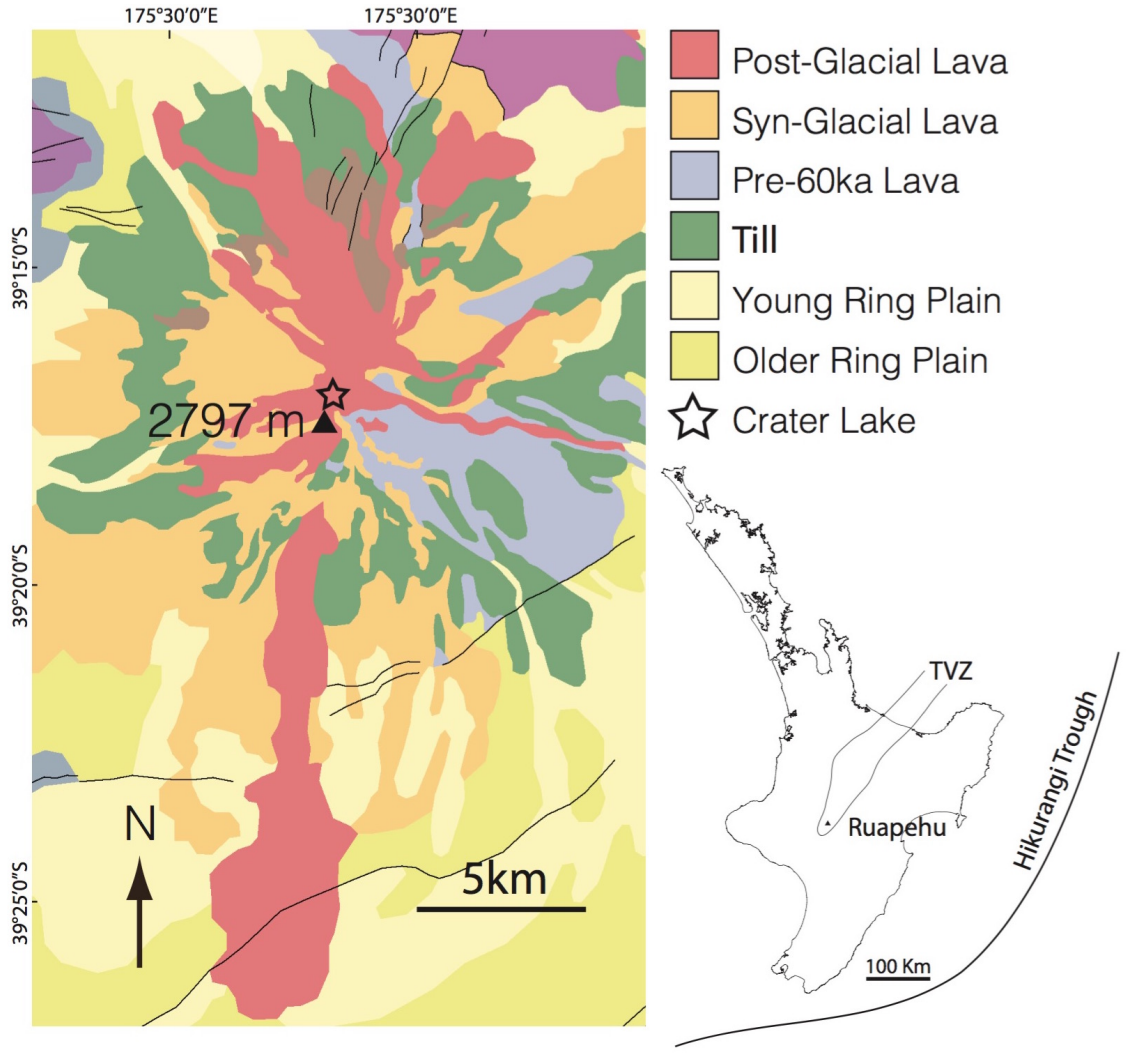

Figure 2.3: Simplified geology of Ruapehu; this map is a major new update to Ruapehu's geological map (G. Leonard and D. Townsend, GNS Science) due for full publication in 2016 (after Conway et al., 2015).

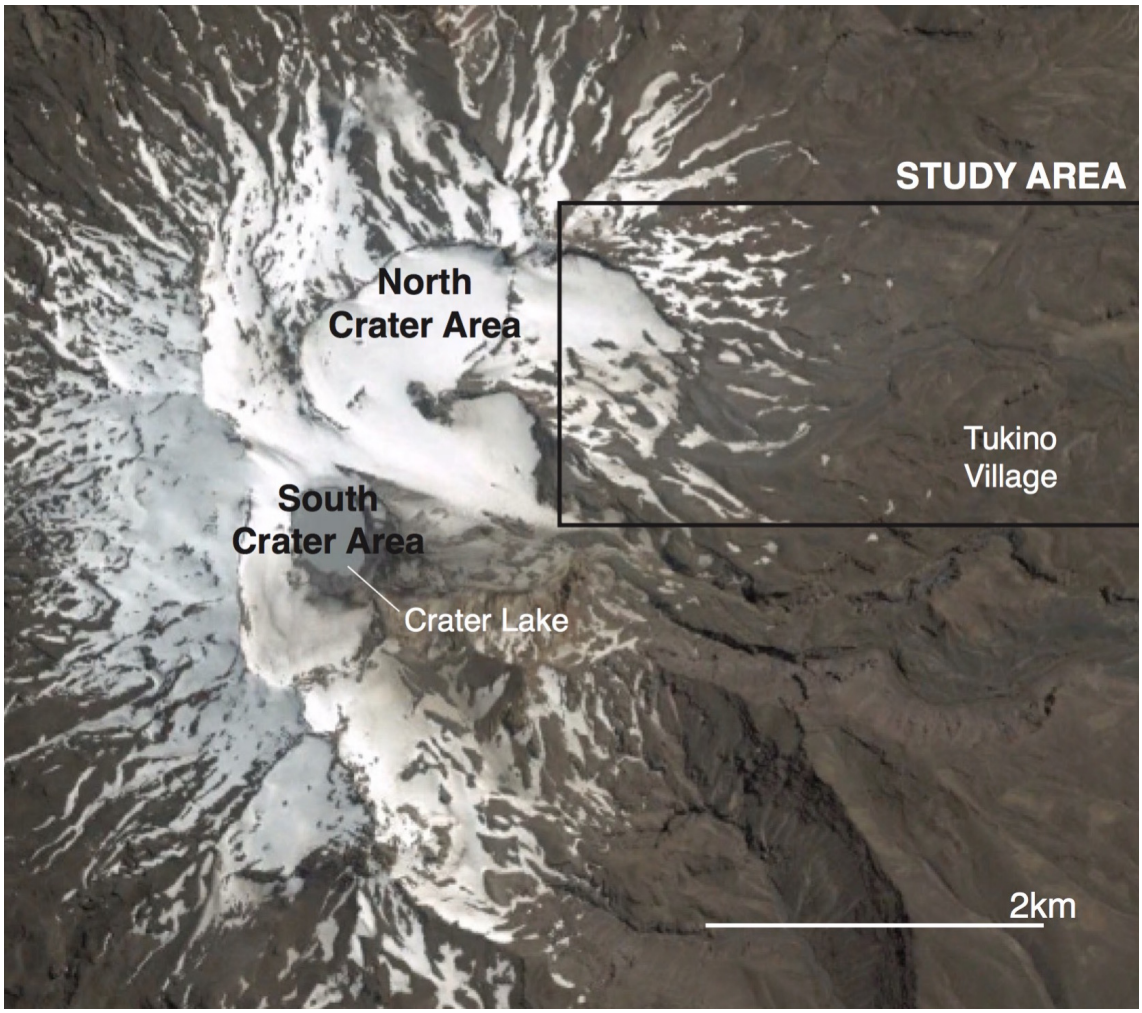

Figure 2.4: The summit area of Ruapehu showing locations referred to in this thesis. During the plinian eruptions of the 27,097 ±957 to ~10,000 cal. years BP Bullot Formation, explosive eruptions appear to have been mostly focused in the North Crater Area (Pardo et al., 2012). However, the ~11.6 ka Taurewa Eruptive Period (including Ruapehu's youngest known plinian eruption, the Okupata-Pourahu eruptive unit; Pardo et al., 2011) has been linked to eruptions in both wider Northern Ruapehu (Topping, 1973; Hackett and Houghton, 1985; Hackett, 1985; Donoghue et al., 1999) as well as the opening of a new vent near the South Crater Area (Pardo et al., 2012, 2014). Since ~9 ka, and more clearly since ~3 ka, eruptive activity has been focused in the South Crater Area, and has been characterised by small-scale, relatively more frequent phreatomagmatic eruptions (Donoghue et al., 1997; Pardo Villaveces, 2012). The modern-day Crater Lake vent is located within the broader South Crater Area; however since the PDCs in this thesis cannot definitively be attributed to the modern vent, the term South Crater Area is preferred. Image date 2/12/2003; Google Earth.

2.2.3 Historical activity at Ruapehu

Historical activity at Ruapehu has been documented for the last ~165 years (Cole and Nairn, 1975), with more than 40 eruptions since 1945 (Kilgour et al., 2013). These are characterised by frequent small phreatic (Nairn et al., 1979; Latter, 1981; Kilgour et al., 2010) and phreatomagmatic eruptions (Healy et al., 1978; Nairn et al., 1979; Houghton et al., 1987) through an acidic crater lake that is usually present in South Crater (Christenson and Wood, 1993). Larger eruptions in 1945 (Oliver, 1945; Reed, 1945; Beck, 1950; Johnston and Neall, 1995) and 1995-96 (Bryan et al., 1996; Nakagawa et al., 1999; Johnston et al., 2000) progressively displaced the crater lake, resulting in drier vulcanian and strombolian eruptions that dispersed ash across much of New Zealand's North Island.

2.2.4 Pyroclastic density currents at Ruapehu

Despite being a common occurrence at many andesitic-dacitic volcanoes, surprisingly few deposits of granular fluid-based PDCs have previously been described at Ruapehu. Hackett (1985) recognised numerous "heterolithic tuff breccias" representing a range of mass flow deposits, and interpreted two small <15 ka deposits in eastern and south-eastern Ruapehu to be from PDCs. One of these, part of Hackett's (1985) <15ka Iwikau Member, is also described by Chapman (1996); though neither authors investigate the physical volcanology of this deposit in detail. This deposit is more fully investigated in this thesis, and is for the first time recognised to represent at least two different PDC events (here referred to as PDC Units 6 and 7; **Chapter 4**).

In the only dedicated PDC study at Ruapehu, Donoghue et al. (1995a) describe magma mingling in the Pourahu PDC from the ~11.6 ka plinian Okupata-Pourahu eruptive unit of the Upper Bullot Formation. Donoghue et al. (1999) suggest that this event emplaced pyroclastic flows in at least 3 drainages, though the main focus of the PDC was the Whangaehu Valley in eastern Ruapehu. Poor deposit preservation led Donoghue et al. (1999) to conclude that primary PDC deposits now only remain in a couple of isolated outcrops on Ruapehu's eastern ring plain, >10km from source.

In a detailed study of the ~27-10 ka Bullot Formation tephras, Pardo et al. (2011) interpreted frothy to expanded pumice textures in the majority of these deposits to represent dry magmatic eruptions and steady eruption columns. However the youngest deposits (<13.6 ka; Ohinewairua eruptive period) showed a change to well-bedded units separated by thin fine ash beds, and characterised by dense-to-coarsely vesicular, fibrous and colour banded pumice fabrics that showed high degrees of heterogeneity within individual stratigraphic layers. Pardo et al. (2011, 2014) interpreted these textures to represent unsteady, oscillating eruption columns associated with generation of pyroclastic density currents. This was supported by field observations of several thin (cm-scale) matrix supported deposits interbedded with the plinian fall deposits, which likely represent deposits from the distal margins of much larger PDCs. Pardo et al. (2011) did not describe any massive deposits associated with the main PDC units; but several of the deposits described in this thesis address this.

In historical times small volume, fully dilute PDCs ("pyroclastic surges") have frequently occurred at Ruapehu during phreatic and phreatomagmatic eruptions through the crater lake, reaching up to ~3km from vent (Houghton et al., 1987). Although to our knowledge no historical granular fluid-based PDCs ("pyroclastic flows") have been described at Ruapehu, two recently rediscovered images from 1945 appear to show a collapsing eruption column and a sizeable PDC decending Ruapehu's south-eastern flank (Figure 2.5). The PDC extends several km from the summit, reaching as far as most of the deposits investigated in this thesis. Furthermore, modelling by Degruyter and Bonadonna (2013) suggested that Ruapehu's 1996 eruption column approached the collapse threshold, and may have only remained buoyant due to the stabilising effect of high atmospheric winds at the time. Both of these examples show that although Ruapehu is not historically known for generating granular fluid-based PDCs, the occurrence and hence the future hazard from PDCs may be currently underestimated.

2.2.5 Volcanic hazards at Ruapehu

Ruapehu is a high risk volcano, combining frequent eruptions with high visitor numbers and significant proximal infrastructure. Major skifields at Whakapapa (north-west Ru-

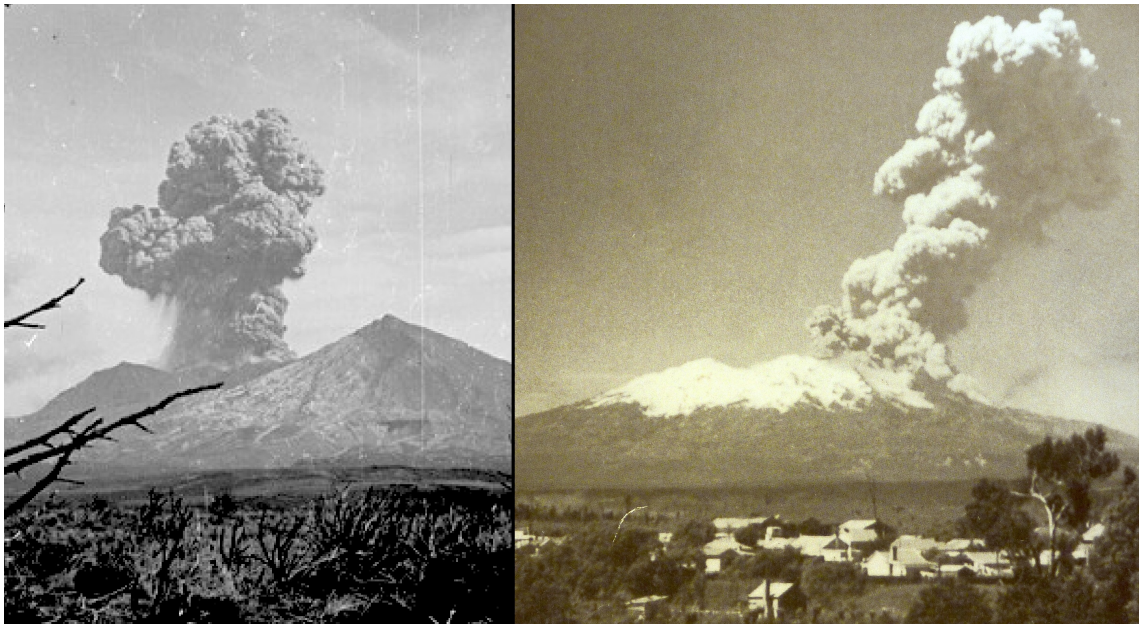

Figure 2.5: Recently rediscovered images from Ruapehu's 1945 eruption appears to show the onset of column collapse (left image), and a sizeable PDC descending several km on Ruapehu's eastern flank (right image). The PDC appears to be descending the deep glacial Wahianoa Valley, though it is also possible that it was focused in the adjacent Whangaehu valley that passes Tukino ski area and the main study area for this thesis. Note that the topography from this angle is obscuring much of the view, so the PDC may have been considerably larger and had a longer runout distance than is seen in this image (Left image: Bruce Valentine Davis, Alexander Turnbull Library Ref: 35mm-00702-a-F. Right image: N. Mosen, Lansdown Collection; In Johnston and Neall, 1995).

apehu) and Turoa (SW), as well as a club ski field at Tukino (E), support ~450,000 skier days each winter, and up to 10,000 people can be present on the mountain at peak times (Bryan et al., 1996; Johnston et al., 2000). Skifield infrastructure reaches within 2km of the active vent, bringing large numbers of people into the proximal hazard zone (Figure 2.6). Historical small-moderate explosive eruptions have often occured at Ruapehu with little warning (e.g. 2007 eruption, Jolly et al., 2010; Kilgour et al., 2010), and frequently produce ballistic hazards and fully dilute PDCs ("pyroclastic surges") that impact the immediate summit area (Houghton et al., 1987).

Figure 2.6: Small eruption at Ruapehu on the 7th October 1995, observed from the West Ridge Chairlift at Whakapapa Ski Area (Photo by Harry Keys, Dept. of Conservation).

Ruapehu is especially known for generating hazardous debris flows (lahars) from its crater lake (e.g. Lecointre et al., 2004; Keys, 2007), including eruption-triggered lahars (Cronin et al., 1997a,b), non-eruptive lahars (triggered by rainfall or lake break-out; Hodgson and Manville, 1999; Massey et al., 2010; Procter et al., 2010), and highly mobile snow-slurry lahars (generated when erupted material mixes with winter snow cover; Cronin et al., 1996a; Lube et al., 2009). The latter pose a particular hazard to Ruapehu's skifields (Figure 2.7). In 1953, a crater lake break-out lahar caused NZ's largest historical volcanic

disaster when the destruction of a rail bridge at Tangiwai resulted in the deaths of 151 train passengers (O'Shea, 1954; Manville, 2004). Subsequent development of Ruapehu's ERLAWS (Eastern Ruapehu Lahar Alarm & Warning System) and EDS (Eruption Detection System) warning systems have helped to mitigate the lahar risks by providing rapid warnings, though the short travel times to the upper skifields means lahars still present a significant proximal hazard (Keys, 2007; Leonard et al., 2008).

Figure 2.7: The deposits from a snow slurry lahar generated by the 25th September 2007 phreatic eruption at Ruapehu reached half way down Whakapapa skifield's Far West T-bar, narrowly missing skifield infrastructure (source: www.geonet.co.nz).

The current iteration of Ruapehu's hazard map reflects the historically observed hazards, and identifies 'flying rocks' and lahars as the major immediate hazards for future 'sudden onset' eruptions (Fig 2.8). Pyroclastic density currents do not feature in this 'sudden onset' hazard map; but in the light of more sustained unrest the map would be updated to reflect additional hazards from larger eruptions (G. Leonard, GNS Science, pers. comm.). However, while Ruapehu's historical activity provides a useful guide for the likely extents of future hazards, it is *not* representative of the longer-term activ-

ity at this volcano. Each of the magmatic or phreatomagmatic eruptions in recent years emitted only small volumes (~0.1 km^3) of juvenile tephra (Nakagawa et al., 1999); an order of magnitude smaller than the largest events of the past 15 ka (e.g Pardo et al., 2011). Similarly, the largest lahars in the past 2000 years were 1-2 orders of magnitude larger than any historically observed (Lecointre et al., 2004; Hodgson et al., 2007). High-particle concentration pyroclastic density currents have not been historically described, and as such have been largely overlooked as a modern-day hazard. However, the ~11.6 ka Pourahu PDC reached ~14 km from source (Donoghue et al., 1995a,b); which today is within range of State Highway 1 and NZ's major north-south power infrastructure. These observations highlight the limitations of assessing volcanic hazards based only on short historical records (Marzocchi et al., 2004), and emphasise the importance of looking to prehistoric deposits to fully characterise a volcano's "typical" eruptive behaviour and the upper limits of potential future hazards (Mendoza-Rosas and De la Cruz-Reyna, 2008).

Key Points:

- ✓ Ruapehu is one of the most active, and most visited volcanoes in New Zealand, and is surrounded by significant infrastructure. Therefore it is essential to properly characterise Ruapehu's eruptive hazards.
- ✓ Historical eruptions at Ruapehu are not representative of its longer-term activity, which includes voluminous lava flows and order-of-magnitude larger explosive eruptions. Therefore the historical activity does not adequately describe the maximum potential hazard.
- ✓ The perception of likely future hazards at Ruapehu has been strongly influenced by the small historical events; consequently voluminous pyroclastic density currents have been largely overlooked.

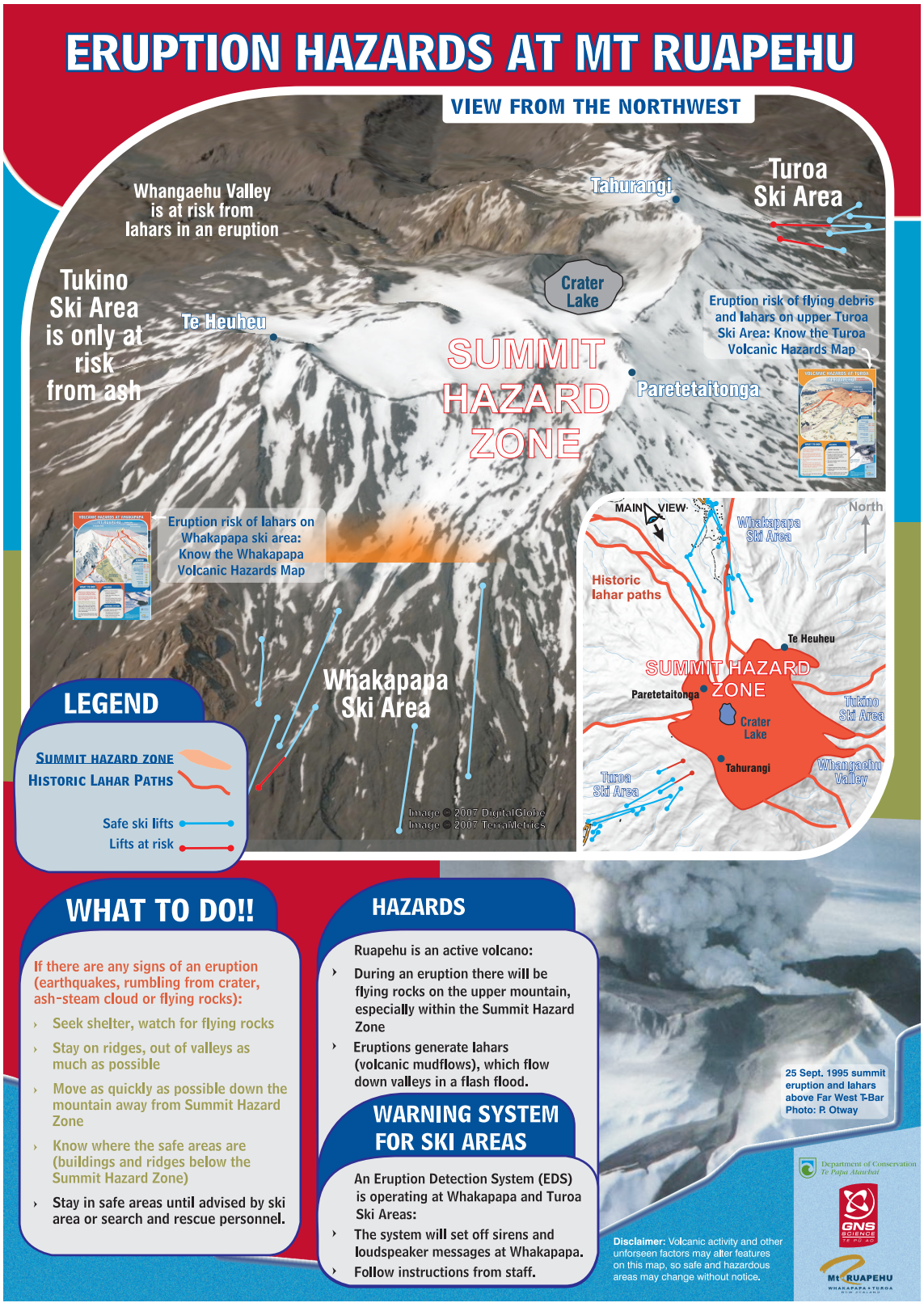

Figure 2.8: The current hazard map for Ruapehu focuses on small, 'sudden onset' eruptions from the Crater Lake area (GNS Science). The map reflects Ruapehu's historical activity, focusing on ballistic hazards and lahars, while granular fluid-based PDCs ('pyroclastic flows') are not included. The young (<13.6 ka) PDC deposits described in this thesis are all observed close to the Tukino Ski Area (left of image), which here is labelled as "only at risk from ash." However, the hazard map shown here specifically targets 'sudden onset' events, and would be updated during periods of heightened unrest.

2.3 Types of PDC that occur at andesitic stratovolcanoes and their associated deposits

Key Questions:

- *What eruption processes can lead to PDC generation at volcanoes like Ruapehu?*
- *What are the resulting deposit charactersitics?*

These concepts provide background for identifying and interpreting Ruapehu's prehistoric PDC deposits in the field (**Chapters 3 and 4**).

Pyroclastic density currents can be generated by any process that results in gravitational collapse of hot erupted material (Druitt, 1998). At cone volcanoes like Ruapehu, high elevations and steep topographic gradients provide multiple opportunities for gravitational collapse of erupted material, and PDCs have been observed to be generated by a wide variety of processes. These can be broadly separated into a) PDCs resulting directly from explosive volcanic eruptions, and b) PDCs resulting from collapse of erupted material already present at the volcano's surface:

PDCs resulting from collapse of explosively erupted material:

- Collapse or sustained fountaining of volcanic eruption columns (e.g. Pinatubo 1991, Rosi et al., 2001; and Ngauruhoe 1975, Nairn and Self, 1978)
- Boiling over (i.e. immediate collapse) of volcanic eruption columns (e.g. Mt Pelee, 1902, Fisher and Heiken, 1982)
- Immediate remobilisation of erupted material falling on steep slopes (e.g. Fuji, 2.5-3.2 ka, Yamamoto et al., 2005)
- PDCs generated by directed volcanic blasts (e.g. Bezymianny 1956, Mount St Helens 1980, and Soufrière Hills, 1997, Belousov et al., 2007)

PDCs resulting from collapse of hot erupted material already present at a volcano's surface:

- Gravitational collapse of lava domes or flows (e.g. Soufriere Hills 1996-7, Cole et al., 1998; Calder et al., 1999; and Colima 1991, Saucedo et al., 2004)
- Explosive disruption of lava domes (e.g. Merapi 1984, Boudon et al., 1993)
- Collapse of rapidly accumulating near-vent piles of erupted material (e.g. Ngauruhoe, 1975, Lube et al., 2007)
- Outpouring of lava following crater-wall collapse (e.g. Arenal, 1993, Alvarado and Soto, 2002; Cole et al., 2005)
- Explosive hydrovolcanic disruption of lava flows travelling over ice or wet ground (e.g. Klyuchevskoy, 1994, Belousov et al., 2011; and Etna, 2006; Behncke et al., 2008)

The resulting PDC deposits span an extensive array of deposit textures (Branney and Kokelaar, 2002; Brown and Andrews, 2015) that reflect the source eruption style and PDC transport and depositional parameters. In general, these processes combine to produce poorly sorted deposits that thicken into valleys and topographic lows. Many PDC deposits show evidence of high clast temperatures at deposition including deposit welding (e.g. Allen, 2004), prismatic jointing within clasts (evidencing in-situ cooling; e.g. Donoghue et al., 1995b), presence of charcoal (Crandell, 1987), gas escape structures (Brantley and Waitt, 1988), or aligned natural remnant magnetism of clasts (Hoblitt and Kellogg, 1979). Away from the immediate vent area evidence of high temperature deposition is often the strongest evidence that a deposit was emplaced by a PDC and not other volcaniclastic processes.

The textures of clasts within PDC deposits reflect the nature of the source material and fragmentation style, plus any modifications (e.g. abrasion, rounding) that occur during transport and deposition. Therefore PDCs generated by explosive eruptions from a vesiculating magma usually contain abundant vesicular clasts (e.g. pumiceous PDCs from collapsing plinian eruption columns), whereas PDCs generated by gravitational collapse of surface lavas (e.g. lava dome collapse) tend to contain denser, often more angular clasts reflecting their more degassed source material (Brown and Andrews, 2015). Therefore, studying the textures of the primary clasts within prehistoric PDC deposits is key to un-

derstanding the PDC generation process.

Key Points:

- ✓ PDCs at stratovolcanoes can be generated by many different explosive and effusive processes that result in gravatational collapse of hot erupted material.
- ✓ High-particle concentration PDCs produce poorly sorted deposits that thicken in valleys and contain abundant clasts of erupted material whose textures reflect their fragmentation and transport histories. These textures therefore provide insight into the type of activity that produced the PDC.

2.4 Physical processes leading to the generation of pyroclastic density currents

Key Questions:

- *What are the main physical parameters controlling PDC generation during volcanic eruptions?*

These concepts introduce the key physical parameters that influence the generation of PDCs during a volcanic eruption. Many of these parameters can be investigated by looking at the textures of clasts in the resulting deposits. This forms the basis for the textural investigations of Ruapehu's PDC deposits presented in **Chapter 5**

Most existing research into PDC generation has focused on modelling the conditions for collapse of volcanic eruption columns (e.g. Sparks and Wilson, 1976; Wilson et al., 1980; Bursik and Woods, 1991; Koyaguchi et al., 2010; Suzuki and Koyaguchi, 2012). These models generally relate column collapse to higher mass eruption rates, lower eruption (exit) velocities, lower exsolved volatile contents, or increases the size of the vent. These models are reviewed in detail in the introduction to **Chapter 5**. However, in broad terms these parameters all relate to the **momentum** and **buoyancy** of the erupting mixture. When pyroclasts and gas are explosively erupted from a volcanic vent, the initial density of the erupted mixture can be several times that of the surrounding ambient air, but the column ascends initially due to the momentum imparted by explosive fragmentation (e.g. Cioni et al., 2015). As this gas-pyroclast mixture ascends, it will expand and turbulently entrain and heat surrounding air, reducing its bulk density. If the bulk density of the eruption column then becomes lower than atmospheric density before it loses its upward momentum, it will continue to ascend as a buoyant plume. However, if the erupted material loses its upward momentum before it has entrained and heated sufficient air to become buoyant, then the column will collapse and continue its motion along the surface as a PDC (Koyaguchi et al., 2010). Despite the many different ways that PDCs can be generated at stratovolcanoes (Section 2.3), these principles of *momentum* and *buoyancy* always apply:

In the case of PDCs generated by lateral blasts or 'boiling over' mechanisms, limited initial upwards momentum means the collapse condition may be reached without appreciable vertical ascent of the erupting mixture. Similarly, in the case of PDCs generated by concentrated ballistic fallout or collapsing lava domes or flows, low initial gas fractions and high pyroclast densities mean the gas-pyroclast mixture has little opportunity to form a buoyant plume.

Since the bulk density of a moving gas-pyroclast mixture directly controls whether that material will ascend as a buoyant plume or travel along a volcano's flanks as a density current, this provides a first-order avenue for investigating why some prehistoric eruptions generated PDCs. Therefore, the densities, vesicularities, and vesicle textures of clasts within prehistoric deposits provide direct insight into the processes contributing to PDC generation. These concepts are explored in detail in **Chapter 5**.

Key Points:

- ✓ PDCs are generated when a moving gas-pyroclast mixture has a bulk density greater than the surrounding atmosphere causing it to travel along a volcano's flanks rather than ascending as a buoyant plume.
- ✓ Numerical simulations suggest that higher mass discharge rates, larger vents, lower exsolved volatile contents, and lower exit velocities all promote column collapse through their effects on the momentum and buoyancy of the erupting mixture.
- ✓ Textures of clasts within prehistoric PDC deposits, including their densities, vesicularities, and vesicle textures, provide insight into why the gas-pyroclast mixture was unable to ascend as a buoyant plume.

2.5 Magmatic systems at intermediate arc volcanoes

Key Questions:

- *What are the characteristic magma storage conditions at volcanoes like Ruapehu?*
- *How might heterogeneities in the magma storage system contribute to PDC generation at volcanoes like Ruapehu?*
- *What methods allow a volcano's pre-eruptive magmatic storage conditions to be investigated.*

These concepts extend the discussion in Section 2.4 to consider how underlying magmatic parameters at arc volcanoes can directly affect the nature of the erupted material, and hence provide insight into PDC generation at volcanoes like Ruapehu (**Chapter 5**).

While the bulk density of a moving gas-pyroclast mixture directly controls PDC generation during a volcanic eruption (Section 2.4), it is the underlying magmatic system that dictates the nature of the erupted material. Magma storage regions at intermediate arc volcanoes like Ruapehu are complex, heterogeneous systems involving frequent small magmatic inputs, mixing and mingling of components (Eichelberger, 1975), and contamination by continental crust (Davidson et al., 2005). In contrast to the traditional view of a single large magma chamber, many intermediate magmas are now thought to be stored in long-lived crystal-mush zones (Bragagni et al., 2014), where ongoing processes such as cooling, crystallisation and degassing are offset by frequent episodes of magma recharge that bring heat and volatiles into the shallow magma system (Cashman and Blundy, 2013). There is abundant textural evidence supporting the open-system nature of these shallow storage zones, including observations of disequilibrium textures and significant geochemical zonation in phenocrysts (Nakamura, 1995; Nakagawa, 2002; Humphreys et al., 2006), entrained antecedent crystals ('antecrysts') in erupted material (Smith et al., 2009; Stewart, 2010), heterogenous melt contents reflected by variations in clast crystallinities (Frey and Lange, 2011), and mingling textures such as mafic enclaves (Christopher et al., 2014) or composi-

tional banding (Donoghue et al., 1995a, 1999). Magmatic recharge is commonly attributed to hot mafic magmas entering more evolved storage zones (e.g. Montserrat; Murphy et al., 1998; Murphy and Sparks, 2000; and Tongariro; Shane et al., 2008), but several studies have also described frequent inputs of hotter, compositionally similar magmas that contribute thermal energy to the crystal mush (e.g. Mt St Helens; Cashman and Blundy, 2013; and Nevado de Toluca; Smith et al., 2009). The resulting subvolcanic storage zones are therefore interpreted to consist of complex networks of sills and dykes containing magmas with different residence times and crystallisation and degassing histories (Roman et al., 2006; Kilgour et al., 2013). At Ruapehu, the young magmatic system is thought to be characterised by frequent injection of small batches of fresh magma that mingle and mix with older stagnant magmas stored in small bodies in the shallow storage zone (Gamble et al., 1999; Nakagawa et al., 1999; Waight et al., 1999; Nakagawa, 2002; Stewart, 2010; Kilgour et al., 2013). Eruptions can disrupt and entrain several such magma bodies, resulting in erupted material whose chemistry and textures reflect these underlying heterogeneities (Figure 2.9). These observations are particularly relevant for Ruapheu's youngest PDC desposits (Units 8-10), and are investigated in detail in **Chapter 5**.

Mixing between remnant magmas and new magmas is a common process at cone volcanoes like Ruapehu (Nakamura, 1995; Nakagawa et al., 1999; Nakagawa, 2002). It has been widely recognised as a mechanism for triggering volcanic eruptions (Sparks et al., 1977; Donoghue et al., 1995a; Eichelberger, 1995), with the influx of fresh magma providing heat and/or volatiles to the resident magma. Because the solubility of dissolved water in magma decreases with increasing temperature, mixing or mingling with a hotter melt is proposed to cause the resident magma to become water-saturated and hence promote exsolution of bubbles. The resulting volume change during exsolution increases the chamber pressure, and hence may trigger an eruption (Snyder, 1997). The physical process of magma mixing occurs through a combination of mechanical and chemical processes (Snyder, 1997). First, as two magmas shear past each other they are mechanically stretched and folded (i.e. mingling), decreasing the distance between particles of each magma and greatly increasing the mingled contact area. At the same time, chemical reactions can occur between the different magmas that release or consume heat and may promote exsolution or dissolution of magmatic components. If the mechanical mingling continues such

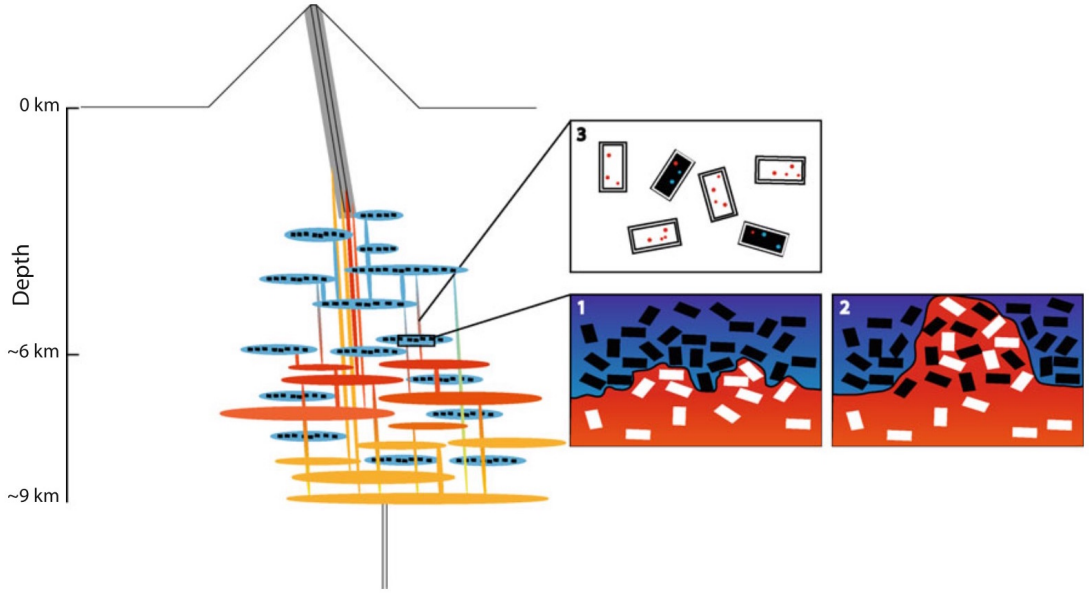

Figure 2.9: Conceptual model for the magmatic system at Ruapehu (from Kilgour et al., 2013). Here, small volume andesitic melts are present in closely spaced dykes and sills between 2-9km depth. Ascending magma interacts with crystal mushes in these storage zones (1), mingling and entraining exotic crystals (2), as well as trapping cognate melt as inclusions (3) that record the magmatic conditions at the time of entrapment.

that the thickness of the ribbons of each magma becomes small compared to diffusive length scales, then diffusion (Sparks et al., 1977) ultimately homogenises the two liquids into one (i.e. mixing). Density differences between the two magmas control their respective buoyancies, with large differences favouring a layered, density-stratified system in which the magmas remain mostly separated and mingling/mixing is minimised. Similarly, large viscosity differences between different magmas also hinders mixing (Sparks and Marshall, 1986), since the shear deformation then mostly occurs only in the lower-viscosity magma. Therefore, mixing/mingling is most efficient when there are only small density and viscosity differences between the different magmatic components (Snyder, 1997).

While the contribution of magma mixing or mingling as an eruption trigger is well studied, few studies have extended this to consider how it affects the eruptive dynamics. Since mixing or mingling of two or more magmas directly affects the physical properties of the erupted material (e.g. composition, volatile content, crystal content, temperature, density, viscosity), this in turn will directly affect the momentum and buoyancy of the erupted mixture. These concepts are addressed more fully in **Chapter 5**, with particular

emphasis on the role of magma mingling in promoting column collapse and PDC generation.

2.5.1 Investigating the magmatic storage conditions

Understanding the pressures and temperatures at which magma is stored prior to eruption is fundamental for unravelling the complexities of the volcanic system (Dahren et al., 2011). This becomes even more important in heterogenous systems, where magmas from multiple storage zones may be involved in a single eruption (Figure 2.9). Traditionally, modelling of magmatic storage pressures has been based on mineral and rock compositional data and calibrated themodynamic formulations to investigate the pressures and temperatures at which the magma and phenocrysts last equilibrated. Widely used approaches include clinopyroxene-melt (Putirka et al., 2003; Putirka, 2008), plagioclase-melt (Housh and Luhr, 1991; Ghiorso et al., 2002; Putirka, 2005, 2008), and clinopyroxene composition (Nimis and Ulmer, 1998; Nimis, 1999) thermobarometers. However, all of these approaches have relatively large standard errors of estimate (SEEs) that exceed ± 150 MPa in the pressure calculations (Dahren et al., 2011). Another frequently used approach uses the concentrations of dissolved H_2O-CO_2 (usually measured in melt inclusions by fourier transform infrared spectroscopy) to calculate the pressure at which the silicate melt would have become vapour saturated (Newman and Lowenstern, 2002; Papale et al., 2006; Moore, 2008). This method is effective for calculating the melt inclusion trapping pressure (i.e. providing the crystallisation depth), *assuming* that the system was vapour saturated at the time of entrapment. Limitations of this method include the significant amount of preparation needed to find, isolate and analyse melt inclusions; and care is also needed to check that further crystallisation of the trapped melt and/or loss of volatiles by diffusion or to vapour bubbles has not affected the measured glass H_2O and CO_2 concentrations. Recently, Gualda and Ghiorso (2014) and Bégué et al. (2014) introduced a new geobarometer using an updated version of the popular themodynamic modelling software rhyolite-MELTS. This geobarometer recognises that the phases crystallising from a magma must be in equilibrium with the host melt at the time of crystallisation, and hence that the saturation curves for each mineral phase will follow unique pressure-temperature paths that are determined by the composition of the melt. Since the melt composition can

be obtained by measuring the major element composition of glass in erupted material (i.e. matrix glass or melt inclusions), this allows the composition-dependent phase saturation paths to be modelled in rhyolite-MELTS across a range of pressures and temperatures using thermodynamic principles. Therefore, if several different phases are inferred to have crystallised simultaneously from the same melt (on the basis of pyroclast/lava textural analyses), then the unique crystallisation conditions *must* be described by the pressure and saturation temperatures at which these curves intersect (Figure 2.10). This method was originally optimised for rhyolite samples crystallising quartz +1 or +2 feldspars. However in this thesis, and in collaboration with the original developers, we extend this method to andesitic compositions using a modified rhyolite-MELTS that has been updated to model equilibrium crystallisation of plagioclase + 2 pyroxenes. The data presented in this thesis is therefore the first time this method has been applied to andesitic compositions. Further details of the method, including its advantages and limitations, are detailed in **Chapter 5**.

Key Points:

- ✓ Intermediate arc volcanoes like Ruapehu typically have heterogeneous magma storage zones comprising numerous small batches of crystallising magma.
- ✓ Mixing and mingling of different magma batches is common; and can serve as both an eruption trigger and also to modify the bulk properties of the erupted material. This affects the eruption dynamics, including the momentum and buoyancy of the erupting mixture, and the potential for PDC generation.
- ✓ There are several different methods for assessing the pressures and temperatures of the pre-eruptive magmatic storage conditions. A new thermodynamic method using rhyolite-MELTS software allows rapid assessment of storage conditions using major element glass composition as the main data input, and is modified here for use with andesitic compositions for the first time (see **Chapter 5**).

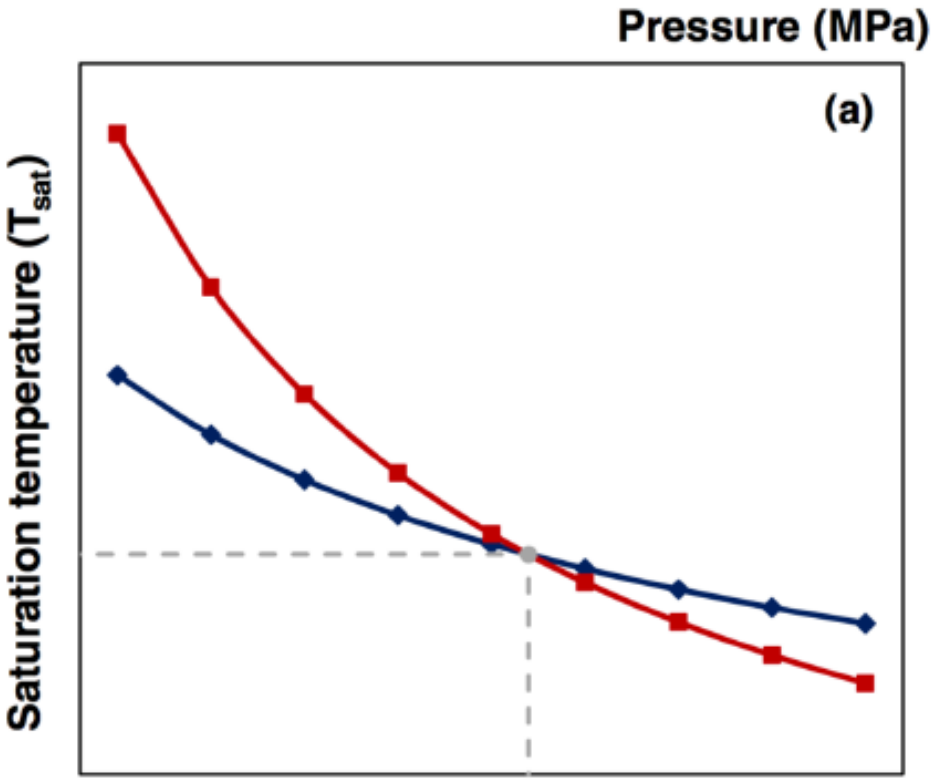

Figure 2.10: The principle behind the rhyolite-MELTS based geobarometer for estimating the pressures and temperatures of crystallising phases (from Gualda and Ghiorso, 2014). a) The two curves represent rhyolite-MELTS modelled saturation curves (T_{sat}) for two different mineral phases known to be crystallising in equilibrium with a given melt composition. If both phases are inferred to have crystallised simultaneousy in equilibrium with the same melt, then the crystallisation temperature and pressure is given by the unique point where the lines intersect. For the Ruapehu samples analysed in this thesis, the model has been updated to address simulataneous crystallisation of plagioclase, orthopyroxene and clinopyroxene in equilibrium with matrix glass compositions.

2.6 The significance of snow and ice

Key Questions:

- *How can the presence of snow or ice affect volcanic processes and hazards?*
- *Why is it important to consider prehistoric snow and ice cover when investigating volcanic deposits?*
- *How do PDCs interact with snow and ice?*
- *What is known about snow and ice cover at Ruapehu?*

These concepts address how snow and ice can affect the textures and preservation of volcanic deposits, and hence are important for identifying and interpreting deposits in the field (**Chapters 3 & 4**). Additionally, snow and ice can directly affect volcanic processes, including affecting the generation, transport and extents of PDCs and lahars (**Chapter 6**).

Stratovolcanoes are tall structures that reach up to 6891m high on Earth (Ojos del Salado, Argentine-Chile border). Consequently, many have permanent ice or snow cover even at low latitudes, and interaction between volcanic material and snow or ice is common. This directly affects a volcano's eruptive styles, hazards, morphology and deposit preservation.

During a volcanic eruption, erupted material can interact with ice in several ways (Major and Newhall, 1989):

- *Glacial meltwater can interact with fragmenting magma:* This changes the eruptive style, resulting in phreatomagmatic fragmentation that may then disperse fine ash over large areas (e.g. Eyjafjallajökull 2010; Gudmundsson et al., 2012)
- *Surface lavas may travel over or burrow into snow and ice:* This results in distinctive lava textures (Lodge and Lescinsky, 2009; Conway et al., 2015), including glassy external margins and fine-scale jointing perpendicular to the ice-contact margins

(Lescinsky and Fink, 2000; Spörli and Rowland, 2006), as well as overthickened lava flows emplaced directly on ridge crests due to diversion by valley-filling ice (Lescinsky and Sisson, 1998). However, although lava flows can produce large volumes of meltwater, the rates of meltwater production are generally too slow to produce hazardous lahars (Major and Newhall, 1989).

- *Glaciers and snowpacks may be melted from below by subglacial eruptions, lava extrusion, or geothermal activity:* This process has been studied in detail in Iceland, (e.g. Stevenson et al., 2006; McGarvie, 2009; Stevenson et al., 2009), producing distinctive volcanic landforms (e.g. flat-topped volcanoes called tuyas; Smellie, 2006), and can result in hazardous floods (jökulhlaups) when ice-dammed meltwater is catastrophically released (Wilson and Head III, 2002).

- *Water ejected from a crater lake may melt and combine with snow and ice:* This can produce mobile "snow-slurry lahars" (Lube et al., 2009; Kilgour et al., 2010) that can incorporate as much as 3500-4000 m^3 of snow for every $1m^3$ of lake water ejected (Cronin et al., 1996a).

- *Tephra may be deposited directly on snow and ice:* This can result in differential ablation (Julio-Miranda et al., 2008; Richardson and Brook, 2010) and destabilisation of the snowpack (Manville et al., 2000), and cause syn- and post-eruptive avalanches and lahars (Manville et al., 2000).

- *Pyroclastic density currents and hot gases may melt, mix and scour snow and ice and generate secondary lahars:* This is discussed in Section 2.6.1 below.

The presence of snow and ice also strongly affects the distribution and preservation of volcanic deposits and the shape of a volcanic edifice (Conway et al., 2015). Hackett and Houghton (1989) and Manville et al. (2000) observed that there is now almost no stratigraphic record of Ruapehu's >40 eruptions in the past 100 years, citing complex interactions between tephra, snow, ice and water for the poor deposit preservation. This highlights how even comprehensive deposit records may significantly under-represent prehistoric activity. Since fragmental volcanic deposits are unlikely to be preserved when emplaced on ice, the locations and extents of ice cover are therefore important considerations when

interpreting prehistoric deposits (**Chapter 4**). Furthermore, since erosive processes dominate between eruptive periods (Hackett and Houghton, 1989), at glaciated volcanoes like Ruapehu much of the surface may therefore reflect glacial rather than volcanic processes (e.g. moraines, glacial valleys; McArthur and Shepherd, 1990).

2.6.1 The effects of snow and ice on PDCs

Pyroclastic density currents can melt, mix, and scour snow and ice during transport, and generate hazardous secondary lahars and mixed avalanches (Major and Newhall, 1989). The most notorious example of this occurred at Nevado Del Ruiz volcano (Colombia) in 1985, when PDCs were emplaced over ~10-18 km^2 of the summit icecap and generated debris flows that killed more than 20,000 people (Pierson et al., 1990; Thouret, 1990). Meltwater-sourced debris flows and mixed avalanches were also generated at Redoubt volcano (Alaska) in 1990 by PDCs generated by repeated collapses of the summit lava dome (Gardner et al., 1994). These events highlight the risks of PDC-ice interaction at other high-risk glaciated volcanoes like Mt. Rainier (USA) and Cotopaxi (Ecuador), both of which have large populations living in the lahar hazard zones (Wood and Soulard, 2009; Pistolesi et al., 2013). However, few studies (e.g. Walder, 2000a,b) have investigated PDC-ice interaction in detail, and none have addressed how transport over ice affects the primary PDC dynamics and hazard. **Chapter 6** addresses these issues by combining experimentally determined rates of meltwater and steam production with high-resolution multiphase numerical models, in order to investigate the large-scale effects of PDC transport over ice for the first time.

In addition to affecting PDC dynamics and the associated secondary lahar hazard, snow and ice has also been observed to directly trigger PDCs by promoting explosive collapse of lava flows on steep (15-35°) ice-covered slopes. At Klyuchevskoy volcano, secondary (rootless) hydrovolcanic explosions resulting from the interaction of hot lava and underlying ice were observed to generate PDCs that reached more than 2km beyond their parental lava flow fronts (Belousov et al., 2011). Therefore, the presence of snow or ice significantly changes the PDC and associated hazards.

2.6.2 Snow and ice at Ruapehu

Ruapehu is the tallest mountain in New Zealand's North Island (2797m) and currently hosts ~20 small glaciers and glacier remnants (Williams, 2013), while thick winter snow cover supports skifields at Turoa, Tukino, and New Zealand's largest commercial skifield at Whakapapa. Ruapehu's edifice has been extensively modified by glaciers, with deep U-shaped valleys and extensive glacial deposits (till) on all flanks (Conway et al., 2015). A large Pleistocene ice cap fed outlet glaciers (McArthur and Shepherd, 1990) that reached as low as 1300m between ~51-41 and ~27-15 ka (Conway et al., 2015), and many Ruapehu lavas show textural evidence for snow and ice contact during emplacement (Spörli and Rowland, 2006; Conway et al., 2015). Consequently many of Ruapehu's proximal eruptive products, including the <13.6 ka PDC deposits described in this thesis, must have interacted with snow or ice during emplacement.

Key Points:

- ✓ Many tall volcanoes have significant snow and ice cover, which can interact with erupting material and directly affect a volcano's eruptive behaviour and associated hazards.
- ✓ PDCs can interact strongly with surface ice, affecting the PDC transport dynamics and generating large volumes of meltwater that can generate hazardous secondary lahars.
- ✓ Snow and ice affects the long-term preservation of volcanic deposits, so understanding the extents of prehistoric ice cover is essential when interpreting the deposit record.
- ✓ Ruapehu had extensive prehistoric ice cover, and many of Ruapehu's Late Pleistocene and Holocene volcanic products will have interacted with ice in some way.

3

A new confidence-based method for identifying poorly exposed pyroclastic flow deposits in the field

Introduction to Chapter 3

In order to understand the nature of the pyroclastic density current (PDC) hazard at Ruapehu, it is important to understand the PDCs that have occurred there before. This relies on identifying and studying deposits in the geological record. However, small volume proximal PDC deposits have low preservation potential (see Chapter 4), and can be difficult to distinguish from other near-source volcaniclastic deposits. Chapter 3 addresses this by introducing a new confidence-based identification method that permits rapid assessment of candidate PDC deposits in the field. This system underpins the identification of 12 PDC units in eastern Ruapehu that are the main focus of the rest of this thesis (Chapters 4 - 6).

Pyroclastic density currents form a continuous spectrum from fully dilute pyroclastic 'surges' to highly concentrated granular fluid-based PDCs (pyroclastic 'flows,' see Box 1.1) that are the main focus of this thesis. Since the same PDC can have both flow-like and surge-like characteristics, the term pyroclastic density current is usually preferred. However, the 'flow' and 'surge' end-members produce very different deposits, and therefore *for the confidence-based deposit assessment system presented here* we retain the terms 'flow' and 'surge,' but acknowledge that the source PDC may have had both 'flow'-like and 'surge'-like characteristics.

The key outcomes are:

1. Recognition that significant textural overlap exists between different volcaniclastic deposits, and that the resulting uncertainties in deposit interpretations are not always acknowledged. Since small, poorly preserved or poorly exposed pyroclastic flow deposits can be especially difficult to distinguish from other deposits containing recently erupted material, these therefore may be frequently misinterpreted or overlooked.

2. Identification key textural criteria that are a) most likely to be observed even in small or poorly exposed volcaniclastic deposits, and b) are most useful for either supporting, excluding, or distinguishing between different volcaniclastic source processes.

3. Development of a new confidence-based system for identifying pyroclastic flow de-

posits in the field. The system assesses how confidently different volcaniclastic processes can explain the observed deposit textures, and hence allows the *most likely* process to have formed the deposit to be determined. A worked example from Ruapehu volcano demonstrates the utility of this system for assessing a difficult-to-identify deposit and determining a likely pyroclastic flow origin.

The chapter is presented in the style of an academic paper, though with slightly expanded detail that will be condensed for submission to a peer-reviewed journal. As such, the relevant contextual background and methods are presented in full.

Abstract

Pyroclastic density currents (PDCs) are a destructive volcanic hazard. Quantifying the types, frequency and magnitudes of PDC events is essential for effective risk management, but since historical records date back at best a few hundred years, this usually relies on identifying deposits in the geological record. However proximal PDC deposits have low preservation potential, especially when emplaced in active drainages or onto snow or ice. Where ancient PDC deposits are preserved they can be difficult to distinguish from other volcaniclastic deposits, and are frequently misinterpreted or overlooked. This has been the case at Mt. Ruapehu; a much visited, high-risk active volcano in New Zealand with no historically observed granular fluid-based PDCs (here termed 'pyroclastic flows'). Here, we introduce a new field method for assessing proximal volcaniclastic deposits of unknown origin at varying degrees of confidence, with a particular focus on identifying deposits from granular fluid-based PDCs (here termed 'pyroclastic flow deposits'). A drawback of previous list-based identification schemes is that they generally lead the user towards making a single interpretation that does not then acknowledge the underlying uncertainties and confidence in that decision. A consequence of these uncertainties is that many small and poorly exposed volcaniclastic deposits are likely to be overlooked in favour of more voluminous and better preserved deposits that can be more easily interpreted and are perceived to represent more significant events. The method presented here differs from previous identification schemes in that it does not attempt to uniquely attribute a deposit to a single depositional process, but instead assesses which volcaniclastic processes *could* have produced the deposits and *how confidently* each of those processes can explain the observed textures. A worked example from the Tukino ski area on Ruapehu's eastern flanks demonstrates the effectiveness of this method for identiying a difficult-to-identify, and previously overlooked proximal pyroclastic flow deposit. This method has applications for consistent, rapid assessment of candidate pyroclastic flow deposits in the field, and the concept can be easily adapted to other types of difficult-to-identify proximal volcaniclastic deposits. The use of confidence levels for deposit interpretations may also provide useful inputs to probabilistic assessments of volcanic hazards.

3.1 Introduction

A fundamental principle in physical volcanology is that a volcano's past behaviour provides insight into the kind of activity that can be expected in the future (Nakada, 2000). Therefore quantifying the distributions, types, frequencies and magnitudes of previous hazards is an essential component of volcanic hazard management. Since historical records only date back at most a few hundred years, this normally relies on identifying deposits in the volcanic record. Therefore, properly assessing even small and poorly preserved deposits is essential for a thorough understanding of a volcano's past activity.

Composite volcanic cones are constructed by repeated eruption of lavas and explosively erupted material from one or more vents. During and between eruptive episodes, non-volcanic erosion and transport processes rework these materials downslope to form a wide variety of fragmental deposits composed almost entirely of volcanic material. Thus, most volcanic surfaces present a diverse mix of intermingled primary and non-primary fragmental deposits ('*volcaniclastic deposits*;' e.g. McPhie et al., 1993) that can be difficult to identify in the field. In the case of historical deposits, identification is usually straightforward since the causative process is either observed directly, or significant amounts of the deposit remain (e.g. Komorowski et al., 2013). Hence, modern deposits are well suited to traditional field identification methods that emphasise broad initial observations of deposit geometry, followed by closer observations of outcrop-scale textures and components (Charbonnier et al., 2013). In contrast, because fragmental deposits are easily reworked on steep proximal volcanic slopes (Smith et al., 1999), many small or ancient deposits are commonly only preserved in a few poorly-exposed locations (e.g. Donoghue et al., 1999) where they lack the broader-scale context that aids interpretation.

The motivation for this study was an observation during fieldwork at Ruapehu volcano of numerous small volcaniclastic surface deposits, some of which contained abundant juvenile/primary clast textures. The small and patchy deposits and relatively poor exposures meant these deposits were difficult to attribute to specific depositional processes. However, initial suspicions were that some of the deposits represented relatively young granular fluid-based pyroclastic density current (PDC) deposits. If true this would be an

important observation at a volcano where no historical granular fluid-based PDCs and very few prehistoric PDC deposits are known. Given the challenges of confidently identifying the deposits, we therefore developed a simple yet systematic method for assessing candidate granular fluid-based PDC deposits in the field and assigning confidence levels to those interpretations.

3.2 Terminology

A wide and often confusing range of terms have been applied to primary and reworked volcaniclastic deposits and their components (for a detailed summary see White and Houghton, 2006), including *pyroclastic* deposits containing explosively fragmented material (Wentworth and Williams, 1932; Fisher, 1966; Fisher and Schmincke, 1984), *autoclastic* (Fisher and Schmincke, 1984) deposits containing material fragmented at the surface of moving lava, and *epiclastic* deposits containing material fragmented or deposited by normal non-volcanic surface processes (Fisher, 1961; Cas and Wright, 1987). On volcanic edifaces, these deposits usually contain either *juvenile* material derived directly from erupting magma, or *lithic* material derived by fragmentation of pre-existing rock or incorporated from unconsolidated sediment. Combining several earlier classifications, White and Houghton (2006) introduced the term *primary volcaniclastic* to describe *all* deposits where particles are mobilised directly by explosive or effusive volcanism and *not stored* prior to arriving at the deposition site. However, even this broad classification introduces difficulties when interpreting ancient deposits. For example, following a large eruption much of a volcanic edifice may be covered in juvenile-textured volcanic material that can then be reworked for years after the eruption ended. Strictly speaking the resulting deposits would be non-primary; however in proximal locations where short transport distances provide little opportunity for clast modification or sorting, the deposits may be texturally indistinguishable from primary deposits that were emplaced at the time of eruption. Hence almost all of the current classification schemes require at least limited interpretation of the source and mode of particle fragmentation, as well as the transport and depositional processes *and* the timing of the events that formed the deposits. In proximal volcanic locations where almost all material begins with an eruptive origin, such *a priori* knowledge is often

impossible; and the same outcrop may be interpreted in different ways by different volcanologists. Therefore for deposit identification purposes, it is preferable to avoid any initial interpretation altogether and only assign genetic names after the most likely depositional process has been assessed. Hence, in the method introduced here, we refer to all fragmental deposits on a volcanic edifice as 'volcaniclastic' until their possible origin has been assessed.

Pyroclastic density currents (PDCs) form a continuous spectrum from highly mobile, fully dilute currents dominated by fluid turbulence (pyroclastic 'surges'), to granular fluid-based currents (pyroclastic 'flows') dominated by particle collisions near the lower flow boundary (Branney and Kokelaar, 2002). In practice the same PDC can exhibit both flow-like and surge-like characteristics at different points in space and time, and as such the term pyroclastic density current is generally favoured (Waitt, 1981; Valentine and Fisher, 1993). However the 'flow' and 'surge' end-member components usually produce very different deposits, and are also significant from a hazards perspective due to differences in their mobility (Nakada, 2000; Valentine and Fisher, 2000, and Chapter 6). 'Standalone' pyroclastic surges are frequently generated by phreatic or phreatomagmatic eruptions (e.g. Kilgour et al., 2010), and the area impacted by them is usually limited to only a few km from the vent due to their low momentum and density (Nakada, 2000). They typically produce thin, fine-grained deposits that have limited preservation potential in the long-term volcanic record. Pyroclastic surges represent a significant near-source hazard (Bryan et al., 1996) capable of overtopping local topography, but rarely have sufficient force to destroy buildings in their path (Nakada, 2000). In contrast, granular fluid-based pyroclastic 'flows' are usually valley-confined and have runout distances that can extend well beyond the volcanic edifice (>10-15km) due to their high momentum (Crandell, 1987). These therefore represent a major hazard to life and infrastructure (Witham, 2005). Pyroclastic flows usually transition vertically into overriding turbulent pyroclastic surges, and these can separate from the denser main body of the pyroclastic flows and impact even greater areas (e.g. Unzen Yamamoto et al., 1993). However the deposits from the denser basal 'flow' component are volumetrically much more significant (Charbonnier et al., 2013) and are more likely to be preserved. Therefore *for the deposit identification purposes outlined in this chapter, we retain the terms 'flow' and 'surge' to describe the main process contributing to the observed deposits*, while nonetheless emphasising that the originating pyroclastic

density current may have had characteristics attributable to both processes. Because of the greater scale and hazard associated with pyroclastic flows, it is these deposits that are the focus of the identification method presented here.

The identification method presented here also focuses primarily on *proximal* volcanic locations, where steep gradients and short transport distances mean many different volcaniclastic processes can produce texturally similar deposits. At Ruapehu, Hodgson and Manville (1999) defined the proximal zone as extending <5 km from the summit, but for the broader deposit identification purposes here we consider 'proximal' to mean any deposits emplaced on the main volcanic edifice; where steep topographic slopes are a major control on clast transport, deposition and subsequent deposit reworking.

3.3 Geological Setting

Mount Ruapehu is an active andesitic-dacitic cone volcano at the southern end of New Zealand's Taupo Volcanic Zone. The ~110-150 km3 edifice (Hackett and Houghton, 1989; Conway et al., 2015) has been constructed from multiple vents over >250ka, and comprises lava flows, plinian and sub-plinian tephras, spatter deposits, debris flow deposits, and rare pyroclastic flow deposits (e.g. Hackett and Houghton, 1989). Extensive glaciation throughout much of Ruapehu's history (McArthur and Shepherd, 1990; Conway et al., 2015), together with infrequent episodes of edifice collapse and normal fluvial and mass-wasting processes means much of Ruapehu's surface has been extensively reworked. Historical phreatic and phreatomagmatic eruptions have frequently produced fully dilute PDCs (pyroclastic surges) that impacted the immediate summit area (e.g Nairn et al., 1979; Kilgour et al., 2010). However destructive granular fluid-based PDCs (pyroclastic flows) have not been historically documented, and very few examples have been described in the volcanic record (e.g. Donoghue et al., 1995a). The results presented here and in Chapter 4 suggest this may be due to misidentification or overlooking of poorly exposed deposits, and is not a reflection of their absence.

3.4 Pyroclastic Flows and their Deposits

Pyroclastic flows (PFs) in their broadest sense are hazardous mass flows of erupted materials and gas that travel downslope due to gravity. They can be generated by any process that results in gravitational collapse of erupting volcanic material on a slope; including collapsing eruption columns (Nairn and Self, 1978; Rosi et al., 2001), gravitational or explosive collapse of lava domes (Boudon et al., 1993; Calder et al., 1999), collapsing lava flows (Saucedo et al., 2004; Belousov et al., 2011), or co-eruptive remobilization of erupted material falling on steep slopes (Yamamoto et al., 2005). In general, pyroclastic flows contain particles that are hotter than ambient temperature, though 'cold' pyroclastic flows and surges generated by phreatic eruptions can contain material well below magmatic temperatures (e.g. 2012 Te Maari (Tongariro) eruption, NZ; Lube et al., 2014).

Pyroclastic flow deposits span an extensive array of textures (Branney and Kokelaar, 2002; Brown and Andrews, 2015) depending on factors including the source eruption style, generation mechanism, nature of the source material (e.g. clast compositions, textures, size distributions), transport parameters (e.g. particle concentration, flow fluidisation, channelisation, particle entrainment, abrasion and communition) and depositional variables (e.g en-mass vs progressive deposition, diachronous deposition [Brown and Branney, 2004], temperature, post-deposition degassing, settling and welding). Furthermore, post-deposition erosion and winnowing can continue to affect the preserved deposit textures even if parts of the deposit remain in-situ, while more extensive reworking can produce new volcaniclastic deposits containing the same components as the original pyroclastic flow (e.g. Brantley and Waitt, 1988). In a very general sense, these processes all combine to produce poorly sorted accumulations of material that contain abundant clasts attributable to the source eruption. However in proximal locations where all material has a volcanic origin, other volcanic mass flows, glacial processes, mass wasting, and even vent-proximal tephras can all produce texturally similar deposits. As such, small and poorly exposed proximal pyroclastic flow deposits can be difficult to identify with confidence.

The difficulties in distinguishing proximal pyroclastic flow deposits from other volcaniclastic deposits have been frequently described. Several authors have commented on

the similarities between pyroclastic flow and debris flow deposits (e.g. Cas and Wright, 1987, p336), and there are often few ways to conclusively differentiate between them. For example, Fisher and Schmincke (1984) point out that the 1902 Nuées ardentes deposits from Mt Pelée and some Mount St Helens pyroclastic flow deposits, are both texturally similar to lithic-rich deposits at Nevado de Toluca volcano that were interpreted as debris flow deposits due to their low pumice and glass contents and lack of breadcrust clasts (Bloomfield and Valastro, 1977). Likewise, pumice-rich debris flows (Bond and Sparks, 1976) can produce deposits that are texturally similar to pumice-rich pyroclastic flows (Fisher and Schmincke, 1984). Even moraines, which are extensive features on many tall stratovolcanoes, are difficult to distinguish from some pyroclastic flow and debris flow deposits (e.g. Hackett, 1985, p.120); for example several of the PF deposits identified at Ruapehu in Chapter 4 have previously been mapped as moraines on the basis of their surface morphology (Chapman, 1996; Spörli and Rowland, 2006).

Evidence of high clast temperatures at the time of deposition is one of the more reliable ways to distinguish pyroclastic flow deposits from other volcaniclastic deposits (Crandell, 1971), especially if the deposit geometry (e.g. channelised deposit) or distance from source rule out hot proximal tephras. However, some pyroclastic flows are relatively cool at deposition and do not preserve high-temperature textures, while some co-eruptive debris flows have also been known to contain hot pyroclasts (Mullineaux and Crandell, 1962). Similarly, it is not uncommon for debris flow deposits to contain charcoal (Crandell, 1971; Fisher and Schmincke, 1984); especially if the debris flows reworked deposits from earlier pyroclastic flows.

In light of the difficulties described above, distinguishing pyroclastic flow deposits from other volcaniclastic deposits usually relies on the judgement and experience of the observer; an essential component in any geological fieldwork, but not one that necessarily promotes consistency (e.g. Aspinall, 2006; Aspinall, 2010). Several authors (e.g. Fisher and Schmincke, 1984; Crandell, 1987) have produced tables of key deposit characteristics to highlight the similarities and differences between pyroclastic flows and other volcaniclastic deposits, and these are helpful for guiding field observations and making an informed interpretation. However these identification tables usually have considerable overlap across

	Lahars	Till (excluding water-laid till)	Unwelded ignimbrite	Fluvial deposits
Large fragments (>2mm)	May have boulders weighing many tons	May have boulders weighing many tons	Extremely large boulders absent	Extremely large boulders rare
Sorting	Poor. May contain abundant clay-size material	Poor. May contain abundant clay-size material	Poor. Clay-size material rare or absent	Poor to good. Clay-size material sparse
Grading	Commonly reverse. May be normal or absent	Commonly absent	Commonly absent, but may be normal or reverse	Commonly normal
Bedding and thickness	Commonly very thick with vague internal bedding	Very thick. Bedding poor or absent	Commonly very thick with vague internal layering	Thin with channels and cross beds. Shingled gravels
Composition	Commonly 100% volcanic. May be pyroclastic or mixed with epiclastic materials. May contain bread crust bombs	Commonly heterolithologic with admixtures from many sources. Plutonic, metamorphic and sedimentary clasts commonly more abundant than pyroclasts	Pyroclastic. May contain abundant bread crust bombs	Material usually 100% epiclastic except in areas of active volcanism
Rounding of large fragments	Commonly angular to subangular	Commonly faceted subangular to subrounded. May be faceted with striations and chatter marks	Commonly subangular	Commonly subrounded to rounded
Carbonaceou matter	Uncharred to charred	Uncharred	Charred	Uncharred if present
Pumice	Common in some lahars	Not present except on active volcanoes	Common	Not present except in areas of active volcanism
Distribution	In valleys spreading onto flat piedmont surfaces	Plains and valleys. May mantle all surfaces. Moraines with steep fronts	Lower parts of valleys and flat piedmont surfaces	Confined to valleys
Lower surfaces	Commonly not erosional	Erosional. Commonly rests on striated bedrock	Commonly not erosional	Erosional

Figure 3.1: Example of an identification table for distinguishing between different volcaniclastic deposits, after Fisher and Schmincke (1984). The red boxes highlight the similarities between the distinguishing criteria.

different volcaniclastic deposit types (Figure 3.1), making them difficult to use with confidence. This is especially the case for small and poorly exposed deposits that rarely contain unambiguous identifying textures. A further drawback of list-based criteria is they generally lead the user towards making a single interpretation that does not then acknowledge the underlying uncertainties and confidence in that decision. A consequence of these uncertainties is that many small and poorly exposed volcaniclastic deposits are likely to be overlooked in favour of more voluminous and better preserved deposits that can be more easily interpreted and are perceived to represent more significant events. However, when investigating the frequencies and characteristics of prehistoric volcanic hazards, it is crucial to identify as many deposits as possible irrespective of the deposits' size or preservation state.

3.5 Methods

In order to identify prehistoric pyroclastic flow deposits at Ruapehu, we developed a new confidence-based system for quickly and reliably assessing the likely origin of the different

volcaniclastic deposits observed. The key aim of this system is to distill the reasoning-based approaches of an experienced field geologist into a reliable and repeatable method for rapidly assessing candidate pyroclastic flow deposits in the field. The system has three objectives:

1. To identify commonly occurring deposit characteristics that support a pyroclastic flow origin.

2. To identify commonly occurring deposit characteristics that support a different (i.e. non-pyroclastic flow) volcaniclastic origin.

3. To use the information in (1) and (2) to assess the confidence by which a volcaniclastic deposit can be attributed to a pyroclastic flow, and compare that to the confidence by which the deposit can be attributed to a different volcaniclastic process.

A thorough literature review revealed characteristic outcrop-scale deposit textures for pyroclastic flows and most other proximal volcaniclastic deposits (Figure 3.2). Each characteristic was also assessed in terms of its likelihood of occurrence and, importantly, its ability to discriminate between the different deposit types. Since there are an almost unlimited number of possible deposit textures, we then focused *only* on those features that:

1. Commonly occur in deposits of any scale (i.e. textures that are most likely to be observed even in small and poorly preserved ancient deposits).

2. Are best able *as a standalone item* to identify specific volcaniclastic processes, and therefore are most useful for identifying or eliminating these processes.

3. Are best able *as a standalone item* to specifically identify pyroclastic flow deposits, and therefore increase confidence that a deposit was emplaced by a pyroclastic flow.

Observation Type	Criteria	PF	Surge	Debris Flow	Spatter Deposit	Moraine	Lava Breccia	Debris Avalanche	Rockfall and Small avalanches	Proximal Tephra	Tephra (less proximal)	Fluvial Deposits	Aeolian deposits	Unknown Regolith	Best for
Bedding	Thick bed (>1m)	Common; not essential	No	Common; not essential	Common; not essential	Common; not essential	Common; not essential	Common; not essential	Common; not essential	Common; not essential	Usually thinner	Not usually	Not usually	Common; not essential	Eliminating surge deposits
Bedding	Bed mantles undulating topography with even thickness (only use if sufficent outcrop to see this)	No	Yes	No	Yes, and can be present on steep slopes	No	No	No	No	Yes	Yes	No	Can do	No	**Identifying fall deposits**
Bedding	Stratified ash	No	Yes	No	No	No	No	No	No	Maybe	Can be ash or lapilli	Yes, can appear this way	Yes, can appear this way	No	Identifying surge and distal tephra
Bedding	Coherent patches maintaining some element of original stratigraphy	No	No	No	No	No	No	Mega blocks, hummocky topography, and jigsaw-fit components are characteristic	No	No	No	No	No	No	**Identifying debris avalanche deposits**
Clast Sizes	Poorly Sorted / Unsorted	Yes	Individual lamellae are generally mod/well sorted but the bulk deposit can be less well sorted	Yes. Can be coarser grained and more poorly sorted than pyroclastic flows	Somewhat poorly sorted in very proximal areas	Yes	Somewhat poorly sorted in very proximal areas	Yes	Yes	Somewhat poorly sorted in very proximal areas	No. Good sorting should be apparent	No. Typically well sorted	No. Typically well sorted	Yes	**Eliminating, surge, fall, fluvial and aeolian deposits**
Clast Sizes	Bomb-sized clasts	Typically abundant	Rare; mostly ash and/or lapilli	Common, can exceed 1m	Yes	Yes	Yes	Yes	Yes	Yes	No	No	No	Yes	Eliminating, surge, distal fall, fluvial and aeolian deposits
Clast Sizes	Fine-grained matrix	Yes, but absence of fines does not proclude PF origin if there has been subsequent winnowing	Somewhat; whole deposit is finer grained ash and lapilli	Yes. Significant clay-size fraction	No	Yes	Low proportion of clasts finer than 2mm. May have open framework	Yes	No	Clast supported with limited fines	Clast supported with very few fines	May contain abundant fine material	Whole deposit is likely to be very fine grained	Yes	**Eliminating spatter, lava breccia, rockfall, and tephra**
Compositions	Abundant clasts characteristic/suggestive of a single source	Yes, especially vesicular clasts & glassy materials but block & ash flows can contain dense lithics	Yes	Maybe, if co-eruptive or associated with a recent eruption. Otherwise typically heterolithologic	Yes, especially vesicular clasts with 'juvenile' textures	Maybe, if emplaced after an eruption or rockfall event.	Yes, monolithologic	Likely heterolithologic, clasts may show hydrothermal alteration	Sometimes (monolithologic, dense lithics, if from single source)	Yes, especially vesicular clasts with 'juvenile' textures	Yes, especially vesicular clasts with 'juvenile' textures	Maybe, if co-eruptive or associated with a recent eruption.	Maybe, if co-eruptive or associated with a recent eruption.	No	**Identifying co-eruptive deposits and deposits following major eruptions**
Compositions	Separate abundant crystal fraction	Yes, and crystal content can be higher in the matrix than in the pyroclasts	Yes, and crystal content can be higher in the matrix than in the pyroclasts	Unlikely	Unlikely	No	Unlikely	No	No	Unlikely	Unlikely	Possible if fractionated by water flow	No	No	Identifying pyroclastic density current deposits
Compositions	Accretionary lapilli	Can occur	Common in wet surges	Unlikely	No	No	No	No	No	Can occur	Can occur	No	No	No	Identifying co-eruptive deposits
Clast Textures	Most clasts have chilled margins	Yes	Maybe	Depends on source material	Maybe	Depends on source material	No	Depends on source material	No	Maybe	Maybe	Depends on source material	Likely to be too fine grained to observe	Depends on source material	**Eliminating lava breccias and rockfall**
Clast Textures	Striated clasts in the deposit	Rare	No	Can occur	No	Yes, but may not be abundant	No	No	No	No	No	No	No	No	Identifying moraines
Clast Shapes	Abrasively rounded fragments (noting that deposit is in proximal locations)	Some rounding during transport	Some rounding during transport	Some rounding during transport	No	Depends on source material	No	Depends on source material	No, generally angular	No	No	Some rounding during transport	Some rounding during transport	Depends on source material	**Eliminating rockfall**
Bedforms	Characteristic fluvial bedding (steep cross beds, ripples)	No	Similar but generally lower angle and longer wavelength	No	No	No	No	No	No	No	No	Yes	Cross beds at angle of repose	No	Identifying fluvial deposits
Bedforms	Characteristic surge bedding (dunes, antidunes, low angle cross beds, pinch and swell)	No	Yes	No	No	No	No	No	No	No	No	Can appear similar	No	No	**Identifying surge deposits**

Bedforms	Elutriation / openwork pipes (can be depleted in fines and enriched in crystal or lithic components)	Very characteristic of PF deposits	Maybe	Dewatering structures can appear similar	No	No	No	No	No	No	No	No	No	No	**Identifying pyroclastic flow deposits**
Bedforms	Evidence of lateral transport of large bomb-sized clasts (e.g. discontinuous lenses, imbrication)	Yes	No	Yes	No	No	Maybe	No, mostly moves as more coherent mass	Maybe	No	No	Unlikely to be as coarse	No	No	**Eliminates proximal tephras and spatter**
Grading	Normal coarse-tail grading of lithics and/or reverse coarse-tail grading of pumices	Common	Maybe	Maybe	No	No	No	No	No	No	No	No	No	No	**Identifying pyroclastic flow deposits**
Grading	Fine grained base	Maybe	Maybe	Common	No	No	No	No	No	No	No	No	No	No	Identifying debris flow deposits
Grading	Reverse graded near base, normal near top	Maybe	Maybe	Characteristic of debris flows not containing pumice	Only if changes in eruption intensity produced this	No	No	No	No	Only if changes in eruption intensity produced this	Only if changes in eruption intensity produced this	Only if changes in flow intensity produced this	No	No	Identifying non-pumiceous debris flow deposits
Thermal	Prismatically fractured clasts in-situ (ie clast is all together)	Yes	Not likely due to fine grain sizes	Possible in large clasts in co-eruptive debris flows	Yes	No	Yes	No, unless significant cryptodome material was involved in the debris avalanche	No	Maybe, for very proximal deposits	No	No	No	No	**Identifying clasts emplaced while hot**
Thermal	Presence of charcoal	Common; although many tall stratovolcanoes lack vegetation	Maybe	Wood is more likely to not be charred, unless next to a large clast, or if the debris flow reworked PF deposits	No	No	No	No	No	No	No	No	No	No	**Identifying pyroclastic flow deposits**
Thermal	Pinkish or reddish-gray alteration, particularly at the top of the deposit	Characteristic of PF deposits	Not likely due to fine grain sizes	No	Clasts can be oxidised red	No	Clasts can be oxidised red	No	No	Clasts can be oxidised red	No	No	No	No	**Identifying pyroclastic flow deposits**
Thermal	Aligned magnetic fabric of clasts determined by portable magnetometer	This is a strong indicator of PDCs. However not all PDCs will be emplaced above the curie point of their magnetic minerals.	Not likely due to fine grain sizes	Debris flows may carry hot clasts & produce similar results; but more usually have randomly aligned NRM, or lower proportion of clasts showing aligned NRM.	Yes	No	Yes	No, unless significant cryptodome material was involved in the debris avalanche	No	Maybe	No	No	No	No	**Identifying deposits emplaced hot**
Thermal	Welding	Characteristic feature if present, but many PFs are unwelded. Can be welded a long way from source	No	No	Yes, but should be relatively proximal to a possible vent	No	Yes	No	No	Maybe	No	No	No	No	**Identifying high temperature deposition**
Geometry	Channel or valley-filling geometry (if observable at this scale)	Yes, but may not be apparent in a single outcrop. Flat topped deposit ponds in valleys and may veneer ridge crests due to high mobility	Somewhat topographically constrained but less so than pyroclastic flows	Typical geometry, but may not be apparent in a single outcrop.	No	Likely to form ridgeforms but may not be observable at this scale	Maybe	Maybe	Maybe	No	No	Typically channellised	No	No	Identifying channelised volcaniclastic processes
Associations	Deposit Associations	Depost may not be located close to a plausible source for the main clast types	Depost may not be located close to a plausible source for the main clast types	Depost may not be located close to a plausible source for the main clast types	Located near a plausible vent source	Associated with glaciers	Associated with lava flow cores.	Depost may not be located close to a plausible source for the main clast types	Associated with cliff faces	Located near a plausible vent source	Associated with other distal tephras	Associated with other fluvial/lacustrine deposits	Not associated with fluvial/lacustrine deposits	No deposit associations to guide other interpretations	**Refining interpretations**

Figure 3.2: Key deposit characteristics resulting from most common volcaniclastic processes (synthesised from Aramaki and Akimoto, 1957; Parsons, 1969; Johnson, 1970; Crandell, 1971; Walker, 1971; Sparks and Walker, 1977; Hoblitt and Kellogg, 1979; Wilson, 1980; Fisher and Schmincke, 1984; Cas and Wright, 1987; Crandell, 1987; McPhie et al., 1993; Druitt, 1998; Freundt et al., 2000; Branney and Kokelaar, 2002; Brown and Andrews, 2015). The 16 deposit characteristics that are most useful for either identifying pyroclastic flows or eliminating other volcaniclastic processes are highlighted in the final row, and form the basis for the 12 criteria used in the confidence-based identification system.

The above process identified 12 criteria (condensed from the 16 criteria in Figure 3.2) that are especially useful for identifying pyroclastic flow deposits, and also for identifying or eliminating other volcaniclastic deposits. If each of these criteria were considered in turn using a traditional flow chart, this would produce $2^{12} = 4096$ different outcomes. This would be completely impractical as a field identification method. Therefore, the method outlined here does not attempt to combine different observations; but instead focuses on standalone criteria that by themselves give good indications of the possible deposit origins. The final 'score' takes into account *only* those textures that are observed in the deposit, and then provides the single *highest* confidence level achieved by any of the individual standalone criteria. The result is a field identification chart that uses 12 commonly occurring outcrop-scale textures to provide a consistent, rapid initial deposit assessment, while nonetheless avoiding a prohibitive number of permutations.

3.6 A new confidence-based method for assessing poorly exposed candidate pyroclastic flow deposits

The new confidence-based system for identifying proximal pyroclastic flow deposits is presented in Figure 3.3. The system is intended to provide a structured *initial* assessment of single outcrops of proximal volcaniclastic deposits of unknown origin, in order to determine whether the deposit characteristics are consistent with emplacement by a pyroclastic flow. As such, it is assumed the volcaniclastic deposit is located on the main slopes of a volcanic edifice, within the reasonable range of pyroclastic flows.

PYROCLASTIC FLOW IDENTIFICATION CHART:

This is intended for INITIAL assessments of single outcrops of unidentified volcaniclastic deposits located on the flanks of a volcano, in the absense of broader deposit geometry or deposit associations that enable identification. The interpretations may change if further outcrops or subsequent investigations provide better undersatnding of the overall deposit textures and geometry.

1 THE DEPOSIT CONTAINS >50% COMPOSITIONALLY & TEXTURALLY SIMILAR VOLCANIC CLASTS (e.g. 'Juvenile,' 'Primary')

NO → The deposit is **UNLIKELY** to have been emplaced by a pyroclastic flow (e.g. applies to 'Heterolithologic,' 'Non-juvenile' deposits etc.)

YES ↓

2 SELECT EITHER: (i.e choose only 1 of the 2 boxes)

3 WHICH OF THE FOLLOWING CRITERIA ARE OBSERVED IN THE DEPOSIT?

TICK **ONLY** THE ROWS THAT APPLY

	POORLY SORTED, and containing fine material												OR	MODERATELY / WELL SORTED										
	Dense PDC (Flow)	Dilute PDC (Surge)	Spatter	Proximal Fall	Fall	Lava Breccia	Debris Flow	Debris Avalanche	Rockfall/Avalanche	Moraine	Fluvial	Unknown Regolith		Dense PDC (Flow)	Dilute PDC (Surge)	Spatter	Proximal Fall	Fall	Lava Breccia	Debris Flow	Debris Avalanche	Rockfall/Avalanche	Moraine	Fluvial	Unknown Regolith
Bed mantles undulating topograpahy with even thickness (if observable)	1	2	2	2	2	5	1	5	1	5	1	5		5	3	3	3	4	5	1	5	1	5	2	5
Coherent patches (maintaining earlier stratigraphy) or megaclasts or hummocky topography	5	5	5	5	5	5	1	3	2	5	5	5		5	5	5	5	5	5	5	2	1	5	5	5
Significant ash-sized matrix between larger clasts	2	2	1	1	5	1	2	1	2	2	1	1		1	1	1	1	5	1	1	1	1	1	1	1
Most clasts have chilled margins around the entire clast	2	2	2	2	2	1	1	1	5	1	1	1		1	2	2	2	3	1	1	1	5	1	1	1
Lateral transport of bomb-sized clasts (abrasive rounding, discontinuous lenses)	2	2	1	1	5	1	2	1	2	1	1	5		2	2	1	1	5	1	2	1	1	1	1	5
Low angle and long wavelength bedding (cross-beds, dunes, pinch and swell bedding)	1	3	5	5	5	5	1	5	5	5	1	5		1	3	5	5	5	5	1	5	5	5	2	5
Elutriation structures (can be crystal and lithic rich and fines depleted) or presence of charcoal	3	3	5	5	5	5	2	1	5	5	1	5		2	3	5	5	5	5	2	1	5	5	2	5
Coarse-tail reverse grading for pumices (if present) +/- coarse-tail normal grading of lithics	3	3	2	2	1	5	2	5	5	5	1	5		3	3	2	2	3	5	2	5	5	5	1	5
High temperature emplacement (abundant prismatically jointed clasts, thermal alteration of deposit, aligned magnetic clast fabric in most interpreted primary clasts, welding)	4	2	4	3	5	4	1	1	5	5	5	5		3	3	3	3	5	3	1	1	5	5	5	5
Deposit not located near a plausible interpreted vent or lava flow source for any of the clast components interpreted to be primary	2	2	5	5	1	5	2	2	2	2	1	2		1	2	5	5	3	2	1	1	5	5	5	5

4 CONSIDERING **ONLY THE TICKED ROWS ABOVE**, FILL IN THE **HIGHEST** VALUE (1-5) IN EACH COLUMN →

5 THE SCORES GENERATED IN (4) SAY HOW CONFIDENTLY THE OBSERVED DEPOSIT FEATURES CAN BE EXPLAINED BY EACH OF THE DIFFERENT VOLCANICLASTIC PROCESSES IN THE COLUMN HEADINGS. IT IS **PERFECTLY ACCEPTABLE** FOR THE USER TO ADJUST THE REPORTED SCORES IN LIGHT OF OTHER TEXTURAL EVIDENCE, BUT THIS SHOULD BE NOTED.

5 = It is **UNLIKELY** that the process in the column heading produced the observed deposits
1 = The process explains the deposit features with **LOW CONFIDENCE**, and other processes may have produced similar deposits
2 = The process explains the deposit features with **MODERATE CONFIDENCE**, but other processes may have produced similar deposits
3 = The process explains the deposit features with **HIGH CONFIDENCE**, but other processes may have produced similar deposits
4 = The process explains the deposit features with **VERY HIGH CONFIDENCE**

Figure 3.3: The new confidence-based system for assessing candidate pyroclastic flow deposits.

The chart begins with straightforward physical volcanological observations that are observable in *any* deposit regardless of size or state of preservation. The first section (Figure 3.3, (1)) is deliberately non-specific, and asks the user to make a decision whether the deposits contain ">50% compositionally and texturally similar volcanic clasts." This broadly separates volcaniclastic deposits that were emplaced either during or soon after an eruption (i.e. most proximal volcanic hazards) from deposits that represent the normal longer-term erosional-depositional system. Section (1) makes no assertion as to the source eruption type, or whether the observed deposit represents co-eruptive emplacement or post-eruptive reworking of recently erupted material. Textural terms such as "juvenile" are deliberately avoided since different eruptive styles (e.g. phreatic vs magmatic, explosive vs effusive) can produce a wide range of fragmental clast types. However in general, high proportions of compositionally and texturally similar volcanic clasts, especially those with 'juvenile' textures (e.g. pumices, breadcrusted or cauliform surfaces, chilled margins), suggest that the clasts *might* be attributable to a single eruption (and hence *might* be from a PF). Such a general approach may seem unreasonable for a classification scheme; but the strength of the confidence-based system is that no matter which way the user interprets any of the criteria, this only affects the final confidence-level. Hence, if a user is *not* confident in the field that the clasts in a deposit are sufficiently similar to have originated from the same eruption, then there *cannot* be confidence that the deposit was emplaced by a pyroclastic flow.

The second section (Figure 3.3, (2)) considers the deposit sorting, with "*poor, including a fine fraction*" vs "*moderate/good*" broadly separating energetic mass-flow deposits from those that have been better sorted in an eruption column or by a fluvial system. In general, transient proximal volcanic hazards such as pyroclastic flows and debris flows produce poorly sorted deposits that contain fine material that has either been entrained or generated within the flow. Again, the confidence-based system does not exclude better sorted pyroclastic flow deposits (e.g. deposits where the fines have been subsequently winnowed away) - but the confidence in the interpretation is likely to be lower in these cases in the absence of context from other deposits.

The remainder of the classification system (Figure 3.3, (3) and (4)) sets about dis-

tinguishing which volcaniclastic processes *might* explain the observed deposits, and how confidently they do so. Section (3) lists 10 standalone deposit textures that either help to identify or eliminate different volcaniclastic processes, or help to increase confidence that the deposit specifically represents a pyroclastic flow. The deposit is therefore inspected for each of the 10 textures, and a tick is placed alongside any that are observed. Section (4) integrates these observations by then carrying forward only the *highest* scores from the ticked rows. This method works because each of the listed textures are treated as standalone items that do not depend on each other. Therefore if one of the observed textures gives "low" confidence that the deposit represents a pyroclastic flow, but another observed texture gives "high" confidence, then the final rating will be "high" confidence. The rating process is repeated for all of the different volcaniclastic processes listed in the column headings, resulting in a series of scores in section (4). These scores list how well the observed deposit features can be explained by each of the different volcaniclastic processes. Thus, the output does *not* say "this is a pyroclastic flow deposit." Rather, it lists all of the different volcaniclastic processes that *could* explain the observed textures, and assigns confidence levels to each of those interpretations. Stage (4) is the only complicated step in the classification, and as such a worked example is presented in Section 3.6.1.

The identification system presented here is intended as an *initial* guide for assessing difficult-to-interpret, poorly exposed deposits at a single outcrop using commonly observed field criteria; but by necessity it cannot cover every possible deposit feature. Thus it is **not** intended to replace or contradict any additional observations that assist the final interpretation. It is therefore perfectly acceptable (and encouraged) for the user to manually increase or decrease the final reported confidence ratings if additional observations, or observations from additional outcrops of the same unit, support this. For example, a pumiceous volcaniclastic deposit may return "high" confidence ratings for both pyroclastic flows and pyroclastic surge deposits on the basis of observed elutriation structures; however if the deposit is also several metres thick, it is reasonable to infer that it is unlikely to represent a pyroclastic surge and hence it is reasonable to reduce the confidence level for that interpretation. The most important point is that the identification system provides a strong *initial* assessment of possible source processes, and leads the user to both justify their final interpretation and quantify any uncertainty.

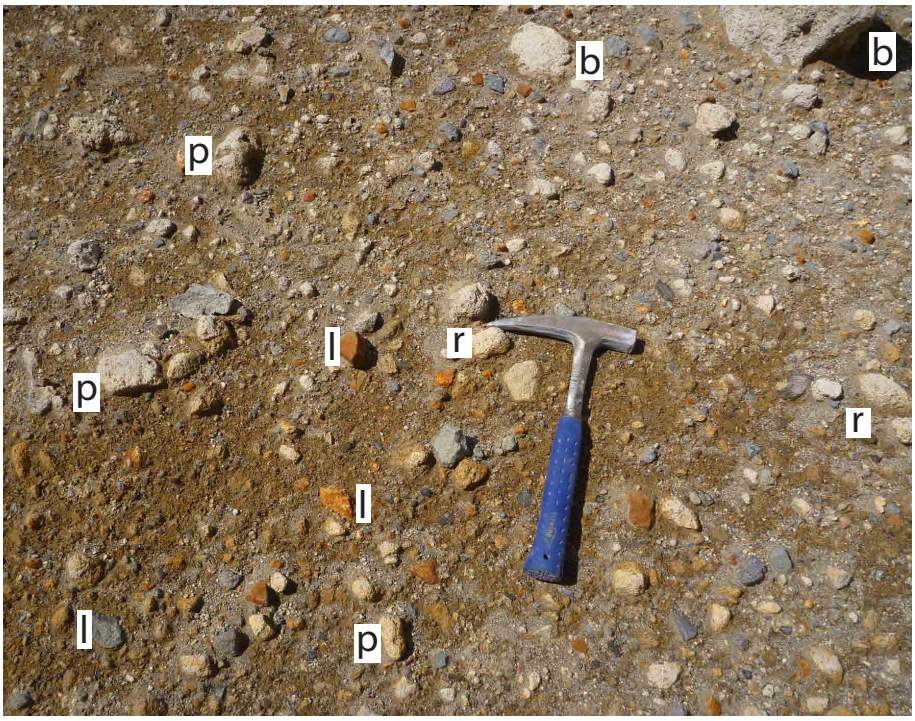

Figure 3.4: Example volcaniclastic deposit from Ruapehu volcano. This poorly sorted deposit contains abundant pumice (p) and lithic (l) clasts in a fine-grained matrix. Many of the pumices are bomb-sized (b) and show signs of abrasive rounding during transport (r).

3.6.1 Application of the method to an unidentified proximal volcaniclastic deposit at Ruapehu volcano

In the study area close to Tukino Ski Village on Ruapehu's eastern flank, almost every volcaniclastic surface or near-surface deposit consists of poorly sorted assemblages of volcanic material resulting from a range of volcanic mass-flow processes. The example deposit shown in Figure 3.4 was mapped by Chapman (1996) as a tephra covered moraine, because its large-scale geometry presents a broadly rounded ridgeform that in one location resembles a glacial close-out loop. However in a few locations, gulleys incised into the deposit reveal small patches of the in-situ deposit. These show that the ridge is composed of at least two different poorly sorted depositional units whose origin is difficult to determine. Thick scree cover means that nowhere are the full deposits exposed; however field observations of an in-situ exposure of the lowermost unit (Figure 3.4) reveal:

1. The deposit is located on Ruapehu's main edifice, but relatively far (~5km) from any reasonably inferred volcanic vents. It is up to 7m thick.

2. Lapilli and blocks/bombs in the deposit are approximately 50% pumice and 50% lithic clasts. The pumices are all texturally and compositionally similar and might have all been produced by a single eruption. At the top of the unit the proportion of pumiceous clasts increases to ~95% (hence the deposit overall contains >50% pumices) and the number of large bomb-sized pumices increases (i.e. reverse coarse-tail grading).

3. The deposit is poorly sorted, and contains both bomb and lapilli-sized clasts and a significant amount of ash matrix.

4. Many of the pumices appear to have been abrasively rounded, though no depositional bedforms are observed in the deposit.

5. Some of the larger pumices readily disintegrated with hints of prismatic jointing; though this is difficult to determine conclusively.

Given these observations, the initial field interpretation was that this represents a post-eruptive debris flow deposit that had reworked recently erupted pumices as well as significant amounts of lithic material. Had we left the interpretation here, this would have been a reasonable experience-based assessment. However, using the new confidence-based method presented here (Figure 3.5), the scores in section (4) of the chart suggest that the observed deposit features are explained by *both* pyroclastic flow and surge deposits with "high" confidence levels, debris flow deposits with "moderate" confidence, and fluvial deposits with "low" confidence. The scores also suggest that other volcaniclastic processes are unlikely to have produced the observed deposits. This therefore forms a starting point for the interpretation, and flags the idea that a pyroclastic flow origin is worth considering. Since the deposit is ~7m thick, it is reasonable at this stage to rule out a pyroclastic surge deposit despite there being no specific criteria for this in the chart. This is an important point; the method cannot include every possible observational criteria, so it is essential that the scores are treated as a starting point to the interpretation rather than an iron-clad assessment. Hence, after ruling out pyroclastic surges, the final deposit rating suggests the deposit is best explained by either a pyroclastic flow (high confidence) or a debris flow (moderate confidence).

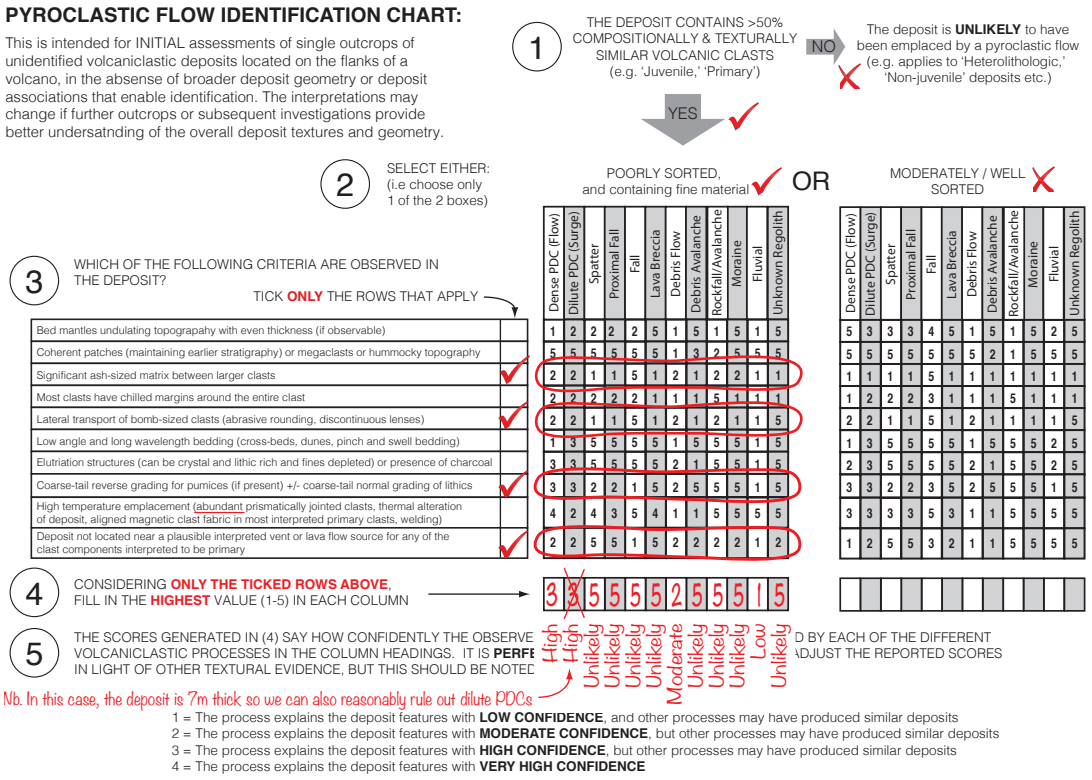

Figure 3.5: Worked example of the new confidence-based deposit assessment system, using the example deposit from Ruapehu volcano. The initial assessment (red) shows that the deposit textures are best attributed to a pyroclastic flow, at a 'high' confidence level. Subsequent investigations with a portable fluxgate magnetometer also showed that the deposit was emplaced hot: this introduces the ninth row in Section 3 of the chart, and hence increases the pyroclastic flow score to 4 (very high confidence).

The process outlined above suggests that attributing the deposit to a pyroclastic flow is a reasonable interpretation, provided that the possibility it could also represent a debris flow deposit is acknowledged. Given these results, we returned to the deposit with a portable fluxgate magnetometer to test for aligned magnetic fabric within the primary clasts. This showed that all of the measured pumices had consistent magnetic orientations*, suggesting the deposit was emplaced while the pumices were still hot. This additional information changes the deposit scores, now increasing the pyroclastic flow score to 4 (very high confidence) and keeping all other scores the same (Figure 3.5). Therefore, the new scores now show that the deposits are much better explained by a pyroclastic flow ("very high confidence") than they are by a debris flow ("moderate confidence"), while all other volcaniclastic processes are considered "unlikely" to have produced the observed deposits.

*12/12 pumices had consistent magnetic polarities in 5 of the 6 measured component directions for the magnetic field. The Ruapehu rocks are very weakly magnetic, and the discrepancies in the 6th component direction are interpreted to be due to the magnetic field being so weak in that direction that it was masked by the effects of irregular (i.e. non-equant) clast shapes and the stronger magnetic fields in the other component directions.

3.7 Discussion

The identification method presented here provides a rapid, repeatable field tool for assessing poorly exposed proximal volcaniclastic deposits using criteria that are easily observed at outcrops of any scale. This differs from previous attempts to discriminate between volcaniclastic deposits that typically only list key deposit characteristics. These list-based identification schemes can be misleading, and frequently present textures that either overlap with other volcaniclastic deposits, or may not commonly be observed in small or poorly exposed outcrops. They also tend to present a picture of an 'ideal' deposit, without acknowledging the significant variability of natural systems. For example, most table-based checklists state that pyroclastic flow deposits are poorly sorted, and therefore are likely to guide against a pyroclastic flow interpretation for better sorted deposits. However, if the other deposit textures (e.g. evidence of high temperature emplacement) suggest that a pyroclastic flow origin is *more* likely that the alternatives, then eliminating a pyroclastic

flow origin on the basis of better sorting would be unreasonable. The system developed here addresses these problems by explicitly acknowledging the uncertainties associated with deposit interpretations, and instead assesses the confidence by which the observed textures can be explained by a particular volcaniclastic process. Using the example of a well-sorted pyroclastic flow deposit, the confidence-based system presented here would not rule out a pyroclastic flow origin, but instead may reduce the stated confidence in that interpretation. In this way, the interpretation can be fully justified in terms of the 'most likely' process that formed the deposit, while nonetheless acknowledging that other processes can also produce similar textures.

The identification system presented here is specifically designed to identify candidate pyroclastic flow deposits in the field, so the chart particularly focuses on PF deposit characteristics. However, a key part of the process involves identifying or ruling out other volcaniclastic deposits, and as such important textures relating to those deposits are also assessed. By deliberately targeting textures that are both common and most useful for identifying or eliminating specific processes, the chart provides a focused structure for rapid and consistent field assessments of most co- and post-eruptive volcaniclastic deposits (i.e. those containing *>50% compositionally and texturally similar volcanic clasts*). This is especially useful as an in-field teaching tool, as it emphasises the importance of identifying the deposit features that are *most* important to the final interpretation. At the same time, the method stresses the need to acknowledge uncertainty in initial deposit assessments, particularly when the observed textures can be attributed to several different volcaniclastic processes.

The strength of the method presented here is that it can be easily and *consistently* applied to any proximal volcaniclastic deposit at any scale. This is advantageous, as it encourages assessment of even poorly-exposed deposits that may otherwise be overlooked. Since many unconsolidated proximal volcaniclastic deposits are emplaced in active drainages and have low preservation potential, small exposures may be all that remain of a nonetheless significant event. This is evidenced by the example deposits described close to Tukino, which had previously been mapped as a tephra-covered moraine. Although the deposit itself is relatively large, it is mostly scree-covered and in-situ exposures are only present

at a few poorly-exposed locations. Despite initially thinking the pumice and lithic-rich deposit probably represented a post-eruptive debris flow, the confidence-based method here flagged the possibility that it may represent a pyroclastic flow. Further investigation using a portable fluxgate magnetometer then confirmed this to be the most likely interpretation. Subsequent investigations, presented in Chapter 4, have now shown that this previously-misinterpreted deposit in fact relates to Ruapehu's largest known plinian eruptions; and is one of the most significant pyroclastic flows known to have occurred at this volcano. This highlights the main value of the identification system in providing rapid and consistent *initial* assessments that then highlight which deposits are worth investigating in more detail.

3.7.1 Limitations of the Method

The new identification system considers multiple observational criteria to assess the confidence that a particular process produced the observed deposit textures, and hence approximates the approach of an experienced field volcanologist. However, this system cannot include every possible textural criteria, and so instead focuses on observations that are either readily observable or are particularly helpful for distinguishing between the different volcaniclastic processes. The system cannot cumulatively integrate all of the different criteria (e.g. in a flow chart) as this would return far too many permutations to be of practical field use. Therefore, the system compromises by giving priority to the observed textures that best support or exclude a particular interpretation (i.e. the highest score in section 3 of the chart). In real terms, this is a reasonable compromise since the strongest observational criteria supporting or excluding a particular interpretation is likely to be the most defining observation. However, an experienced field investigator is able to integrate multiple lines of evidence in a way that is not possible here. Therefore, the chart is not intended to replace field experience or to overlook other textural features that may change the interpretation. Instead, it is seen as an effective *initial* system for rapidly and consistently assessing volcaniclastic deposits, such that it can then highlight those deposits that most warrant further study. Future digital iterations of the system, perhaps as a smartphone or tablet application, may be able to overcome some of these limitations by allowing more textural features (and hence more permutations) to be considered before

determining the deposit confidence ratings.

3.8 Conclusions

Here we present a new confidence-based method for rapidly assessing poorly exposed volcaniclastic deposits in the field, with particular emphasis on identifying candidate pyroclastic flow deposits. The system addresses the difficulties in distinguishing between different proximal volcaniclastic deposits, and overcomes some of the limitations of previous systems by assigning confidence levels to the different interpretations. This provides a method for consistent, rapid field assessments of small and poorly exposed deposits that can therefore highlight targets for further investigation. The system may be useful as a teaching tool that emphasises the importance of acknowledging uncertainty, and may also be useful for encouraging interpretation of poorly preserved ancient deposits that nonetheless may represent significant volcanic events. Recognition of prehistoric pyroclastic flow deposits is crucial for quantifying the frequency and magnitudes of the hazard, and rapid confidence-based deposit assesments such as this could therefore provide a valuable input for future probabilistic hazard assessments (e.g. Marzocchi et al., 2004) at high-risk volcanoes like Ruapehu.

4

Proximal pyroclastic density currents at a glaciated volcano; Mount Ruapehu, New Zealand

Introduction to Chapter 4

This chapter presents detailed field observations of 12 small-volume PDC deposits preserved in eastern-Ruapehu, identified using the confidence-based system presented in Chapter 3. We focus on field-based observations of deposit distributions and textures to investigate the types of eruption that have previously generated PDCs at Ruapehu, as well as the factors that affected PDC transport and deposit preservation. These results therefore provide insight into Ruapehu's possible future PDC hazard.

The key outcomes are:

1. Identification of at least 12 young (<13.6 ka) proximal PDC deposits that are preserved close to the Tukino ski area on Ruapehu's easten flank. These include a) pumice-dominated deposits from some of Ruapehu's largest plinian eruptions (Units 1-4), b) scoria-dominated welded deposits (Units 6 & 7) that are interpreted to have resulted from periodic collapse of accumulating spatter/cinders on steep topographic slopes, and c) small-volume deposits (Units 8-10) generated by smaller eruptions of more degassed magma from the historically active South Crater area. Most of these deposits have never previously been described.

2. Observation that deposit distributions, textures, and interpreted ages compared with Ruapehu's glacial record all suggest that many of Ruapehu's PDCs encountered glacial ice during transport. This is interpreted to have affected the preservation and extents of the PDC deposits, and may also have significantly affected the PDC transport dynamics. This concept is investigated in detail in Chapter 6.

3. Recognition that hazardous PDCs have been generated by most of Ruapehu's known eruption magnitudes and styles, including smaller eruptions similar in magnitude to Ruapehu's historical activity (Units 8-12). PDCs would therefore not be unexpected from future eruptions similar to Ruapehu's 1945 or 1995/6 activity, and would represent a significant threat to life and proximal infrastructure.

The chapter is presented in the style of an academic paper, though with expanded detail that will be condensed for submission to a peer-reviewed journal. As such, the relevant

contextual background and analysis methods are presented in full. Due to the large number of PDC units identified, the results for each of the main PDC facies are each immediately followed by their respective interpretations; while the discussion section is reserved for the wider whole-mountain implications.

Abstract

Pyroclastic density currents (PDCs) are a destructive volcanic hazard. Quantifying the types, frequency and magnitudes of PDC events in the geological record is essential for effective risk management. However small-medium volume valley-confined PDC deposits have limited preservation potential, especially when emplaced in active drainages or onto snow or ice. Where PDC deposits are preserved they can be difficult to distinguish from other volcaniclastic deposits and are frequently misinterpreted or overlooked. This is the case at Mt. Ruapehu; a much visited, high-risk active volcano in New Zealand with few significant historical PDCs. Through systematic field observations we identify 12 young proximal andesitic PDC units exposed on Ruapehu's eastern flanks. The oldest deposits (Units 1-5), are massive pumice-rich deposits, and include deposits from Ruapehu's largest plinian eruptions (Units 1-3; Ohinewairua PDCs, <13.6 ka) that are preserved up to 7 km from source (North Crater area). Stratigraphically younger, the pumice-rich Pourahu PDC deposit (Unit 4) reaches more than 14 km from source (South Crater area) and correlates with Ruapehu's last known plinian eruption (~11.6 ka). Two unusual variably welded, layered deposits containing clasts of welded spatter (Units 6 and 7) are interpreted to represent multiple failures of accumulating near-vent (North Ruapehu) spatter/cinders, and are the youngest known PDCs from the North Crater area (Unit 6 ~11.6 ka). Here, PDC initiation was controlled by high vent-proximal deposition rates and oversteepening of the spatter/cinders deposit on steep topographic slopes. PDC Unit 6 is chemically similar to the plinian-sourced Pourahu PDC, yet represents a different style of eruption that may reflect more open-system conditions in Northern Ruapehu. Finally, Units 8-12 are locally preserved PDC deposits with denser primary clasts that represent PDCs from smaller eruptions. These include at least three young (<11.6 ka.) deposits (Units 8-10) exposed next to the Tukino ski village from eruptions near South Crater that are not dissimilar to Ruapehu's modern activity. The patchy distribution and small volumes of the Ruapehu deposits highlight the limited preservation of PDC deposits on steep volcanic flanks. Additionally, deposit ages, textures, distributions, and associations with moraines indicate that many of Ruapehu's PDCs encountered glacial ice during transport. This affected their distribution, mobility, and preservation; and has implications for assessing the PDC hazard at Ruapehu and other glaciated volcanoes.

4.1 Introduction

Pyroclastic density currents (PDCs) are destructive mass flows of pyroclastic materials and gas (Yamamoto et al., 2005) that have killed almost 60,000 people since 1783 (Tanguy et al., 1998). Small-volume ($<10^7 m^3$, Stinton and Sheridan, 2008) granular fluid-based PDCs ('pyroclastic flows') are a frequent occurrence at many composite volcanoes, and present a significant threat to life and infrastructure (e.g. Merapi 2010; Jenkins et al., 2013). They can be triggered by any process that results in gravitational collapse of hot volcanic material, including collapsing eruption columns (Nairn and Self, 1978; Rosi et al., 2001), collapsing lava domes and flows (Boudon et al., 1993; Calder et al., 1999; Saucedo et al., 2004; Behncke et al., 2008; Belousov et al., 2011), and co-eruptive remobilisation of erupted material deposited on steep slopes (Yamamoto et al., 2005). At volcanoes where granular fluid-based PDCs have not been historically observed, prehistoric deposits are the only evidence of their occurrence. However poor preservation on steep, glacially modified proximal slopes, together with challenges in identifying small-volume deposits, means that small-volume prehistoric PDC deposits are often overlooked. This is the case at Ruapehu volcano in the North Island of New Zealand, where an absence of historically observed granular fluid-based PDCs means they have been underestimated as a significant hazard.

4.2 Geological setting

Mount Ruapehu is the largest and most active andesitic-dacitic volcano in the North Island of New Zealand. The ~150 km^3 cone is located at the southern end of the Taupo Volcanic Zone (Cole and Nairn, 1975; Hackett and Houghton, 1989; Conway et al., 2015) and is surrounded by an equally voluminous ring plain composed mostly of laharic, fluvial and distal plinian and subplinian tephras (Palmer et al., 1993; Cronin et al., 1996b; Lecointre et al., 1998; Donoghue and Neall, 2001). The edifice was constructed over the past ~250 ka by episodes of voluminous lava extrusion from multiple vents, (Hackett, 1985; Graham and Hackett, 1987; Waight et al., 1999; Gamble et al., 2003), often in the presence of glacial ice which has exerted a major control on edifice morphology and deposit preservation (Conway et al., 2015). Historical activity has consisted of frequent small phreatic and phreatomagmatic eruptions from Crater Lake in the South Crater Area (Figure 2.4; Healy

et al., 1978; Nairn et al., 1979; Kilgour et al., 2010), with larger subplinian, vulcanian and strombolian eruptions in 1945 (Oliver, 1945; Reed, 1945; Beck, 1950; Johnston and Neall, 1995) and 1995-96 (Bryan et al., 1996; Nakagawa et al., 1999; Johnston et al., 2000).

Pyroclastic density currents at Ruapehu

For an active volcano with a rich pyroclastic explosive record, comparatively few prehistoric PDC deposits have been observed at Ruapehu. Hackett (1985) briefly described two small <15 ka deposits in eastern and south-eastern Ruapehu, and Donoghue et al. (1995a) found plinian-sourced deposits from the ~11.6 ka Pourahu pyroclastic flow exposed on Ruapehu's eastern ring plain. Pardo et al. (2011) interpreted several thin (cm-scale) matrix supported deposits interbedded with plinian tephras of the ~27-10 ka B.P. cal Bullot formation as PDCs, and Pardo et al. (2014) studied the conditions leading to increasingly common column collapse in the period ~13.6-10 ka on the basis of disequilibrium bubble textures in the plinian fall deposits. However, these studies did not observe any proximal evidence of massive deposits associated with these PDCs.

In historical times small fully dilute PDCs ('pyroclastic surges') have frequently occurred at Ruapehu during phreatic and phreatomagmatic eruptions through the crater lake, reaching up to ~3km from vent (Houghton et al., 1987; Kilgour et al., 2010). Hazardous longer-runout granular fluid-based PDCs ('pyroclastic flows') have not been historically observed, though recently re-discovered images from Ruapehu's 1945 eruption suggest one such PDC may have been emplaced in eastern Ruapehu but was not reported (Figure 4.1a).

The frequency, types, magnitudes and locations of previous PDCs reflect their characteristic nature at a given volcano. At volcanoes like Ruapehu with no historically documented granular fluid-based PDCs, recognising small-volume prehistoric deposits is essential for properly assessing the likely future hazard. The PDC deposits may also be the only evidence of eruptions whose deposits are not preserved in the tephra-fall record. Here, we investigate the proximal record of PDCs at Ruapehu, and describe 12 young deposits exposed near the Tukino ski village on Ruapehu's north-eastern flank.

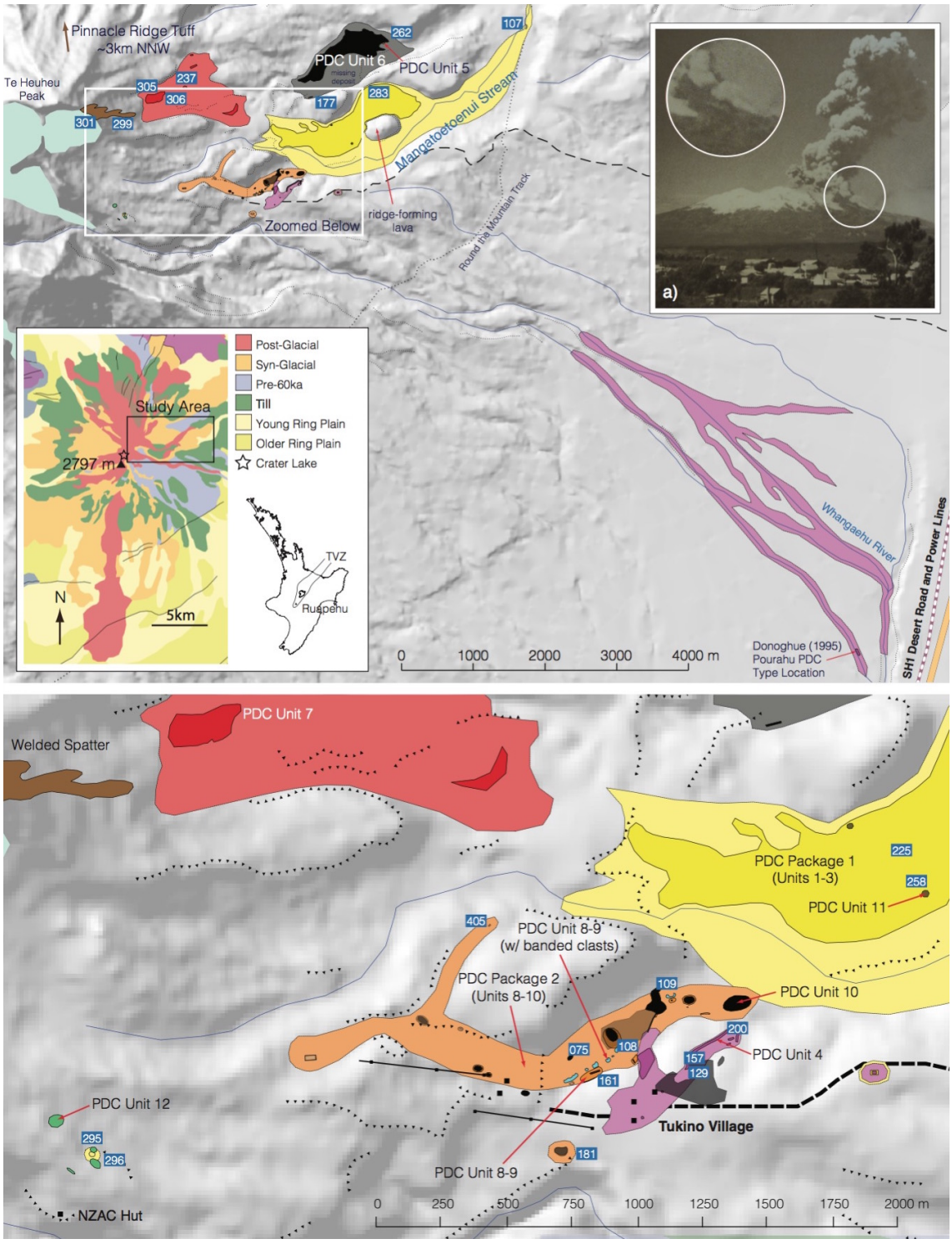

Figure 4.1: Location of the PDC deposits near to Tukino Ski Area, eastern Ruapehu. PDC units and GPS waypoints (blue) are labelled. Darker shading shows the observed deposits, lighter shading indicates interpreted depositional areas. For PDC Package 2 (Units 8-10) only the interpreted distribution of Units 8-9 (orange) is shown as Unit 10 (black) overlaps this. Unit 4's (Pourahu PDC) interpreted deposition is only schematic due to very limited preservation (e.g. Donoghue et al., 1995a, 1999). The overview map is a major update to Ruapehu's geological map due for full publication in 2016 (GNS Science and Conway et al., 2015). Inset a) shows a newly re-discovered photograph of Ruapehu's 1945 eruption showing an unreported PDC in eastern Ruapehu, with equivalent runout to the deposits reported here (N. Mosen, Lansdown Collection; In Johnston and Neall, 1995).

4.3 Methods

Field identification of the PDC deposits

Small-volume granular fluid-based PDC deposits are typically poorly sorted accumulations of erupted pyroclasts, ash and entrained lithic clasts whose distribution usually reflects channelised transport (Brown and Andrews, 2015). In proximal locations where all source material is volcanic, distinguishing PDC deposits from other volcaniclastic units is challenging (Fisher and Schmincke, 1984), but careful observation of deposit textures allowed candidate PDC deposits to be identified using the confidence-based methodology detailed in Chapter 3.

Where possible, support for the textural interpretations of PDC units was obtained in the field by measuring the natural remnant magnetisation (NRM) of in-situ pyroclasts within the deposits (Hoblitt and Kellogg, 1979). Magnetic fabric is imparted to individual pyroclasts as magnetic minerals cool through their Curie temperatures (~350-580°C for the titanomagnetite in Ruapehu rocks; McClelland and Erwin, 2003). Therefore, if a deposit was emplaced at high temperatures most clasts should have developed uniform magnetic orientations as the deposit cooled. For the suspected Ruapehu PDC deposits, the NRM of at least 10 primary bomb-sized clasts was measured in six component directions using an FG Instruments BR-2 portable fluxgate magnetometer (Platz et al., 2012). Uniform magnetic orientations in 7/10 clasts was considered strong evidence of hot emplacement. However, Ruapehu's pyroclasts are so weakly magnetic that it was often difficult to obtain a sufficiently strong signal in all 6 field directions, and variations in clast shape made readings difficult in the weakest field directions. Therefore, it was frequently found that field directions would match in 5 of the 6 component directions, but that in the very weakest field direction it was difficult to get consistent results even at the highest detector sensitivity. This observation is supported by measurements of PDC Unit 6 (Section 4.4.4), which is known to have been emplaced hot due to welding textures within the deposit. Here, 2 of the 11 measured clasts still had indeterminate readings in one direction. Therefore, some discretion is needed in interpreting the results, and this is detailed in Table 4.1.

Field descriptions of the identified PDC deposits were designed to facilitate comparison

between field sites and subsequent laboratory analyses. At measured sections the maximum pumice, maximum lithic, estimated average clast size, and estimated pumice:lithic ratios were all recorded vertically throughout the section to document any vertical changes. In order to allow direct comparison with laboratory sieving data clasts were measured along their intermediate axes, and follow the terminology of White and Houghton (2006). Here, we use the term *matrix* to refer to the dominant ash-sized particle fraction (<2mm; finer than -1Φ), but note that in truly poorly sorted PDC deposits there is a continuous range of particle sizes rather than a bimodal *clasts-in-matrix* size distribution. Additional in-field estimates of the % of material finer than 1cm (medium-coarse lapilli) were recorded throughout all sections to provide a rapid field assessment of the changing amounts of fine material in the deposits. The 1cm threshold was chosen for practical reasons, since this was the smallest particle size easily discerned by in-field visual estimates.

Deposit Dating

Determining the age of proximal PDC deposits is difficult in alpine environments due to a lack of vegetation, and hence absence of charcoal within the units for radiometric dating (e.g. Crandell, 1987). Where the deposits correlate with or are bounded by tephra fall deposits of a known age, then a relative stratigraphic position can be estimated. However, high rates of physical erosion and glaciation removes many of these deposits in proximal locations, and for PDCs from smaller eruptions there is often no correlatable tephra preserved. Here, PDC deposit ages are estimated by their relative stratigraphic positions and textural/chemical correlations with plinian fall deposits on Ruapehu's ring plain (Pardo et al., 2011). However, for the youngest units the absence of dated cover beds means only a maximum age estimate of ~11.6 ka B.P. cal is available.

Runout distance and volume estimates

Ruapehu's proximal PDC deposits are often poorly preserved and exposed at only a few outcrops, so estimating primary PDC deposit volumes is impossible with accuracy. Uncertainty in the original deposit distribution can be further exacerbated by deposition over glacial ice (Chapter 6), where volumetrically significant deposits may then never be

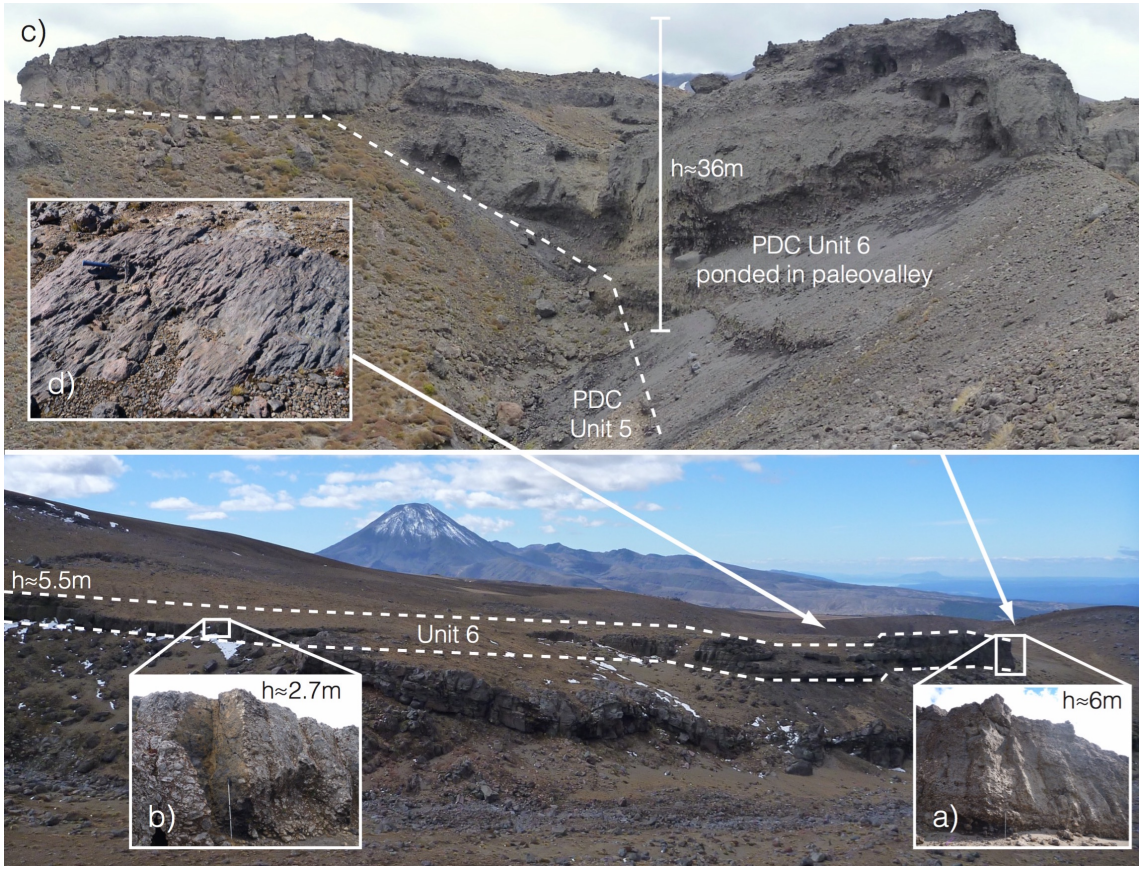

Figure 4.2: Considerations involved in estimating PDC unit thicknesses for volume calculations; a) Most of the PDC Unit 6 deposit appears to originally have been ~5.5-6m thick. However, b) many outcrops no longer preserve the full unit thickness, while c) at WP262 the PDC has ponded in a palaeovalley and the deposit reaches ~36m thick. Finally, d) glacial striations on the deposit's upper surface suggest a portion of the original deposit was removed by subsequent glacial erosion. Accurately determining the average unit thickness is therefore difficult; here, a judgement-based value of 6.5m is estimated, providing a conservative correction above the observed 5.5-6m unit thickness to allow for the effects of localised ponding in palaeovalleys and removal of the deposit's upper surface by later erosion.

preserved. Figure 4.1 shows the mapped extents of the modern-day PDC deposits, as well as conservative interpretations of the original depositional areas that are used here for the minimum volume estimates (Table 4.3). Average unit thicknesses were estimated from measured sections, field observations and field photographs in reflection of the patchy preservation and valley vs ridge deposition patterns (Figure 4.2)

Granulometry

At PDC type sections, between 35-105 kg of PDC material (average ~50 kg, comparable to Lube et al., 2007) was carefully excavated and hand-sieved at -7, -6, -5 and -3.5 ϕ size fractions. Samples larger than -7 ϕ were weighed and measured along their intermediate

axes for allocation to an appropriate sieve size fraction. In rare instances where the largest clasts could not be removed, or where they disintegrated upon removal, a nearby clast of equivalent size and density from the same unit was selected as a suitable proxy for measurement. Each sieved size fraction was weighed at field moisture contents using a portable field scale, then subsamples of material smaller than -5 ϕ were taken by pouring from height into a cone and dividing. The subsamples were dried overnight at 65°C and sieved at 1 ϕ intervals down to +5 ϕ. The ~50 kg sample size was limited by field constraints, but is sufficient to adequately represent the finer than -5 ϕ fraction that is usually reported for pyroclastic deposits (e.g. Walker, 1971, 1983). The grain size distribution of the larger components is rarely reported (due to the much greater volumes of sieved material required), but is included here for indicative purposes. In order to combine the field (larger than -5 ϕ, damp clasts) and laboratory (smaller than -5 ϕ, dry) datasets, the field data was recalculated to dry equivalent weights based on the percentage weight loss of the -5 to -3.5 ϕ samples following drying in the laboratory. Corrections were also applied to account for finer material adhered to the surface of the damp clasts in the field, again based on the amount of fines liberated from the -5 to -3.5 ϕ samples following drying (Appendix 3.2). This methodology allows a closer estimation of the total grain size distribution by permitting semi-quantitative integration of both the field and laboratory data across the full range of grain sizes.

For each unit, samples from the sieved -5ϕ to -4ϕ fraction were also classified in terms of clast type. In many of the PDCs, several classes of juvenile clasts were observed, including:

1. Juvenile clasts of the dominant magma type. Hereafter, these clasts are referred to as the "primary clasts."

2. Juvenile clasts of a secondary magmatic component (if present); these represent fresh, vesicular clasts that appear in hand sample to be entirely composed of a secondary magmatic component. These clasts are hereafter referred to as "secondary clasts."

3. Colour banded juvenile clasts; these reflect either pre-eruptive mingling of two different magma types, or mingling of different textural domains within the same magma (Chapter 5). These are hereafter referred to as "banded clasts," and may contain both "primary" and "secondary" magmatic components.

Geochemistry

Geochemical analyses were conducted at the University of Canterbury Geological Sciences Department using a Phillips PW2400 Sequential Wavelength Dispersive X-Ray Fluorescence Spectrometer calibrated against certified international standards, and based on methods by Norrish and Chappell (1967) and Norrish and Hutton (1969). Samples were cut and ground to remove surface weathering, rinsed in deionised water and dried overnight at 65°C. The samples were crushed in clean conditions before grinding to a fine powder. Whole rock major elements were analysed using fusion beads and a rhodium tube set at 50KV/55mA, with loss on ignition calculated after fusion. Selected results from primary pyroclasts in the PDC deposits are presented in Table 4.2 and Figure 4.6.

4.4 Results

Three main proximal PDC deposit facies outcrop close to the Tukino ski village on the eastern flank of Ruapehu (Fig 4.3), including at least 12 separate units emplaced during the past 13.6 ka B.P cal. These are:

1. Pumice-dominated PDC deposits mostly erupted from northern Ruapehu (Figure 4.3 a-b).

2. Scoria-dominated variably welded PDC deposits containing rounded clasts erupted from northern Ruapehu (Figure 4.3 c-d).

3. Heterogeneous small-volume PDC deposits containing denser juvenile clasts and lithics associated with eruptions near the presently active South Crater (Figure 4.3 e-f).

A summary stratigraphic log of all of the PDC deposits is presented in Chapter 5 (Figure 5.4).

For this study, the PDC deposits are primarily classified into PDC *units* and *packages*. Each unit reflects a distinct, stratigraphically identifiable depositional layer with clear textural or compositional boundaries separating the top and bottom of the unit and is interpreted to be the product at least one distinct PDC. However, in some cases a unit may

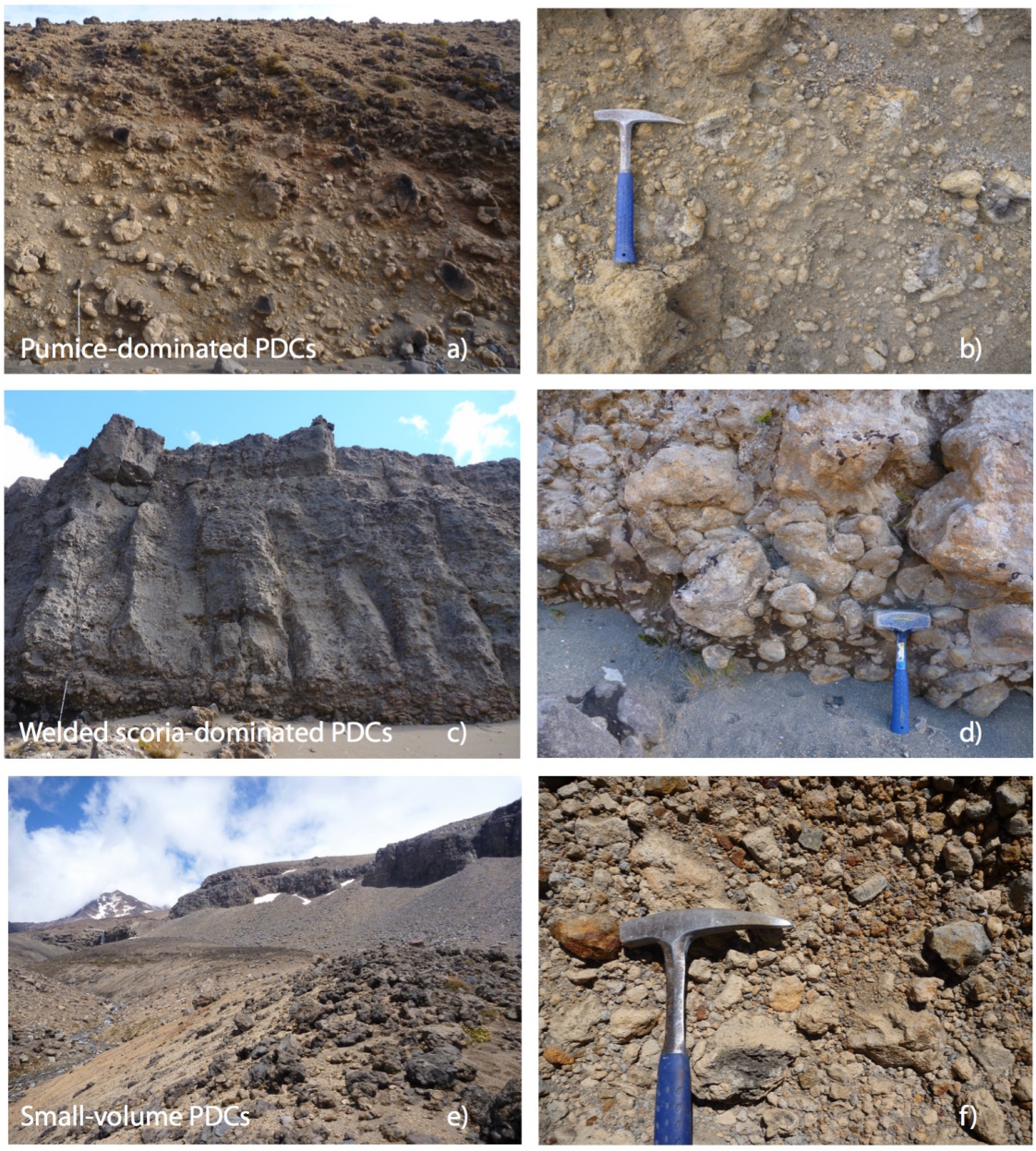

Figure 4.3: PDC deposit facies observed in eastern Ruapehu. a-b) Pumice-dominated PDCs; c-d) Scoria-dominated variably welded, bedded, monolithologic PDCs containing unusually rounded clasts; e-f) Heterogeneous small-volume deposits containing denser juvenile clasts, cauliflower-textured bombs, and lithics. Pole in a) and c) is 1m long, and the entire sequence of deposits in e) is ~9m thick.

represent the combined deposits from several flows whose depositional boundaries cannot be readily distinguished. In some locations, multiple PDC units sharing similar textural features have combined to produce larger pyroclastic "packages." Here, limited exposures make correlation of individual units difficult between outcrops, but comparisons with other volcanoes shows that PDC packages are commonly built up from multiple small-volume PDCs (e.g. Merapi 2010, Charbonnier et al., 2013; Cronin et al., 2013). Therefore for each PDC package we present field observations from representative stratigraphic sections, but recognise that the number of PDC units described may under-represent the total number of PDCs contributing to the overall package.

4.4.1 Pumice-dominated PDC deposits

These PDC deposits are characterised by poorly sorted, unconsolidated accumulations of highly vesicular yellowish pumice lapilli and bombs in a fine-to-medium ash matrix (Figure 4.3 a & b).

1. PDC Package 1 (containing PDC Units 1, 2 and 3)

PDC Package 1 is mostly exposed as a 2km long, up to 25m thick flat-topped sequence of pumiceous PDC deposits lining the northern lateral margin of the Mangatoetoenui valley ~1km NE of Tukino Village. Here, the Mangatoetoenui valley divides into two branches around a thick glacially-emplaced ridge-forming lava flow (Lescinsky and Sisson, 1998; Conway et al., 2015). The preserved pyroclastic package completely fills the northern valley branch, terminating at a ~25m high face where it rejoins the main valley downstream of the ridge-forming lava. Only one small deposit remains in the active southern valley branch that hosts the modern river (PDC Unit 3, WP107; Figure 4.1). These PDC deposits were earlier mapped by Chapman (1996) as tephra covered moraines, but were not investigated further.

Field Characteristics

The unconsolidated deposits are poorly exposed along minor channels and gulleys incised into the main deposit, and consist of multiple localised sequences of poorly sorted deposits that combine to form a flat-topped, valley-filling package. Correlation between outcrops

is difficult due to local variability, poor exposures and diffuse unit boundaries, but at the type section at WP225 (Figure 4.1) at least two pumiceous PDC deposits (Units 1 and 2) are clearly separated by laminated pinkish-white fine ash beds containing accretionary lapilli (Figure 4.4). Field magnetic investigations using a portable fluxgate magnetometer show that both units were emplaced hot, with most bomb-sized clasts showing aligned NRM (Table 4.1).

PDC Unit	**Aligned NRM**	**Notes**
PDC Unit 1	12/12	The clasts consistently disagree in one magnetic component direction (W), where they are split 7 and 5 for - and + components respectively.
PDC Unit 6	11/11	One of the clasts had an indeterminate reading in one magnetic component direction (E) and one differed in one magnetic component direction (E).
PDC Unit 8a	8/11	
PDC Unit 8b	8/11	2 of the 8 clasts with aligned NRM had an indeterminate reading in one magnetic component direction each (E and Up)

*Clast magnetic polarities (+/-) were measured in 6 component directions (N, E, S, W, Up, Down, with N nominally pependicular to the outcrop) in order to resolve the overall magnetic orientation. Due to the weak magnetism of the Ruapehu rocks and lack of equant clasts, some discretion is used where resolved fields differ only in a single component direction. This is supported by the results for Unit 6 (2 indeterminate readings), which is *known* to have been emplaced hot due to the deposit welding.

Table 4.1: Portable fluxgate magnetometer results for the Ruapehu PDC deposits.

The oldest Unit (Unit 1) has a distinctive lithic-rich base that is is at least ~10m thick at the type section (the log starts 3m above the base of the gulley due to poor exposure) and contains up to 50% orange-white weathered and hydrothermally altered lithic clasts (Figure 4.5). When observed at other locations, this lithic-rich unit is always exposed near the base of the PDC package. Reverse coarse-tail grading of pumices is also observed in Unit 1, with large pumices up to 1m only present at the unit top (Figure 4.4). However, the pumices in both Unit 1 and Unit 2 are texturally similar, and in the absence of clearly exposed unit breaks it is almost impossible in the field to separate the top of Unit 1 from the base of Unit 2. Although the type section provides the best exposure of the different PDC units, multiple fine-then-coarse pumiceous layers at other locations (e.g. WP283, Figure 4.1) suggest that the upper parts of PDC Package 1 is composed of numerous flow units that cannot easily be correlated between outcrops.

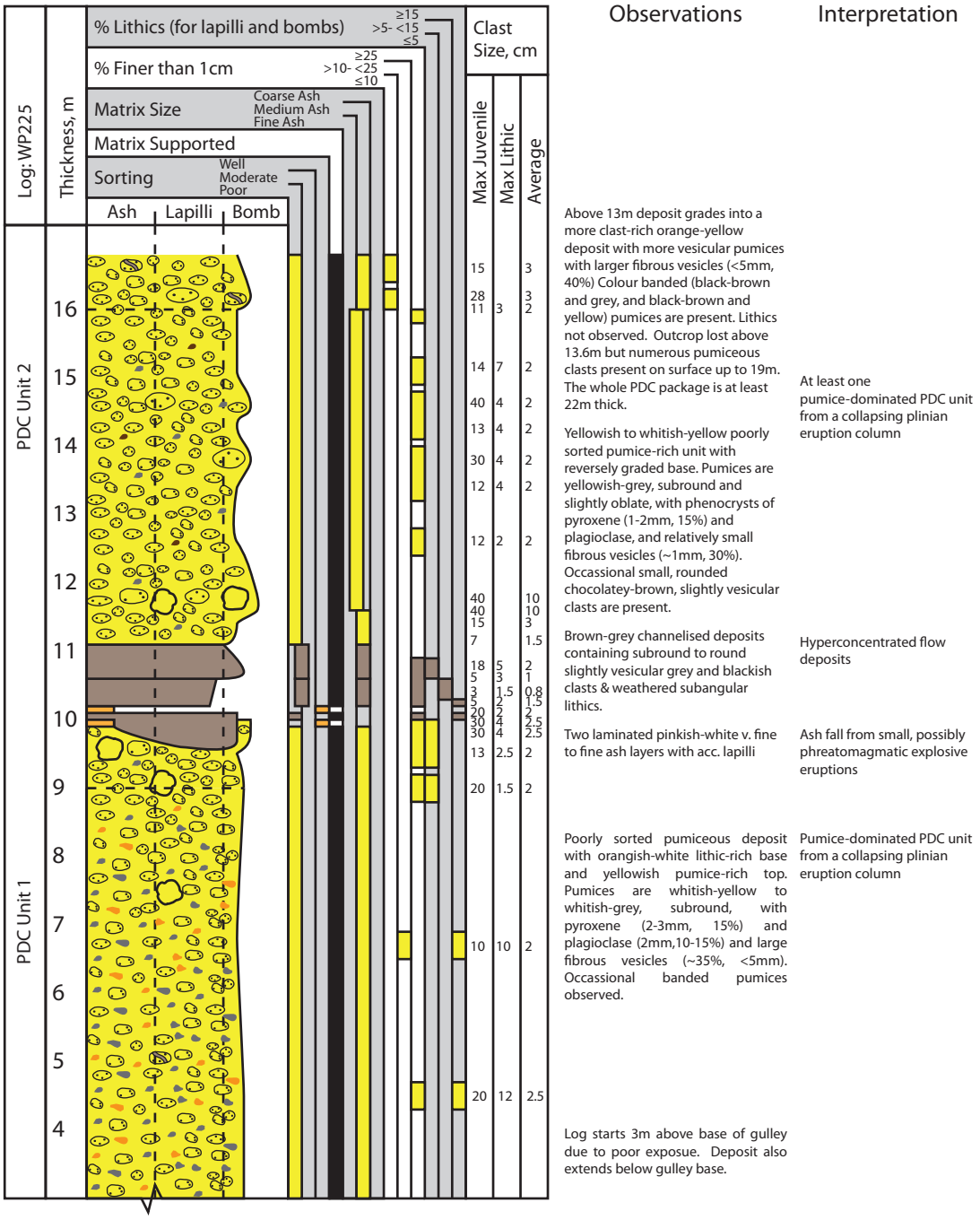

Figure 4.4: Representative stratigraphic log for PDC Package 1, containing PDC Units 1 and 2 at WP225.

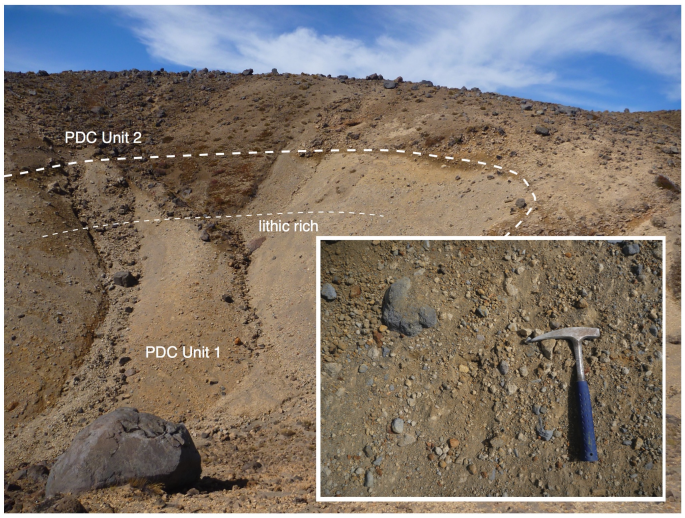

Figure 4.5: The basal ~10m of PDC Unit 1 is extremely lithic-rich, containing up to ~50% lithic clasts. Unit 1 is ~13m thick from the base of the valley, while the whole PDC package (to the ridge crest) is at least 22m thick.

2 km downstream from the main PDC deposits, a ~20m long, channelised, pumiceous PDC deposit (Unit 3) at WP107 (Figure 4.1) is the only deposit from PDC Package 1 preserved in the active Mangatoetoenui Valley. Unit 3 is a poorly sorted, orangish-brownish-yellow PDC deposit containing orangish-yellow pumices in an ash matrix. The unit is bounded below and above by 3-5cm thick fine ash layers rich in accretionary lapilli, with accretionary lapilli also present in the first few cm of the PDC deposit. As also observed in PDC Unit 2 (Figure 4.4), the Unit 3 deposit contains ~3% chocolatey-brown vesicular lapilli that are interpreted as clasts of a secondary magma (Chapter 5). However Unit 3 is considerably more matrix-rich, with field estimates for the amount of material finer than 1cm increasing from 25% at the base of the deposit to 40% at the top.

Laboratory Characteristics

Primary pumices in PDC Package 1 (Units 1-3) range from 55.6 to 59.1 (bulk, anhydrous) % SiO_2 (Table 4.2, Figure 4.7), and form a distinct group in the CaO-MgO variation diagram (Figure 4.6) with significantly higher CaO and MgO than Units 4-6 and significantly lower CaO and MgO than PDC Package 2 (Units 8-10).

The sieved data reinforces the field observations, with Unit 1 transitioning from a

Sample	Flow Unit	Clast Type	SiO_2	TiO_2	Al_2O_3	Fe_2O_3T	MnO	MgO	CaO	Na_2O	K_2O	P_2O_5	LOI	Total
X225AA	Unit 1 Lower	Primary clast	56.315	0.73	16.805	7.372	0.116	4.088	6.716	3.222	1.636	0.125	2.84	99.965
X225AB	Unit 1 Lower	Primary clast	57.575	0.738	16.881	7.205	0.115	4.163	6.922	3.32	1.677	0.126	1.17	99.892
X225AC	Unit 1 Lower	Denser primary	58.887	0.735	16.482	7.224	0.113	4.218	6.888	3.251	1.676	0.131	0.07	99.675
X225BA	Unit 1 Top	Primary clast	57.142	0.73	16.65	7.29	0.115	4.283	6.865	3.186	1.548	0.126	2	99.935
X225BC	Unit 1 Top	Primary clast	56.681	0.734	16.348	7.022	0.116	4.19	6.657	3.237	1.704	0.134	3.09	99.913
X225BD	Unit 1 Top	Denser primary	58.703	0.721	16.691	7.098	0.111	4.279	6.82	3.292	1.682	0.13	0.34	99.867
X225BB	Unit 1 Top	Denser primary	56.323	0.729	16.789	7.258	0.122	4.386	6.877	3.21	1.608	0.126	2.44	99.868
X225BE	Unit 1 Top	Larger primary	58.083	0.717	16.897	7.061	0.113	4.21	6.819	3.286	1.7	0.132	0.9	99.918
X225AD	Unit 1 Lower	Secondary clast type	58.264	0.73	16.448	7.49	0.117	4.372	7.052	3.162	1.568	0.122	0.51	99.835
X225CA	Unit 2 Bottom	Primary clast	54.452	0.722	17.133	6.886	0.109	4.009	6.612	2.999	1.472	0.13	5.4	99.924
X225CH	Unit 2 Bottom	Primary clast	58.538	0.728	17.006	7.2	0.116	4.266	6.922	3.344	1.692	0.135	-0.08	99.867
X225CB	Unit 2 Bottom	Denser primary	54.261	0.729	16.658	7.16	0.109	4.23	6.861	3.105	1.497	0.127	5.1	99.837
X225CE	Unit 2 Bottom	Denser primary	58.728	0.718	16.663	6.994	0.114	4.259	6.782	3.328	1.71	0.134	0.44	99.87
X225CG	Unit 2 Bottom	Larger primary	58.14	0.734	17.049	7.08	0.117	4.224	6.702	3.275	1.727	0.133	0.78	99.961
X225DA	Unit 2 Upper	Primary clast	54.781	0.812	18.534	8.329	0.128	4.82	6.944	2.835	1.192	0.116	1.38	99.871
X225DB	Unit 2 Upper	Denser primary	55.673	0.73	17.658	7.17	0.114	4.298	6.504	3.099	1.504	0.13	3.01	99.89
X225DE	Unit 2 Upper	Denser primary	58.426	0.759	17.054	7.351	0.12	4.379	6.678	3.163	1.625	0.133	-0.18	99.508
X225EA	Unit 2 Top	Larger primary	58.167	0.726	17.355	7.169	0.119	4.37	6.798	3.207	1.661	0.129	0.18	99.881
X225CC	Unit 2 Bottom	Poss. secondary clast	55.384	0.726	16.699	7.605	0.12	4.899	7.469	3.082	1.37	0.122	2.34	99.816
X225CD	Unit 2 Bottom	Secondary clast type	57.582	0.665	17.283	6.781	0.115	3.429	6.596	3.369	1.597	0.132	2.35	99.899
X225DG	Unit 2 Upper	Poss. secondary clast	58.216	0.74	16.975	7.216	0.114	4.246	6.702	3.33	1.736	0.129	0.53	99.934
X225DH	Unit 2 Upper	Secondary clast type	58.683	0.731	16.946	7.279	0.115	4.276	6.736	3.253	1.62	0.129	-0.6	99.168
X225DC	Unit 2 Upper	Secondary clast type	58.31	0.759	16.967	7.428	0.117	4.326	6.686	3.24	1.635	0.133	-0.54	99.061
X225DF	Unit 2 Upper	Grey-black lithic	58.638	0.72	16.828	7.184	0.118	4.425	6.813	3.238	1.737	0.133	0.1	99.934
X225DD	Unit 2 Upper	Grey-black lithic	58.395	0.719	16.903	7.185	0.115	4.297	6.809	3.204	1.627	0.131	-0.31	99.075
X107A1	Unit 3	Primary clast	58.022	0.749	17.188	7.272	0.116	4.118	6.629	3.211	1.685	0.138	0.81	99.938
X129AA	Unit 4	Primary clast	58.157	0.732	18.041	6.496	0.11	3.622	5.926	3.157	1.764	0.141	0.2	98.346
X129AC	Unit 4	Primary clast	58.054	0.726	17.995	6.623	0.112	3.752	5.898	3.134	1.727	0.151	0.55	98.722
X129AD	Unit 4	Primary clast	58.145	0.767	17.533	6.882	0.117	3.947	5.912	3.124	1.795	0.148	0.21	98.58
X129AB	Unit 4	Secondary clast type	59.608	0.707	17.156	6.535	0.11	3.636	5.972	3.325	1.83	0.138	-0.41	98.607
X262Y1	Unit 5 Top	Primary clast	59.329	0.685	17.066	6.629	0.108	3.722	6.427	3.388	1.867	0.133	0.6	99.954
X262AA	Unit 6, base	Primary clast	59.97	0.675	17.127	6.563	0.11	3.692	6.573	3.401	1.754	0.131	-0.2	99.796
X262AB	Unit 6, base	Blockier primary clast	59.705	0.671	17.133	6.642	0.109	3.685	6.596	3.425	1.716	0.133	0.04	99.855
X262AD	Unit 6, base	Primary clast	60.198	0.688	16.584	6.613	0.11	3.847	6.329	3.362	1.876	0.136	0.19	99.933
X262AE	Unit 6, base	Primary clast	60.448	0.689	16.598	6.486	0.106	3.725	6.346	3.375	1.912	0.135	0.03	99.85
X262A3	Unit 6, near top	Primary clast	59.454	0.705	16.815	6.613	0.108	3.821	6.295	3.34	1.935	0.137	0.69	99.913
X306A1	Unit 7	Primary clast	58.479	0.695	17.11	7.063	0.117	4.601	6.37	3.305	1.657	0.135	0.35	99.882
X109AC	Unit 8a	Banded primary clast	56.335	0.76	16.898	8.109	0.135	5.26	8.034	2.962	1.201	0.118	-0.12	99.692
X109AA	Unit 8a	Primary clast	53.086	0.76	17.444	8.17	0.137	5.297	8.083	2.825	1.103	0.119	2.92	99.944
X109AB	Unit 8a	Primary clast	54.482	0.755	16.966	8.239	0.14	5.401	8.148	2.974	1.176	0.118	1.54	99.939
X108AA	Unit 8b	Primary clast	54.589	0.775	17.777	8.212	0.134	5.189	7.804	2.987	1.219	0.125	1.06	99.871
X108AB	Unit 8b	Primary clast	54.64	0.751	17.817	8.209	0.131	5.309	7.83	2.838	1.171	0.121	1.07	99.887
X108AC	Unit 8b	Primary clast	57.234	0.742	16.822	7.777	0.124	4.929	7.438	3.045	1.395	0.124	-0.37	99.26
A108AD	Unit 8b	Primary clast	56.511	0.746	16.833	8.008	0.131	5.194	7.796	3.012	1.283	0.121	0.19	99.825
X108BA	Unit 9b	Primary clast	52.575	0.814	18.133	8.628	0.135	5.459	7.619	2.699	1.032	0.131	2.57	99.795
X108BB	Unit 9b	Primary clast	54.41	0.775	17.83	8.289	0.132	5.349	7.829	2.82	1.1	0.124	1.18	99.838
X108BC	Unit 9b	Primary clast	54.809	0.773	17.854	8.351	0.132	5.311	7.859	2.852	1.103	0.122	0.73	99.896
X108BD	Unit 9b	Larger primary	55.764	0.744	17	8.169	0.135	5.343	8.012	3.089	1.273	0.125	0.25	99.904
X161AC	Unit 10	Primary clast	56.462	0.741	16.91	7.922	0.128	5.125	7.799	3.006	1.27	0.122	0.36	99.845
X108CA	Unit 10	Larger primary	55.479	0.762	17.1	8.312	0.135	5.429	7.867	3.025	1.243	0.122	0.4	99.874
X161AA	Unit 10	Primary clast	57.808	0.737	17.177	7.291	0.122	4.287	6.549	3.164	1.678	0.127	0.94	99.88
X161AB	Unit 10	Primary clast	54.609	0.761	17.456	8.108	0.137	5.201	7.862	2.995	1.231	0.122	1.47	99.952
X225EB	Unit 11	Primary clast	56.99	0.73	18.17	7.45	0.12	4.11	7.20	3.39	1.41	0.13	0.22	99.92
X296A1	Unit 12	Primary clast	55.463	0.73	18.819	7.805	0.128	4.153	7.007	3.345	1.269	0.115	1.1	99.934
X301A1	Te Heuheu Welded Spatter		56.709	0.795	17.567	8.015	0.128	4.608	7.483	3.252	1.424	0.135	-0.24	99.876
X301A4	Te Heuheu Welded Spatter		54.876	0.806	17.145	9.438	0.131	4.73	7.043	2.963	1.509	0.17	1.05	99.861
X299A1	Te Heuheu Welded Spatter		55.199	0.829	17.177	9.263	0.136	4.96	6.895	2.943	1.411	0.149	0.99	99.952
X274A1	Pinnacle Ridge Tuff	Primary clast	60.157	0.62	16.554	5.922	0.099	3.877	6.087	3.562	1.886	0.124	1.07	99.958
X274A3	Pinnacle Ridge Tuff	Primary clast	59.853	0.644	16.884	5.941	0.098	3.84	6.082	3.507	1.844	0.129	1.1	99.922

Table 4.2: XRF major element chemistry of samples from Ruapehu's PDC deposits. Samples not representing the dominant magma types are highlighted in grey. The data here is presented in full, showing loss on ignition and analyses totals. However values reported in the main text and used in Figures 4.6 and 4.7 are recalculated to 100% anhydrous. Two analyses with large LOI values are highlighted in yellow and should be treated with caution. The low analysis totals for the PDC Unit 4 samples may result from the presence of an element that has not been analysed; however the normalised data (Figure 4.6) is consistent with previous analyses of pyroclasts from this unit (Donoghue et al., 1995a).

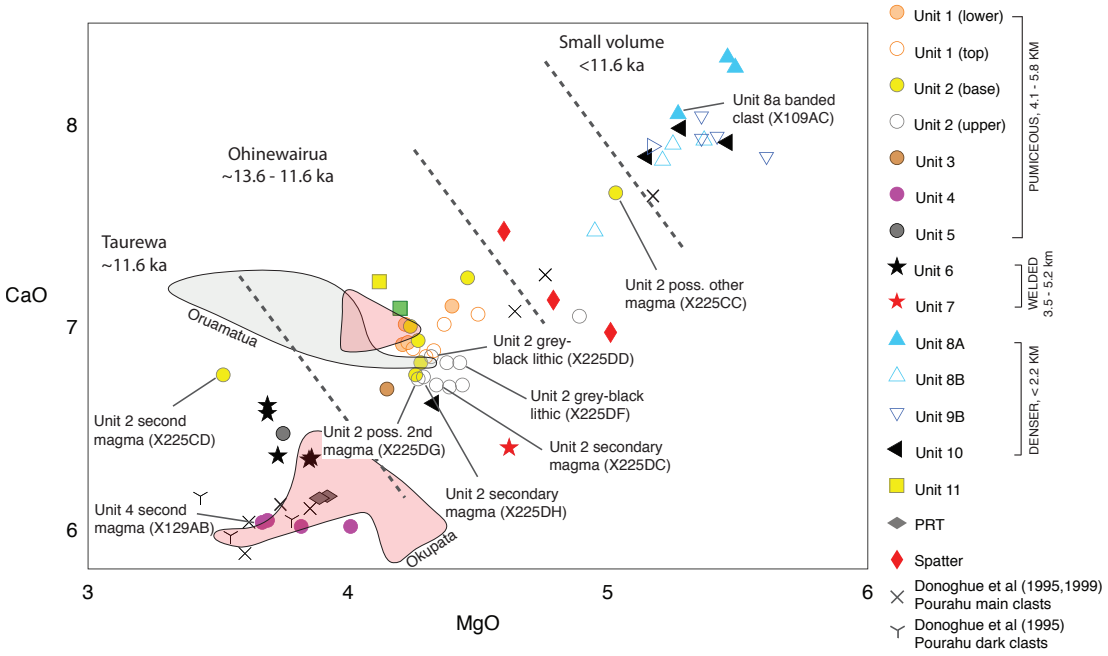

Figure 4.6: Geochemical variation diagram for pyroclasts from the Ruapehu PDC deposits (100% anhydrous). The MgO-CaO diagram shown here is representative of all of the major element variation diagrams, but clearly shows the distinct groupings of PDC chemistry by eruption age. This data supports tentative field-based correlations that Units 11 & 12 belong to the same eruptive period as Units 1-3. Similarly, the field correlations between Units 4, 5, 6 & the Pinnacle Ridge Tuff are fully supported by the chemistry. These chemical correlations add confidence to the interpretated ages in the absence of well-defined stratigraphic controls. Fields for Pardo Villaveces' (2012) Oruamatua (one of three plinian eruptions in the Ohinewairua eruptive period, of which PDC Units 1-3 are interpreted to be associated) and Okupata (part of the Okupata-Pourahu eruptive unit, of which PDC Unit 4 is interpreted to be associated) tephras are also shown, as well as Donoghue et al's (1995a, 1999) analyses of primary and secondary clasts in the Pourahu PDC (PDC Unit 4).

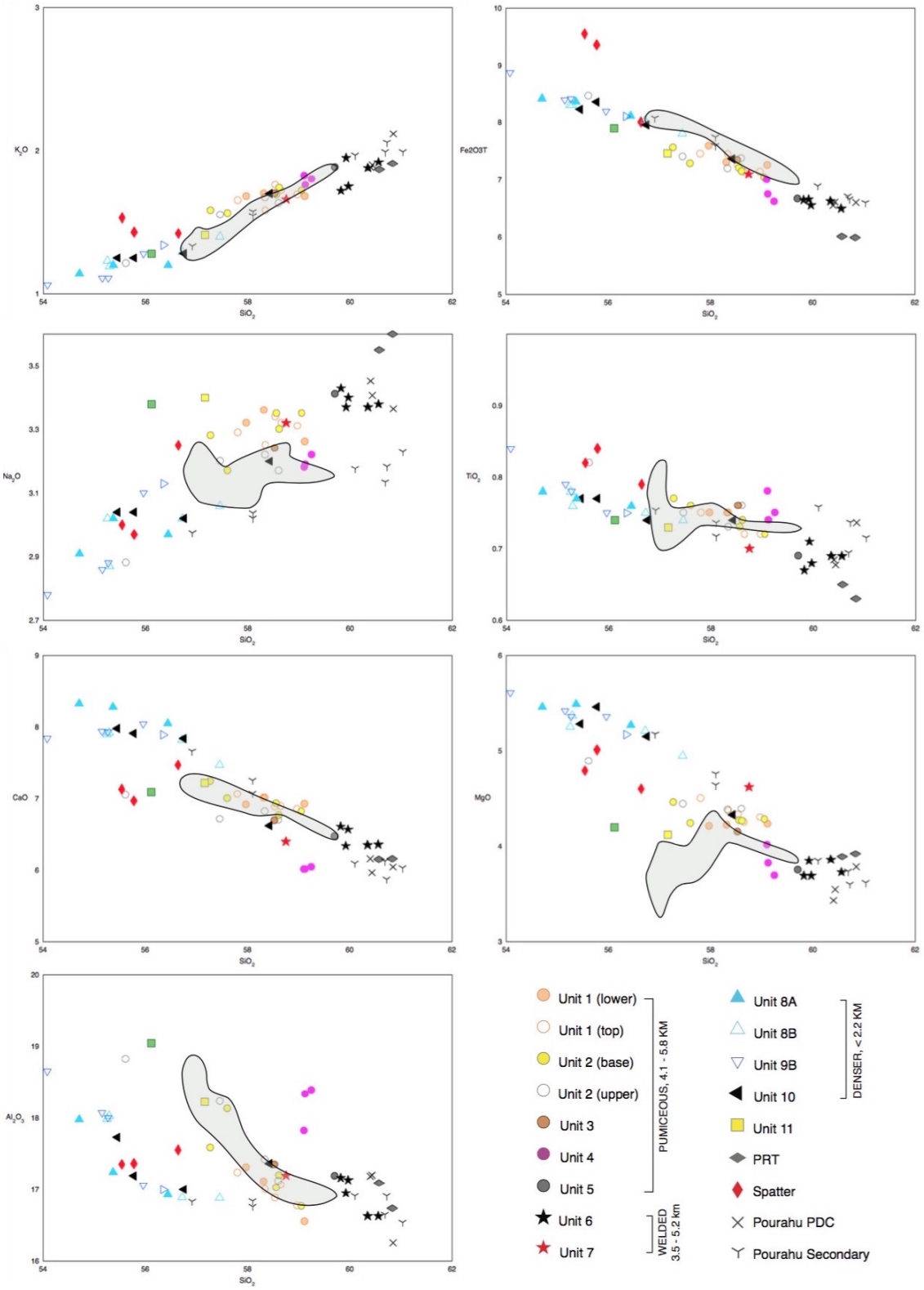

Figure 4.7: Major element variation diagrams for pyroclasts from the Ruapehu PDC deposits (100% anhydrous). Fields for Pardo Villaveces' (2012) Oruamatua tephra (one of three plinian eruptions in the Ohinewairua eruptive period, of which PDC Units 1-3 are interpreted to be associated) are also shown, as well as Donoghue et al's (1995a, 1999) analyses of primary and secondary clasts in the Pourahu PDC deposit (PDC Unit 4).

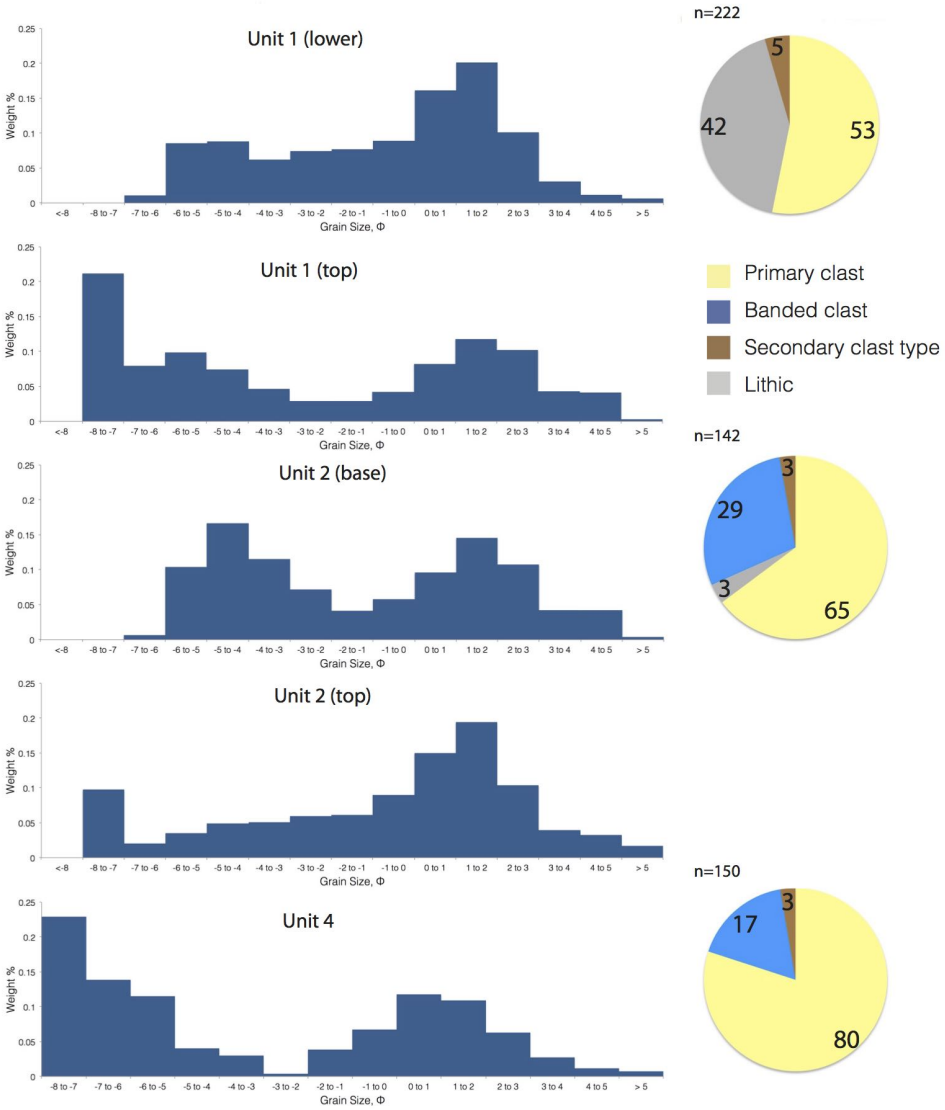

Figure 4.8: Total grain size distribution and corresponding whole-clast componentry from the -5ϕ to -4ϕ sieved size fraction for Ruapehu's pumiceous PDC Units 1, 2 and 4 deposits.

unimodal grain size distribution in the lower lithic-rich part of the deposit to a bimodal distribution at the top, as a result of the reverse coarse-tail grading of the largest pumices (Figure 4.8). Unit 2 has a bimodal distribution at its base, and it is difficult to reliably discriminate between the top of Unit 1 and the base of Unit 2 on the basis of grain size. Both units fall comfortably within the PDC fields on the Walker (1971, 1983) size-sorting diagram (Figure 4.9).

Although pumices in PDC Package 1 cannot readily be distinguished in the field, laboratory dried samples *are* subtly different. Unit 1 pumices are pale white-grey, and are slightly denser than Unit 2 pumices (see Chapter 5) which are pale yellow. Unit 1 also

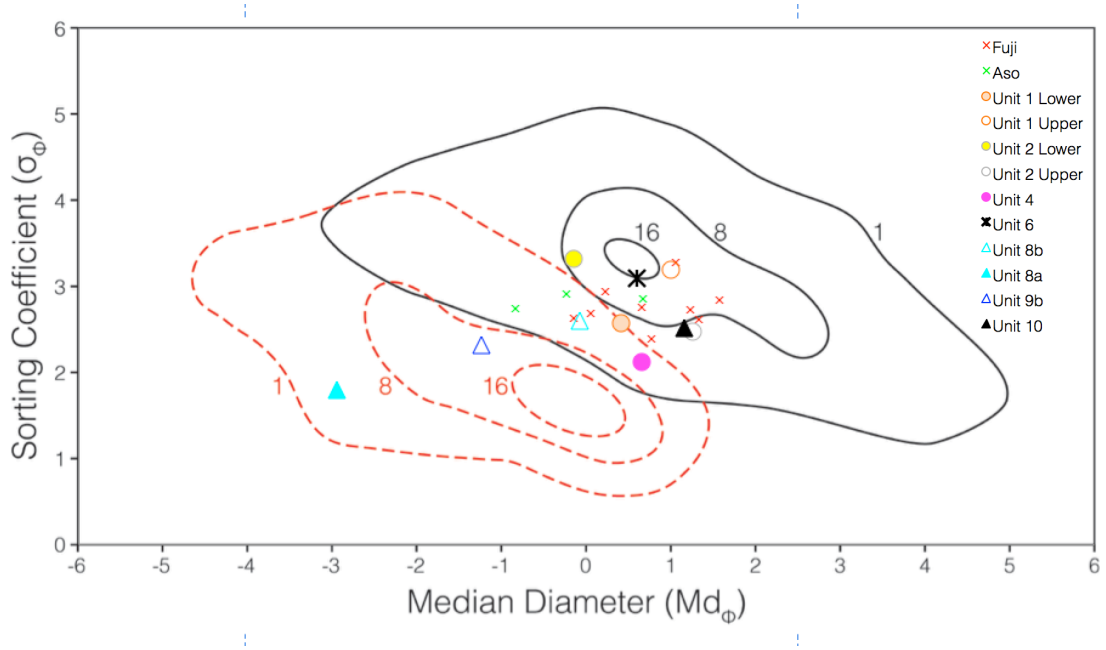

Figure 4.9: Median diameter vs sorting coefficient of grain size data (finer than -5 Φ fraction) for the Ruapehu PDCs. The outlined areas show the 1, 8 and 16% contours of Walker (1971, 1983) for PDCs (solid line) and fines-depleted deposits associated with PDCs (dashed lines), including ground layers, fines-depleted ignimbrite and elutriation pipes. Basaltic spatter-fed PDCs from Fuji (initiated due to steep topograpical gradients, similar to Unit 6; Yamamoto et al., 2005) and Aso (containing abundant cauliflower-bombs, similar to Units 8-10; Miyabuchi et al., 2006) shown for comparison.

contains ~5% slightly vesicular grey clasts (Figure 4.8) that are similar to the white-grey primary pumices and are only readily distinguished after drying. These are intepreted as secondary clasts, and in Unit 2 the same secondary magma appears as grey bands within the primary pumices (29% banded clasts, Figure 4.8). Again, this banding is too subtle to be observed unless the clasts are completely dry.

2. PDC Unit 4

PDC Unit 4 is exposed at the base of three minor gulleys north of Tukino ski village (Locations WP108, WP157, and WP200, Figure 4.1), immediately beneath the moraine ridge that separates the Whangaehu and Mangatoetoenui Valleys. Pumiceous clasts from Unit 4 are also observed at the ridge crest in the ski village parking area, though undisturbed outcrop is not present here. Unit thickness varies from a thin veneer where it mantles pre-existing slopes, to up to 2m thick where the PDC ponded in valley bottoms (e.g. Locations WP108 and WP157, Figure 4.1).

Field Characteristics

The Unit 4 deposits are poorly to very poorly sorted, clast-supported deposits containing highly vesicular whitish-yellow subround coarse pumice lapilli and bombs in a medium to coarse ash matrix (Figure 4.14). The deposits are texturally similar to the Unit 2 deposits, but contain very few lithics (none at WP157, ~3% at WP108) and more abundant strongly banded pyroclasts (with black-brown bands, as opposed to the mostly subtle grey banding in Unit 2). Additionally, a higher proportion of pumices in Unit 4 have pale pinkish thermal oxidation, though this is generally too subtle to observe in the field if the clasts are not completely dry.

Laboratory Characteristics

Primary pumices in PDC Unit 4 are the most silicic andesites of Ruapehu's pumiceous PDCs, ranging from 59.1 to 60.2 % (anhydrous) SiO_2 (Table 4.2, Figure 4.7). Together with Units 5 & 6, they from a distinct group in the CaO-MgO variation diagram (Figure 4.6) with significantly lower CaO and MgO than all other deposits.

The sieved data show that the deposit is significantly coarser grained than the Ohinewairua deposits with a bimodal distribution that is skewed towards the bomb size fractions and an all-clasts median diameter of -4.6 ϕ (Figure 4.8). This is consistent with the field observations of clast supported coarse lapilli and bombs with relatively little matrix. The deposit falls within the PDC field on the Walker (1971, 1983) size-sorting diagram (Figure 4.9).

Laboratory drying reveals abundant pinkish alteration (3% of clasts from the -5ϕ to -4ϕ size fraction are distinctly pink, and another 17% have subtle pink sections) that is not easily visible in the field when the clasts are damp. This easily distinguishes the Unit 4 pumices from Ruapehu's other pumiceous PDC deposits when the clasts are dry. In addition to the clearly banded bomb-sized clasts observed in the field, laboratory drying also reveals that 17% of the Unit 4 lapilli have subtle grey bands, and 3% of the lapilli are black-brown secondary clasts (Figure 4.8). These characteristics highlight the strong

similarities between the Unit 4 and Unit 2 deposits.

3. PDC Unit 5

PDC Unit 5 is an at least 8m thick, poorly sorted pumiceous PDC deposit that is only exposed in a ~10m-long section at Location WP262 (Figure 4.1), where it directly underlies deposits from another PDC (PDC Unit 6, see Section 4.4.4 and Figure 4.11). Texturally similar pumiceous clasts are occasionally observed in other locations by digging beneath Unit 6, suggesting that these two units have similar distributions.

Field and Laboratory Characteristics

In the field this unit appears similar to PDC Units 1-4, being a whitish-yellow poorly sorted pumiceous deposit with subround pumice lapilli in a medium ash matrix of crystals and broken pumice. However after cleaning and drying, the pumices lack the characteristic pinkish alteration that typifies the Unit 4 clasts, and they also appear to be denser than those in Units 2-4. Pumices at the base of the deposit are a pale whitish-yellow similar in appearance to those PDC Unit 1, but clast colour changes upwards to a distinct pale brown colour not seen in any of the other pumiceous units. Banded clasts with pale-grey to yellow (primary magma) or black-brown colour bands (secondary) are present throughout PDC Unit 5 but also increase in number towards the top of the unit. Chemically, sample X262Y1 suggests that the Unit 5 pumices most closely resembles those in both PDC Unit 4 and the overlying Unit 6 (Figure 4.6).

4.4.2 Interpretation of the pumice-dominated PDC deposits YAY

4.4.3 Interpretation of the pumice-dominated PDC deposits

The poorly sorted, matrix supported, pumice-rich nature of the deposits supports their interpretation as pyroclastic density current deposits using the assessment system developed in Chapter 3 (Figure 3.3). Unit 1 can be explained by a PDC origin with 'very high' confidence due to the reverse coarse tail grading of large pumices and magnetic evidence of hot emplacement. Units 2-5 *initially* score 'moderate' confidence since the generally

poorly exposed deposits did not present definitive evidence of high-temperature emplacement, these units were not tested with the portable magnetometer. However, no other volcaniclastic processes explain the observed textures with higher confidence levels in the initial assessment. Direct textural and spatial associations with other PDC units (Units 2 & 3 correlate with Unit 1, Unit 4 correlates with known deposits of the Pourahu PDC, Donoghue et al., 1995a, 1999), as well as larger-scale deposit geometries observed over multiple outcrops (Unit 2 forms a flat-topped, valley filling deposit and Unit 4 has pond-and-veneer geometry), increases the confidence that these are also PDC deposits, and we therefore give them an adjusted rating of 'high' confidence).

Pyroclasts within PDC Package 1 (Units 1-3) are texturally and chemically similar to plinian fall deposits from the ~13.6-11.6 ka B.P. cal. Ohinewairua eruptive period described by Pardo et al. (2011), encompassing the "Oruamatua," unnamed "Unit 28," and "Akurangi" eruptive units. These were some of the largest plinian eruptions at Ruapehu, sourced from North Crater. Pardo et al. (2011, 2012, 2014) previously hypothesised that these eruptions were accompanied by voluminous PDCs from oscillating and collapsing eruption columns, on the basis of disequilibrium lapilli vesicle textures and observation of several cm-scale matrix supported units interbedded with the Ohinewairua fall deposits. The massive deposits described here confirm that hypothesis. Pardo's (2011) cm-scale deposits are therefore now interpreted to represent the laterally distal PDC facies associated with the massive PDC deposits identified here. The whole rock chemistry for Units 1-3 is distinct from all other Ruapehu PDC deposits and overlaps Pardo's (2012) results for the Oruamatua fall deposits (Figure 4.6). However the PDC pyroclasts have greater chemical diversity than the Oruamatua fall deposts, and since whole rock analyses for Pardo's (2011) "Unit 28" and "Akurangi" tephras are not available it is therefore unknown which of the Ohinewairua eruptions produced Units 1-3. PDC Package 1 had a minimum runout distance of 7.8 km and an interpreted minimum combined deposit volume of 0.051 km^3 (Figure 4.1 and Table 4.3). This is equivalent to 10% of the Oruamatua or 8% of the Akurangi plinian fall deposit volumes (Pardo et al., 2012, using the method of Sulpizio, 2005), depending which (if not all) of the Ohinewairua eruptions generated PDC Package 1.

The distinctive highly vesicular pumices with pinkish alteration in PDC Unit 4 corre-

Unit	Interpreted area, km^2	Deposit thickness, m	Interpreted average thickness, m	Volume, km^3	Furthest runout (from preserved deposits), km	Comments
PDC Package 1 (Units 1-3)	2.54			0.051	5.7 (Units 1 and 2) to 7.8 (Unit 3)	Difficult to correlate individual units, at least 3 PDC units described. PDCs equivalent in volume to either 10% of Oruamatua (0.5km^3) or 8% of Akurangi (0.6km^3) fall deposit volumes, assuming the PDCs belong to only one of these eruptive periods.
- Upstream of front face of Units 1-2	1.49	>22m (WP225) to 25 at front face of Units 1-2	25	0.037		
- Downstream of front face of Units 1-2	1.06	25m at front face of Units 1-2 to 1m at WP107	13	0.014		
PDC Unit 4	2.66	Surface veneer to 2m thick at Tukino, 1.1m at Donoghue Type Location	1	0.003	14.6	Outcrops close to Tukino represent PDC overbank deposits. Donoghue (1995) reports primary deposits on the ring plain. Lack of exposures means that the interpreted depositional area (and hence volume) is very tentative
PDC Unit 5	0.90	8m thick at WP262, no other exposure	1	0.001	5.4	Only one small outcrop, but area is tentatively interpreted to be similar to PDC Unit 6. 1m thickness reflects this uncertainty and the fact that overlying Unit 6 at WP262 is substantially overthickened in a paleovalley.
PDC Unit 6	0.90	2m to 36m in palaeovalley at WP262	6.5	0.006	4.3	Runout distance from inferred location of accumulating then collapsing spatter deposit below Te Heuheu peak; not from original vent.
PDC Unit 7	1.17	10m thick at WP306, less thick in other locations	5	0.006	3	Unit thicknesses are poorly constrained.
PDC Package 2 (Units 8-10)	0.33			0.002	5	Difficult to correlate individual units, at least 3 PDC units described.
- Units 8-10 in valley by Tukino	0.17	8.75m at WP108	8.75	0.002		
- Unit 8-10 outside of main valley	0.15	Scattered surface clasts	0.25	3.86 x $10^{-}5$		
PDC Unit 11	Insufficent deposit	Scattered surface clasts at WP258			4.7	Insufficent deposit for volume estimates
PDC Unit 12	Insufficient deposit	Scattered surface clasts at WP295 and WP296			2.3	Insufficent deposit for accurate volume or runout estimates
Total				**0.119**		

Table 4.3: Depositional areas, minimum runout distances, and interpreted volumes for Ruapehu's PDC Units 1-12. Grey rows show calculations that account for different average deposit thicknesses in different parts of the deposits.

late texturally and chemically with deposits previously described for the ~11.6 ka Pourahu PDC and associated plinian Okupata tephra (Donoghue et al., 1995a; Pardo et al., 2011). We therefore interpret that the Unit 4 deposits identified here also belong to the Pourahu PDC. This is the only PDC deposit previously studied in detail at Ruapehu (Donoghue et al., 1995a), and was emplaced at ~11.6 ka during the "Okupata-Pourahu eruptive unit" (Pardo et al., 2011) of the "Taurewa eruptive period" (Donoghue et al., 1995b, 1999). The Okupata-Pourahu eruptive unit is the youngest known plinian eruption at Ruapehu, and was previously interpreted by Hackett and Houghton (1989) and Donoghue et al. (1999) to have been erupted from a North Crater source. However, detailed mapping by Pardo et al. (2011, 2012) now suggests that this eruption opened a new vent near to the presently active South Crater. The observed PDC distribution in the southern edge of the study area supports this interpretation (Figure 4.1). Donoghue's (1995b) type location for primary Pourahu PDC deposits is "The Chute" in the Whangaehu river fan on Ruapehu's eastern

ring plain (Figure 4.1), and it was previously proposed that no primary deposits were emplaced <10km from source due to flow channelisation in the proto-Whangaehu Gorge. The primary deposits described ~4.6 km from source therefore greatly extend the known depositional extent. Like the Ohinewairua PDCs, Unit 4 is interpreted to have formed by collapse or partial collapse of a plinian eruption column. The PDC had a minimum runout distance of 14.6 km (Table 4.3). The deposit is preserved in too few locations to give an accurate estimate of its original depositional area, but a hypothetical depositional extent is shown in Figure 4.1. If the original deposit is interpreted to have been 1m thick over this area (the unit is 1.1m thick at Donoghue's 1999 type location on Ruapehu's ring plain), it would have a volume of 0.003 km^3.

PDC Unit 5 is chemically similar to the directly overlying Unit 6 (Section 4.4.4 and Figure 4.6). Since there is no field evidence of a substantial time break between Units 5 and 6 (Figure 4.11), it is therefore interpreted to represent an initial small and short-lived pumiceous phase of the same eruptive sequence (see Section 4.4.4). While Unit 5 is also chemically similar to the ~11.6 ka Unit 4 (Pourahu PDC), the primary pyroclasts are texturally distinct with denser juvenile clasts that lack the characteristic pinkish alteration. However, we propose that Units 4 (South Crater), and 5 & 6 (North Crater) were all erupted at a similar time from different vents (see Section 4.4.5), so in the absence of other stratigraphic controls this suggests that Unit 5 was emplaced at ~11.6 ka B.P. cal. Unit 5 has a minimum runout distance of 5.4 km, but lack of exposed deposits prohibits a reliable volume estimate. However, assuming it was emplaced over a similar area to the directly-overlying Unit 6 (as supported by occasional texturally similar pumiceous clasts beneath Unit 6 in other locations) we suggest this unit may have had a volume of ~0.001 km^3 (Table 4.3).

4.4.4 Scoria-dominated variably welded pyroclastic density currents

These PDC deposits are characterised by poorly sorted, monolithologic, variably welded and bedded deposits containing unusually round black scoriaceous clasts (compared to Ruapehu's other PDC deposits; see Chapter 5, Section 5.4.3) in a medium ash matrix.

1. PDC Unit 6

PDC Unit 6 is a grey-black, variably welded, layered sequence of PDC deposits that forms a flat-topped plateau in a broad valley immediately downslope of Te Heuheu Peak and Ruapehu's North Crater (Figure 4.1). The unit was previously identified by Hackett (1985) and later mapped by Chapman (1996). Deposition was concentrated downstream of a pronounced break in slope, and the deposit then extends for ~1.3km at an observed thickness of ~2 to 36m (Figure 4.2). The southern part of the deposit is not preserved (see Section 4.5.3), but an isolated outcrop at WP177 (Figure 4.1) reveals the original southern extent where there deposit laps against a thick ridge-bounded lava flow.

Field Characteristics

Unit 6 contains subround to rounded, monolithologic, black scoriacous lapilli and bombs in a coarse-to-medium ash matrix of the same composition. Unusually high degrees of clast rounding are distinctive features at such short (4.3 km) distances from source (Figure 4.3 d and Section 5.4.3). Isolated large bombs up to ~3m diameter, and occasional bombs composed of welded spatter (Fig 4.10) are also present, and many clasts have chilled rinds up to 1cm thick. Metre-scale deposit layering has been overprinted by partial welding, evidenced by vertical cooling joints that extend continuously through most of the deposit, as well as changes in deposit induration and minor clast flattening (Figures 4.3 (c) and 4.2 c). The base of the unit is typically unwelded, grading vertically into a more welded core before in places returning to a less welded top (Figure 4.3 c). Protrusions from the mostly flat welded upper surface of the deposit show linear striations and have gentle stoss and steeper lee sides consistent with glacial erosion (Figure 4.2 d).

At the distal end of Unit 6 (WP262, Figures 4.1 and 4.2) the deposit thickens up to ~36m thick in a palaeovalley (Figure 4.11). In the bottom 13.2m of this section, the deposit alternates between thicker (0.4 - 4.35m), coarser-grained layers with reverse graded bases and dominantly bomb-sized average clast sizes, and thinner (all <35 cm apart from the uppemost layer which is 1m thick) layers with dominantly lapilli-sized clasts (Figure 4.11). The layers are distinct but their contacts are sufficiently gradational to prevent allocation to separate PDC units. Above 13.2m, the deposit contains dominantly bomb sized

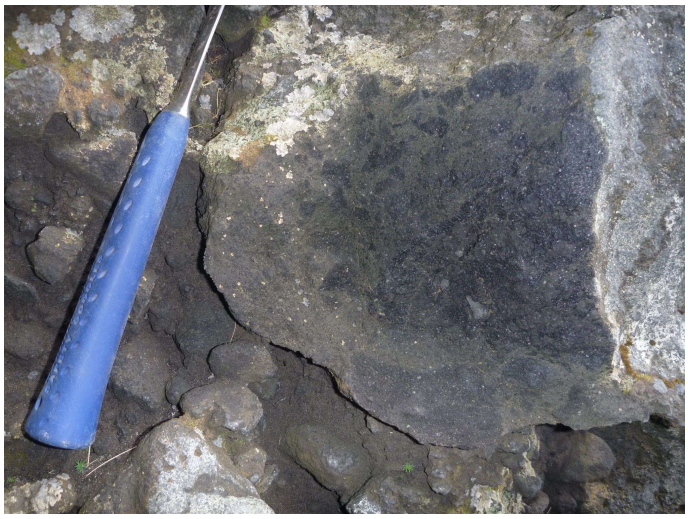

Figure 4.10: Clast within variably welded PDC Unit 6 composed of agglutinated spatter that is interpreted to have welded prior to transport within the PDC.

clasts in layers up to 7m thick, with the densest welding occurring between 17.2 and 23m in section (Figure 4.11). In total, a continuous stack of 16 layers were identified at this section.

Laboratory Characteristics

Unit 6 has the most silicic pyroclasts observed, ranging from 59.8 to 60.6 % (anhydrous) SiO_2 (Table 4.2, Figure 4.7). It is chemically similar to pumiceous Units 4 (Pourahu PDC) and 5, and these three units form a distinct group on the CaO-MgO variation diagram with significantly lower CaO and MgO than Ruapehu's other PDC units (Figure 4.6.

Sieved data from the unwelded base of the deposit emphasises the coarse grained nature of the deposit, with a bimodal distribution skewed towards the bomb-sized clasts, and an all-clasts median diameter of -2.7 ϕ (Figure 4.12). The deposit falls close to the centre of the PDC field on the Walker diagram (Figure 4.9). Componentry of the sieved -5ϕ to -4ϕ lapilli shows that the deposit is not completely monolithologic, with 4% denser lithic clasts. However most of these are very slightly vesicular and unweathered, and hence may be associated with the primary magma.

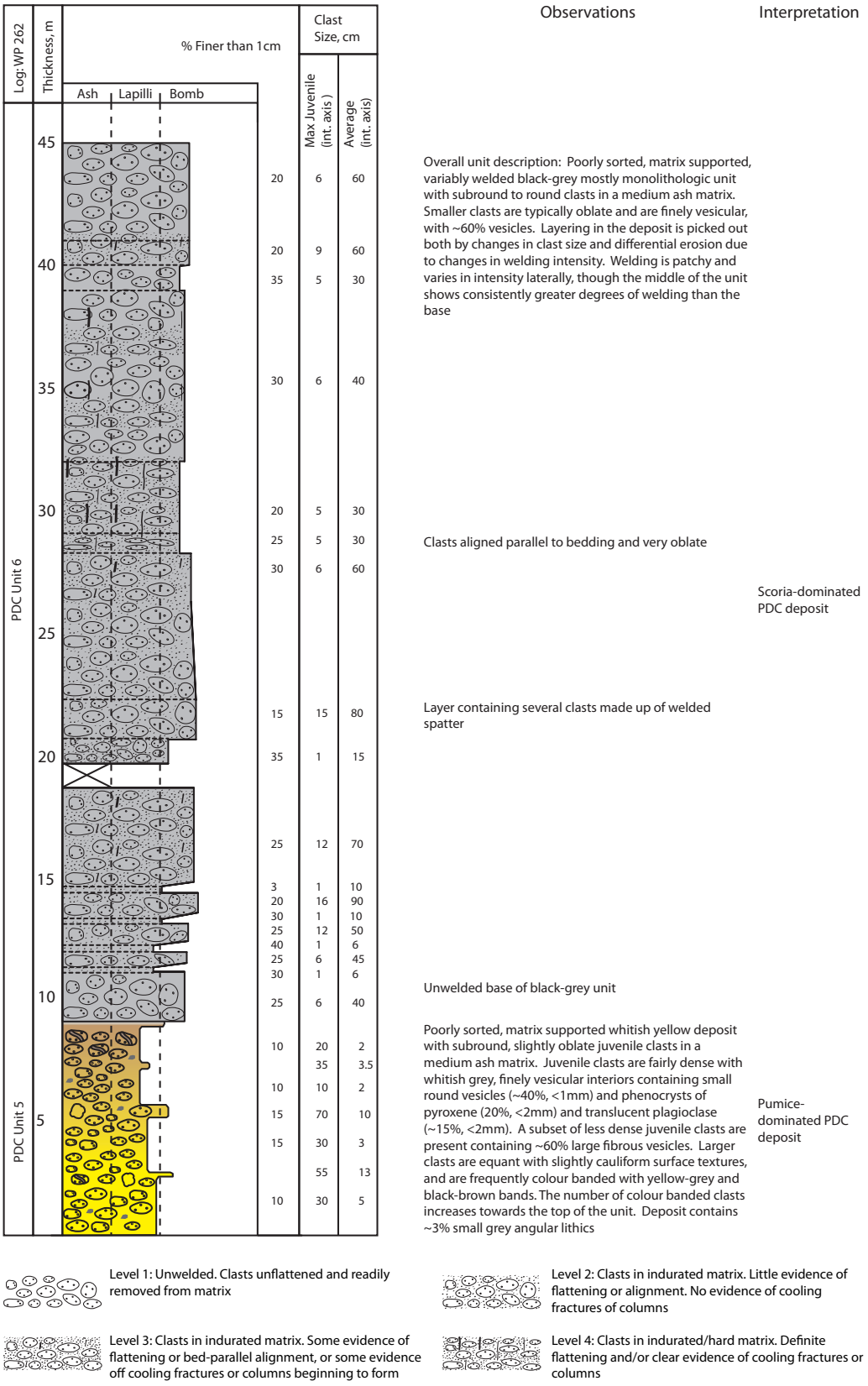

Figure 4.11: Representative stratigraphic log for PDC Units 5 and 6 at WP262.

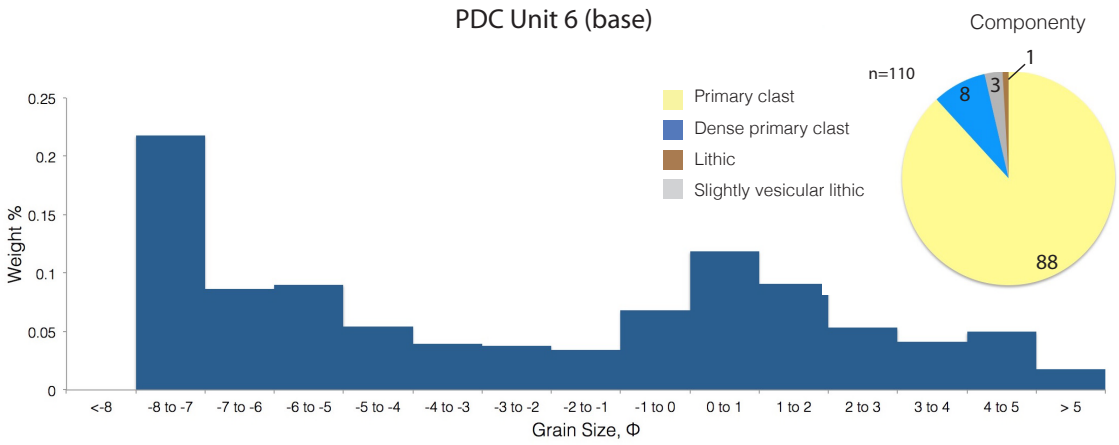

Figure 4.12: Total grain size distribution and corresponding whole-clast componentry from the -5ϕ to -4ϕ sieved size fraction of Ruapehu's variably welded PDC Unit 6 deposit.

PDC Unit 7

PDC Unit 7 is exposed in several small (<300m) outcrops directly upslope of PDC Unit 6, towards North Crater and Te Heuheu Peak (Figure 4.1).

Field and Laboratory Characteristics

The Unit 7 deposits are texturally indistinguishable from PDC Unit 6, and given their spatial association upslope of Unit 6 they were initially mapped as the same unit by Hackett (1985) and Chapman (1996). However Unit 7 is chemically distinct from Unit 6, and does not plot with any of the other PDC fields on the CaO-MgO diagram (Figure 4.6). The variably welded Unit 7 deposits contain rounded black scoriaceous lapilli and bombs in fine-medium ash matrix. Localised sections of the deposit are thermally oxidised to a bright red colour (e.g. Location WP237, Figure 4.13), and this becomes more pervasive further upslope where most of the deposit is oxidised.

4.4.5 Interpretation of the Variably Welded PDCs

The poorly sorted, matrix supported, scoria-rich, valley-filling nature of the observed deposits, and the textural (welding) and magnetic evidence of hot emplacement supports the interpretation that Units 6 and 7 are PDC deposits with 'very high' confidence using the assessment system developed in Chapter 3 (Figure 3.3). The deposit layering containing numerous reverse-graded beds, together with the presence of clasts composed of

Figure 4.13: Parts of PDC Unit 7 have been oxidised to a bright red colour which becomes more prevalent further upslope. Outcrop is ~1m high.

previously-welded spatter, supports an interpretation that multiple small-volume PDCs were generated by repeated gravitational collapse of accumulated near-vent spatter and cinders on steep (~35°) proximal slopes. This process has been directly observed at neighbouring Ngauruhoe volcano (Lube et al., 2007). Near-continuous cooling columns bisecting most layers show the entire sequence was emplaced in rapid succession (i.e. minutes to hours) before the early units had cooled. PDC Unit 6 had a minimum runout distance of 4.3 km and an interpreted deposit volume of 0.006 km^3. Unit 7 had a minimum runout distance of 3 km and a tentative volume of 0.006 km^3 based on limited unit thickness data (Figure 4.1 and Table 4.3).

In the most proximal locations upslope of Units 6 and 7, densely welded spatter mantles the slope below Te Heuheu peak (Te Heuheu welded spatter deposit, Figure 4.1). The densely welded spatter grades vertically into a black deposit that is texturally indistinguishable to both Units 6 and 7. Given the spatial relationships and the presence of spatter clasts in Unit 6, all three deposits were initially mapped here and by Hackett (1985) as a single unit. However, Units 6, 7 and the Te Heuheu welded spatter deposit are all chemically distinct. Based on this we suggest that these should not be correlated (Figure 4.6). Evidence for these being different units is further supported by the deposit distributions, which appear to have been largely controlled by the changing distributions of glacial ice at the times of emplacement (See Section 4.5.3). Therefore, these three units instead evidence *multiple* spatter-forming eruptions from the North Crater area, some of

which transitioned to PDCs when the accumulating tephras collapsed on oversteepened proximal slopes.

New insights into the Taurewa eruptive period

The PDC Unit 6 deposit is texturally and chemically similar to the Pinnacle Ridge Tuff (PRT); a grey-black variably welded spatter deposit that mantles the slopes of Pinnacle Ridge at Location WP276 in north-western Ruapehu (Figures 4.1 and 4.6). Given these similarities, we therefore propose that Unit 6 and the PRT may have been erupted at a similar time. The PRT has previously been interpreted to have been emplaced during a subplinian eruption in Northern Ruapehu (Hackett, 1985) that may have covered most of the northern slopes in up to 1m of tephra (Donoghue et al., 1999). Hackett and Houghton (1985) and Donoghue et al. (1999) also suggest that the PRT eruption was associated with the ~11.6 ka plinian Okupata-Pourahu eruptive unit (i.e. including the Okupata tephra and PDC Unit 4), and this is supported by the presence of occasional pumices in the PRT deposits that are similar to those in the Okupata-Pourahu deposits (Donoghue et al., 1999). Furthermore, the chemical data presented here shows that PDC Units 4, 5, 6 and the PRT *all* form a distinct group with higher SiO_2 (Table 4.2) and lower CaO and MgO than the other PDC units (Figure 4.6). However, while the Okupata tephra was originally interpreted as having a Northern Ruapehu source (Topping, 1973; Donoghue et al., 1999), detailed isopach mapping by Pardo et al. (2012, 2014) later related this to the opening of a new vent near the South Crater Area (Figure 2.4). This better explains the Pourahu PDC's (Unit 4) southerly distribution in the Whangaehu valley, but then does not satisfactorily explain the more northern distributions of Units 5, 6, and the PRT if these were part of the same eruption sequence. Therefore, we propose that the deposit distributions and chemical evidence described here suggest there may have been closely spaced eruptions of chemically similar magma from *both* Southern and Northern Ruapehu, all of which are interpreted to have occurred around the same time as the Okupata-Pourahu eruptive unit and form part of the Taurewa eruptive period (Donoghue et al., 1999; Pardo et al., 2011). In this model, batches of chemically-similar, volatile-rich andesitic magmas were emplaced beneath both Northern and Southern Ruapehu at ~11.6 ka B.P. cal. The pre-existing conduit in Northern Ruapehu is interpreted to have allowed more efficient degassing, resulting

in a short-lived explosive eruption (emplacing pumiceous Unit 5) followed by more sustained fountaining that deposited thick accumulations of spatter/cinders on the upper ediface. These deposits are interpreted to have welded in-situ on shallower slopes (i.e. forming the Pinnacle Ridge Tuff), but repeatedly collapsed on the steeper slopes near Te Heuheu Peak (Figure 4.1) to form PDCs (i.e. PDC Unit 6). In contrast, the absence of a pre-existing conduit in southern Ruapehu is interpreted to have encouraged explosive excavation of a new vent, producing the plinian Okupata tephra and the Pourahu PDC (Unit 4). These hypotheses are further investigated in Chapter 5.

4.4.6 Heterogeneous small volume PDC deposits

These young PDC deposits are characterised by poorly sorted unwelded deposits containing denser, poorly vesicular juvenile clasts (see Chapter 5) with cauliflower surface textures.

PDC Package 2 (containing PDC Units 8-10)

PDC Package 2 is comprised of at least 3 different PDC units (PDC Units 8-10) that outcrop along a ~800m length of a small tributary valley of the Mangatoetoenui stream, immediately north of Tukino Village (Figure 4.1). Here the deposits form the main (basal) part of a valley-filling pyroclastic and colluvial deposit sequence.

Field Characteristics

The unconsolidated deposits are poorly exposed along a small stream and minor gulleys, and consist of localised PDC deposits making correlation between units difficult over distance. The uppermost unit (Unit 10) is a distinctive black deposit containing large cauliflower and breadcrust bombs (Figure 4.14, and Figure 5.21 in Chapter 5), and is the only unit that can easily be traced between outcrops. This is a useful stratigraphic marker. At least two poorly sorted orangish-yellow deposits (PDC Units 8 and 9) are observed in several locations in sequence beneath Unit 10. However these units cannot always be confidently correlated between outcrops due to differences in deposit and clast textures at the different locations. We therefore refer to the lower of the two as Unit 8, and the upper as Unit 9, but acknowledge the difficulties in confident correlations. Isolated surface patches

of Units 8-10 are observed upslope of Tukino village and also near the Whangaehu Gorge (WP181, Figure 4.1), extending their known areas of deposition towards a source near to South Crater and suggesting that parts of the PDCs may have also travelled along the Whangaehu valley. At Location WP108 (Figure 4.1), Units 8-10 immediately overly deposits from Unit 4 (Pourahu PDC), indicating that they are <11.6 ka B.P. cal. Field magnetic investigations show Unit 8 was emplaced hot with 8/11 clasts in both Unit 8a and Unit 8b showing aligned NRM (Table 4.1).

At location WP075 and several other locations alongside the tributary stream, small dense cauliflower bombs with very distinctive golden bands are commonly found near the base of the exposed deposits (Figure 4.15). These clasts easily disintigrate along prismatic joints, indicating that they were emplaced hot and only later developed these joints as the deposit cooled. At location WP109 (Fig 4.1), two texturally identical units (here referred to as PDC Unit 8a and 9a) *both* contain these distinctive banded clasts (Figure 4.15). However at the type section at location WP108 (Figure 4.14), the two units (Units 8b & 9b) do not contain any golden-banded bombs and are here separated by a lithic-rich deposit interpreted as a debris flow deposit or till (Figure 4.14). Despite the difficulties correlating Units 8 and 9 between locations, in *all* cases Units 8 and 9 contain moderately dense orangish-yellow primary clasts with olivey-brown interiors, in a medium to coarse ash matrix. In contrast to Units 8 and 9, Unit 10 is monolithologic and lacks the abundant lithic lapilli present in the underlying units (Figure 4.16). Despite these differences, the very top of Unit 9 appears to grade into PDC Unit 10; with a decrease in lithic contents and emergence of texturally similar large cauliflower bombs (Figure 4.14). This suggests that Units 9 and 10 were emplaced in quick succession.

Laboratory Characteristics

Primary pumices in PDC Package 2 (Units 8-10) range from 54.7 to 58.4 (bulk, anhydrous) % SiO_2 (Table 4.2, Figure 4.7) and form a distinct group in the CaO-MgO variation diagram (Figure 4.6) with significantly higher CaO and MgO than all other PDC Units.

The sieved data (Figure 4.16) highlights the relative lack of fines in Units 8 and 9,

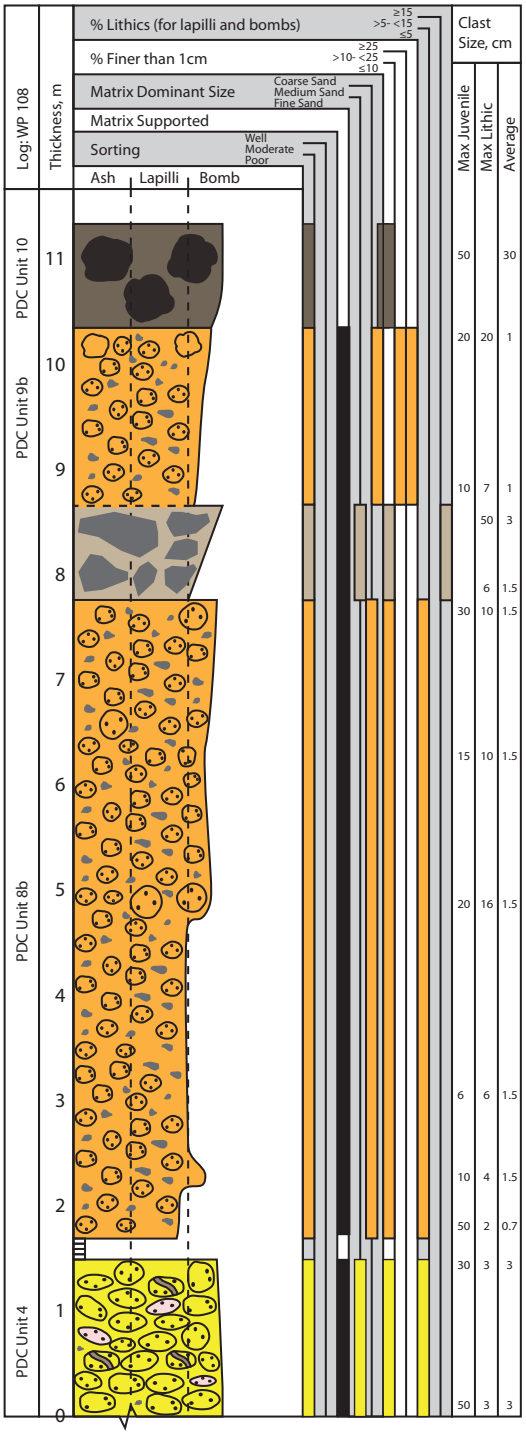

Observations	Interpretation
Monolithologic black-grey unit containing large cauliflower-textured juvenile bombs and occasional dense grey breadcrust bombs in a black matrix of subround lapilli and coarse ash. Contact with underlying unit has sharp colour change but texturally the large bombs at the top of Unit 9b are very similar	PDC Deposit
Increasing amounts of bomb sized clasts (<35cm) with cauliform textures near top of orange unit.	
Pale orangish yellow unit texturally similar to Unit 8b containing subround juvenile lapilli that are 2.5-5cm (long axis) and have plag (15%, 1-2mm), px (15-20%, 1-3mm) and small vesicles (<1mm). Base of unit gradational with underlying lithic-rich unit. Deposit is matrix supported but almost clast supported.	PDC Deposit
Very poorly sorted, lithic rich, orangish pink breccia with polymictic angular to subangular andesite lithics in an indurated fine to medium sand matrix	Proximal debris flow deposit or till
Top of Unit 8b has a sparse line of large (<30cm) equant cauliflower-textured bombs. .	
Above 5.2m, bombs (<20cm long axis) make up ~5% of the deposit but these are mostly absent below this point.	
Orangy-brown unit containing subround juvenile lapilli. Majority of deposit contains small (<1.5cm), relatively dense juvenile lapilli and ~5% lithics, with larger pumices (<10cm long axis) making up ~7% of clasts. Larger juvenile clasts contain plag (~25%, 1mm) and px (10%, 1mm) and have black interiors with small vesicles (<1mm). Smaller juvenile clasts have small vesicles (<0.5mm). Lithics are subangular and heterolithological with orange and red weathered surfaces. Deposit is matrix supported but almost clast supported.	PDC deposit
Thinly and thickly laminated orange, pink and grey fine sands.	Fluvial deposits
Very poorly sorted, pumice rich, whitish yellow deposit containing large equant bombs. Coarse lapilli and small bombs (<10cm) in a framework of <2cm pumice lapilli. Pumices are highly vesicular with large (<3mm) vesicles and have whitish-yellow to grey-brown interiors containing plag (10%, <2mm) and px (15%, <3mm). Occasional banded clasts with brown bands. At this location lithics are <3 % of all lapilli. Deposit is matrix supported (though nearly clast supported) here; in other locations it is clast supported.	Pumice-dominated PDC deposit

Figure 4.14: Representative stratigraphic log for PDC Unit 4 and PDC Package 2; Units 8-10, at WP108.

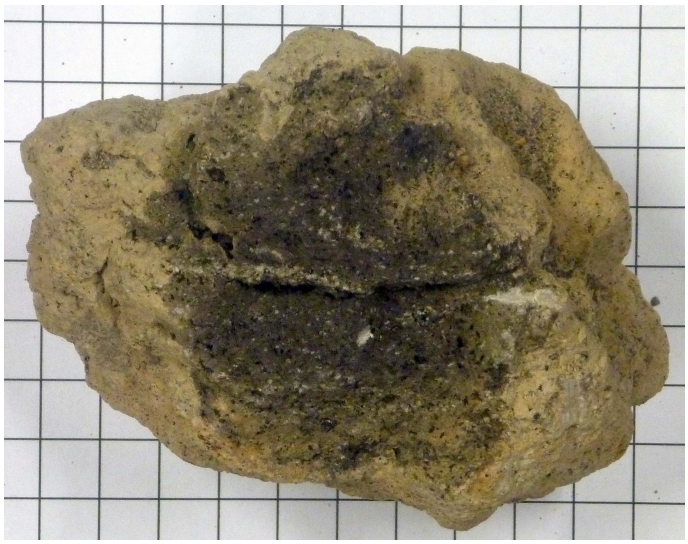

Figure 4.15: Banded sample X109AC from PDC Unit 8a, showing distinctive cauliflower surface texture and olivey-gold banding. Grid is 1cm squares.

with mainly unimodal grain size distributions and broad peaks spanning between -4 ϕ and 2 ϕ (medium lapilli to medium ash). In contrast, the dominance of large clasts in Unit 10 is reflected by a bimodal size distribution that peaks in the bomb size fraction and has an all-clasts median grain size of -3 ϕ, but also contains abundant medium-fine ash matrix (Figure 4.16). The very poorly sorted Unit 10 therefore falls comfortably within the PDC field on the Walker size-sorting diagram (Figure 4.9), while Units 8 and 9 all fall in Walker's fields for fines-depleted deposits associated with PDCs. This is in keeping with the field observations and sieved data that show these deposits lack abundant very fine matrix. The componentry of the -5 ϕ to -4 ϕ sieved fractions also support the field observations of high lithic contents in Unit 8 (28 to 33 % lithic clasts; Figure 4.16), as well the monolithologic nature of Unit 10 (100% primary clasts).

PDC Units 11 and 12

PDC Units 11 and 12 contain relatively dense cauliflower-textured bombs similar to those observed in PDC Package 1.

Field and Laboratory Characteristics

PDC Unit 11 directly overlies PDC Package 1 (Units 1-3), where it is preserved as discrete concentrations of large (up to 0.6m) grey-black cauliform clasts and occassional breadcrust

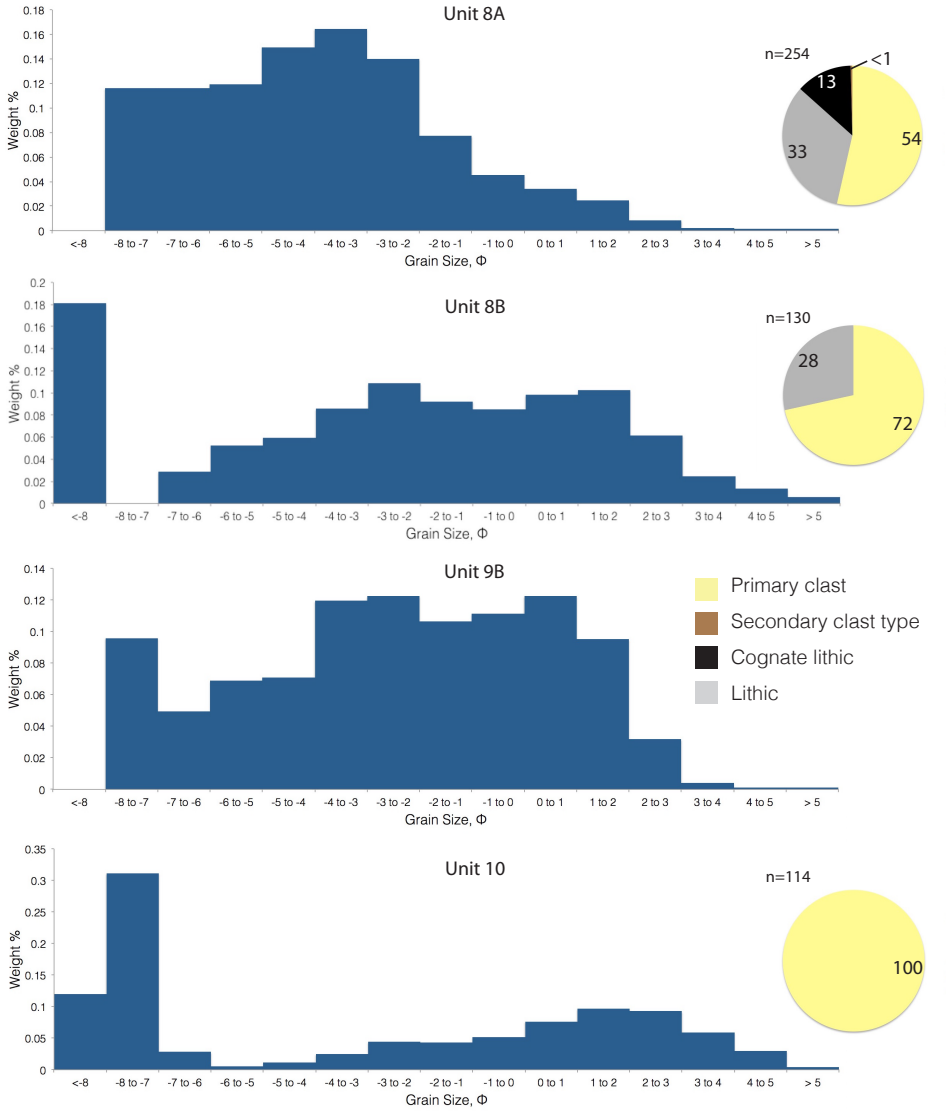

Figure 4.16: Total grain size distribution and corresponding whole-clast componentry from the -5ϕ to -4ϕ sieved size fraction for Ruapehu's heterogeneous small volume PDC Units 8a, 8b, 9b and 10 deposits. The coarse clasts in Unit 8b may reflect ballistic bombs that fell into the main PDC.

bombs (~3% of clasts) on the upper surface of PDC Package 1 (e.g. WP258; Figure 4.1). The deposits are superficially similar to PDC Unit 10, but the primary clasts are denser and greyer (Unit 10 is black) and have more weathered surfaces.

PDC Unit 12 is preserved close to Ruapehu's summit at Locations WP295-6 (Figure 4.1), where grey-black and red (oxidised) cauliflower-textured clasts up to 50cm in size mantle the surface. The cauliform clasts most closely resemble those in Unit 11, being slightly denser and less black than those in Unit 10. These deposits stratigraphically overlie

a small and extremely poorly exposed pumiceous deposit at Location WP295 that somewhat resembles the pumiceous PDC Package 1 Units. Both Units 11 & 12 are chemically similar to the underlying pumiceous PDC Package 1 (Table 4.2), and have significantly lower CaO and MgO than the texturally similar PDC Package 2 deposits (Figure 4.6).

4.4.7 Interpretation of the heterogeneous small volume PDCs

The poorly sorted, juvenile-rich deposits, together with evidence of hot emplacement (Unit 8), and reverse coarse-tail grading (Unit 9) gives 'very high' (Unit 8), 'high' (Unit 9) and 'medium' (Units 10-12) confidence that these are PDC deposits (Chapter 3, Figure 3.3). However, the direct deposit associations between these units and Ruapehu's other PDCs increase the confidence that *all* of these units are PDC deposits (adjusted ratings = 'very high' to 'high').

The deposits' small volumes, limited distribution, dense juvenile clasts, high lithic contents (Units 8a and 8b) and lack of known correlative tephras suggests subplinian or vulcanian-style eruptions of small batches of volatile-poor magma, possibly assisted by phreatomagmatic fragmentation (see Chapter 5 Section 5.4.6). We therefore propose that Units 8-12 were generated by collapses from small-moderate eruption columns not dissimilar to those observed at Ruapehu in 1995/96. Indeed, numerical modelling by Degruyter and Bonadonna (2013) found that Ruapehu's 1996 eruption column may have approached the envelope for collapse, and was possibly only stabilised by high atmospheric wind speeds at the time. PDC deposits from the 1975 vulcanian eruption of neighbouring Ngauruhoe volcano are texturally very similar to Ruapehu's Unit 10 (Figure 5.21 in Chapter 5), and eyewitness observations led Lube et al. (2007) to attribute those PDCs to ongoing collapses of rapidly accumulating piles of poorly welded proximal agglutinate, with lesser contributions from the collapsing part of the eruption column; we therefore suggest that Unit 10 was generated in a similar way.

PDC Package 2 (Units 8-10) indicates that at least 3 small PDCs were emplaced near Tukino ski village (Figure 4.1), with a minimum runout distance of 5 km and an estimated combined volume of 0.002 km^3 (Figure 4.1 and Table 4.3). The deposits directly overlie

deposits from the Pourahu PDC and so are <11.6 ka B.P. cal. The Tukino PDCs have no known correlative tephras, but their age (<11.6 ka), and their distribution supports a source at or near the presently active South Crater. This is in with keeping Ruapehu's shift to smaller, mainly phreatomagmatic and subplinian/vulcanian eruptions since the opening of South Crater at ~11.6 ka B.P. cal (e.g. Donoghue et al., 1997; Donoghue and Neall, 2001; Pardo et al., 2011). In this case, these are the youngest known PDCs to have occurred from the kind of small-moderate explosive eruptions that have characterised Ruapehu's historical activity.

PDC Units 11 and 12 are texturally similar to Unit 10, suggesting similar ascent, fragmentation and transport of small batches of relatively degassed magma (see Chapter 5). However, their stratigraphic and chemical associations with the underlying pumiceous PDC Package 1 suggests that these units were emplaced at the end of the ~13.6-11.6 ka plinian Ohinewairua eruptive period. This is consistent with modern observations of smaller eruptions of degassed residual magma continuing for some time after major plinian events (e.g. Mt St Helens, Cashman, 1992).

4.5 Discussion

4.5.1 Eruptive History

The PDC deposits preserved near to Tukino provide insight into the evolution of Ruapehu's eruptive activity during the past ~13.6 ka. The proposed eruption sequence based on the field observations is summarised in Figure 4.17. In general, the deposits support previous studies' interpretations (Donoghue et al., 1995b; Donoghue and Neall, 2001; Pardo et al., 2011) of a major shift at ~11.6 ka from large-scale plinian eruptions near North Crater to smaller scale activity from a new vent(s) near South Crater. However, since few airfall deposits are preserved on the main cone (Hackett and Houghton, 1989), Ruapehu's small volume PDC deposits resolve detail in the pyroclastic record that is not recorded by ring plain tephras (Figure 4.17).

PDC Units 1-3 confirm Pardo's (2014) hypothesis that increasingly unstable plinian

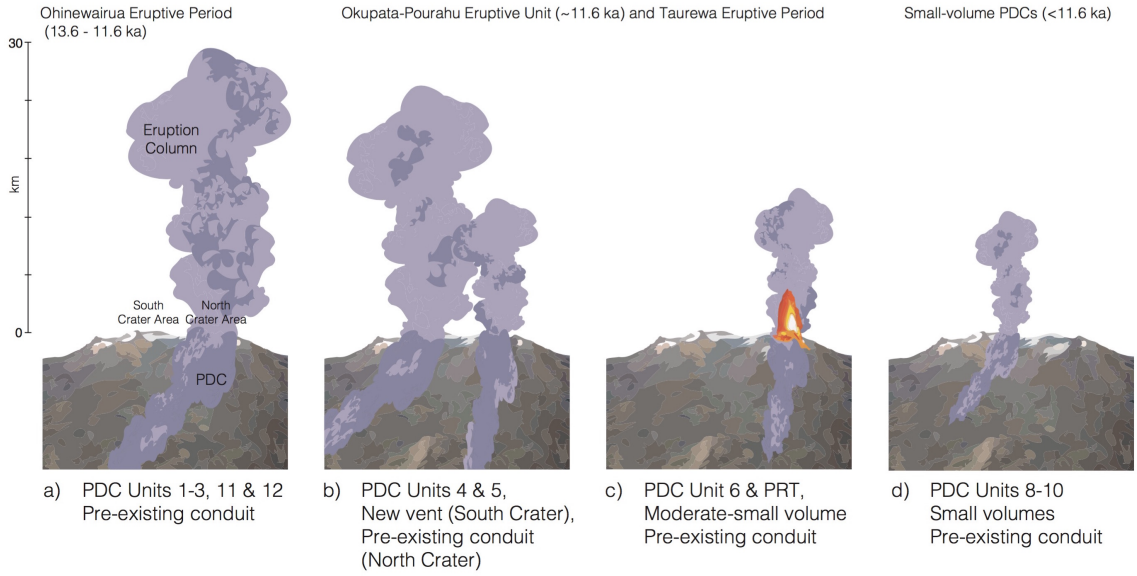

Figure 4.17: Schematic eruption sequence inferred from Ruapehu's PDC deposits. Column heights are drawn to approximate (interpreted) scale, and ice-cover at the time is not shown. a) Between 13.6 - 11.6 ka, plinian eruptions from the North Crater area produced increasingly unsteady eruption columns (Pardo et al., 2014) accompanied by sizeable PDCs in the Mangatoetoenui valley (pumiceous Units 1-3). The plinian sequence ended with smaller eruptions from more degassed magma that produced small-volume Units 11 and 12. b) At ~11.6 the plinian Okupata-Pourahu eruption explosively excavated a new vent near South Crater to produce the Okupata tephra (Pardo et al., 2011) and pumiceous PDC Unit 4 in the Whangaehu valley. At a similar time the pre-existing (i.e. more open-system) conditions in Northern Ruapehu permitted magma degassing and ascent, resulting in a short-lived eruption of a frothy magma (pumiceous Unit 5) followed by c) eruption of hot, more degassed magma through energetic fire-fountaining/spatter-forming eruptions that emplaced the welded Pinnacle Ridge Tuff and welded PDC Unit 6 deposits. Lack of stratigraphic controls prevents interpretation of the ages of welded PDC Unit 7 and the Te Heuheu welded spatter, but their preservation higher up the mountain suggests younger emplacement when the upper edifice was more ice-free. d) Ruapehu's activity then shifted (<11.6 ka) towards smaller (subplinian/vulcanian) eruptions from relatively degassed magmas sourced near the now semi-open southern vent. These eruptions emplaced small volume PDC Units 8-10 in the southern parts of the Mangatoetoenui and Whangaehu valleys.

eruption columns between 13.6-11.6 ka produced sizeable PDCs from Ruapehu's North Crater area. The stratigraphic position of Unit 11 on top of the pumiceous deposits, and chemical and textural similarities between Units 11 and 12, suggests that the plinian sequence ended with smaller eruptions from more degassed magma that also produced hazardous PDCs. This detail is not easily picked up in the ring plain tephras.

At ~11.6 ka, previous studies suggested large-scale eruptions in Northern Ruapehu produced the plinian Okupata tephra, Pourahu PDC (Unit 4), and Pinnacle Ridge Tuff (Hackett and Houghton, 1985; Hackett, 1985; Donoghue et al., 1999), which is also physically and chemically similar to the deposits identified in this paper as PDC Units 6 and 7 (Section 4.4.4). In contrast, Pardo et al. (2012, 2014) reinterpreted the Okupata-Pourahu eruptive unit as having a source near to South Crater on the basis of detailed isopach mapping in Ruapehu's eastern ring plain. The PDC deposits may partially resolve these conflicting interpretations (Section 4.4.5). Here, we suggest that a large body of volatile-rich, chemically distinct magma was emplaced under much of Ruapehu's edifice, near-simultaneously supplying vents in both the north and south. The mostly southern distribution of the Pourahu PDC along the proto-Whangaehu valley supports Pardo's (2011) interpretation that the source for this event was located near the presently active South Crater Area, and we therefore propose that the previously absent conduit in Ruapehu's southern summit area (i.e. a mostly closed degassing and magma ascent pathway) promoted explosive excavation of a new vent and produced the plinian Okupata tephra and pumiceous Pourahu PDC (Figure 4.17b). However, at a similar time the pre-existing conduit in Northern Ruapehu (i.e. a relatively more open degassing and ascent pathway) permitted pre-eruptive magma outgassing and magma ascent to shallower levels, resulting in a short-lived eruption of a frothy magma cap (pumiceous PDC Unit 5) followed by sustained eruption of hot, more gas-depleted magma (Chapter 5) through energetic fire-fountaining/spatter-forming eruptions that emplaced the welded Pinnacle Ridge Tuff and welded PDC Unit 6 deposits (Figure 4.17c). Lack of stratigraphic controls prevents interpretation of the ages of welded PDC Unit 7 and the welded spatter deposit near Te Heuhue peak. However, their presence shows that the well-establised Northern Ruapehu vent system provided an efficient mechanism for magma degassing and fire-fountaining/spatter eruptions on at least two other occasions.

Since ~11.6 ka, Ruapehu's activity appears to have shifted towards smaller (sub-plinian/vulcanian) eruptions from relatively degassed magmas (Chapter 5) sourced near the now semi-open southern vent. These eruptions emplaced hazardous PDCs (Units 8-10) in the southern parts of the Mangatoetoenui and Whangaehu valleys (Figure 4.17d), and the resulting deposits may now be the only record of these small but hazardous eruptions that are similar in scale to Ruapehu's modern activity.

4.5.2 Preservation potential of PDC deposits

Unconsolidated PDC deposits have low preservation potential and are particularly susceptible to laharic and fluvial erosion on a volcano's steep proximal flanks. Snow and glacial ice further reduces deposits' opportunities for preservation by limiting access to a solid substrate and providing meltwater for deposit reworking. Long-term preservation of primary PDC deposits is therefore reliant on the deposits physically escaping a volcano's active glacial and fluvial systems, either by deposition away from active erosion or by rapid burial (Figure 4.18).

Long-term preservation of PDC Package 1 (Units 1-3) appears to have only occurred due to a pre-existing split-valley topography that then isolated parts of the deposit from Ruapehu's active erosional system (Figure 4.18 a-d). Holocene erosion has since removed *almost all* trace of the deposits in the main valley, demonstrating just how rapidly even young and sizeable PDC deposits can be erased from a volcano's geological record. Had the split-valley topography not provided a conduit for deposit preservation (Figure 4.18 d), the entire PDC deposits from some of Ruapehu's largest plinian eruptions might have been completely overlooked.

PDC Unit 4 (Pourahu PDC) was mostly emplaced within the simple active valley system of the proto-Whangaehu gorge. Donoghue et al. (1999) found no primary Pourahu PDC deposits within 10km of source, and proposed that the channelised nature of the PDC restricted deposition until the flow emerged onto Ruapehu's ring plain. We suggest that poor preservation in the presence of glacial ice and an active glacio-fluvial system also

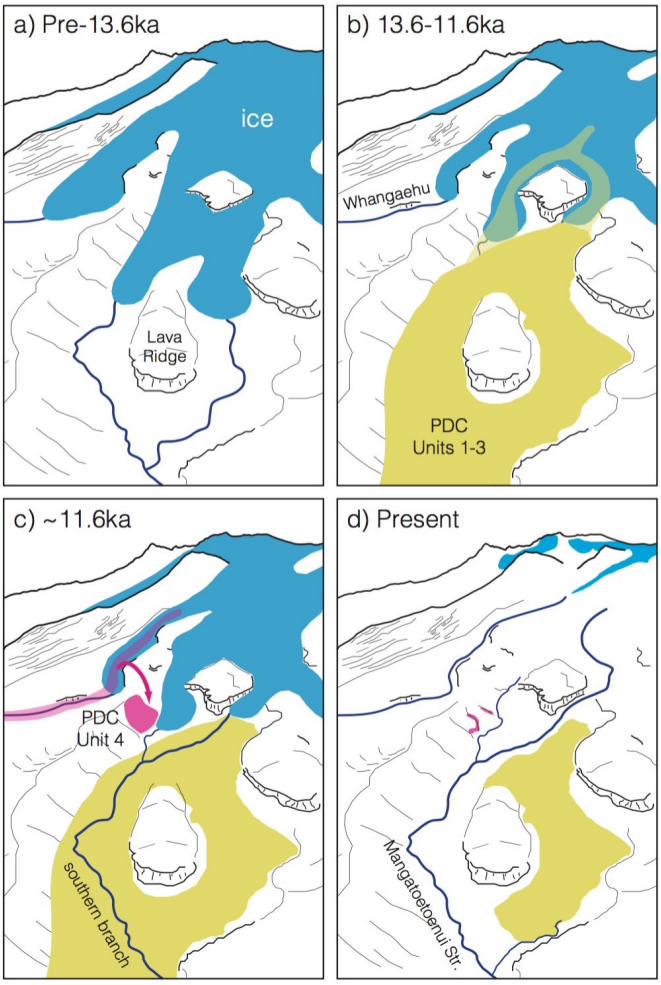

Figure 4.18: Interpreted deposition and preservation sequence for PDC Package 1 (Units 1-3; Ohinewairua PDCs) and PDC Unit 4 (Pourahu). a) The Mangatoetoenui valley originally split into two branches around a glacially-emplaced ridge-forming lava flow (cf. Lescinsky and Sisson, 1998). b) Units 1-3 (yellow) were deposited on proximal glacial ice and on ice-free ground in the Mangatoetoenui valley, temporarily blocking the valley and shutting off stream flow. c) The glacially-fed Mangatoetoenui stream re-established in only the southern valley branch, permanently abandoning its northern course. At a similar time, Unit 4 (pink) was emplaced along the proto-Whangaehu Gorge. At a bend in the flow path, upper parts of the PDC overtopped the moraine that forms the valley side, possibly assisted by valley-filling ice. d) PDC deposits in the main Mangatoetonui and Whangaehu valleys were then completely removed by erosion, whereas the Units 1-3 deposits in the now-inactive northern valley branch, and small patches of Unit 4 on the southern valley margins were preserved due to their locations away from the main glacio-fluvial system.

explains the lack of deposits, rather than just non-deposition. Although no proximal Unit 4 deposits remain in the Whangaehu valley, primary PDC deposits are preserved where they have overtopped the lateral moraine that forms the valley side by Tukino village. This process may have been assisted by valley-filling ice that subdued topography and promoted lateral dispersal (Fig 4.18 c). By overtopping the moraine the PDC deposits became physically removed from the active glacio-fluvial system, increasing their preservation potential. However, the resulting deposits may therefore *not* be representative of the bulk PDC, since they only represent the upper part of the PDC that escaped from its main channel. This may explain the low lithic contents (0 to ~3%) and large average pumice sizes (md_ϕ -4.6) observed (Section 4.4.1); reflecting the upper lower-density parts of a density-stratified flow. Similarly, the preserved deposit thickness is unlikely to be representative of the bulk main flow at this point, as it only reflects the time-integrated flow fraction that overtopped the moraine at the valley side.

The Ruapehu PDC deposits therefore illustrate three important considerations for both finding and interpreting proximal-medial PDC deposits in the field;

1. In the long term, unconsolidated deposits from small volume PDCs are more likely to be preserved at valley margins than in the main valley flow path.

2. Thicknesses and componentries of deposits at PDC margins will reflect only the portions of the flow sampled during deposition, including any vertical and lateral fractionation. They therefore may not be representative of the bulk PDC.

3. The poor preservation potential of unconsolidated PDC deposits means that prehistoric deposits, even when preserved, may significantly under-represent the size of the original PDC and extent of the hazard.

4.5.3 The significance of snow and ice

Snow and ice has significantly influenced Ruapehu's morphology, eruptive styles, deposit preservation, and hazards (Chapter 6). Ruapehu (2797m) currently hosts ~20 small glaciers and glacier remnants (Williams, 2013) as well as skifields at Turoa, Tukino, and New Zealand's largest commercial skifield at Whakapapa. A large Pleistocene ice cap fed out-

let glaciers (McArthur and Shepherd, 1990) that reached as low as 1300m between ~51-41 and ~27-15 ka (Conway et al., 2015), and many Ruapehu lavas show textural evidence for snow and ice contact during emplacement (Spörli and Rowland, 2006; Conway et al., 2015). Consequently it is very likely that many of Ruapehu's proximal eruptive products, including the PDC deposits described here, interacted with snow or ice for some of their transport (e.g. even today, significant snow covers the volcano for >4 months each year at elevations corresponding to the majority of the interpreted PDC deposits' transport paths). However, it is poorly understood whether this interaction would have an observable impact on the deposits.

Despite extensive ice cover at many modern stratovolcanoes, there have been relatively few studies addressing PDC deposit textures that directly indicate pyroclast-ice interaction. In modern examples of both ice-transported PDCs (Pierson et al., 1990; Gardner et al., 1994) and volcanic mixed avalanches (Pierson and Janda, 1994), large blocks of ice were observed to be incorporated into the primary deposits. Once melted, this caused significant deposit deformation (Pierson and Janda, 1994), but this would be difficult to identify in prehistoric deposits due to PDC deposits' already-poor sorting. At Klyuchevskoi volcano (Belousov et al., 2011), 10–20% of the bomb-sized clasts in PDC deposits emplaced over ice were observed to have quenched surfaces crisscrossed by a dense network of thin cracks, while at Nevado del Ruiz (Pierson et al., 1990) and Redoubt volcanoes (Pierson and Janda, 1994), thin fine-grained deposit basal layers were also observed. However, in general modern ice-transported PDC deposits do not appear to differ significantly to those from PDCs that did not interact with ice, making identification of prehistoric PDC-ice interaction difficult. This is the case at Ruapehu, where many of the unwelded PDC deposits do *not* show direct textural evidence of ice interaction. The lack of definitive ice-contact textures may also be due to a) limited basal deposition during transport that isolates most of the PDC from direct ice contact, b) insufficient meltwater/steam fluxes to significantly affect PDC textures, or c) sufficient ice-free transport at the end of the flow paths to remove any ice-contact clast textures before deposition. Nevertheless, some elements of the glacial story *can* be inferred from the *distributions* of the preserved deposits since prehistoric PDC deposits emplaced directly onto ice are unlikely to have been preserved. Therefore, the locations of remaining deposits can help to constrain the extent of ice cover

at Ruapehu at the time of emplacement. This could explain the relative lack of observed deposits within ~4km of source, consistent with new data (Conway et al., 2015, and C. Conway pers. comm.) that shows lava-ice contact features down to ~1700m as recently as 8.8 ± 2.2 ka. This approximately matches the starting elevation of all of the preserved ~13.6-11.6 ka Units 1-6 deposits.

In contrast to Ruapehu's unwelded PDC deposits, the Unit 6 deposits exhibit several textures (Section 4.4.4) that, when considered together, suggest the PDC may have interacted with snow or ice:

1. *The deposits contain very few weathered lithics*: The deposit appears nearly monolithologic, implying the PDC was mostly isolated from the volcanic surface during transport.

2. *Chilled clast margins up to ~1cm thick*: These reflect rapid clast quenching during transport, possibly assisted by water and steam from melting snow/ice.

3. *Unusually rapid clast rounding compared to Ruapehu's other PDC deposits*: Patel et al. (2013) found that rates of abrasion were significantly higher for quenched pumices compared to non-quenched samples; so continuous quenching, abrading, and then re-quenching of freshly exposed hot clast surfaces during transport over ice could explain the rapid rounding of the Unit 6 pyroclasts. This process would produce abundant ashy matrix of the same composition which, when coupled with meltwater or steam, could also generate an abrasive clast-ash slurry within the PDC (similar to that proposed by Walder, 2000b). We propose that such a slurry might further enhance the rounding efficiency, since the same principle is used in sand-and-water 'rock tumblers' to efficiently polish gemstones. However, further studies are needed to demonstrate this process in the context of PDCs.

4. *Glacial striations on the top of Unit 6* (Fig 4.2 d): These evidence later advance of glacial ice, and therefore indirectly support the presence of nearby ice at the time of deposition.

Most of these criteria are not *individually* diagnostic of pyroclast-ice interaction; PDCs

do not always entrain material they travel over (Roche et al., 2013), and phreatomagmatic fragmentation may also contribute to producing chilled clast margins similar to those observed here. However, explosive phreatomagmatism might also be expected to generate significant amounts of accessory lithic pyroclasts (McPhie et al., 1993), and these are not observed in the Unit 6 deposits. Similarly clast rounding is common in all PDC deposits, and so further studies are needed to demonstrate that the high rates of rounding in the Unit 6 deposits are best explained by transport over ice. Nonetheless, when all of these features are considered together, *and especially when combined with Ruapehu's known prehistoric ice extents* (Conway et al., 2015), we propose that these observations support the interpretation that PDC Unit 6 interacted with snow or ice during transport.

Ice may also explain the 'missing' (not preserved) southern parts of the welded Unit 6 deposit (Section 4.4.4), whose full original distribution is evidenced by a single small outcrop at WP177 where it was emplaced against an older ridge-bounded lava flow (Figure 4.1). Although fluvial processes may subsequently have eroded the 'missing' deposit, the remaining preserved parts of welded Unit 6 have shown considerable resistance to erosion. However, an alternative hypothesis is provided by new multiphase numerical simulations of meltwater generation when PDCs are transported over glacial ice, presented in Chapter 6. Here, we show that a PDC transported over ~2km of ice (i.e. the interpreted ice extent for Unit 6 at the time of deposition) can generate meltwater volumes equivalent to at least 50% of the volume of the main PDC bedload. Therefore, if this meltwater became sufficiently channelised in a pre-existing valley, it could then have *immediately* remobilised the 'missing' southern parts of Unit 6 *before* the deposit had a chance to weld.

In comparison to the Unit 6 deposits, the texturally similar but chemically distinct deposits from PDC Unit 7 higher upslope must have been emplaced at a time when the upper flanks were more ice-free, allowing access to a solid substrate for long-term deposit preservation. This supports the chemical evidence and the interpretation here that Unit 7 is a different PDC deposit to Unit 6, in contrast to Hackett (1985) and Chapman's 1996 earlier interpretations that these and the Te Heuheu welded spatter deposit were all part of the same unit. The bright red colour of parts of the Unit 7 deposits (Figure 4.13) suggests efficient *localised* thermal oxidation, and this might be explained by steam

from melting snow or ice acting as a high-temperature oxidant (Deal and Grove, 1965; Walker and Croasdale, 1971). Again, thermal oxidation is *not* uniquely diagnostic of ice interaction, and oxidised pyroclasts are a common feature of many proximal deposits from magmatic eruptions (e.g. Red Crater, Tongariro volcano, NZ; Wadsworth et al., 2015). However, the patchy, localised nature of the oxidation in parts of Unit 7 (Figure 4.13) is here interpreted to suggest that there was at least some snow/ice present at the time of deposition of PDC Unit 7.

In summary, given Ruapehu's glacial history (Conway et al., 2015) and the distributions of the preserved PDC deposits, it is likely that most, if not all, of the PDCs described here interacted with snow or ice in some way. However, only the Unit 6 deposits hint at this in the deposit textures. This therefore represents a significant challenge when interpreting prehistoric PDC deposits at similar glaciated volcanoes worldwide.

4.5.4 Hazard Implications

Perceptions of likely future hazards are strongly dictated by a volcano's known past activity. Therefore, with no historical granular fluid-based PDCs and few previously documented prehistoric deposits, the extent of Ruapehu's PDC hazard has been largely underestimated. The deposits described here record 12 young (<13.6 ka) granular fluid-based PDC units that span nearly all of Ruapehu's known eruptive styles. Additionally, poor preservation of small-volume unconsolidated deposits, as well as extensive prehistoric ice extents, suggests that significantly more PDCs may have occured at Ruapehu during this time. Newly rediscovered images of a possible granular fluid-based PDC in 1945 (Figure 4.1 a), as well as numerical modelling by Degruyter and Bonadonna (2013) that suggests high wind speeds may have stabilised Ruapehu's 1996 eruption column, both suggest that the absence of significant historical PDCs may not be representative of the modern hazard. Most of the PDC deposits described in this study reach >4 km from source (Table 4.3), demonstrating that even small-volume PDCs can impact Ruapehu's skifields and present significant risk to life and infrastructure. Units 8-12 represent PDCs from smaller eruptions not dissimilar to Ruapehu's modern activity, while steep topographic gradients appear to have also been significant in generating PDCs (Units 6 & 7) from collapse of proximal

spatter/cinders emplaced by fountaining/spatter eruptions not normally associated with a PDC hazard. Summit snow or ice may have exacerbated the collapse of accumulating proximal material (e.g. Belousov et al., 2011), and may also have contributed to increased PDC mobility (Chapter 6). Therefore, steep vent-proximal topographic gradients and summit snow/ice are important considerations for identifying areas of heightened future PDC risk. The proximal deposits observed near to Tukino underscore that hazardous PDCs can occur at Ruapehu across a full range of eruptive styles and magnitudes, and represent a significant future risk to life and infrastructure.

4.6 Conclusions

Despite absence of significant PDCs in historical time, newly described deposits close to Ruapehu's Tukino ski village evidence at least 12 granular fluid-based PDCs at Ruapehu during the past ~13.6 ka.

1. Hazardous PDCs have been generated at Ruapehu across a wide range of eruption styles, including collapsing plinian eruption columns (Units 1-4), periodic collapse of accumulating erupted material on steep slopes (Units 6-7), and collapsing eruption columns from smaller eruptions similar to Ruapehu's modern activity (Units 8-12).

2. The deposits provide a detailed record of prehistoric variability in eruption styles and sources at Ruapehu not resolved in the tephra-fall record, including resolving contrasting eruptions from multiple vents at ~11.6 ka as part of the Taurewa eruptive period (PDC Units 4-6). The PDC deposits also reveal smaller-scale eruptions from more degassed magma at the end of the plinian Ohinewairua eruption sequence (Units 1-3, 11 & 12) . These observations are investigated in more detail in Chapter 5.

3. The glacial record suggests most of Ruapehu's PDCs encountered ice during emplacement, which appears to have affected their transport and preservation. The locations of prehistoric deposits may reflect the limit of prehistoric ice extents rather than the onset of PDC deposition. The effects of ice on PDC transport are further investigated in Chapter 6.

4. Small volume proximal PDCs are the most frequent but least-well preserved PDCs at many volcanoes. Long-term deposit preservation is most likely at PDC margins away from active valley erosional systems, but for every deposit preserved many more may never make it into the geological record; especially when emplaced in the presence of glacial ice. Therefore systematic identification of *all* prehistoric PDC deposits (Chapter 3), even where poorly preserved, is essential to properly characterise a volcano's PDC hazard.

5

Textural insights into PDC generation at Mount Ruapehu, New Zealand

Introduction to Chapter 5

This chapter extends the field-based observations presented in Chapter 4 to consider the underlying magmatic, conduit and eruption-level processes that led to PDC generation at Ruapehu. We take a deeper look at the chemical and physical properties of pyroclasts within the PDCs, and assess how Ruapehu's heterogenous magmatic system has directly contributed to PDC events. This data is used to address the broad-scale factors affecting PDC generation at Ruapehu across a wide range of eruptive styles.

The key outcomes are:

1. Recognition that bulk pyroclast densities underpin the conditions for PDC generation through their direct effect on the buoyancy of the erupted pyroclast-gas mixture.

2. Testing and application of a new MELTS-based geobarometer being developed at Vanderbilt University, USA, to assess the magmatic storage conditions for Ruapehu's PDC-forming eruptions. These pre-eruptive conditions directly affect the pyroclast densities and the stability of the erupting mixture.

3. Observation that the very heterogenous magma system at Ruapehu, most visually expressed by abundant banded pyroclasts, frequently results in less stable eruption styles that are more likely to generate PDCs. This is an important consideration when assessing the future PDC hazard at Ruapehu and similar volcanoes worldwide.

The chapter is presented in the style of an academic paper, though with expanded detail that will be condensed for submission to a peer-reviewed journal. As such, the relevant contextual background and analysis methods are presented in full. The chapter follows the same structure as Chapter 4 by considering each of Ruapehu's PDC types in turn. Thus, the results for the pumicous PDCs, welded PDCs, and heterogenous small-volume PDCs are each immediately followed by their respective interpretations, while the discussion section is reserved for the wider whole-mountain implications.

Abstract

Pyroclastic density currents (PDCs) are a major volcanic hazard that have killed nearly 260,000 people since 1783. Understanding the types of PDCs that have occurred at a volcano and the processes leading to their generation is essential for hazard assessment and risk management. At Mt. Ruapehu, large PDCs have been absent in historical time, but >12 young deposits on Ruapehu's eastern and southern flanks reveal that they have been a frequent occurrence over the past ~13.6 ka. Here, we present results from detailed textural studies of Ruapehu's PDC deposits to gain insight into the processes that led to PDC generation. We combine these textural observations with results from a new rhyolite-MELTS based method for characterising the pressure-temperature regime of Ruapehu's magma storage systems. The textural and geochemical modelling results link PDCs to most of Ruapehu's known eruptive styles, and suggest that the type of PDC is strongly dictated by the underlying magmatic system. Magma storage depths and temperatures, proportions of magma mingling, and open vs. closed systems have strongly influenced the eruptive styles and nature of the PDC hazard. Our field and textural observations suggest that these factors control the amount of pre-eruptive degassing and hence clast density. Large column collapse PDCs accompanied Ruapehu's largest plinian eruptions from deep (4.1-6.0 km), and hence initially gas-rich magmas (PDC Units 1-4). Here, we interpret PDC generation to be affected by both vent widening (PDC Unit 1) and also densification of the erupting mixture due to mingling with denser secondary melts (PDC Unit 2). Mingling may also have been instrumental in triggering these eruptions (e.g. PDC Unit 4). Hazardous PDCs have also occurred from smaller column collapse and 'boiling over' style eruptions (PDC Units 8-10) of shallow (<2.2 km), relatively gas-poor magmas somewhat similar to Ruapehu's modern-day magma system. A third kind of PDC (Units 6 & 7) has been generated at Ruapehu on at least 2 occasions where hot, slightly degassed erupted material has rapidly accumulated as spatter/cinders on steep slopes and then repeatedly collapsed to form PDCs. Heterogeneous storage and ascent pathways and the ubiquity of magma mingling at Ruapehu, as well as the role of shallow magma degassing, are therefore important considerations when assessing the PDC hazards at this volcano.

5.1 Conditions leading to PDC Generation

Pyroclastic density currents can be triggered by any process that results in gravitational collapse of hot volcanic material, including collapsing eruption columns (Nairn and Self, 1978), collapsing lava domes and flows (Boudon et al., 1993; Saucedo et al., 2004; Belousov et al., 2011), and co-eruptive remobilisation of erupted material deposited on steep slopes (Yamamoto et al., 2005). In general, these processes fall into one of two categories a) collapse of explosively erupted volcanic material, or b) collapse of freshly erupted material already resting on the the volcano's surface.

5.1.1 Pyroclastic density currents generated by collapse of explosively erupted material

When pyroclasts and gas are explosively erupted from a volcanic vent, the initial density of the erupted mixture can be several times that of the surrounding ambient air, but it will initially move due to its momentum. This material may then either follow ballistic trajectories (Breard et al., 2014; Fitzgerald et al., 2014) in which the pyroclasts travel mostly decoupled from erupted or entrained gas, it may entrain and heat surrounding air and form an eruption column, or it may be expelled laterally in a directed blast (Lube et al., 2014). In each case, PDCs can be generated if the erupted material collapses and continues its motion along the volcanic flanks.

In the case of ballistically-transported components, small PDCs can be generated if large numbers of erupted pyroclasts land on proximal slopes and continue downslope under their own momentum (e.g. Yamamoto et al., 2005). If the avalanching material entrains fine material and air it can then transform into a coupled pyroclast-and-gas density current. This process was observed at the base of the sub-plinian eruption column from Ngauruhoe volcano in 1975, where low spatter/fountaining at the base of the eruption column directly fed PDCs (Lube et al., 2007; Figure 5.1).

When the explosively erupted gas-pyroclast mixture forms an eruption column, the column must first collapse in order to generate a PDC. This occurs if the erupted material loses its upward momentum before it has entrained and heated sufficient air to reduce its

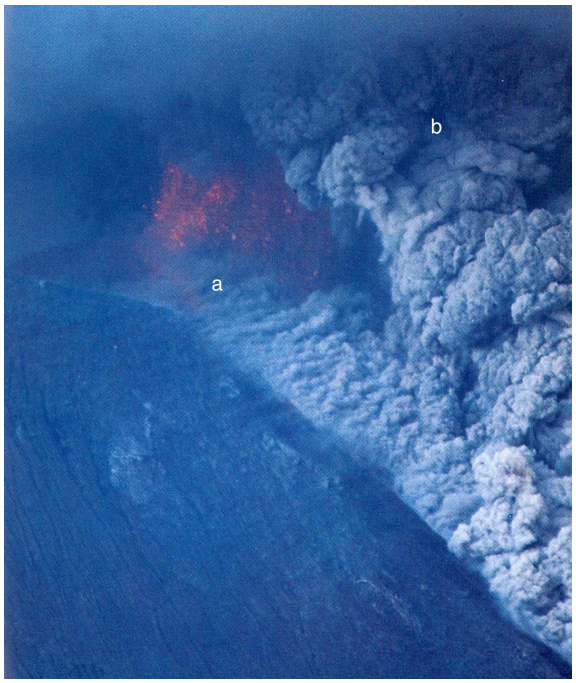

Figure 5.1: Nguaruhoe volcano's 1975 sub-plinian eruption column demonstrating two simultaneous mechanisms that may have contributed to PDC generation: a) Spatter/fountaining at the base of the column with the ballistic blocks landing on the steep proximal flanks, continuing downslope and possibly transitioning into a pyroclastic density current as they mobilise additional material. b) 'Boiling-over' or low collapse of part of the main erupted pyroclast-gas mixture that has insufficient momentum and buoyancy to ascend with the main column, instead transitioning immediately into a PDC.

density below that of the surrounding atmosphere (Koyaguchi et al., 2010). In this case, the column will collapse and continue its motion along the surface as a PDC. In contrast, if the bulk density of the eruption cloud becomes lower than atmospheric density before losing its upward momentum, it will instead continue to ascend as a buoyant plume and will not collapse.

Early 1-dimensional models of eruption column stability related the collapse condition to increasing vent radius (r_v) or mass discharge rate ($\dot{m}$), and decreasing water content (n) or exit velocity (u_0) of the erupting mixture (Fig 5.2, Wilson et al., 1980). This led to the theory that plinian-style eruption columns are likely to transition during the course of an eruption from stable to collapsing regimes as a result of vent widening by erosion and/or eruption of progressively deeper magma (with lower exsolved water contents) from a stratified chamber.

More recent 1-, 2- and 3-dimensional numerical models have investigated the effects of

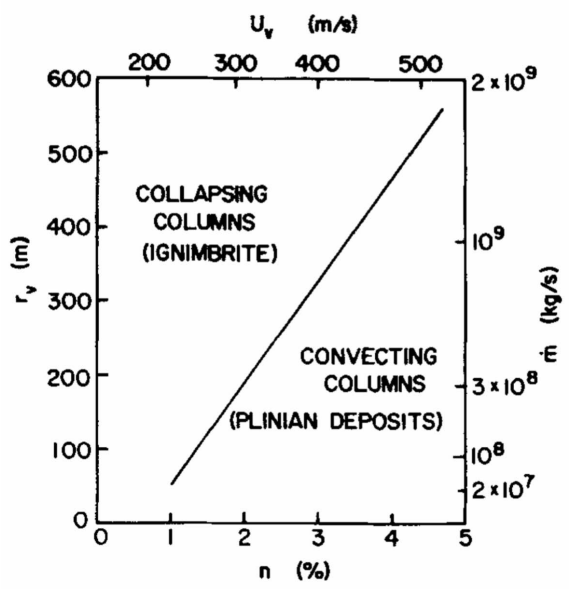

Figure 5.2: Conditions for collapse of volcanic eruption columns from 1D numerical simulations (Wilson et al., 1980). Eruption exit velocity u_v is considered to be primarily controlled by exsolved water content n, and is used interchangeably. Likewise, mass discharge rate $\dot{m}$ is considered to primarily be a function of vent radius r_v for constant exit velocity.

additional physical parameters to eruption column stability, including the contribution of turbulent mixing between the erupting mixture and the surrounding air (Carazzo et al., 2008), the importance of over-pressure at the vent (Ogden et al., 2008a,b), and the effects of conduit shape and the presence of a volcanic crater (Koyaguchi et al., 2010). These studies, and constraints from the May 18th 1980 eruption of Mt St Helens (Carey et al., 1990), revealed that in some cases even decreasing mass eruption rate can to lead column collapse (Koyaguchi et al., 2010). This emphasises the importance of detailed multiphase modeling of all components of the erupting system from the chamber upwards. Nevertheless, the latest 3D models (e.g. Suzuki and Koyaguchi, 2012) still usually associate the collapse condition with increasing mass discharge rates and/or decreasing exit velocities of the erupting mixture (Figure 5.3 and Box 5.1). The general considerations for PDC generation by collapse of volcanic eruption columns can also be extended to PDCs directly generated by directed blasts (e.g. Mt St Helens, 1981; Belousov et al., 2007) and/or 'boiling over' (Fisher and Heiken, 1982) style eruptions (e.g. Ngauruhoe 1975, Fig 5.1). Here, the major difference in both cases is that the erupted mixture reaches the collapse threshold without first ascending as part of a vertical column.

Box 5.1: Physical parameters affecting mass discharge rate and exit velocity:

The mass discharge rates ($\dot{m}$) and exit velocities (u_v) of an erupting mixture from a circular vent are related by the formula:

$$\dot{m} = \pi \rho_0 u_0 L_0^2 \tag{5.1}$$

where ρ_0 is the initial density of the erupting mixture and L_0 is the vent radius. In turn, the initial density of the erupting mixture ρ_0 is a function of the magma density, volatile content, pressure and temperature. Similarly, u_0 is primarily a function of magmatic water content, but again also relates to the magmatic density, pressure and temperature. *These therefore define the key underlying parameters involved in understanding collapse of volcanic eruption columns.*

An apparent contradiction of column collapse models presenting mass discharge rate and exit velocity as independent discriminators of column collapse is that Equation 5.1.1 shows these parameters are directly correlated; such that a reduction in exit velocity (i.e. moving *towards* the collapse condition) also results in a decreased mass discharge rate (i.e. moving *away from* the collapse condition). The contradiction is resolved by the fact that column collapse is more sensitive to exit velocity, such that a 50% reduction in u_0 (and accompanying 50% reduction in $\dot{m}$) nonetheless moves the erupting mix closer to the collapse threshold (Figures 5.2 & 5.3).

5.1.2 Pyroclastic density currents generated by gravitational collapse of erupted material already resting on the volcanic surface

In addition to PDCs directly generated by volcanic explosions, PDCs can also be produced by gravitational collapse of lava domes (Cole et al., 1998; Calder et al., 1999) and lava flows (Saucedo et al., 2004). Here, the gravitational potential energy of lava effusively emplaced on a volcano's surface provides much of the initial energy for fragmentation and movement, though decompression of volatiles in the lava (e.g. Sparks, 1997) during the collapse event can also promote further fragmentation. Following fragmentation, exsolution of volatiles and entrainment of ambient air allows rapid transition to a pyroclastic density current. In

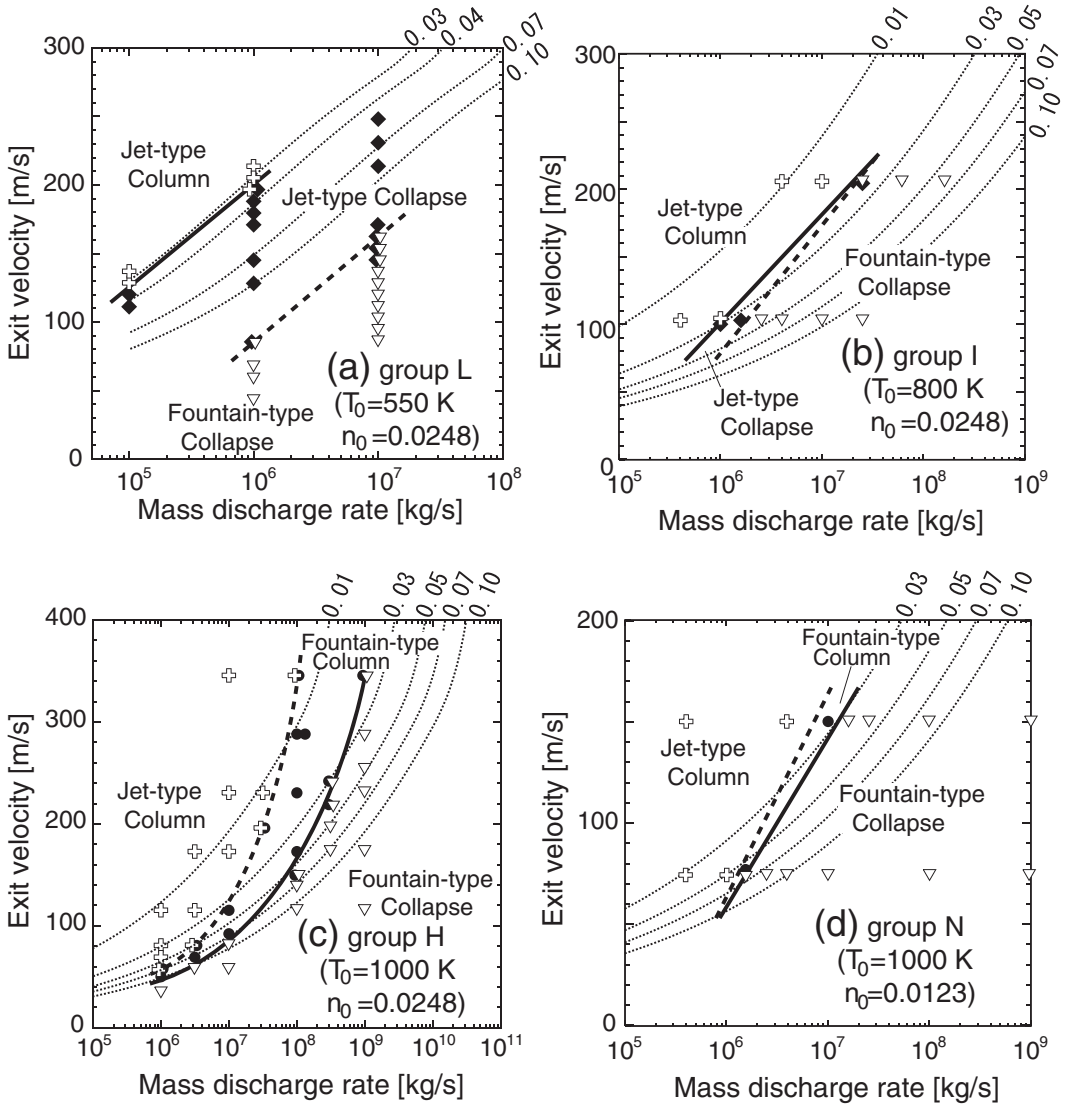

Figure 5.3: Conditions for collapse of volcanic eruption columns from 3D numerical simulations (after Suzuki and Koyaguchi, 2012). Intial temperatures (T_0) and water contents n_0 of the model runs are listed in each box. Eruption columns are modelled to typically develop an annular structure with a dense inner core surrounded by an outer shear zone that turbulently mixes with the surrounding atmosphere. In this context, 'fountain-style' collapse occurs in columns whose inner core has remained isolated prior to collapse, whereas 'jet-style' collapse occures when the column has fully mixed before collapsing.

practical terms, PDC generation by pure gravitational failure is only an end member, and explosive disruption of dome material (e.g. Fink and Kieffer, 1993; Voight and Elsworth, 2000) or hydrovolcanic disruption of lava flows travelling over ice or water (Belousov et al., 2011) is common. In keeping with explosively generated PDCs, the density and buoyancy of the resulting pyroclast-gas mixture is key to the PDC behaviour. Again, this is largely controlled by the temperature, pressure (≈ atmospheric), density and volatile content of the lava immediately prior to collapse. However, unlike explosively generated PDCs, the initial velocity of the material is near-zero, and initial volatile contents in the lava are likely to be lower due to the effusive nature of lava eruptions.

A third kind of PDC generated by gravitational failure is the co-eruptive collapse of unstable near-vent piles of erupted material. This process was reported at Ngauruhoe in 1975 (Lube et al., 2007) and directly observed and filmed in 1984 at Manam volcano, Papua New Guinea (Appendix 7.1, B. Scott pers. comm). At Manam, regular but intermittent strombolian activity was observed to construct a spatter rampart that periodically collapsed between explosions (i.e. during non-eruptive periods) to produce PDCs. Unlike collapsing lava domes and flows, the pyroclastic material in this case *is* first explosively erupted, but has then temporarily come to rest *before* collapsing en-mass to produce a PDC.

5.1.3 Magmatic Systems at Intermediate Arc Volcanoes

While the bulk density of a moving gas-pyroclast mixture directly controls PDC generation, it is the underlying magmatic system that dictates the nature of the erupted material. Magma storage regions at intermediate arc volcanoes like Ruapehu are often complex, heterogeneous systems involving frequent small magmatic inputs and mixing and mingling of components (Eichelberger, 1975) within long-lived crystal-mush zones (Bragagni et al., 2014). Ongoing processes such as cooling, crystallisation and degassing are offset by frequent episodes of magma recharge that bring heat and volatiles into the shallow magma system (Cashman and Blundy, 2013). Recharge is commonly attributed to hot mafic magmas entering more evolved storage zones (e.g. Montserrat; Murphy et al., 1998; Murphy and Sparks, 2000, and Tongariro; Shane et al., 2008), but several studies

have also described inputs of hotter, but *compositionally similar* magmas that contribute thermal energy to the crystal mush (e.g. Smith et al., 2009; Cashman and Blundy, 2013). Mixing between existing magmas and new magmas is common (Nakamura, 1995; Nakagawa et al., 1999; Nakagawa, 2002) and has been widely recognised as a mechanism for triggering volcanic eruptions through the input of heat and/or volatiles to the resident magma (Sparks et al., 1977; Donoghue et al., 1995a; Eichelberger, 1995). Mixing/mingling is most efficient when there are only small density and viscosity differences between the different magmatic components (Snyder, 1997), and directly affects the physical properties of the erupted material (e.g. composition, volatile content, crystal content, temperature, density, viscosity). This in turn will directly affect the momentum and buoyancy of the erupted mixture, and hence is also significant for PDC generation.

5.1.4 General considerations for pyroclastic density current generation and transport

Despite the many different ways that PDCs can be generated (Sections 5.1.1 and 5.1.2), in all cases they require an initial input of moving fragmented material on the surface of a volcano, and they then travel as coupled pyroclast-gas mixtures whose bulk density is greater than that of the surrounding atmosphere. Therefore, the 'recipe' for producing PDCs of any kind can be considered in terms of *momentum* and *buoyancy*:

1. *Momentum:* PDC generation requires fragmented erupted material (i.e. mass) to be set in motion along the flanks of a volcano (i.e. velocity): this can be caused by directed volcanic blasts, collapse of an eruption column, fall-out of ballistic clasts onto a slope, or explosive and non-explosive collapse of lava domes or flows.

2. *Buoyancy:* A PDC requires incorporation of sufficient gas (whether primary volcanic gas or entrained air) that the moving mixture behaves as a coupled pyroclast-gas current whose bulk density is greater than the atmospheric density (i.e. not buoyant). The thermal energy of the erupting mix is important, and increases buoyancy by heating entrained air and reducing the bulk density of the coupled pyroclast-gas mixture.

Table 5.1 outlines the *key parameters* controlling PDC momentum and buoyancy, and

the methods used in this study to measure and investigate these controls. As a general observation, Table 5.1 shows that *denser melt and pyroclasts* (Shea et al., 2011), *lower pre-fragmentation volatile contents, and lower pyroclast temperatures* are all conducive to PDC generation. In this chapter, we consider each of these parameters in order to provide insight into the processes that led to the generation and transport of Ruapehu's prehistoric PDCs (Chapter 4).

5.2 Overview of Ruapehu's PDC deposits

12 young (~13.6 ka) PDC deposits are exposed near the Tukino Ski Area on Ruapehu's eastern flanks. Initial field observations presented in Chapter 4 suggest these were formed by a variety of different eruption and PDC generation mechanisms, including:

1. Collapsing plinian eruption columns that produced large pumice-dominated PDC deposits.

2. Repeated collapses of proximally accumulating spatter on steep slopes that combined to produce variably welded, bedded, scoria-dominated PDC deposits.

3. Smaller collapsing eruption columns that produced heterogenoues small-volume PDC deposits.

Figure 5.4 summarises the stratigraphy and correlative eruptive periods of the 12 PDC Units outlined in Chapter 4. Here, we expand upon these field-based observations by detailing the chemical and textural features of clasts within the PDC deposits, as well as modelling the magmatic storage conditions prior to the PDC-forming eruptions.

5.3 Methods

5.3.1 Chemical pyroclast analyses

The whole rock and glass chemistry of the primary pyroclasts reflect the magma (melt + crystals) and melt compositions at the time of eruption. These directly affect the density of the erupted solid fractions (i.e. dense rock equivalent density and glass density of the

Momentum (input energy)	**Buoyancy (bulk density of the gas-pyroclast mix)**	**Observation method**
Gravitational potential energy		Not directly measured but controlled by eruptive parameters and column height
Magma composition	Magma composition	CHEMISTRY: XRF whole rock
Melt composition	Melt composition	CHEMISTRY: SEM-EDS glass analysis
Magma/melt density	Magma/melt density	CHEMISTRY: Melt density from chemistry; TEXTURES: pyroclast densities
Magmatic / eruption pressures		MODELLING: New MELTS-based geobarometer; Requires glass composition and knowledge of crystallising phases
Magmatic / eruption temperatures	Eruption temperature (heats gas phase and lowers bulk density)	MODELLING: Maximum chamber temperature estimated using new MELTS-based geobarometer; provides a general indication of eruption temperature
Magmatic volatile content (affects ascent, fragmentation, eruption and initial density of the erupting mixture)	Magmatic volatile content (affects pyroclast vesicularity)	MODELLING: Water contents estimated using new MELTS-based geobarometer
Pre- or syn- eruptive degassing/outgassing (affects eruptive volatile contents)	Pre- or syn- eruptive degassing/outgassing (affects pyroclast vesicularity)	TEXTURES: Pyroclast vesicle textures in thin section and tomographic images
Mass-eruption rate and exit velocities		Not directly measured but controlled by the eruptive parameters e.g. volatile content
	Entrained (non-magmatic) gas fraction	Not measured
	Grain size distribution of the erupted mixture and PDC	TEXTURES: Field and laboratory sieving of deposit grain sizes
	Componentry of the erupted mixture (including vent erosion and lithics) and PDC (including entrained lithics)	TEXTURES: Clast componentry of the -5 to -4 ϕ lapilli
	Density of the clast components	TEXTURES: Bulk density measurements of the -5 to -4 ϕ lapilli; Calculated melt densities
	Vesicularity and vesicle structures of the clast components	TEXTURES: SEM imagery, Synchrotron tomography

Table 5.1: Parameters affecting the momentum (or input energy) and buoyancy (or bulk density) of erupting fragmental material, and the investigation methods used here to provide insight into PDC generation at Ruapehu.

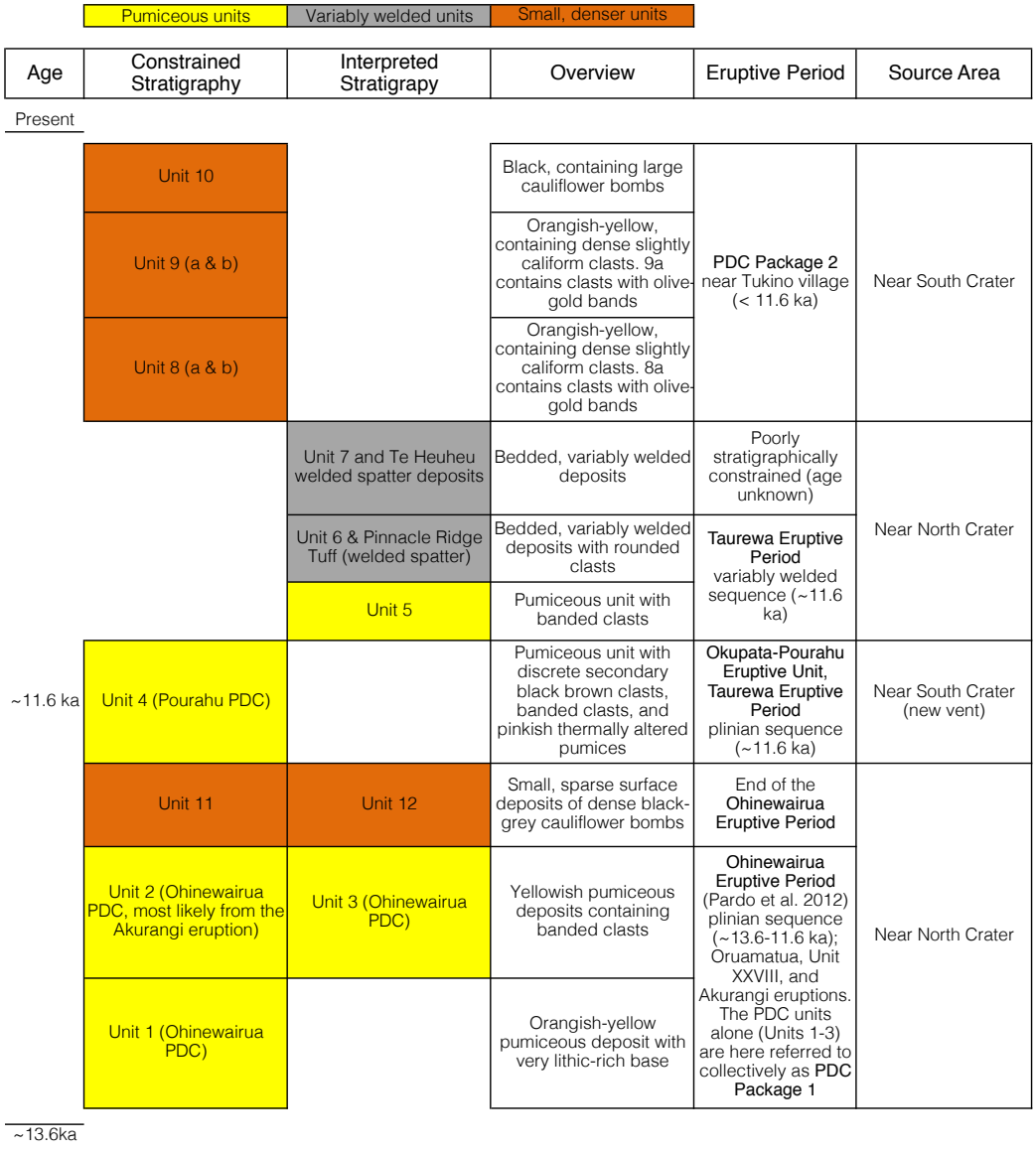

Age	Constrained Stratigraphy	Interpreted Stratigrapy	Overview	Eruptive Period	Source Area
Present					
	Unit 10		Black, containing large cauliflower bombs	PDC Package 2 near Tukino village (< 11.6 ka)	Near South Crater
	Unit 9 (a & b)		Orangish-yellow, containing dense slightly caliform clasts. 9a contains clasts with olive-gold bands		
	Unit 8 (a & b)		Orangish-yellow, containing dense slightly caliform clasts. 8a contains clasts with olive-gold bands		
		Unit 7 and Te Heuheu welded spatter deposits	Bedded, variably welded deposits	Poorly stratigraphically constrained (age unknown)	Near North Crater
		Unit 6 & Pinnacle Ridge Tuff (welded spatter)	Bedded, variably welded deposits with rounded clasts	Taurewa Eruptive Period variably welded sequence (~11.6 ka)	
		Unit 5	Pumiceous unit with banded clasts		
~11.6 ka	Unit 4 (Pourahu PDC)		Pumiceous unit with discrete secondary black brown clasts, banded clasts, and pinkish thermally altered pumices	Okupata-Pourahu Eruptive Unit, Taurewa Eruptive Period plinian sequence (~11.6 ka)	Near South Crater (new vent)
	Unit 11	Unit 12	Small, sparse surface deposits of dense black-grey cauliflower bombs	End of the Ohinewairua Eruptive Period	Near North Crater
	Unit 2 (Ohinewairua PDC, most likely from the Akurangi eruption)	Unit 3 (Ohinewairua PDC)	Yellowish pumiceous deposits containing banded clasts	Ohinewairua Eruptive Period (Pardo et al. 2012) plinian sequence (~13.6-11.6 ka); Oruamatua, Unit XXVIII, and Akurangi eruptions. The PDC units alone (Units 1-3) are here referred to collectively as PDC Package 1	
	Unit 1 (Ohinewairua PDC)		Orangish-yellow pumiceous deposit with very lithic-rich base		
~13.6ka					

Figure 5.4: Summary stratigraphy and simplified deposit characteristics of the 12 PDC units observed near to the Tukino Ski Area in eastern Ruapehu (Chapter 4).

pyroclasts), as well as pre- and syn-eruptive dynamics through the effect of composition on magma buoyancy, viscosity and the associated movement of exsolved volatiles.

Whole-rock XRF Analyses

Pyroclast whole-rock geochemistry (Appendix 2) is here used to distinguish broad-scale geochemical trends for PDC suites linked by common eruptive styles (Chapter 4), and to investigate geochemical heterogeneity and magma mingling processes that may have contributed to PDC generation.

Whole-rock analyses were conducted at the University of Canterbury using a Phillips PW2400 Sequential Wavelength Dispersive X-Ray Fluorescence Spectrometer calibrated against certified international standards, and based on methods by Norrish and Chappell (1967) and Norrish and Hutton (1969). Samples from primary and secondary clast types (Section 5.3.3) were cut and ground to remove surface weathering, rinsed in deionised water and dried overnight before grinding to a fine powder. Whole rock major elements were analysed using fusion beads and a rhodium tube set at 50KV/55mA, with loss on ignition calculated after fusion.

Pyroclast glass analyses: Quantitative Energy Dispersive X-ray Spectroscopy

Pyroclast glass chemistry is here used to distinguish different melt components in mingled clasts, and is also the required input to a new rhyolite-MELTS based geobarometer (Section 5.3.2, below) used here to model Ruapehu's magmatic storage system.

Glass compositions were measured on polished thin sections by Quantitative Energy Dispersive X-ray Spectroscopy (EDS) using the Scanning Electron Microscope (SEM) at Vanderbilt University, USA. The quality of the analyses were checked against reference standards (Glass Mountain Rhyolite, RGM-1 and AGV Andesite). For each target glass, multiple compositional spectra were acquired and then averaged to provide the average glass composition. While individual EDS analyses are considered reliable, as supported by repeated analyses of reference standards, the averaging process is advantageous since it allows identification and removal of any outliers (e.g. altered glass or glass containing microlites), and also averages any small-scale heterogeneities in the glass composition.

Therefore, we developed a fast but robust statistical method for identifying chemical outliers using the median and median absolute deviation (MAD) values of the compositional analyses for each target glass. The MAD is similar to, but more robust than, the standard deviation when dealing with datasets containing outliers since it is not as strongly affected by those values. For any single set of glass analyses, any spectra in which *any* of the measured oxide values exceeded the $median \pm 2.5MAD$ were excluded, ensuring that *all* of the remaining analyses were consistent across all oxides. Only the remaining 'good' analyses were then averaged to provide the final glass compositions (Appendix 4).

5.3.2 Modelled magma storage conditions: rhyolite-MELTS

The Ruapehu PDC samples, being geologically young and unaltered, provided an ideal test-bed for a new rhyolite-MELTS based geobarometer under development at Vanderbilt University, USA. The geobarometer applies strict thermodynamic considerations to assess the pressures at which crystallising phases are found to be in equilibrium with the pre-eruptive melt, now preserved as matrix glass. This method has previously been used for felsic assemblages crystallising in rhyolites where it has been shown to reliably reproduce pressures assessed using H_2O-CO_2 solubility models and amphibole geobarometry (Bégué et al., 2014; Gualda and Ghiorso, 2014). However this is the first time that the thermodynamic model has been adapted for mafic phases crystallising from andesitic rocks.

The principles behind the rhyolite-MELTS geobarometer are explained in detail in Figure 5.5. The governing assumption is that any crystallising phase *must* be in equilibrium with the surrounding melt composition at the time of crystallisation. Therefore, the saturation curves for each mineral phase will follow unique pressure-temperature paths that are determined by the composition of the melt (Figure 5.5 a). Hence, if several different phases are inferred to have crystallised simultaneously from the *same* melt (on the basis of textural analyses), then those crystallisation conditions must be described by a unique pressure and saturation temperature where these curves intersect (Figure 5.5 b). At Ruapehu, all of the PDC units described in this thesis appear to have crystallised plagioclase + clinopyroxene + orthopyroxene in equilibrium with their respective melts prior to eruption (Figure 5.6), and so the thermodynamic model was adapted to account

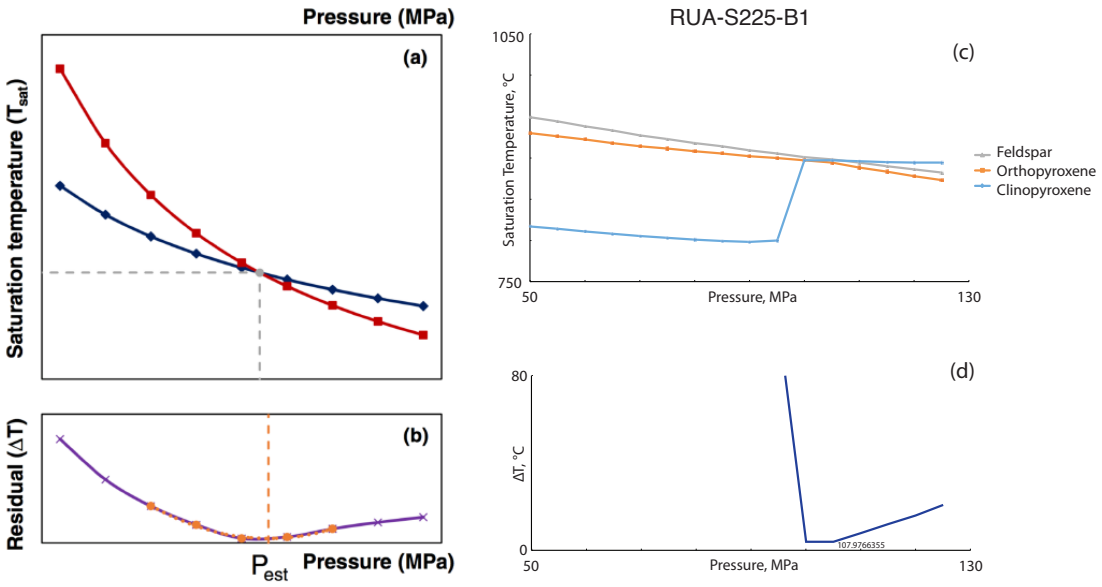

Figure 5.5: The principles behind the rhyolite-MELTS geobarometer for estimating the pressures and saturation temperatures of crystallising phases in the Ruapehu magmas (after Gualda and Ghiorso, 2014). a) The two curves represent saturation curves (T_{sat}) for two different mineral phases as a function of pressure for a given melt composition. If the different phases are inferred to have crystallised simultaneously, then the crystallisation temperature and pressure is given by the point where the lines intersect. b) Because the rhyolite-MELTS calculations are at discrete pressure intervals, the final estimated crystalisation pressure (P_{est}) is calculated by plotting the absolute difference between the different saturation temperatures (ΔT) at two points either side of the crossover, then fitting a curve to these residuals to find the minimum (ΔT_{min}). c) For the Ruapehu samples, the model has been updated to address simulataneous crystallisation of plagioclase, orthopyroxene and clinopyroxene in equilibrium with matrix glass compositions. d) In these real world examples, the curves sometimes approach very closely without crossing at a unique point. In earlier model versions for rhyolites, a threshold of $\Delta T_{min} \leq 5$°C was therefore used as a cutoff for the pressure estimates. However for the andesitic Ruapehu samples a ΔT_{min} value up to 10°C is allowed (see Box 5.2). In the example from sample RUA-S225-B1 shown here, the saturation curves do not all cross at a unique point, but ΔT_{min} reaches 4°C at ~108 MPa and this is therefore accepted for the pressure calculations.

for these phases (see Harmon, Cowlyn, Gualda & Ghiorso, 2015, American Geophysical Union conference abstract; Appendix 5.3).

In practice, the measured real-world glass compositions do not always result in absolute convergence of the modelled saturation curves, as shown in Figure 5.5 c&d. This can be because: a) the measured glass compositions may be inaccurate due to small-scale sample alteration or analytical errors, or b) rhyolite-MELTS incorrectly modelled the phase relations. These, and other errors and limitations associated with the method, are discussed in Box 5.2.

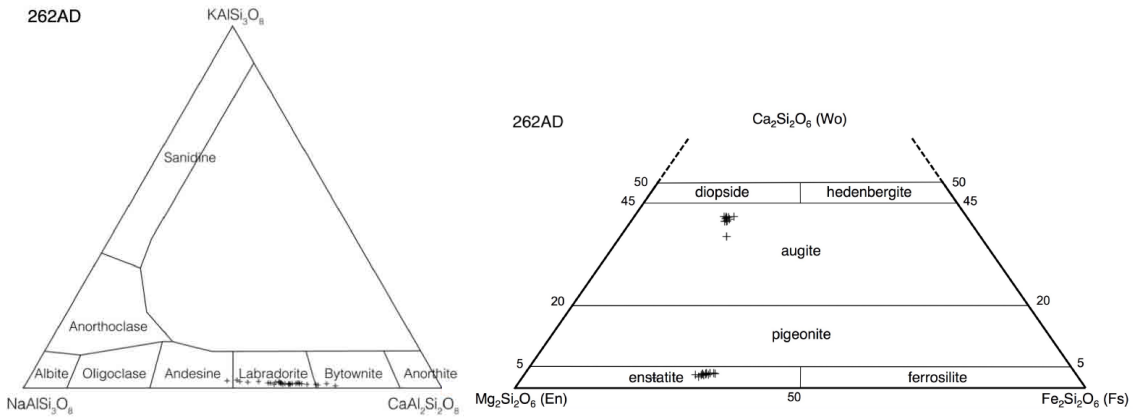

Figure 5.6: Feldspar and pyroxene compositions from sample X262AD, PDC Unit 6. These compositions are representative of the crystallising phases for all of Ruapehu's PDC units; and together with measured groundmass glass compositions these phases constrain the input conditions for a new rhyolite-MELTS based geobarometer applied here for the first time to andesitic samples.

Box 5.2: Errors and limitations of the rhyolite-MELTS geobarometer:

Gualda and Ghiorso (2014) investigated the errors associated with the rhyolite-MELTS geobarometer in detail, and separated the errors into a) those associated with the calibration of rhyolite-MELTS and b) those associated with errors in the measured glass compositions.

Errors associated with the calibration of rhyolite-MELTS: While there are certainly uncertainties associated with the calibration of rhyolite-MELTS, Gualda and Ghiorso (2014) considered these difficult-to-impossible to assess due to a lack of experimental results that can be used as calibration points (see Gualda et al., 2012). However, Gualda and Ghiorso (2014) concluded that since the uncertainties associated with the calibration of rhyolite-MELTS will result in systematic errors, they can be effectively neglected for practical purposes as long as the method is shown to produce results that are consistent with other geobarometers, as confirmed by Bégué et al. (2014). Furthermore, these errors can effectively be neglected when comparing *relative* pressure differences between results that were all generated using the rhyolite-MELTS method (as is the case in this thesis).

Errors associated with the measured glass compositions: Uncertainties associated with the measured glass compositions are the main source of non-systematic error for the pressure determinations, and are a combination of analytical uncertainties and the effects of sample inhomogeneities due to small degrees of alteration. In order to assess these errors, Gualda and Ghiorso (2014) employed a Monte Carlo approach using natural glass inclusion data from the Bishop Tuff as a starting composition (including estimated errors for each oxide from Anderson, Jr. et al., 2000). They then created a set of 1000 new compositions by assuming the errors had a Gaussian distribution with means equal to the observed concentration and standard deviations equal to the estimated error for each oxide. Application of the rhyolite-MELTS geobarometer to each of these compositions yielded errors of ± 20-45 MPa when modelling equilibrium crystallisation of three crystal phases (here; quartz + 2 feldspars). However, Gualda and Ghiorso (2014) note that the published uncertainties for Na_2O (Anderson, Jr. et al., 2000) are much larger (~13%) than is geologically reasonable for most cases, and therefore suggest that in most cases the pressure errors due to compositional uncertainties are likely to be at the lower end of the range (± 20-25 MPa).

An unexpected benefit of the method is that the pressure calculations are very sensitive to the quality of the glass analyses as a result of the stringent phase-equilibria constraints used, and will fail in the light of unreasonable compositions due, for example, to sample alteration. In their analyses of rhyolitic compositions, Gualda and Ghiorso (2014) allowed for small discrepancies by allowing the modelled saturation curves to converge within 5°C (referred to as the residual, ΔT, Figure 5.5 d) rather than strictly enforcing that the curves must cross at exactly the same P,T point. Even so, only 57% of the modelled compositions yielded results, demonstrating how effectively the rhyolite-MELTS geobarometer filters out spurious compositional data. For the andestic method used here for the first time (using plagioclase + 2 pyroxenes), the rhyolite-MELTS model is more sensitive to factors including fO_2 and H_2O, and as such it can be harder to get absolute convergence of the saturation curves even for 'good' glass compositions. Therefore, after considerable consultation (G. Gualda pers. comm.) we suggest that convergence of the saturation curves within $\Delta T_{min} \leq 10$°C is reasonable for andesites, and that in this case the previously assessed ± 25 MPa error will still be a reasonable estimate of the non-systematic error. Future work along the lines of Gualda and Ghiorso (2014), however, will allow this error to be confirmed more precisely.

When attaining the pressures for the Ruapehu samples presented in this thesis, it was noted that some analyses appeared to graphically converge but the saturation curves did not reach the required $\Delta T_{min} \leq 10$°C cutoff. However, allowing a larger cutoff (up to 32°C) nonetheless returned pressure estimates that were *consistent* with the results from the higher quality analyses. Because of the challenges in obtaining pressures for andesitic compositions, we have decided to include these results in this thesis when they provide further insight that is not possible without this data (e.g. in analysis of mingled magma domains within clasts); however we acknowledge that the associated errors are greater when the curves do not converge within $\Delta T_{min} \leq 10$°C. The ΔT_{min} of each pressure estimate is listed with the results, and those that do not achieve a $\Delta T_{min} \leq 10$°C are highlighted as less reliable.

Temperatures: When modelling the phase saturation pressures, rhyolite-MELTS also calculates the saturation temperature for each phase. In this sense, the method also serves as a thermometer as well as barometer. There is much more uncertainty regarding rhyolite-MELTS' ability to constrain temperatures, and limited experimental results on rhyolites suggest it may overestimate absolute temperatures by as much as 40°C (G. Gualda pers. comm.). However, in a relative sense the errors will be much lower, and therefore using the method to qualitatively assess temperature *differences* between different magma storage zones is appropriate.

Oxygen fugacity and water contents: In addition to generating magma storage pressures and phase saturation temperatures, the rhyolite-MELTS geobarometer currently requires iterative testing of magmatic water contents and oxygen fugacites in order to find the optimal conditions for model convergence. Therefore, estimated magmatic water contents and fO_2 values that result in the best thermodynamic solutions are also available directly from the rhyolite-MELTS model.

Comparison of the new rhyolite-MELTS method for andesitic compositions to other data and methods.

As a new method for use on andesitic systems, the rhyolite-MELTS geobarometer is untested against other existing methods for estimating the magmatic storage conditions. Here, we briefly look at the (albeit limited) available experimental data for validating this

technique, and also compare some of the modelled storage pressures and temperatures calculated for the Ruapehu PDC deposits to other geothermometers.

1. Experimental comparisons:

Relatively few experimental studies of shallow plagioclase + othopyroxene + clinopyroxene bearing andesites are available for comparison with the new rhyolite-MELTS barometer. However Harmon et al. (in prep) have applied the rhyolite-MELTS geobarometer to 15 experimentally constrained glass compositions taken from the Library of Experimental Phase Relations (LEPR) database. These compositions were chosen based on their crystallising mineral assemblages (plag+opx+cpx), pressure (upper crustal pressures ranging from 100 MPa to <1 GPa), and water-contents where available. Of the 15 compositions tested, 4 yielded viable triple-junction model convergence from the rhyolite-MELTS geobarometer (L. Harmon, pers. comm.). Selected results, including 2 of the successful model runs, are presented in Table 5.2. The analyses that yielded model convergence for cpx+opx+plag in the rhyolite-MELTS geobarometer produced storage P and T estimates that agree well with the experimental data (Table 5.2). Although the majority of the 15 compositions tested did not yield model convergence, this is not problematic since the emphasis is showing that, for the times when the rhyolite-MELTS geobarometer does achieve convergence, it produces results that are consistent with the experimental results. As a general observation, the experimental glass compositions that were water saturated and were ran at lower pressures (<200 MPa) yielded more consistent rhyolite-MELTS model convergence (L. Harmon, pers. comm.). This provides confidence in the P-T results for the Ruapehu PDC deposits in this thesis, all of which were found to have erupted from shallow, water-rich magmatic storage conditions (this Chapter).

2. Comparison with other geothermometers:

In addition to obtaining pyroclast glass analyses for the Ruapehu samples, we also acquired select crystal compositions by Quantitative Energy Dispersive X-ray Spectroscopy (EDS) using the Scanning Electron Microscope (SEM) at Vanderbilt University, USA. Therefore, we are able to estimate magmatic storage pressures and temperatures using

LEPR Index	Experiment	Author	Method	Duration (hours)	T, C	err T, °C	rhyolite-MELTS T, °C	P, Gpa	err P, Gpa	rhyolite-MELTS P, Gpa	Δ T cut-off	fO2 cond	Phases	SiO_2	H_2O+
1426	PIN98s	Prouteau & Scaillet (2003)	EMP,SEM	63	950	5		0.4	0.002			NNO+3.2	liq + plag + cpx + spn + opx		
1622	8	Kawamoto (1996)	EDS,EMP	73	975	15		0.5	20			NNO+1.3	cpx + opx + plag + spn		
2478	85-41-9	Grove et al. (2003)	EMP	48	940			0.2				NNO	liq + cpx + opx + plag + spn	57.79	
3603	PEM12-11	Moore & Carmichael (1998)	EMP	48	1000	5		0.0441	5			NNO+2.8	liq + opx + plag + ox + cpx	62.64	0.8
3607	PEM12-19	Moore & Carmichael (1998)	EMP	48	975	5	984	0.1008	5	0.09	6	NNO+1.1	liq + opx + plag	62.64	0.8
4037	TJ-34	Auwera & Longhi (1994)	EMP	72	1085	2		0.0001				NNO	liq + plag + opx + cpx + ilm + spn	49.54	
4799	1140mf #27	Grove et al. (1997)	EMP	47	940		920	0.1		0.14	9	NNO	liq + opx + cpx + plag + spn	56.3	
4801	1140mf #29	Grove et al (1997)	EMP	25	910			0.1				NNO	liq + opx + cpx + plag + spn	56.3	
4806	1140mf #41	Grove et al (1997)	EMP	38	915			0.15				NNO	liq + opx + cpx + plag + spn	56.3	

Table 5.2: Comparison of rhyolite-MELTS estimated storage pressures and temperatures with experimental data from the Library of Experimental Phase Relations database. For the rhyolite-MELTS results that succesfully produced model convergence (highlighted), it can be seen that the estimated pressures and temperatures closely match the experimental results.

Sample	rhyolite-MELTS		2 pyroxene, Putirka 2008					CPX-liquid, Putirka et al 2003			Feldspar-liquid, Putirka 2005			
	P	T	T, C Eqn 36	T, C Eqn 37	P, Mpa, Eqn 38	P, Mpa, Eqn 39	OPX-liquid Equilibrium Test (should be 1.09 +/- 0.14)	T	P, Mpa	Equilibrium Test (should be 0.27)	T, C Eqn 23	T, C Eqn 24a	P, Mpa Eqn 25a	Equilibrium Test (should be: 0.1 +/- 0.11 if T <1050, or 0.27 +/- 0.05 if T >1050)
X225AC (phenocryst analysis)	111	896	1028.1	1020.3	730	690	0.725	955.6	70	0.17	1062.2	1041.9	250	0.06
X225DE (phenocryst analysis)	134	878	1043.3	1020.6	1020	770	0.804	956.8	290	0.17	1076.1	1061	260	0.05
RUA-S129-A3a (phenocryst analysis)	158	833									1083.9	1068.7	260	0.05
RUA13-262-Y1 / X262Y1 (phenocryst analysis)	134	876	1084.6	1051.6	1020	780	0.573	954.9	240	0.12	1071.6	1056.4	280	0.05
X262AD (phenocryst analysis)	138	861	1020.9	1006.9	640	590	0.76	929.8	110	0.15	1042.1	1016.1	290	0.06
108A1 glass btwn. microlites (phenocryst analysis)	22	1030	1035.4	1091.3	780	470	0.475	1033.2	-40	0.11	1103.5	1096	210	0.1
161AC glass btwn. microlites (phenocryst analysis)	58	986	1035.4	1039.5	670	490	0.74	1015.5	-240	0.12	1109.4	1097.9	380	0.15
161AC glass btwn. microlites (microlite analysis)	58	986	1167.3	1210.1	660	480	0.966	1063.2	-70	0.15	1112.5	1102	350	0.14

Table 5.3: Comparison of rhyolite-MELTS estimated storage pressures and temperatures with calculations using thermobarometers from Putirka et al. (2003) and Putirka (2005, 2008). Calculations that achieve the equilibrium test criteria are highlighted.

the Putirka (2008) two-pyroxene, Putirka (2008) clinopyroxene-glass, and Putirka et al. (2003) feldspar-glass thermobarometers, and compare them to the pressures and temperatures calculated by rhyolite-MELTS. In each case, within the limitations of the available data, we have used crystal compositions that most closely represente equilibrium with the melt (i.e. phenocryst rims, microlites, and in one instance the core from a small phenocryst). The results of these comparisons are presented in Table 5.3 and Figure 5.7.

Only two of the calculations meet requirements the basic equilibrium tests offered by the Putirka spreadsheets (Table 5.3), suggesting that the Putirka et al. (2003) and Putirka (2005, 2008) results should be treated with caution. However, in this context, Figure 5.7 shows that there is tremendous variability in both the estimated pressures and temper-

atures from the different models. The rhyolite-MELTS pressure estimates are broadly consistent with those from the Putirka et al. (2003) clinopyroxene-liquid thermobarometer, though the latter returns negative pressures for the 2 more mafic samples 108A1 and 161AC. The other geobarometers return significantly higher estimated storage pressures, though the most important observation is that *all* of the methods show broadly similar *relative* changes. The same is true for the estimated temperatures, with rhyolite-MELTS returning the lowest temperature estimates and the clinopyroxene-liquid thermometer producing the most comparable results. This contrasts with limited experimental results for rhyolitic samples that suggest rhyolite-MELTS may overestimate absolute temperatures by as much as 40°C for rhyolitic compositions (G. Gualda, pers comm; Box 5.2). Again, however, the relative temperature changes are broadly consistent across all of the different geothermometers. Since this thesis' observations are mostly concerned with the *relative* changes in storage conditions (this Chapter) for the different PDC source magmas (as opposed to the absolute storage depths and temperatures, which do not affect the broad interpretations), this validates the use of the rhyolite-MELTS model for assessing the storage conditions prior to eruption of the Ruapehu PDCs.

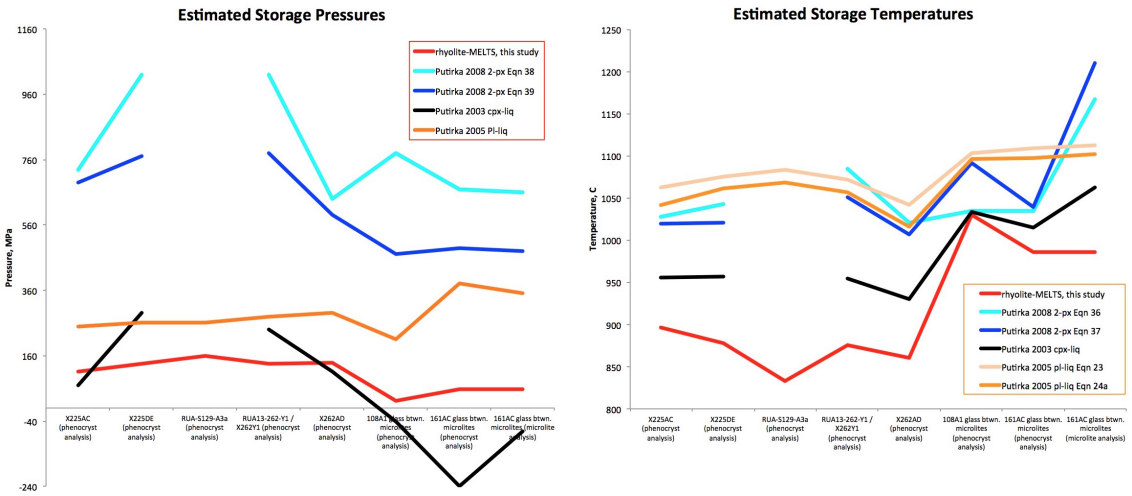

Figure 5.7: Graphical comparison of rhyolite-MELTS estimated storage pressures and temperatures with calculations using thermobarometers from Putirka et al. (2003) and Putirka (2005, 2008). Although the different methods produce significantly different results, all of the methods show the same relative pressure and temperature trends.

3. Comparison with other Ruapehu Data

a) Pressures

Kilgour et al. (2013) investigated the magmatic storage pressures of Ruapehu's historical eruptives using volatile contents of melt inclusions following the calculations of (Papale et al., 2006). Here, Kilgour et al. (2013) found that the Ruapehu melt inclusions suggest a minimum (volatile saturation) trapping pressure of 50–270 MPa (at temperatures between 920 and 1,030°C). Kilgour et al. (2013) also found that these values were in agreement with estimates from the phenocryst-melt and two-pyroxene geobarometers of Putirka (2008). Assuming a crustal density of 2,600 kgm^{-3} and volatile saturation, this suggests that the historical magma storage region beneath Ruapehu extends from ~2 to 9 km below the volcano. This is fully consistent with the rhyolite-MELTS estimated magmatic storage pressures presented in this Chapter for Ruapehu's PDC deposits, which mostly range from ~2-5.8km depth.

Pardo Villaveces (2012) reported that melt inclusions from the Oruamatua eruptive unit (part of the Ohinewairua eruptive period) contain 1.8 % of total H_2O, and hence appear to either be degassed or represent a minimum pre-eruptive storage depth of 1.4 km. The rhyolite-MELTS estimates for the equivalent Ohinewairua PDC deposits (PDC Units 1-3) presented here give estimated storage depths from 4.1-5.6 km, and hence appear to support Pardo's (2012) assertion that those melt inclusions had degassed. For melt inclusions from the Okupata tephra (part of the Okupata-Pourahu eruptive unit that produced the PDC Unit 4 deposit), Pardo Villaveces (2012) measured total H_2O of 5.1-5.4 wt. %, representing a minimum saturation depths of 6.8-7.5 km. The comparable rhyolite-MELTS estimates for PDC Unit 4's storage depth range from 4.3-5.8km, somewhat shallower than Pardo's (2012) estimates.

b) Temperatures

Kilgour et al. (2013) investigated the magmatic storage temperatures of Ruapehu's historical eruptives using plagioclase-liquid (Putirka, 2008), clinopyroxene-liquid (Putirka, 2008), orthopyroxene-liquid (Putirka, 2008) and two-pyroxene (Frost and Lindsley, 1992) geothermometers, with an assumed H2O content of ~1.5 wt % and an assumed pressure of 250 MPa. These different geothermometers yielded temperature estimates for Ruapehu's

historical magmas that often differed by up to ~100°C, though the different geothermometers all showed similar overall trends. All of the data plotted between 910-1080°C, with the majority clustering between 950 and 1050°C.

The whole rock compositions of Kilgour et al.'s (2013) historical Ruapehu magmas (57.6 - 61.1 wt% SiO_2, hydrous) are most comparable to the deposits from PDC Units 1-6. The relevant Ruapehu PDC thin section samples that are compared here are X225AC (58.89 wt% SiO_2, hydrous, Table 4.2), X225DE (58.43 wt% SiO_2), S129A3a (no whole-rock XRF data for this sample, but other Unit 4 samples have 58.1-59.6 wt% SiO_2) and X262AC (60.51 wt% SiO_2). These samples yielded temperatures between 930 and 1085°C using the Putirka et al. (2003) and Putirka (2005, 2008) cpx-liquid, plagioclase-liquid and 2-pyroxene calculations, here using anhydrous compositions with no prior assumed storage pressure. Therefore, in a general sense these temperature estimates are consistent with the results of Kilgour et al., 2013 for Ruapehu samples of similar composition. By contrast, the rhyolite-MELTS method yielde temperatures between 861-896°C for the same PDC samples, highlighting that rhyolite-MELTS method appears to underestimate the storage temperature compared to the other methods.

Pardo Villaveces (2012) estimated the temperatures of magmas from the Oruamatua eruptive unit (comparable to the PDC Units 1-3 deposits) and The Okupata tephra (comparable to the PDC Unit 4 deposit) using the two-pyroxene method of Putirka (2008). This yielded results of 974°C (Oruamatua) and 977°C (Okupata), compared to ~900°C (PDC Units 1-3) and 837-886°C (Unit 4) using rhyolite-MELTS. This again highlights that that the rhyolite-MELTS method appears to underestimate the storage temperature in comparison to the other geothermometers.

Melt density and viscosity

The melt density (i.e. free of crystals, bubbles or xenoliths) is important in terms of magma ascent, mingling, and also affects the glass density in the erupted pyroclasts. It is a function of the melt composition (X), temperature (T) and pressure (P), and can be

calculated empirically using the relation:

$$\rho = \Sigma X_i M_i / \Sigma V_i \tag{5.2}$$

where X_i is the mole fraction, M_i is the molar mass, and V_i is the fractional volume of the ith oxide component in the melt. Although V_i does have some compositional dependency, it is mostly a function of temperature and pressure under normal magmatic compositions, and hence can be calculated using published values (Spera, 2000) of partial molar volume $\bar{V}_i$, partial molar isobaric thermal expansion, $(\partial \bar{V}_i / \partial T)_P$ and partial molar isothermal compressibility $(\partial \bar{V}_i / \partial P)_T$:

$$V_i(T, P, X) = \bar{V}_{i,T_r,P_r} + (\partial \bar{V}_i / \partial T)_P (T - T_r) + (\partial \bar{V}_i / \partial P)_T (P - P_r) \tag{5.3}$$

where T_r and P_r are constant reference conditions, usually 1673K and 10^{-4} GPa.

It is therefore straightforward to calculate the pre-eruptive volatile-free melt densities (Appendix 5.2) for Ruapehu's PDCs using the measured glass compositions (Section 5.3.1) and modelled P,T storage conditions (Section 5.3.2).

The melt viscosity is also important in terms of magma mingling, ascent, and the ability of bubbles to move through the melt, and is here calculated for the measured glass compositions and rhyolite-MELTS modelled storage conditions using the viscosity model of Giordano et al. (2008).

5.3.3 Physical pyroclasts analyses

The physical characteristics of the PDC deposits and the primary pyroclasts reflect the combined inputs of the underlying magmatic system, the fragmentation and eruption mechanisms, and the transport and depositional processes occurring within the PDCs.

PDC macro textures and grain size characteristics

Major deposit and pyroclast textural features were observed in-field and are described in Chapter 4 and Figure 5.4. The grain-size characteristics of the PDC deposits (Chapter 4 and Appendix 3.2) reflect both the initial grain-size distribution of the fragmenting mixture, as well the subsequent transport processes within the eruption column and PDCs, and were measured using the sieving methods outlined in Chapter 4, Section 4.3.

Lapilli componentry and textures

The textural aspects of pyroclasts within Ruapehu's PDC deposits were primarily investigated using bulk subsamples of lapilli from the -5ϕ to -4ϕ sieved size fraction. This size fraction was selected in order to allow a full suite of analyses on the same samples, while nonetheless being small enough to have quenched and reasonably preserved the vesicularities and vesicle textures of the ascending and fragmenting magma (e.g. Houghton and Wilson, 1989). In contrast, larger samples would be expected to undergo additional post-fragmentation vesiculation, and would not therefore reflect conduit-level processes.

For each unit, samples from the sieved -5ϕ to -4ϕ fraction were classified in terms of clast type (Chapter 4), shape, and density. In many of the PDCs, several classes of juvenile clasts were observed, including:

1. Juvenile clasts of the dominant magma type (generally labelled Type 1 and 1D, where 'D' refers to distinctly denser clasts in hand sample); these represent the 'main' magmas. Hereafter, these clasts are referred to as the 'primary clasts.'

2. Juvenile clasts of a secondary magmatic component (if present); these represent fresh, vesicular clasts that appear in hand sample to be entirely composed of a secondary

magmatic component. These are hereafter referred to as 'secondary clasts.'

3. Colour banded juvenile clasts; these reflect either pre-eruptive mingling of two different magma types, or mingling of different textural domains within the same magma. These are hereafter referred to as 'banded clasts,' and may contain both 'primary' and 'secondary' components.

Pyroclast shapes were assessed semi-quantitatively using a modified Krumbein roundness scale (Fig 5.8, Krumbein, 1941), in which roundness was scored from 1-9 on the basis of comparison with standardised shapes. Although this method only gives semi-quantitative results, it was preferred over other techniques (e.g. digital image analysis) as it allowed the full surface of the clasts to be inspected, and also allows comparative studies of in-situ deposits in the field. The advantage of the Krumbein scale over other roundness scales (e.g. Powers, 1953) is the high number of example shapes provided for comparison, providing consistency across all of Ruapehu's texturally different PDC deposits. For broken clasts, the original Krumbein scale calls for a roundness value that is half of the roundness observed for the non-broken surfaces. However, in the case of PDC deposits this provides a misleading representation of the total rounding processes within the PDC, since clasts may break at any point during transport. Therefore, for broken clasts we instead report the roundness of the non-broken faces, as this most closely reflects the total clast rounding experienced during transport.

Lapilli density

Whole clast pyroclast densities (Appendix 3.1) directly affect the bulk density of the erupting mixture, and hence are critical to PDC generation. In order to relate pyroclast densities to the other physical parameters outlined above, the bulk densities of the same -5 to -4 ϕ clasts were assessed following methods outlined by Houghton and Wilson (1989), Barker et al. (2012), and Rotella (2013). Here, dry clasts were first sprayed with a silicon sealant to seal vesicles <~1mm, before clast specific gravities (S.G) were measured by comparing the weight of the clast in air with that in water (Archimedes' principle; Fig 5.9). Whole-clast densities (ρ_{clast}) were then determined by dividing the clast specific

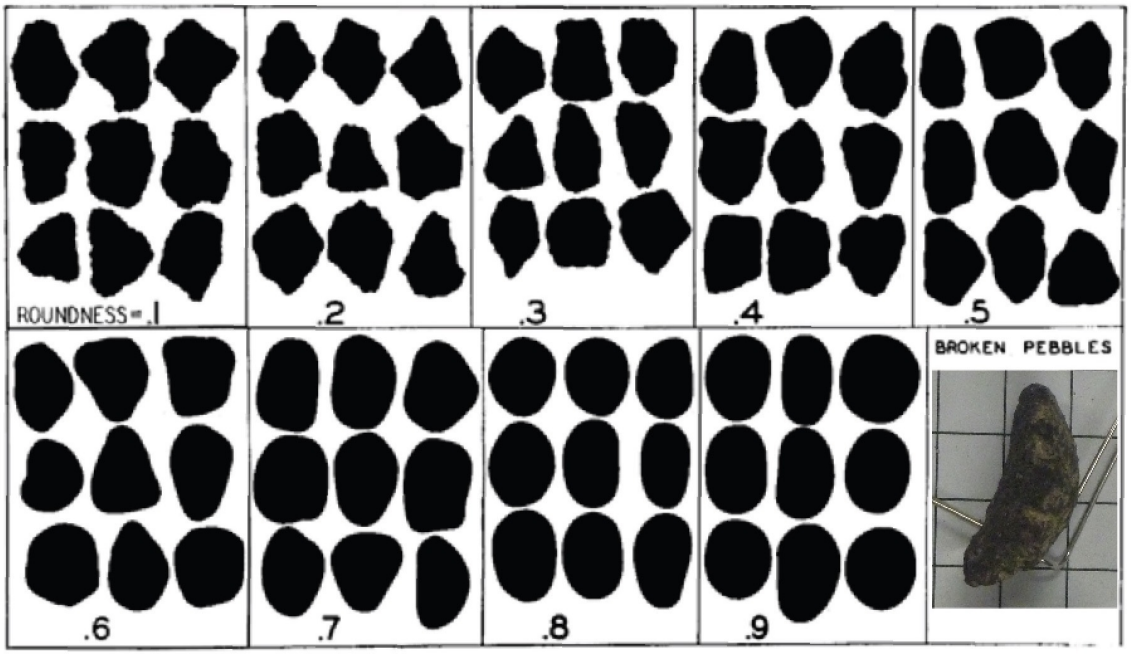

Figure 5.8: Modified Krumbein roundness scale for assessing the shape of clasts within Ruapehu's PDCs (after Krumbein, 1941). Here, clasts are assigned a roundness value by comparing their shape to the standardised shapes. In the case of broken clasts, a modified roundness is assigned on the basis of just the unbroken surfaces. Therefore, the example clast has a primary roundness of ~6 despite being broken on one side.

gravities by the density of water:

$$\rho_{clast} = \frac{S.G.}{\rho_{water}} = \frac{W_{clast(air)}}{\rho_{water}[W_{clast(air)} - W_{clast(water)}]} \tag{5.4}$$

where ρ_{water} is the density of water (1g/cm^3), and W_{clast} is the weight of the clast measured in both air and water.

Clasts with larger open vesicles additionally required wrapping in parafilm wax to prevent water ingress, while floating clasts were also ballasted using a cage. Equation 5.4 was therefore adjusted to account for these:

$$\rho_{clast} = \frac{W_{clast(air)}}{\rho_{water}[W_{clast(air)} + W_{wax(water)} + W_{cage(water)} - W_{clast+wax+cage(water)}]} \tag{5.5}$$

where W_{wax} is the parafilm wax weight (if used) and W_{cage} is the cage weight (if used). Wrapping the clasts in parafilm reduced their measured bulk density, and this is interpreted to result from the trapping of air beneath the wax. Repeat measurements on 21 clasts from the Ruapehu deposits, as well as a detailed repeatability study by Barker et

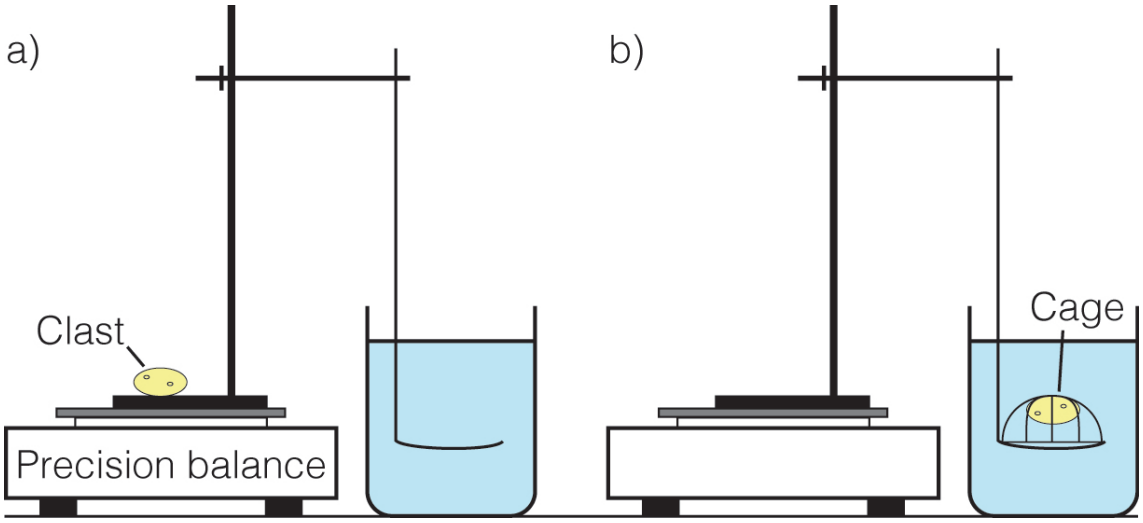

Figure 5.9: Experimental setup for measuring pyroclast density. Prior to measuring, all clasts are sprayed with a silicon sealant to seal vesicles <~1mm, while clasts with larger open vesicles are also wrapped in parafilm wax to prevent water ingress. a) Dense clasts are weighed dry and then weighed again when submerged in water; b) floating clasts are kept below water with the use of a cage, whose weight in water is subtracted from the total.

al. (2012), showed the parafilm reduced the measured densities by a maximum of 0.12 gcm^{-3}. However this did not significantly affect the shapes of the resulting density histograms (Appendix 3.1.3).

While the measured lapilli densities provide insight into the eruptive and PDC processes, it is important to emphasise that fractionation processes acting during each stage of transport means they nonetheless will not exactly reflect the bulk densities of either the erupting mixture or the bulk PDCs.

Vesicularity and vesicle textures

Pyroclast vesicle textures provide the only physical record of the exsolved gas phase during eruption, and therefore compliment the density analyses in reflecting the eruptive and PDC generation processes. Broad characterisation of pyroclast vesicularity was achieved by comparing calculated whole-clast densities with published dense rock equivalent (DRE) densities of equivalent fall deposits for the Ohinewairua eruptive unit (2770 g/cm^3; correlating with PDC Units 1-3) and Okupata-Pourahu eruptive unit (3024 g/cm^3; correlating with PDC Units 4-6) eruptions (Pardo Villaveces, 2012). Where published DRE values

were unavailable (i.e. PDC Units 8-10), the higher value 3024 g/cm^3 was used in recognition that Units 8-10 also have the highest calculated melt densities (Table 5.5).

Qualitative study of vesicle textures was achieved using 2-dimensional Scanning Electron Microscope (SEM) imagery of representative thin sections from samples from Ruapehu's PDC deposits. Additional high resolution tomographic images of representative ~1cm lapilli were collected using the Australian Synchrotron's Imaging and Medical Beamline, allowing select 3-dimensional analyses of vesicle textures from several of the units. The ~1cm lapilli size favours rapid quenching of the erupting pyroclasts, providing direct insight into the ascent and fragmentation-level vesicle structures.

5.4 Results

In order to understand the general magmatic and eruptive processes leading to PDC generation and transport at Ruapehu, we here present the detailed chemical and physical characteristics from each of the three main PDC deposit types (Chapter 4): pumice-dominated PDC deposits (Units 1-5), variably welded scoria-dominated PDC deposits (Units 6 & 7), and heterolithologic small-volume PDC deposits (Units 8-10).

5.4.1 Pumice-dominated PDCs: Results

Macro-scale textures and whole rock chemistry

PDC Units 1-3, 4 (Pourahu PDC), and 5 all contain poorly sorted yellowish andesite pumices ranging from 55.6 to 59.7, recalculated anhydrous, wt% SiO_2 (Table 5.4 and Appendix 2). Sieved analysis of Units 1, 2 and 4 show bimodal distributions, with bomb-sized pumices supported in a medium-to-coarse ash matrix (Chapter 4, Figure 4.8 and Appendix 3). The oldest unit, PDC Unit 1, contains an at least ~10m thick lithic-rich base containing up to ~50% lithic clasts (Chapter 4, Figure 4.5). This grades vertically into a ~3m pumice-rich top (up to ~95% pumiceous clasts), with an accompanying increase in bomb-sized clasts at the top of the deposit interpreted to be due to kinetic sieving of the largest pumices during PDC transport (Chapter 4, Figure 4.4). All of the pumiceous PDCs

Sample	Flow Unit	Clast Type	SiO_2	TiO_2	Al_2O_3	Fe_2O_3T	MnO	MgO	CaO	Na_2O	K_2O	P_2O_5	LOI	Total
PDC Unit 1														
X225AA	Unit 1 Lower	Primary clast	56.315	0.73	16.805	7.372	0.116	4.088	6.716	3.222	1.636	0.125	2.84	99.965
X225AB	Unit 1 Lower	Primary clast	57.575	0.738	16.881	7.205	0.115	4.163	6.922	3.32	1.677	0.126	1.17	99.892
X225AC	Unit 1 Lower	Denser primary clast	58.887	0.735	16.482	7.224	0.113	4.218	6.888	3.251	1.676	0.131	0.07	99.675
X225BA	Unit 1 Top	Primary clast	57.142	0.73	16.65	7.29	0.115	4.283	6.865	3.186	1.548	0.126	2	99.935
X225BC	Unit 1 Top	Primary clast	56.681	0.734	16.348	7.022	0.116	4.19	6.657	3.237	1.704	0.134	3.09	99.913
X225BD	Unit 1 Top	Denser primary clast	58.703	0.721	16.691	7.098	0.111	4.279	6.82	3.292	1.682	0.13	0.34	99.867
X225BB	Unit 1 Top	Denser primary clast	56.323	0.729	16.789	7.258	0.122	4.386	6.877	3.21	1.608	0.126	2.44	99.868
X225BE	Unit 1 Top	Larger primary clast	58.083	0.717	16.897	7.061	0.113	4.21	6.819	3.286	1.7	0.132	0.9	99.918
X225AD	Unit 1 Lower	Secondary magma type	58.264	0.73	16.448	7.49	0.117	4.372	7.052	3.162	1.568	0.122	0.51	99.835
PDC Unit 2														
X225CA	Unit 2 Bottom	Primary clast	54.452	0.722	17.133	6.886	0.109	4.009	6.612	2.999	1.472	0.13	5.4	99.924
X225CH	Unit 2 Bottom	Primary clast	58.538	0.728	17.006	7.2	0.116	4.266	6.922	3.344	1.692	0.135	-0.08	99.867
X225CB	Unit 2 Bottom	Denser primary clast	54.261	0.729	16.658	7.16	0.109	4.23	6.861	3.105	1.497	0.127	5.1	99.837
X225CE	Unit 2 Bottom	Denser primary clast	58.728	0.718	16.663	6.994	0.114	4.259	6.782	3.328	1.71	0.134	0.44	99.87
X225CG	Unit 2 Bottom	Larger primary clast	58.14	0.734	17.049	7.08	0.117	4.224	6.702	3.275	1.727	0.133	0.78	99.961
X225DA	Unit 2 Upper	Primary clast	54.781	0.812	18.534	8.329	0.128	4.82	6.944	2.835	1.192	0.116	1.38	99.871
X225DB	Unit 2 Upper	Denser primary clast	55.673	0.73	17.658	7.17	0.114	4.298	6.504	3.099	1.504	0.13	3.01	99.89
X225DE	Unit 2 Upper	Denser primary clast	58.426	0.759	17.054	7.351	0.12	4.379	6.678	3.163	1.625	0.133	-0.18	99.508
X225EA	Unit 2 Top	Larger primary clast	58.167	0.726	17.355	7.169	0.119	4.37	6.798	3.207	1.661	0.129	0.18	99.881
X225CC	Unit 2 Bottom	Possible secondary magma	55.384	0.726	16.699	7.605	0.12	4.899	7.469	3.082	1.37	0.122	2.34	99.816
X225CD	Unit 2 Bottom	Secondary magma type	57.582	0.665	17.283	6.781	0.115	3.429	6.596	3.369	1.597	0.132	2.35	99.899
X225DG	Unit 2 Upper	Possible secondary magma type	58.216	0.74	16.975	7.216	0.114	4.246	6.702	3.33	1.736	0.129	0.53	99.934
X225DH	Unit 2 Upper	Secondary magma type	58.683	0.731	16.946	7.279	0.115	4.276	6.736	3.253	1.62	0.129	-0.6	99.168
X225DC	Unit 2 Upper	Secondary magma type	58.31	0.759	16.967	7.428	0.117	4.326	6.686	3.24	1.635	0.133	-0.54	99.061
X225DF	Unit 2 Upper	Grey-black lithic	58.638	0.72	16.828	7.184	0.118	4.425	6.813	3.238	1.737	0.133	0.1	99.934
X225DD	Unit 2 Upper	Grey-black lithic	58.395	0.719	16.903	7.185	0.115	4.297	6.809	3.204	1.627	0.131	-0.31	99.075
PDC Unit 3														
X107A1	Unit 3	Primary clast	58.022	0.749	17.188	7.272	0.116	4.118	6.629	3.211	1.685	0.138	0.81	99.938
PDC Unit 4														
X129AA	Unit 4	Primary clast	58.157	0.732	18.041	6.496	0.11	3.622	5.926	3.157	1.764	0.141	0.2	98.346
X129AC	Unit 4	Primary clast	58.054	0.726	17.995	6.623	0.112	3.752	5.898	3.134	1.727	0.151	0.55	98.722
X129AD	Unit 4	Primary clast	58.145	0.767	17.533	6.882	0.117	3.947	5.912	3.124	1.795	0.148	0.21	98.58
X129AB	Unit 4	Secondary magma type	59.608	0.707	17.156	6.535	0.11	3.636	5.972	3.325	1.83	0.138	-0.41	98.607
PDC Unit 5														
X262Y1	Unit 5 Top	Primary clast	59.329	0.685	17.066	6.629	0.108	3.722	6.427	3.388	1.867	0.133	0.6	99.954

Table 5.4: Major element XRF chemistry for Ruapehu's pumice-dominated PDCs. Analyses of clasts of secondary magma types are highlighted. Analyses X225CA and X225CB have high loss on ignition (LOI) values and should be treated with caution.

contain banded clasts and/or discrete clasts of one or more secondary, darker (black-brown or grey) magmatic components (Fig 5.10).

The componentry of whole clasts from the -5ϕ to -4ϕ sieved fractions highlights the prevalence of mingling within Ruapehu's pumiceous PDCs. Unit 4 contains 17% banded clasts, with an additional 3% discrete black-brown secondary clasts, and mingling is even more prevalent at the base of Unit 2, with 29% banded clasts and 3% discrete black-brown secondary clasts (Chapter 4, Figure 4.8). However, much of the banding in Unit 2 is subtle and observed as light grey patches that are easily missed in the field when the deposits are damp (Fig 5.10). Unit 1 contains ~5% grey clasts that may result from more complete mingling of a similar secondary magma to that seen in Unit 2, though no definitively banded clasts were observed in the sieved samples (Chapter 4, Figure 4.8). Distinctive pinkish thermal alteration (Donoghue et al., 1995b) is also present in ~3% of clasts in Unit 4 (Pourahu PDC), and another 17% have subtle pink sections. This pink alteration is mostly absent in the other units (Figure 5.10), although this is easily missed in the field

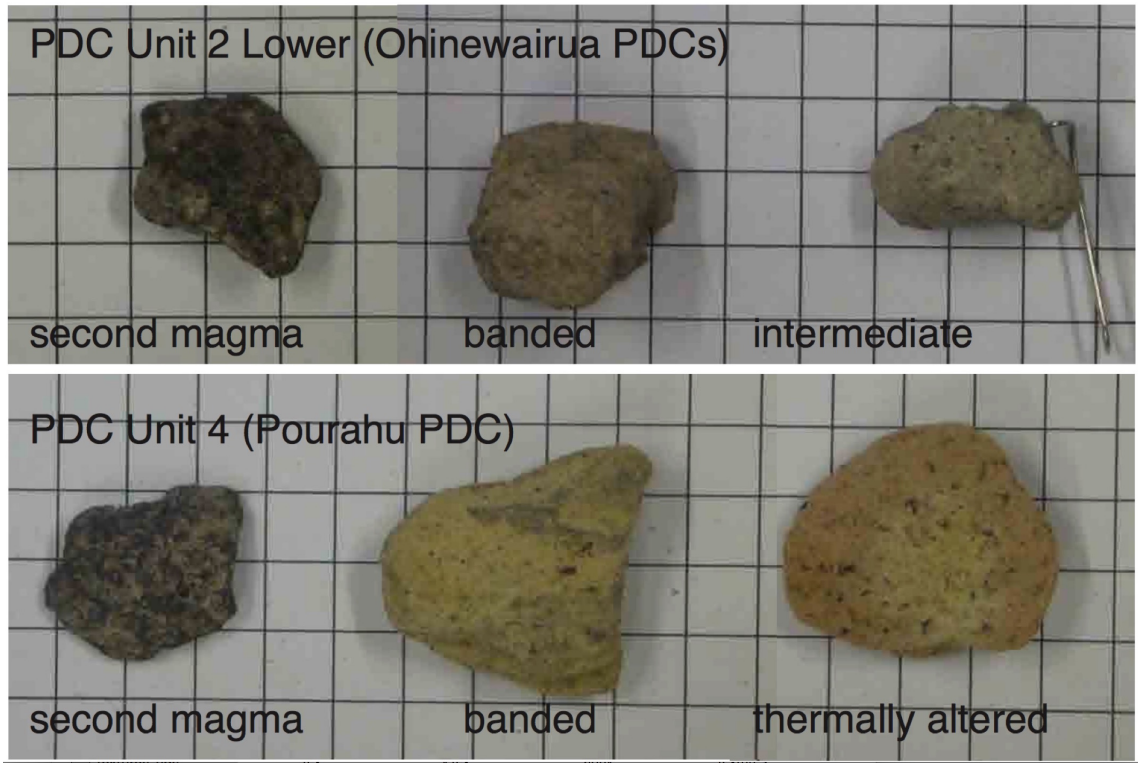

Figure 5.10: Secondary components and banded clast textures in PDC Units 2 and 4. The primary (main) clasts are similar to the banded clasts, but lack the darker bands. The grid is in 1cm intervals.

when the clasts are damp (Chapter 4, Section 4.4.1).

Despite the distinct appearance of the darker secondary clasts (Fig 5.10), whole-rock major element analyses from Units 2 and 4 *mostly* show similar chemistries for the primary and secondary clast types (Table 5.4). This observation is supported by Donoghue et al's (1995a) whole-rock analyses of the Pourahu PDC (Unit 4), which also found few major element differences between light (primary) and dark (secondary) clasts (Fig 5.11). However, two secondary clasts from Unit 2 *do* have significantly different whole-rock chemistries to the primary clasts: One (X225CD, Figure 5.11) is much more evolved and is chemically similar to the younger Units 4-6, while the other (X225CC; Fig 5.11) is much more mafic and has similar characteristics to the even younger Units 8-10 (Section 5.4.5).

Glass chemistry

Ruapehu's pumice-dominated PDCs all have primary glass that straddles silicic dacite to rhyolite in composition (69.3-72.1% SiO_2, anhydrous; Table 5.5), while the secondary glass

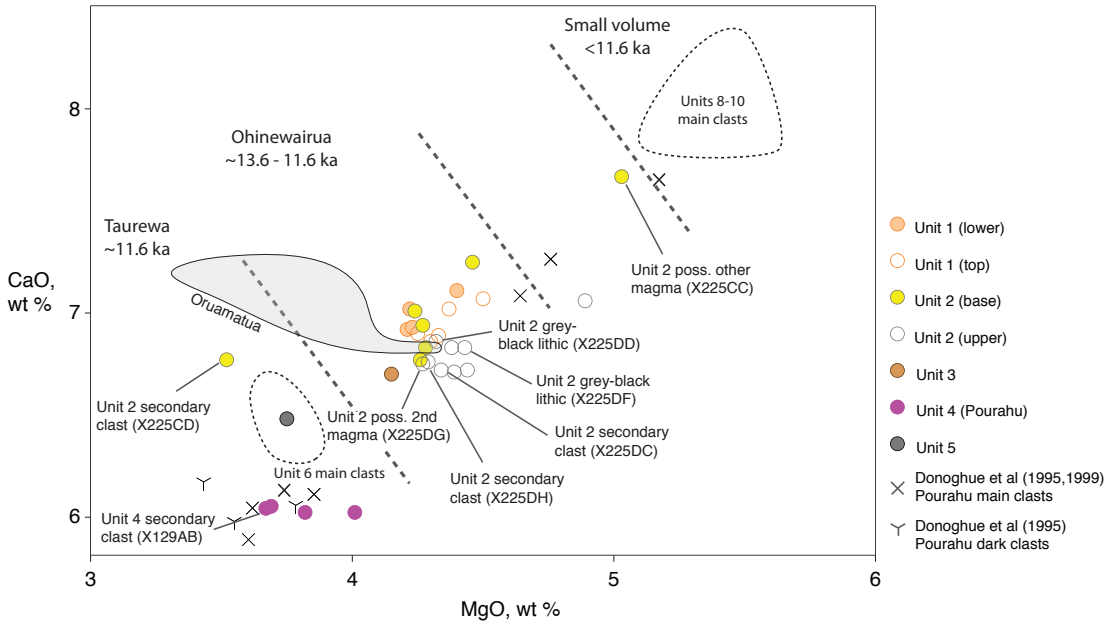

Figure 5.11: Whole-rock major element CaO vs MgO chemistry of clasts from Ruapehu's pumice-dominated PDC deposits. In general the mingled and secondary magmas are compositionally similar to the primary magmas; though two secondary clasts from PDC Unit 2 show significantly different major element chemistries - one more silicic (X225CD) and one more mafic (X225CC). Donoghue et al.'s (1995a, 1999) Pourahu (Unit 4) anayses of the main and mingled components are shown for comparison.

components show a similar mingling story to the whole rock chemistry (Figure 5.12). In Unit 2, one secondary component (Sample S225-D3a, Figure 5.12) is more mafic than the primary glass, and is preserved as a lower-vesicularity domain within a blackish secondary clast (Figure 5.15 e). The corresponding more-vesicular band (S225-D3b; Figure 5.15 d) has glass chemistry consistent with the main primary magma (Figure 5.12). In Unit 4, glass from another black-brown secondary clast (Sample S129-A5, Figure 5.12) is slightly *more* silicic than the primary glass, but is not sufficiently chemically different to definitively attribute this clast to a secondary magma on the basis of chemistry alone. We did not observe any secondary mafic glass in Unit 4, but Donoghue et al. (1995a) described several such components (shown on Figure 5.12) and interpreted mingling with a more mafic magma as being instrumental in triggering the Unit 4 eruption.

Sample	Unit	Clast Type	Storage P, Mpa	Storage T, °C	Δ T	Log Viscosity, Pas	Melt density, kgm^{-3}	SiO_2	TiO_2	Al_2O_3	FeO(T)	MgO	CaO	Na_2O	K_2O	Total	Fe_2O_3**	FeO**	H_2O**
PDC Unit 1																			
X225AC	Unit 1 Lower	Denser primary clast	111	896	2	4.26	2304	69.51	0.82	14.78	3.64	0.94	2.98	3.99	3.34	100.00	0.98	2.62	3.75
RUA-S225-A1	Unit 1 Lower	Primary clast	106	893	17	4.28	2304	69.60	0.83	14.51	3.99	0.77	2.90	3.86	3.54	100.00	1.06	2.88	3.80
RUA-S225-B1	Unit 1 Top	Primary clast	108	896	4	4.33	2306	69.73	0.80	14.67	3.53	0.92	3.03	3.89	3.45	100.00	0.96	2.54	3.63
RUA12-225-5B / X225BE	Unit 1 Top	Primary clast	138	878	4	4.17	2270	70.09	0.74	14.66	3.32	0.84	2.69	4.25	3.41	100.00	0.91	2.36	4.27
PDC Unit 2																			
X225CE	Unit 2 Base	Denser primary clast	148	867	2	4.23	2263	70.32	0.73	14.66	3.32	0.78	2.60	4.12	3.47	100.00	0.90	2.35	4.43
RUA-S225-C1	Unit 2 Base	Primary clast						69.32	0.79	14.89	3.68	1.03	2.93	4.10	3.25	100.00	0.99	2.64	3.96
X225DE	Unit 2 Upper	Denser primary clast	134	878	2	4.30	2282	70.10	0.78	14.61	3.39	0.84	2.72	4.09	3.47	100.00	0.92	2.42	4.05
RUA-S225-D1	Unit 2 Upper	Primary clast	108	901	3	4.29	2310	69.49	0.75	14.78	3.54	0.95	3.08	4.00	3.42	100.00	0.97	2.54	3.55
RUA-S225-D3a	Unit 2 Upper	2nd magma: Less vesicular, lower SiO2 glass						68.04	0.93	15.18	4.51	0.84	3.64	3.85	3.03	100.00			
RUA-S225-D3b	Unit 2 Upper	2nd magma: More vesicular, higher SiO2 glass	113	890	4	4.37	2305	69.74	0.77	14.65	3.72	0.89	2.84	3.70	3.70	100.00	0.99	2.68	3.69
PDC Unit 3																			
RUA13-107 / X107A1	Unit 3	Primary clast	119	907	15	4.14	2301	69.68	0.73	14.67	3.61	0.99	2.96	4.00	3.37	100.00	0.98	2.59	3.75
PDC Unit 4																			
X129AC	Unit 4	Primary clast	153	837	1	4.64	2242	72.06	0.62	13.92	2.82	0.60	2.26	3.71	4.00	100.00	0.78	1.98	4.45
RUA-S129-A3a	Unit 4	Primary w/ grey-brown bands: Band glass	158	833	0	4.62	2235	72.09	0.59	14.17	2.88	0.58	2.15	3.64	3.89	100.00	0.79	2.04	4.62
RUA-S129-A3b	Unit 4	Primary w/ grey-brown bands: Primary glass	113	886	13	4.42	2316	69.68	0.80	14.45	4.16	0.78	2.93	3.64	3.552	100.00	1.09	3.02	3.67
RUA-S129-A5	Unit 4	Second magma type						72.62	0.51	14.03	2.45	0.55	2.06	3.78	3.99	100.00			
PDC Unit 5																			
RUA13-262-Y1 / X262Y1	Unit 5 Top	Primary clast	134	876	3	4.34	2281	70.45	0.76	14.40	3.40	0.83	2.71	4.07	3.39	100.00	0.93	2.43	4.06

Table 5.5: Glass chemistry, modelled magma storage pressures and temperatures, and calculated melt densities and viscosities of Ruapehu's pumice-dominated PDCs. Glass chemistry is 100% anhydrous as this was provided directly from the EDS analyses. Numbers of analyses and standard deviations are provided in Appendix 4. Secondary magmatic components are highlighted in grey. Modelled storage conditions that did not reach the required $\Delta T_m in \leq 10°C$ are highlighted in pink, and will have greater associated errors (Box 5.2). **Fe2O_3, FeO and H_2O are calculated by the MELTS thermodynamic model, and wt. %s are recast to include the hydrous phases. They are included for reference only since not all of the analyses were able to be modelled in this way.

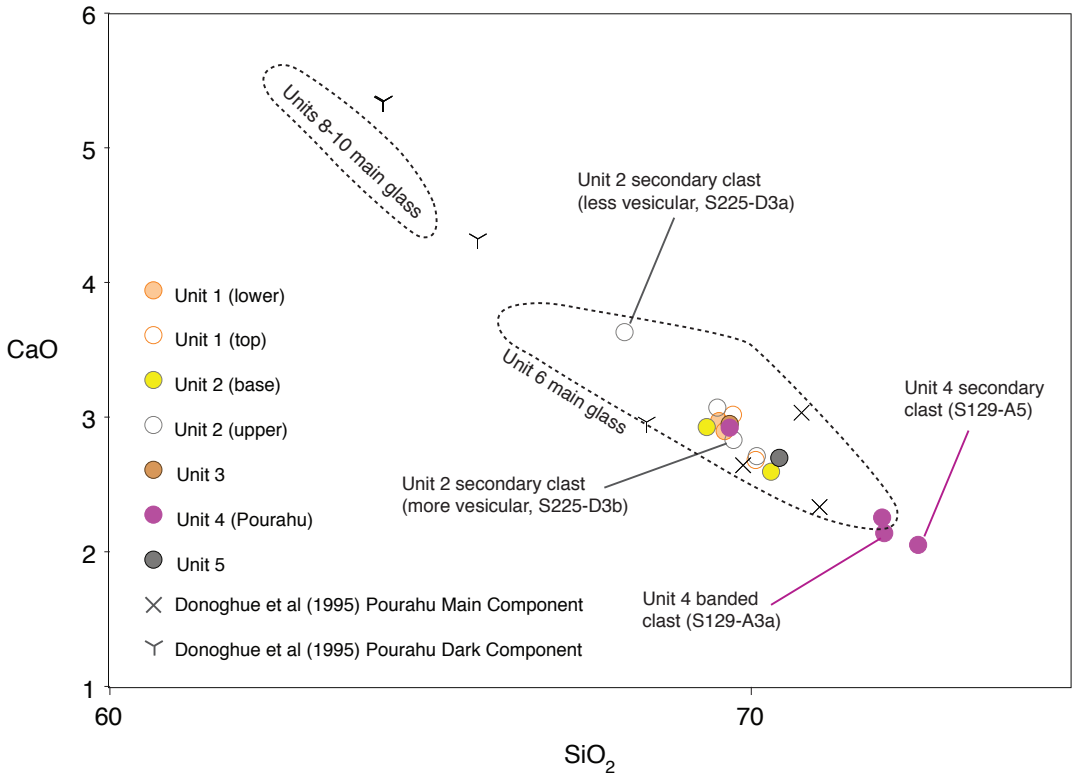

Figure 5.12: CaO-SiO_2 glass chemistry of clasts from Ruapehu's pumice-dominated PDC deposits, highlighting the differences between the main and mingled components. The CaO-SiO_2 diagram is representative of the other major element variation diagrams, but best highlights the differences between the PDC units that are also seen on the CaO-MgO whole-rock diagram (Figure 5.11). Fields for the primary pyroclasts from variably welded Unit 6 and denser Units 8-10 are shown for comparison.

Magma storage conditions

SEM and thin section analyses (Appendix 4) show that all of Ruapehu's pumice-dominated PDCs crystallised plagioclase (labradorite ± bytownite), clinopyroxene (augite), orthopyroxene (enstatite), and titanomagnetite, while ilmenite was only observed in two samples. Plagioclase phenocrysts in the pumiceous PDCs commonly show micro-jigsaw-fit textures separating parts of the crystals by a few microns (Figure 5.15 a &b), similar to those reported by Kennedy et al. (2005).

Rhyolite-MELTS modelling of simultaneous crystallisation of plagioclase, orthopyroxene and clinopyroxene in equilibrium with the measured glass chemistries suggests that all of Ruapehu's pumiceous PDCs were erupted from water-rich magmas (3.55-4.62 wt. %, Table 5.5) stored at pressures exceeding 108 MPa (Table 5.5, Figure 5.28). This equates

to depths >4.1km assuming an average crustal density of 2600kgm^{-3} (after Kilgour et al., 2013). Units 1-3 were sourced from ~4.1 to 5.6km (108-148 MPa), with a slight increase in storage depth from Unit 1 to Unit 2. Maximum chamber temperatures were ~900 °C on the basis of crystallising phase saturation temperatures. Unit 4 was sourced from a slightly deeper chamber than Ruapehu's other plinian units (~4.3-5.8km, 113-153 MPa), with maximum chamber temperatures between ~837-886 °C (Table 5.5).

In the case of the secondary (mingled) components, many of the glass analyses did not return definitive P-T results (Table 5.5). This supports the notion that they represent external magmas not in equilibrium with the crystallising plag-cpx-opx assemblage at the time of mingling and eruption, and demonstrates the sensitivity of the rhyolite-MELTS geobarometer for filtering out data that does not meet the strict thermodynamic constraints (Box 5.2). Of the secondary clast analyses that did return results, sample RUA-S225-D3b (Unit 2 secondary clast, more vesicular domain, Figure 5.15 d) returned P-T results of 113 MPa and 890°C. This fits within the broader Unit 2 storage field (Figure 5.28), reinforcing the glass chemistry observations that this likely represents a band of primary magma mingled within the secondary black-brown clast. The less vesicular domain (RUA-S225-D3a), reflecting the secondary magma type and containing more mafic glass, did not provide equilibrium convergence.

For Unit 4, only one mingled component from banded sample RUA-S129-A3a returned reliable P-T results (Table 5.5, Figure 5.28), here suggesting a similar, though marginally deeper, storage to the main Pourahu magma (P=158 MPa and T=833 °C). A second whole-clast sample of Unit 4's interpreted secondary component (RUA-S129-A5) did not return reliable P-T estimates.

Density

Ruapehu's pumiceous PDC deposits have the lowest pyroclast densities of all of the observed PDC deposits (Figures 5.13 and 5.14), mostly averaging <1000 kgm^{-3} for the primary clasts.

PDC Unit 1 has the highest average pyroclast density of the pumiceous PDC deposits ($\bar{\rho}$ = 1405 kgm^{-3}), and has a wide range of primary clast densities (673 to 1632 kgm^{-3}, average, $\bar{\rho}$ = 1087 kgm^{-3}) evidencing heterogeneity in the vesiculating primary magma. Secondary clasts ($\bar{\rho}$ = 1603 kgm^{-3}) in Unit 1 have consistently higher bulk densities than the primary clasts from the main magma (Fig 5.13). PDC Unit 2 has a very wide range of primary clast densities (322 to 1388 kgm^{-3}, average, $\bar{\rho}$ = 935 kgm^{-3}), again evidencing heterogeneity in the vesiculating primary magma. Banded ($\bar{\rho}$ = 1103 kgm^{-3}) and discrete secondary clasts ($\bar{\rho}$ = 1277 kgm^{-3}) in Unit 2 have consistently higher bulk densities than the primary clasts from the main magma (Fig 5.13).

PDC Unit 4 has lower and less variable bulk pyroclast densities than the older Units 1-3 (Fig 5.14), and unlike Unit 2 the banded clasts do not have significantly different average densities to the primary clasts (809 kgm^{-3} for the banded clasts and 804 kgm^{-3} for the primary clasts). However, discrete clasts of the darker secondary clast type in Unit 4 *do* have consistently higher densities, consistent with Ruapehu's other pumice-dominated PDC deposits ($\bar{\rho}$ = 930 kgm^{-3}, Figure 5.13).

Total (all clast types included) pyroclast densities of the pumice-dominated PDC deposits show the same trends as the primary clasts, but the inclusion of secondary and lithic components increases the average overall pyroclast densities (Figure 5.14). This is particularly the case for lithic-rich PDC Unit 1 (42% lithic clasts; Chapter 4, Figure 4.8) with an all-clasts average density of 1405 kgm^{-3} compared to 1087 kgm^{-3} for the primary clasts alone.

Calculated melt densities (Table 5.5) for PDC Units 1-3 range from 2263-2310 kgm^{-3} for the primary magmas. The interpreted secondary (mingled) component in Unit 2 (RUA-S225-D3b) has a similar density of 2305 kgm^{-3}. For Unit 4, the primary magma has densities between 2242-2316 kgm^{-3}, with the banded glass from sample S129-A3a falling just over these values (2335 kgm^{-3}). This is consistent with the observation that Unit 4 banded clasts do not have significantly different bulk densities to the non-banded clasts.

The calculated viscosities of the primary and mingled components (Table 5.5) in PDC

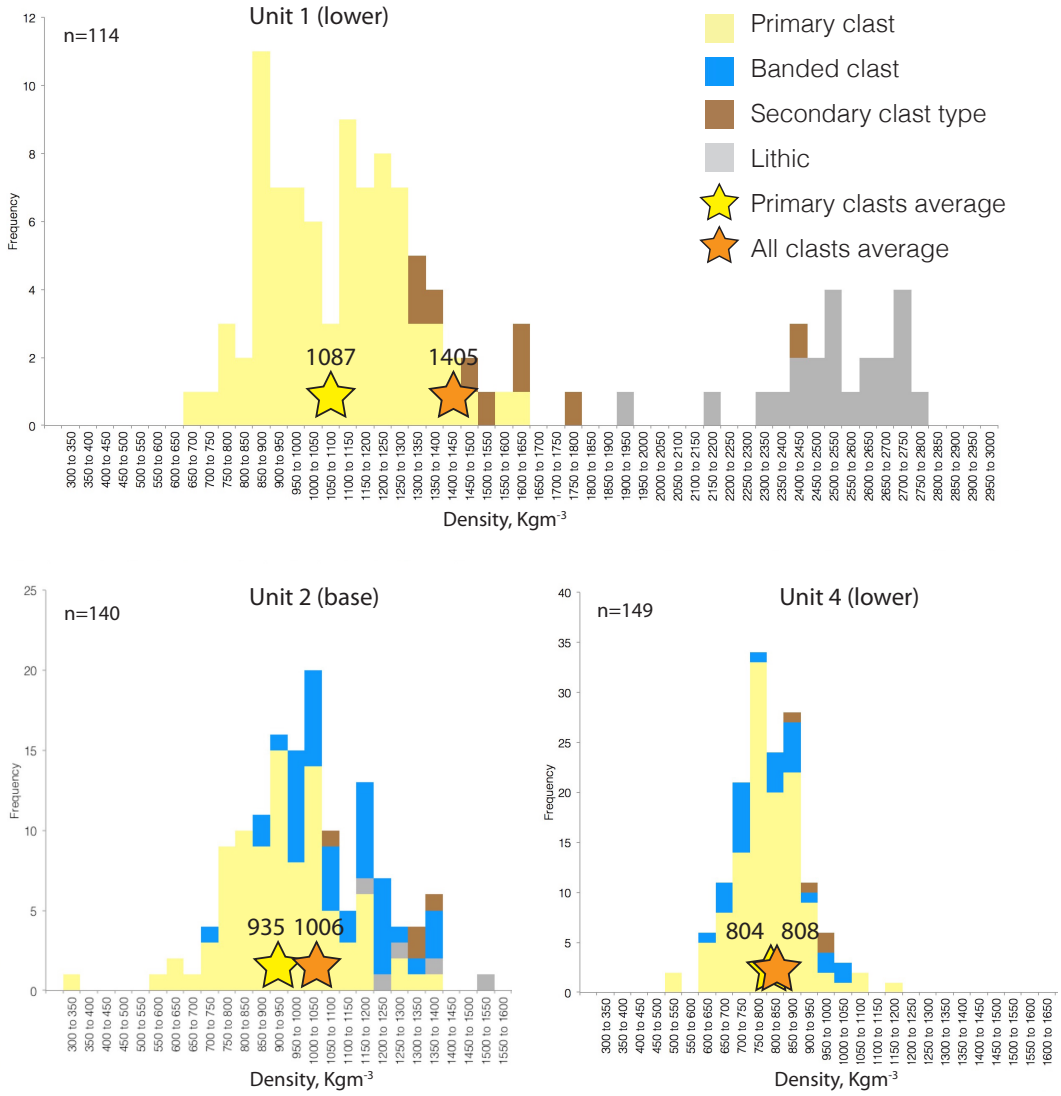

Figure 5.13: Whole-clast densities of clasts from the -5ϕ to -4ϕ sieved size fractions for Ruapehu's pumice-dominated PDC Units 1, 2 and 4 deposits.

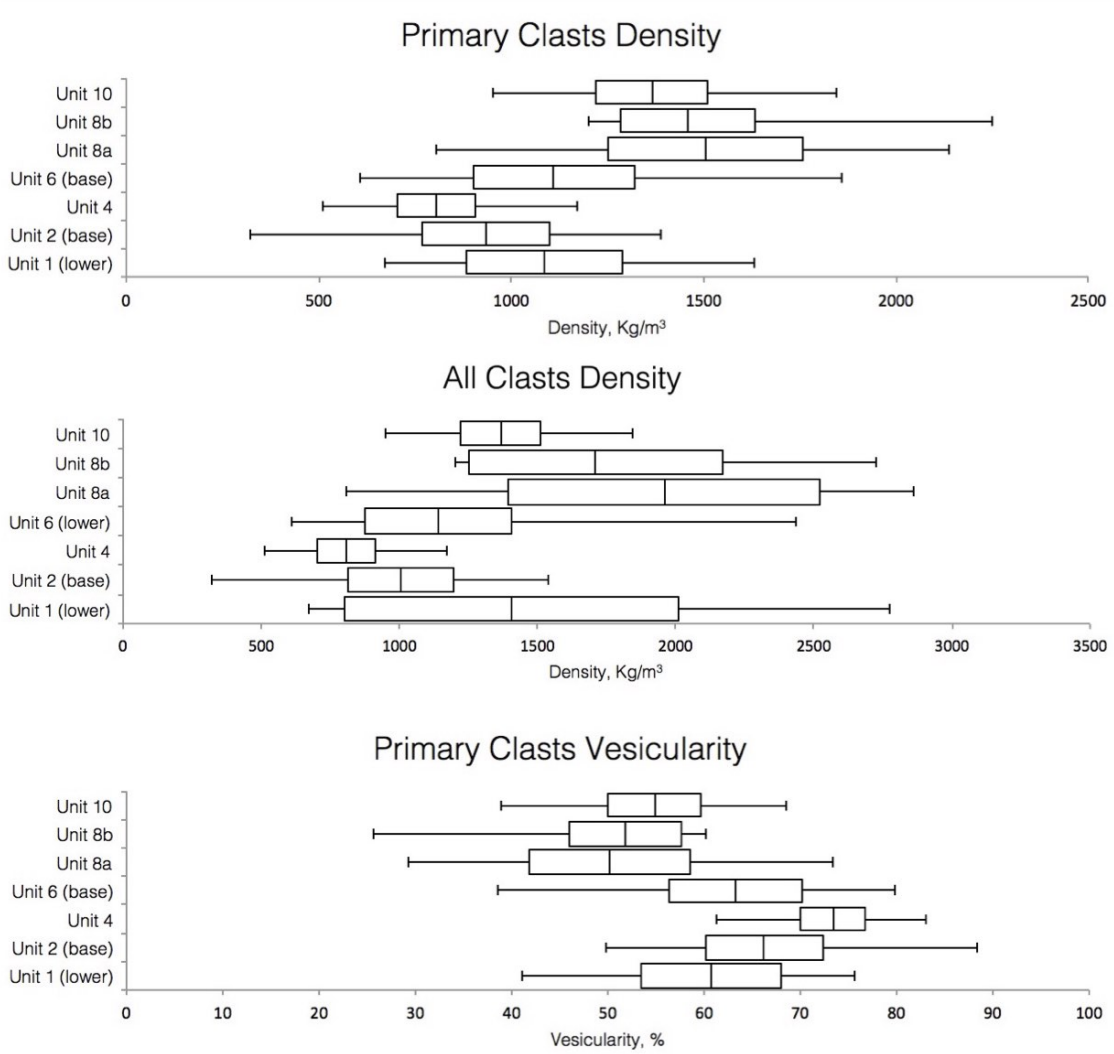

Figure 5.14: Whole-clast densities and vesicularities of clasts from the -5ϕ to -4ϕ size fractions for Ruapehu's PDCs. Boxes show average values ± 1 s.d., whiskers show min and max density values.

Units 1-3 are broadly similar, and range from log 4.14 to log 4.37 Pa s. In Unit 4, the primary components have similar calculated viscosities (log 4.42-4.64 Pa s) to the interpreted mingled component in sample S129-A3a (log 4.62 Pa s).

Micro-scale textures, vesicularity and vesicle shapes

Figures 5.15 and 5.16 present vesicle textures from lapilli within Ruapehu's pumice-dominated PDCs. The units all contain vesicular pumice lapilli with highly interconnected bubble networks and thin cuspate bubble walls.

The oldest units (PDC Units 1-2; Ohinewairua eruptive period) show distinct textural changes from older Unit 1 to younger Unit 2. Unit 1 contains highly connected, vesicular lapilli (average vesicularity = 61%) with thin microlite-free bubble walls (Figure 5.15 a) and very small (<10μm) to very large (>2mm) bubbles that show variable amounts of shear (Figure 5.16 a). In contrast, Unit 2 still contains highly-connected vesicle networks (average vesicularity = 66%), but the networks are narrower (Figure 5.16 b) and have thicker (compared to Unit 1), microlite-rich bubble walls (Figure 5.15 b), and the lapilli also lack both the very small and very large bubbles (Figure 5.16 b).

The calculated average vesicularities of the secondary magmatic components in Units 1 and 2 are lower than the primary clasts (Unit 1: 42% for secondary grey clasts, 60% for primary pumices. Unit 2: 60% for banded clasts, 54% for discrete secondary blackish clasts, 66% for the primary pumices). This observation is supported by vesicle textures in secondary clast RUA-S225-D3 from the top of Unit 2 (Figure 5.15 c-e), which in thin section has very finely vesicular, more isolated vesicles and thicker vesicle walls (Figure 5.15 e). This clast is cross-cut by a more-vesicular band of the primary melt (Figure 5.15 d), and the boundary between these two domains is marked by aligned feldspar phenocrysts, evidencing differential flow (shear) at the interface between the two magmas (Figure 5.15 c).

Primary pumices from PDC Unit 4 (Figure 5.15 f and Figure 5.16 c) are characterised by very highly interconnected vesicles separated by thin cuspate glass walls. The samples

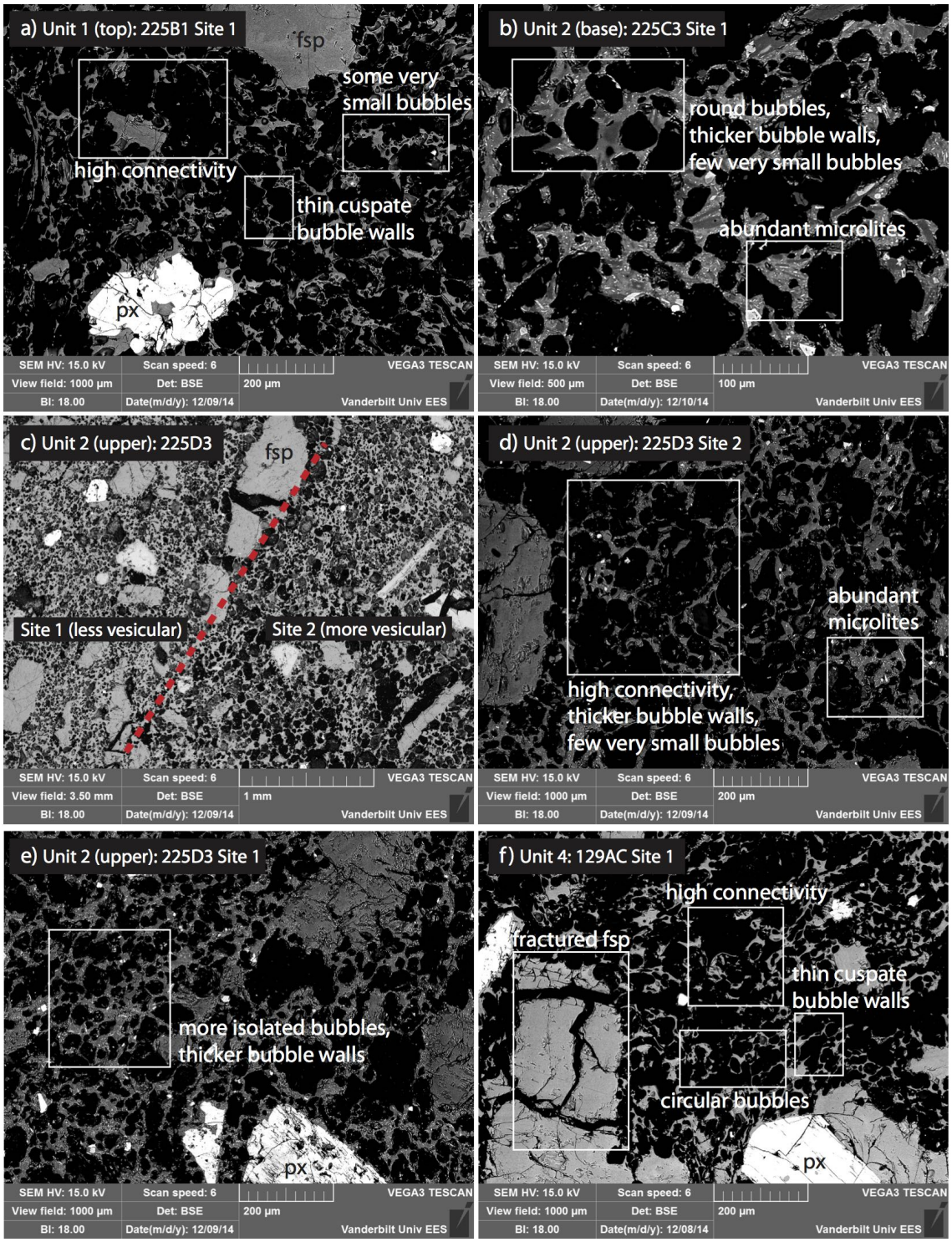

Figure 5.15: Vesicle textures in Ruapehu's pumice-dominated PDCs. All of the units have highly interconnected vesicles with thin cuspate glass walls, but b) bubble wall thickness and microlite abundance increases from Unit 1 to Unit 2. c) Banding in Unit 2 sample RUA-S225-D3 presents as less vesicular and more vesicular domains. d) The more vesicular domain represents the primary melt, while e) the less vesicular domain has slightly more mafic glass. Note the alignment of the plagioclase phenocrysts (labelled 'fsp' in c) along the boundary between the two domains, reflecting shearing between the two magmas. f) Unit 4 has very highly connected, circular bubbles, and jigsaw-fit fractured phenocrysts that probably opened as the magma explosively decompressed (Kennedy et al., 2005)

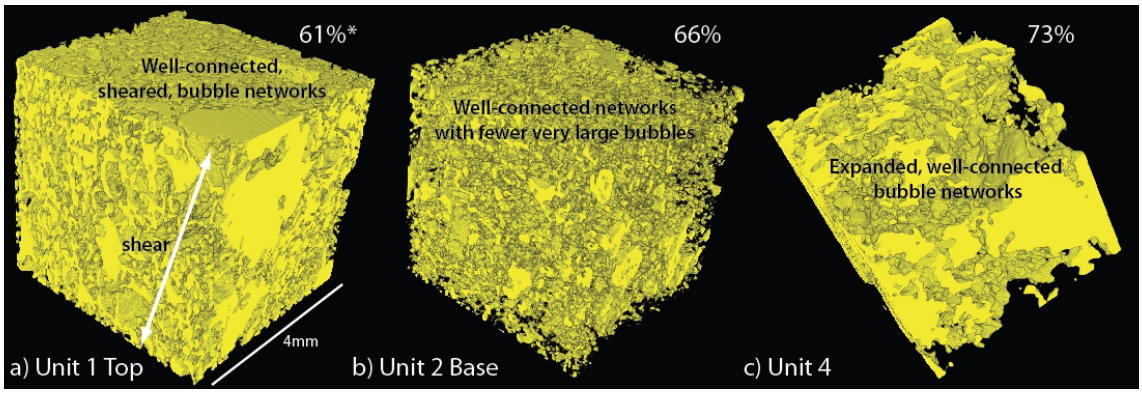

Figure 5.16: 3D vesicle textures in Ruapehu's pumice-dominated PDC deposits from high resolution synchrotron tomography of ~1cm lapilli, reflecting fragmentation-level vesicle structures. In these images the vesicles are filled and the glass is transparent in order to show the vesicle surface structures. The sides of each cube are 4mm long. All units show highly connected vesicle networks that are frozen in the process of growth and coalescence. a) Unit 1 has large and distinctly sheared vesicles (arrow), whereas b) Unit 2 has a much more narrowly connected network that lacks the very large bubbles. c) Unit 4 is more coarsely vesicular, with expanded and very highly connected vesicles. Average primary clast vesicularities calculated from the density data are shown for comparison.

from Unit 4 have the highest vesicularities of all of Ruapehu's PDCs, ranging from 61.3 to 83.0% (average = 73.4%) using Pardo's (2012) dense rock equivalent value of 3024 kgm^{-3} for corresponding clasts from the Okupata-Pourahu eruptive unit tephras. At Tukino, Unit 4 (Pourahu PDC) is only preserved where it has overtopped the valley sides of its main channel (See Chapter 4), and so it is likely that the deposits described here preferentially sampled only the lowest density components from a density-stratified flow. They therefore may not represent the bulk flow, which is not preserved.

All of the results show that Ruapehu's pumiceous PDCs were erupted from deep, water-rich magmas that mingled with other magmatic components prior to eruption and PDC generation. The key observations are presented in Table 5.6

5.4.2 Interpretation of the pumice-dominated PDCs

The modelled storage conditions and high primary pyroclast vesicularities suggest Ruapehu's pumice-dominated PDC Units were generated during plinian eruptions of initially

Deposit Features	Chemistry	Magma Storage (MELTS)	Mingling	Densities	Vesicularity
Lithic-rich base (Unit 1 only); Pumice-rich (all units). Bimodal GSDs.	Andesite with silicic dacite-to-rhyolite glass.	Deepest (4.1-6 km); Lowest T (<900°C); H_2O-rich (>3.55%); Units 1-3 from pre-exisitng system (North Crater area), Unit 4 from closed system (South Crater area).	Banded and discrete clasts of darker magmatic component(s). One mingled component in Unit 4 falls within older Unit 2 storage field.	Lowest (<1000 kgm^{-3}); Secondary and mingled clasts have higher densities than the primary clasts.	Highly interconnected (gas-rich) vesicle networks with thin cuspate bubble walls, Unit 2 has slightly thicker, microlite-rich walls and lacks very large or very small vesicles. Variable degrees of shearing.

Table 5.6: Summary of the key observations for Ruapehu's pumice-dominated PDC Units 1-4

gas-rich, water saturated magmas from deep (4.1 - 5.8 km) storage chambers. This agrees with the interpretations made by (Pardo Villaveces, 2012) for equivalent ring-plain tephras. All of the PDCs are interpreted to have resulted from collapsing eruption columns; however, the interpreted processes leading to column collapse differ between units. Table 5.6 summarises the key textural results that provide the basis for the interpretations here.

PDC Units 1-3 (Ohinewiarua eruptive period):

The at least ~10m thick lithic-rich base of Unit 1 suggests rapid conduit erosion and vent widening resulted in generation of the first of the 13.6-11.6 ka Ohinewairua PDCs. This process contributed to collapse of the plinian column in two ways. Firstly, if the exit velocity and density of the erupting mixture remained approximately constant, vent widening will have directly correlated with an increase in mass eruption rate (Equation 5.1.1). This will have limited the column's ability to entrain and heat sufficient air to remain buoyant, therefore moving the erupting mixture towards the collapse threshold (Fig 5.2 and 5.3). Secondly, incorporation of a high proportion of dense lithic clasts (~42%, based on the -5 to -4ϕ components from the sieved analyses) eroded from the conduit walls increased the bulk density of the erupting mixture (Shea et al., 2011), also increasing the mass eruption rate (Equation 5.1.1) and again moving the column towards the collapse threshold.

PDC Unit 2 is interpreted to have been emplaced from a separate eruption shortly after PDC Unit 1, since there are intervening ash layers but no evidence for a substantial

time break (Chapter 4). The Unit 2 deposits have relatively few lithic clasts and hence there is little evidence of vent widening, probably reflecting the already-widened conduit established during eruption of Unit 1. Importantly, the presence of a pre-existing widened vent means that continued eruptions from the same vent were therefore already closer to the column collapse threshold, suggesting even relatively small changes in exit velocity and/or mass eruption rate may then have led to further column collapse. In Unit 2, this appears to have been driven by densification of the erupting mixture by both limited degassing/outgassing and mingling with a denser secondary magmatic component:

Degassing: Degassing is interpreted to have been ongoing throughout the PDC Units 1-3 eruption sequence, with Unit 2 erupting a slightly more degassed magma from deeper in the chamber than Unit 1. This is evidenced by a slight thickening in vesicle walls and higher microlite contents consistent with limited degassing and degassing-induced crystallisation (Figure 5.15 b). The increase in modelled storage depths (up to ~5.6 km) and absence of very small vesicles in Unit 2 (which *are* present in Unit 1) suggests a longer magma residence time (compared with Unit 1) allowing coalescence of smaller vesicles and development of a highly connected vesicle network (Figure 5.16 b) that permitted limited pre-eruptive degassing. This will have increased the bulk density of the pyroclasts and contributed lower exsolved gas contents for driving the eruption. The variable microlite contents and wide range of densities and vesicularities in the primary Unit 2 pyroclasts evidence rheological hetrogeneity in the ascending magma column, and this may have further contributed to column instability by promoting variable ascent rates and differences in the depth of the fragmentation front (as proposed by Pardo Villaveces, 2012).

Mingling: PDC Unit 2 appears to have mingled with at least 2 different magmas; one more mafic and one more silicic than the main magma. The silicic component is chemically similar to the immediately-following Unit 4 magma, and may represent this magma's first arrival in the Ruapehu system. Since the mingled and primary components both have similar melt densities and viscosities (Table 5.5), mingling between new and resident magma will have been efficient (Snyder, 1997), and this explains the high proportion of mingled clasts observed in the deposits. The ~29% banded clasts (average density 1103 kgm^{-}3) and ~3% discrete secondary clasts (1277 kgm^{-}3) in Unit 2 are more dense than

the primary clasts, and therefore increased the bulk density of the erupting mixture. This in turn will have moved the column closer to the collapse threshold. Additionally, the lower bulk vesicularities of these clasts (54% for discrete secondary clasts compared with 66% for the primary clasts) suggests they also contributed lower exsolved gas fractions to the erupting mixture, thereby reducing exit velocities and again favouring column collapse.

PDC Unit 4 (Pourahu PDC):

PDC Unit 4 is also interpreted to have resulted from collapse of a plinian eruption column. The rhyolite-MELTS modelling shows that Unit 4 was erupted from the deepest storage zone of any of the pumice-dominated PDCs (up to 5.8 km), and it was also the lowest temperature and most silicic composition, with the corresponding highest viscosity (Table 5.5). Again, mingling ± limited degassing appears to have been important in moving the column towards collapse.

Degassing: Unit 4 pumices have very highly connected vesicles and large bubbles, evidencing extensive bubble growth and coalescence. Pardo Villaveces (2012) interpreted the high connected porosity of Okupata-Pourahu clasts in the corresponding fall deposits to reflect slow decompression rates that favoured coalescence and the development of connectivity, enabling outgassing and limited vesicle collapse during ascent (Burgisser and Gardner, 2004; Rust and Cashman, 2011). Our observations mostly support this, though we do not observe evidence of significant bubble collapse. Therefore, we interpret that *limited* degassing/outgassing through highly-connected permeable bubble networks resulted in reduced exit velocities and lower mass discharge rates that therefore moved the eruption column slightly closer to the collapse threshold. This is also supported by field isopach data (Pardo Villaveces, 2012) that shows the Okupata-Pourahu eruption had *lower* column heights (<25km) and *lower* mass discharge rates (9.2 x 10^7 kg/s) than the preceding Ohinewairua (i.e. Units 1-3) eruptions (>30km; 4.5-6 x 10^8 kg/s). Furthermore, the lower temperature of the Unit 4 magma (compared to Units 1-3) will have further reducing the buoyancy of the eruption column through less efficient heating of entrained air, again moving the column closer to the collapse condition.

Mingling: Unit 4 appears to have mingled with 2 or more different magmas; a more mafic component not observed in this study but reported by Donoghue et al. (1995a) to be the dominant secondary magma (supported by published glass analyses), and a secondary silicic component observed here as black-brown bands or discrete black-brown secondary clasts. As with PDC Unit 2, magma mingling is interpreted to have favoured column collapse and PDC generation by increasing the bulk density of the erupting mixture, and this is reflected by the slightly higher densities of the observed discrete black-brown secondary clasts compared to the primary pumices (Figure 5.13).

Sampling considerations: A possible explanation for the absence of Donoghue et al.'s (1995a) mafic component in the deposits described here is that the observed deposits represent density-fractionated deposits that are only preserved where the less-dense upper part of the PDC overtopped the valley side at a bend in the proto-Whangaehu valley near to Tukino village, while the denser main flow continued along the main valley and was not preserved (see Chapter 4). If the mafic clasts had a higher bulk density than other components in the PDC, they may then have remained in the main channelised part of the flow while the less-dense upper part overtopped the valley side. This may also explain the absence of lithic components (Chapter 4) and the much narrower and lower range of observed clast densities than the other PDC deposits; despite Pardo's (2012) observations of very high levels of textural heterogeneity in the corresponding fall deposits. It may also explain why the observed banded and secondary clasts do *not* have significantly different densities to the primary clasts in Unit 4. Again, if the deposit only represents the upper part of a density-stratified flow, any denser secondary clasts (i.e. as observed in Unit 2) would likely not have been preserved here. Therefore, the densifying effect of the magma mingling may be significantly under-represented in the deposits described here, and may have played a greater role in the generation of PDC Unit 4. These considerations emphasise the significant effect that deposit preservation can have on the resulting deposit interpretations (Chapter 4).

5.4.3 Variably welded scoria-dominated PDCs: Results

Macro-scale textures and whole rock chemistry

PDC Units 6 and 7 contain poorly sorted, grey-black rounded andesite clasts ranging from 58.75 to 60.56 wt% (anhydrous) SiO_2 (Table 5.7 and Appendix 2). The deposits are bedded and variably welded, with cooling columns extending across multiple reverse graded layers (Chapter 4). The deposits are texturally similar to the Pinnacle Ridge Tuff welded spatter deposit (interpreted in Chapter 4 to correlate with Unit 6), and a welded spatter deposit below Te Heuheu Peak immediately upslope of Units 6 and 7. Sieved analysis from the unwelded base of Unit 6 (Chapter 4, Figure 4.12) shows a bimodal grain size distribution, with abundant bomb-sized clasts in a coarse ash matrix that peaks in the 0 to 1ϕ size fraction. In the field the Unit 6 deposit appears monolithologic, and this is confirmed by the detailed componentry with less than 4% lithic clasts, of which most (3/4) are very slightly vesicular and may be cognate (Chapter 4). No weathered/altered lithics are observed. Two distinct juvenile clast types are present; the main type (Type 1, 88%) are rounded black scoriaceous clasts with chilled margins and vesicular interiors, while a subordinate number (Type 2, 8%) are clasts of the same composition that are distinctly blockier (average roundness = 3.7, Appendix 3.1.2) and generally higher density (Figure 5.19). In addition, several large bomb-sized clasts appear to be composed of agglutinated spatter that must have formed prior to incorporation into the PDC (Chapter 4, Figure 4.10). The primary clast rounding is unusually high (average roundness = 5.2) compared to the older pumice-dominated PDC units (average roundness = 4.9), especially considering the relatively short Unit 6 transport distances (~4.3 - 5.4 km, Chapter 4). Many of these features have been interpreted as evidence that Unit 6 travelled over snow or ice for much of its transport (Chapters 4 & 6). Whole rock major element analyses from Unit 6 show relatively consistent chemistry (Table 5.7), with no evidence for mingling of chemically different magmas unlike the older pumice-dominated PDCs.

Sample	Flow Unit	Clast Type	SiO_2	TiO_2	Al_2O_3	Fe_2O_3T	MnO	MgO	CaO	Na_2O	K_2O	P_2O_5	LOI	Total
PDC Unit 6														
X262AA	Unit 6, base	Primary clast	59.97	0.675	17.127	6.563	0.11	3.692	6.573	3.401	1.754	0.131	-0.2	99.796
X262AB	Unit 6, base	Blockier primary clast	59.705	0.671	17.133	6.642	0.109	3.685	6.596	3.425	1.716	0.133	0.04	99.855
X262AD	Unit 6, base	Primary clast	60.198	0.688	16.584	6.613	0.11	3.847	6.329	3.362	1.876	0.136	0.19	99.933
X262AE	Unit 6, base	Primary clast	60.448	0.689	16.598	6.486	0.106	3.725	6.346	3.375	1.912	0.135	0.03	99.85
X262A3	Unit 6, near top	Primary clast	59.454	0.705	16.815	6.613	0.108	3.821	6.295	3.34	1.935	0.137	0.69	99.913
Pinnacle Ridge Tuff														
X274A1	PRT	Primary clast	60.157	0.62	16.554	5.922	0.099	3.877	6.087	3.562	1.886	0.124	1.07	99.958
X274A3	PRT	Primary clast	59.853	0.644	16.884	5.941	0.098	3.84	6.082	3.507	1.844	0.129	1.1	99.922
PDC Unit 7														
X306A1	Unit 7	Primary clast	58.479	0.695	17.11	7.063	0.117	4.601	6.37	3.305	1.657	0.135	0.35	99.882
Te Heuheu Welded Spatter														
X301A1	Welded Spatter		56.709	0.795	17.567	8.015	0.128	4.608	7.483	3.252	1.424	0.135	-0.24	99.876
X301A4	Welded Spatter		54.876	0.806	17.145	9.438	0.131	4.73	7.043	2.963	1.509	0.17	1.05	99.861
X299A1	Welded Spatter		55.199	0.829	17.177	9.263	0.136	4.96	6.895	2.943	1.411	0.149	0.99	99.952

Table 5.7: Major element XRF chemistry for Ruapehu's welded PDCs, Pinnacle Ridge Tuff, and Te Heuheu welded spatter deposits.

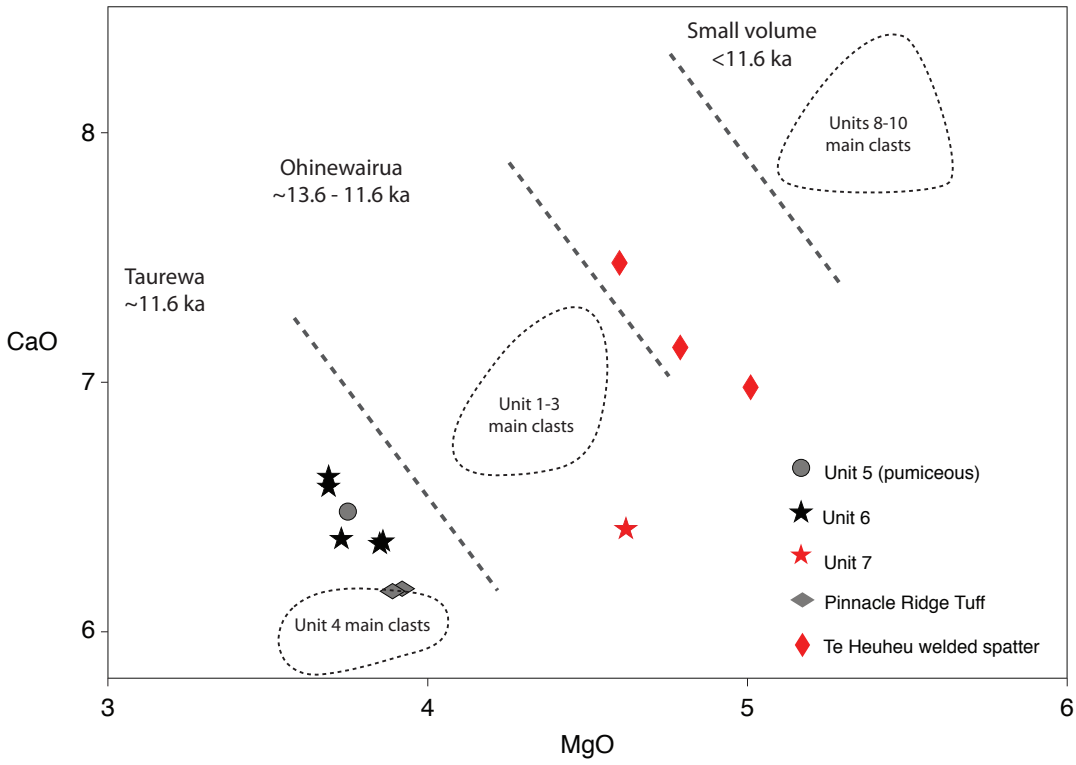

Figure 5.17: Whole-rock major element CaO vs MgO chemistry of clasts from Ruapehu's variably welded PDCs, Pinnacle Ridge Tuff, and Te Heuheu welded spatter deposits. Fields for Units 1-3, 4, and 8-10 are shown for comparison.

Glass chemistry

PDC Unit 6 has primary-component glass that straddles dacite to rhyolite in composition, ranging from 66.31 to 72.05% SiO_2 (Table 5.8 and Figure 5.18). Unlike the whole-rock major element chemistry, glass analyses from Unit 6 show significant variability; and may become more mafic in the upper deposit layers (one analysis, sample 13-262-4, Table 5.8). In thin section, sample 13-262-4 presents texturally distinct bands with different vesicularities (Figure 5.20). However the glass from each of these two domains have very similar chemistry and may not represent different magmas.

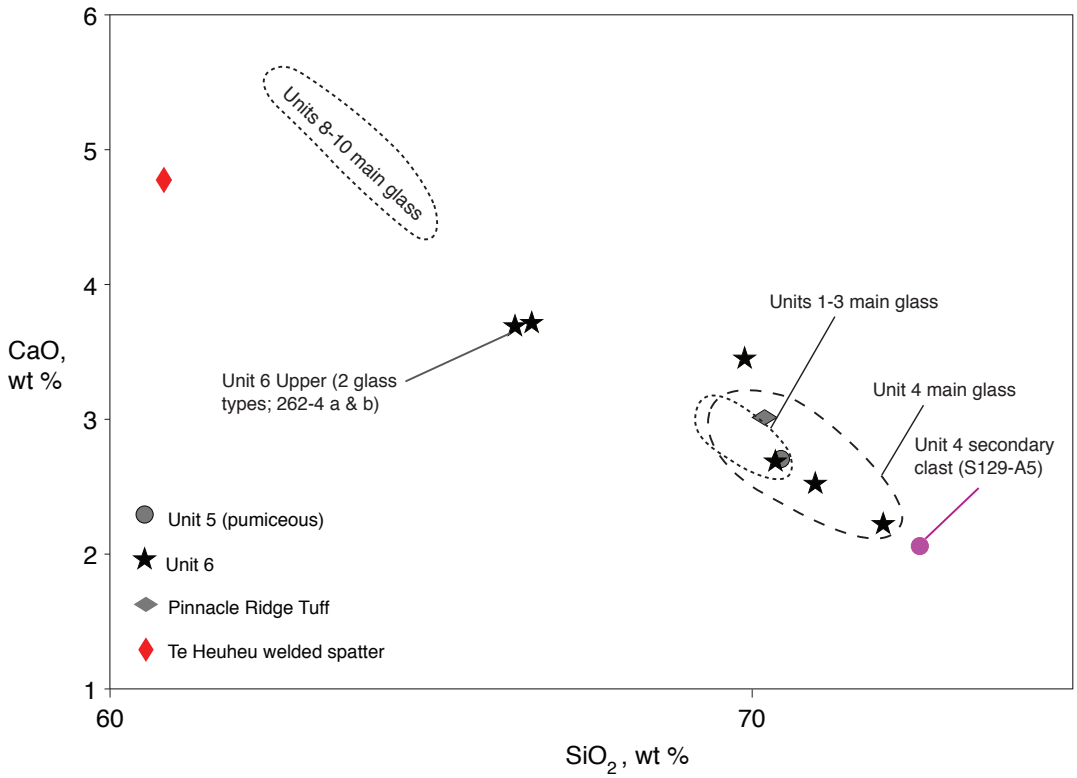

Figure 5.18: SiO_2-CaO glass chemistry of Ruapehu's variably welded PDC Unit 6, Pinnacle Ridge Tuff, and Te Heuheu welded spatter deposits. Fields for the primary pyroclast glass from the pumiceous PDCs 1-3, 4, and denser Units 8-10 are shown for comparison.

Sample	Unit	Clast Type	Storage P, Mpa	Storage T, Degrees C	Delta T	Log Viscosity, Pas	Melt density, kgm^{-3}	SiO2	TiO2	Al2O3	FeO(T)	MgO	CaO	Na2O	K2O	Total	Fe2O3**	FeO**	H2O**
PDC Unit 6																			
X262AD	Unit 6, base	Larger primary clast	138	861	2	4.44	2267	70.99	0.73	14.18	3.25	0.73	2.52	3.93	3.65	100.00	0.89	2.31	4.21
RUA12-259-1-2a	Unit 6, welded section	Primary clast in welded section, interior	92	913	18		2324	69.89	0.72	14.85	3.44	0.86	3.45	3.46	3.34	100.00	0.94	2.48	3.20
RUA12-259-1-2b	Unit 6, welded section	Primary clast in welded section, chilled margin	113	906	30		2295	70.37	0.75	14.36	3.46	0.94	2.69	3.50	3.95	100.00	0.93	2.49	3.65
RUA12-259-1-2c	Unit 6, welded section	Welded section matrix between clasts						72.05	0.64	14.06	2.51	0.73	2.22	3.67	4.11	100.00			
RUA13-262-4a	Unit 6, near top	Primary clast, isolated vesicle domain	58	969	6	4.04	2407	66.31	0.91	15.41	4.72	1.43	3.69	3.63	3.91	100.00	1.25	3.47	2.39
RUA13-262-4b	Unit 6, near top	Primary clast, connected vesicle domain	94	959	19		2377	66.57	0.97	15.52	4.83	1.49	3.71	4.01	2.91	100.00	1.26	3.54	3.18
Pinnacle Ridge Tuff																			
RUA13-274-1 / X274A1	PRT		145	877	14	4.24	2267	70.20	0.63	15.10	3.15	0.74	3.01	3.94	3.24	100.00	0.86	2.23	4.29
Te Heuheu Welded Spatter																			
RUA13-301-1 / X301A1 (Only 2 analyses)	Welded Spatter							60.84	0.26	20.66	2.59	0.83	4.78	4.13	5.93	100.00			

Table 5.8: Glass chemistry, modelled magma storage pressures and temperatures, and calculated melt densities and viscosities of Ruapehu's variably welded PDCs. Glass chemistry is 100% anhydrous as this was provided directly from the EDS analyses. Numbers of analyses and standard deviations are provided in Appendix 4. Secondary magmatic components are highlighted in grey. Modelled storage conditions that did not reach the required $\Delta T_m in \leq 10°C$ are highlighted in pink, and will have greater associated errors (Box 5.2). **$Fe2O_3$, FeO and H_2O are calculated by the MELTS thermodynamic model, and wt. %s are recast to include the hydrous phases. They are included for reference only since not all of the analyses were able to be modelled in this way.

Magma storage conditions

SEM and thin section analyses (Appendix 4) show that PDC Unit 6 crystallised plagioclase (labradorite ± bytownite ± andesine), clinopyroxene (augite), orthopyroxene (enstatite), titanomagnetite and ilmenite. rhyolite-MELTS modelling of simultaneous crystallisation of plagioclase, orthopyroxene and clinopyroxene in equilibrium with the measured glass compositions suggests that Unit 6 was erupted from water-rich magmas (2.4 - 4.2 wt %, considering only the higher-quality rhyolite-MELTS analyses, Table 5.8) mostly stored between 3.5-5.2 km (92-138 MPa, here including the lower quality rhyolite-MELTS pressure estimates due to limited data), at temperatures between 861-969°C (Table 5.8). This is slightly shallower and hotter, but nonetheless overlapping, the storage regime of the older pumice-dominated Units 1-3 (Figure 5.28). However, it is significantly shallower and hotter than compositionally similar Unit 4 (153 MPa and 835°C), which has been interpreted in Chapter 4 to belong to the same eruptive period (Taurewa eruptive period). The storage conditions for the Pinnacle Ridge Tuff, also interpreted by Hackett and Houghton (1985) and Donoghue et al. (1999) to be associated with the Okupata-Pourahu eruptive unit of the Taurewa eruptive period, falls between the modelled conditions for Unit 4 and Unit 6 with a storage pressure of 145 MPa and maximum temperature of 877°C (Table 5.8).

Although there is no definitive chemical evidence for mingling in the PDC Unit 6 samples, RUA13-262-4 has separate domains with distinctly different vesicle textures (Figure 5.20 a). The less vesicular melt domain (RUA13-262-4a) returned P-T results of 58 MPa (~2.2km) and 969°C; significantly shallower than the modelled storage for the more vesicular domain from the same sample which falls within the main Unit 6 storage zone (RUA-13-262-4b, 94 MPa and 959°C). However, as noted in Section 5.4.3 the two glasses have very similar chemistry, and may reflect similar magmas with different storage histories.

Density

The densities of primary clasts (Types 1 and 2) in the -5 to -4ϕ sieved fraction of PDC Unit 6 are the most variable of any of Ruapehu's PDCs, ranging from 609 to 1858 kgm^{-3} with an average of 1110 kgm^{-3} and standard deviation of 209 kgm^{-3} (Figure 5.19 & Figure

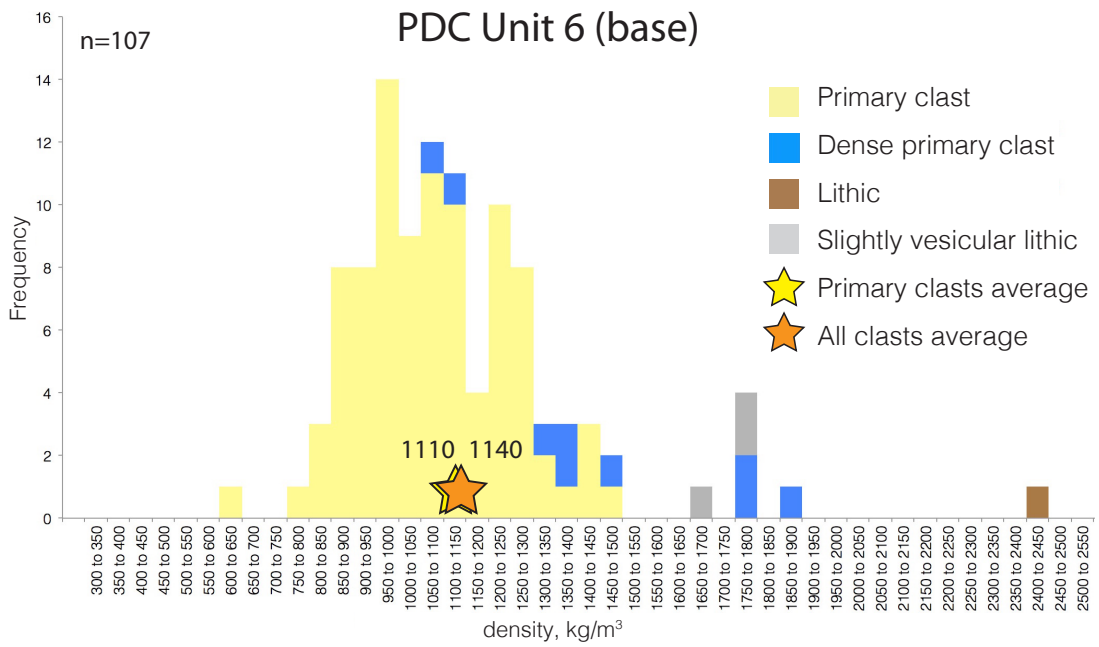

Figure 5.19: Whole-clast densities of clasts from the -5ϕ to -4ϕ sieved size fractions for Ruapehu's variably welded PDC Unit 6 deposits.

5.14). The main Type 1 rounded clasts have an average density of 1076 kgm^{-3}, higher than all of the preceding pumice-dominated PDCs, and the blockier Type 2 clasts have much higher average densities of 1469 kgm^{-3}. Total (all clasts) densities are very similar due to the almost monolithological nature of the deposits, only slightly increasing the average to 1140 kgm^{-3}. Calculated melt densities (Table 5.8) show only limited variability, but do increase slightly from 2267 kgm^{-3} near the base of Unit 6 to 2377-2407 kgm^{-3} for the more mafic clasts near the unit top.

Micro-scale textures, vesicularity and vesicle shapes

PDC Unit 6 contains vesicular lapilli (average vesicularity = 63%) that in 2-dimensions (Figure 5.20 b-c) appear to have smaller, more isolated vesicles than the preceding pumiceous PDC units. Compared to PDC Unit 4 (which is interpreted to belong to the same eruptive episode; Chapter 4), the vesicles are more irregularly distributed, have more irregular shapes, and are separated by thicker microlite-free bubble walls (Figure 5.20 b). Pinched and sheared vesicles (Figure 5.20 c) are frequently observed, and vesicles often have flattened sides where their growth has been impeded by crystals. In 3-dimensions the highly irregular vesicles form narrow, sheared connected networks that may have deflated during

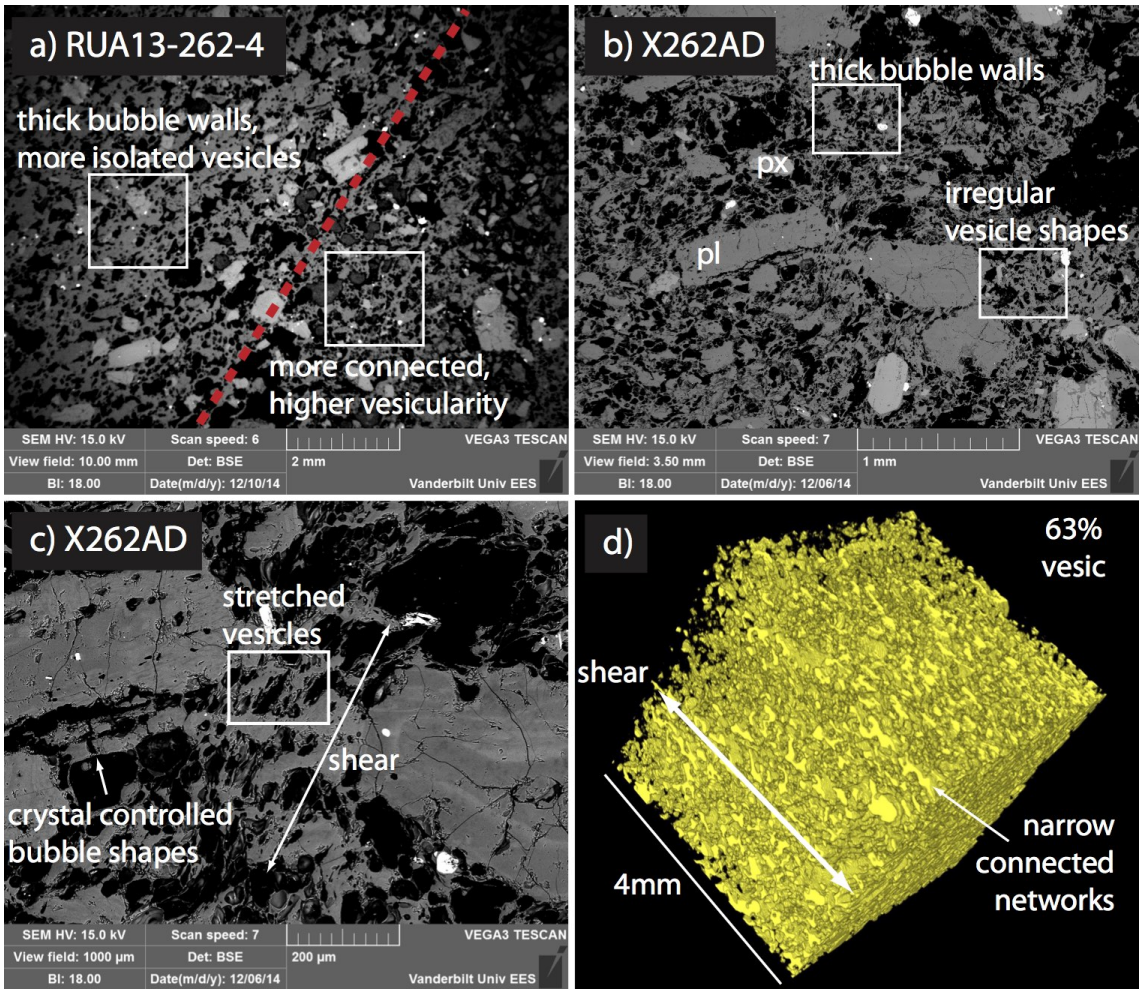

Figure 5.20: Vesicle textures in Ruapehu's variably welded PDC Unit 6 sample deposits. a) Sample RUA13-262-4 has two texturally different, but chemically similar textural domains that also have different modelled storage conditions. The less vesicular, isolated vesicle domain (left) is modelled to have been stored at 58 MPa (2.2 km), while the more vesicular domain (right) falls within the main Unit 6 storage field (94 Mpa, 3.5 km). b-d) Unit 6 pyroclasts typically have irregularly shaped, sometimes sheared vesicles connected in narrow networks with relatively thick vesicle walls. Average primary clast vesicularities (63 %) is shown for comparison.

outgassing (Figure 5.20 d).

Using Pardo's (2012) dense rock equivalent value of 3024 kgm^{-3} for clasts from the Okupata-Pourahu eruptive unit, the calculated vesicularities evidence significant textural heterogeneity. Primary clast vesicularities range from 38.5-79.9 vol %, with an average of 63.3 vol % (Figure 5.14). The main, rounded Type 1 clasts have an average vesicularity of 64.4%, while the blockier Type 2 clasts have a lower average vesicularity of 51.4%.

Deposit Features	Chemistry	Magma Storage (MELTS)	Mingling	Densities	Vesicularity
Variably welded; bedded; rounded pyroclasts; spatter clasts. Bimodal GSD with slightly coarser matrix than the pumiceous units.	Andesite (Unit 6 is the most silicic andesite of Ruapehu's PDCs) with dacite-rhyolite glass.	Moderately deep (3.5-5.2km); Intermediate T (861-969°C); H_2O-rich (>2.39%). Erupted from pre-existing system (North Crater area).	Sample 262-4 consists of 2 chemically similar but different vesicularity domains. The lower-vesicularity domain has much shallower modelled storage conditions (2.2 km)	Intermediate (average 1110 kgm^{-3}) and highly variable.	Vesicles more irregular than the pumiceous PDCs, forming narrow, sheared, connected networks with thicker, microlite-free bubble walls. Degassing textures dominant.

Table 5.9: Summary of the key observations for Ruapehu's welded PDC Unit 6.

All of the results show that Ruapehu's variably welded PDC Unit 6 was erupted from moderately-deep, water-rich magmas, whose pyroclast vesicle textures reflect higher amounts of pre- or syn-eruptive degassing. The key observations are presented in Table 5.9

5.4.4 Interpretation of the variably welded scoria-dominated PDCs

PDC Unit 6 was generated by eruption of silicic magma from 3.5-5.2 km depth. The deposit is chemically similar to pumice-dominated PDC Unit 4, and together with the welded fall deposits of the Pinnacle Ridge Tuff (PRT) is interpreted to have been erupted around the same time as the ~11.6 ka Okupata-Pourahu eruptive unit in the Taurewa eruptive period (Chapter 4 and Donoghue et al., 1999). However, clasts of welded spatter, multiple reverse graded deposit layers, and variable welding in the Unit 6 deposits show that this unit had very different generation and transport mechanisms to the preceding pumice-dominated PDCs.

Whereas pumice-dominated Unit 4 is interpreted to have resulted from a collapsing plinian eruption column from gas-rich magma explosively erupted from a new vent (Section 5.4.2), the Unit 6 and Pinnacle Ridge Tuff deposits were erupted from a shallower pre-existing magmatic system near North Crater. This is interpreted to have promoted active pre- and syn-eruptive degassing, supported by the higher clast densities, lower average vesicularites (63% in Unit 6 vs. 73% for Unit 4), and vesicle textures reflecting significant

outgassing and bubble collapse through narrow (partially deflated) connected networks (Kennedy et al., 2016). Compared with Unit 4, the Unit 6 magma was hotter (861-969°C vs 833-837°C) and lower viscosity (Log viscosity 4.04-4.44 Pas vs. 4.64-4.93 Pas, Table 5.8), and this is interpreted to have permitted more decoupled ascent of the gas phase. The Unit 6 eruption is therefore interpreted to have produced a fountaining/spatter-forming eruption column that rapidly deposited hot pyroclasts near to the vent. This is supported by the deposit welding and clasts of welded spatter within both the PRT and PDC Unit 6 deposits (Chapter 4, Figure 4.10), despite the modest modelled magma storage temperatures (877°C for the PRT, and 861-959°C for Unit 6) that are similar to those for the unwelded pumice-dominated PDC Units 1-3. Here, a relatively low fountaining-style eruption column, higher clast densities, and rapid near-vent accumulation rates are all interpreted to have limited the amount of clast cooling in the eruption column, therefore allowing some clasts to weld on deposition and form the larger spatter clasts observed in the Unit 6 deposits. Where the accumulating pyroclasts landed on relatively shallow slopes, they are interpreted to have remained in-situ and produced the welded PRT deposit. In contrast, when the pyroclasts landed on steeper slopes we interpret that they temporarily remained in-place before reaching a critical thickness and collapsing en-mass to produce PDC Unit 6 (as also observed at Ngauruhoe volcano, Lube et al., 2007; and Manam volcano, Appendix 7.1). Multiple reverse graded layers in the Unit 6 deposit (Chapter 4, Figure 4.11) evidence numerous accumulation-collapse cycles, while the presence of vertical cooling columns cross-cutting multiple deposit layers suggest these PDCs were emplaced over a short time (minutes to hours). Texturally similar PDC Unit 7 is interpreted to have formed in the same way.

5.4.5 Heterolithologic small volume PDC deposits: Results

Macro-scale textures and whole rock chemistry

PDC Units 8-10 (Tukino PDCs), 11 and 12 all contain dense (Section 5.4.5), blocky (average primary clast roundness = 4.2 in Unit 8b, 4.5 in Unit 10, Appendix 3.1.2) basaltic-andesite to andesite clasts ranging from 54.08 to 58.43 wt% SiO_2. Sieved grain size analyses from Units 8a, 8b, and 9b show nearly unimodal trends with broad peaks between medium lapilli and medium ash (Chapter 4, Figure 4.16). This reflects both a lack of very large

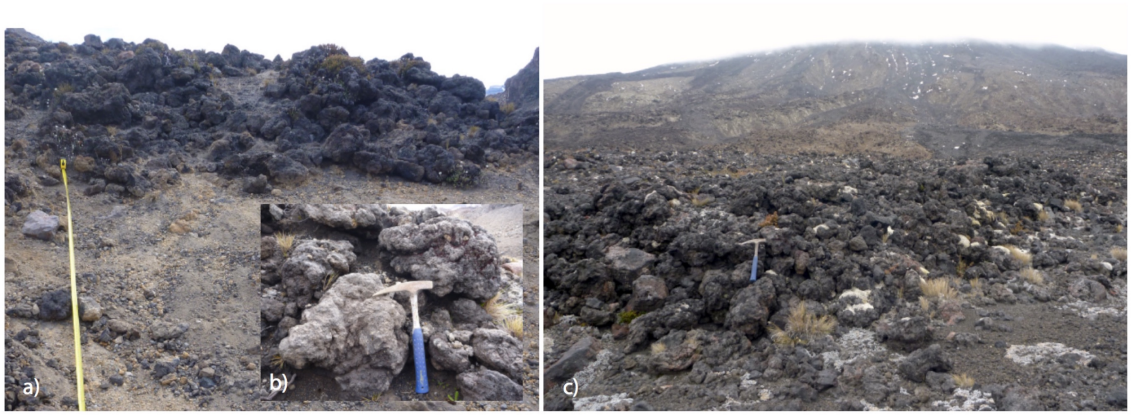

Figure 5.21: Comparison of Ruapehu's Unit 10 deposit textures with modern PDC deposits from Ngauruhoe volcano. a) & b) Unit 10 is dominated by large, clast-supported cauliflower textured bombs, and is c) texturally very similar to modern PDC deposits from the 1975 eruption of neighbouring Ngauruhoe volcano (see also Figure 5.1.

bomb-sized clasts in the deposit, and also a lower contribution of fine material generated in-flow than the preceding less-dense Units 1-6. Grain size increases rapidly at the very top of Unit 9 and into Unit 10, which has a more characteristic bimodal distribution with large bombs in a medium-to-fine ash matrix (Chapter 4, Figure 4.16).

The most distinctive macro-scale textures in Units 8-12 are the presence of dense, cauliflower textured bomb-sized clasts in all units (Figure 5.21). In the sequence of small PDC deposits immediately north of Tukino village (Units 8-10, Chapter 4), the oldest unit (Unit 8) contains very distinctive orangish-yellow cauliform clasts that have dense black-grey interiors and striking olive-gold banding (Chapter 4, Figure 4.15). These clasts are absent higher in the sequence. The youngest unit in the sequence (Unit 10) contains very large (up to ~1m) black cauliflower bombs and occassional breadcrust bombs, and is almost identical to PDC deposits from the 1975 eruption of neighbouring Ngauruhoe volcano (Fig 5.21). The major difference between the Ngauruhoe deposits and Ruapehu's Unit 10 is that the Ruapehu PDC was much more mobile - travelling at least 5km from source compared to less than 2.3 km at Ngauruhoe.

Whole-rock major element analyses from Units 8-10 (Table 5.4.5) show relatively little variability; however two clasts (X108AC and X161AA) are significantly more silicic andesites despite no obvious difference in their macro-scale textures. Sample X161AA is chemically most similar to the earlier PDC Units 1-3, and is significantly different to all

Sample	Flow Unit	Clast Type	SiO_2	TiO_2	Al_2O_3	Fe_2O_3T	MnO	MgO	CaO	Na_2O	K_2O	P_2O_5	LOI	Total
PDC Unit 8a														
X109AC	Unit 8a	Banded primary clast	56.335	0.76	16.898	8.109	0.135	5.26	8.034	2.962	1.201	0.118	-0.12	99.692
X109AA	Unit 8a	Primary clast	53.086	0.76	17.444	8.17	0.137	5.297	8.083	2.825	1.103	0.119	2.92	99.944
X109AB	Unit 8a	Primary clast	54.482	0.755	16.966	8.239	0.14	5.401	8.148	2.974	1.176	0.118	1.54	99.939
PDC Unit 8b														
X108AA	Unit 8b	Primary clast	54.589	0.775	17.777	8.212	0.134	5.189	7.804	2.987	1.219	0.125	1.06	99.871
X108AB	Unit 8b	Primary clast	54.64	0.751	17.817	8.209	0.131	5.309	7.83	2.838	1.171	0.121	1.07	99.887
X108AC	Unit 8b	Primary clast	57.234	0.742	16.822	7.777	0.124	4.929	7.438	3.045	1.395	0.124	-0.37	99.26
A108AD	Unit 8b	Primary clast	56.511	0.746	16.833	8.008	0.131	5.194	7.796	3.012	1.283	0.121	0.19	99.825
PDC Unit 9b														
X108BA	Unit 9b	Primary clast	52.575	0.814	18.133	8.628	0.135	5.459	7.619	2.699	1.032	0.131	2.57	99.795
X108BB	Unit 9b	Primary clast	54.41	0.775	17.83	8.289	0.132	5.349	7.829	2.82	1.1	0.124	1.18	99.838
X108BC	Unit 9b	Primary clast	54.809	0.773	17.854	8.351	0.132	5.311	7.859	2.852	1.103	0.122	0.73	99.896
X108BD	Unit 9b	Larger primary clast	55.764	0.744	17	8.169	0.135	5.343	8.012	3.089	1.273	0.125	0.25	99.904
PDC Unit 9c														
X405A1	Unit 9c	Primary clast	56.316	0.75	16.986	8.109	0.135	5.163	7.89	3.131	1.34	0.123	-0.04	99.903
PDC Unit 10														
X161AC	Unit 10	Primary clast	56.462	0.741	16.91	7.922	0.128	5.125	7.799	3.006	1.27	0.122	0.36	99.845
X108CA	Unit 10	Larger primary clast	55.479	0.762	17.1	8.312	0.135	5.429	7.867	3.025	1.243	0.122	0.4	99.874
X161AA	Unit 10	Primary clast	57.808	0.737	17.177	7.291	0.122	4.287	6.549	3.164	1.678	0.127	0.94	99.88
X161AB	Unit 10	Primary clast	54.609	0.761	17.456	8.108	0.137	5.201	7.862	2.995	1.231	0.122	1.47	99.952
PDC Unit 11														
X225EB	Unit 11	Primary clast	56.99	0.73	18.17	7.45	0.12	4.11	7.20	3.39	1.41	0.13	0.22	99.92
PDC Unit 12														
X296A1	Unit 12	Primary clast	55.463	0.73	18.819	7.805	0.128	4.153	7.007	3.345	1.269	0.115	1.1	99.934

Table 5.10: Major element XRF chemistry for Ruapehu's heterogenous small volume PDCs. Analyses of clasts of secondary magma types are highlighted.

other analysed clasts from Units 8-10 (Figure 5.22). Whole-rock major element analyses of primary clasts from Units 11 and 12 are most comparable to PDC Units 1-3 (Table 5.4.5 and Figure 5.22), consistent with the field stratigraphic interpretations that these units were emplaced at the end of the pumiceous Units 1-3 sequence (Chapter 4).

Glass chemistry

Ruapehu's heterogeneous small volume PDCs have primary-component dacitic glass ranging from 63.01 to 64.88 wt% SiO_2 for Units 8-10, and 68.75 wt% SiO_2 in the sample from Unit 11 (Table 5.11 and Figure 5.23).

PDC Unit 8, the oldest of the small PDCs preserved next to Tukino village, shows evidence of complex magma mingling with visibly banded clasts. Sample X109AC from PDC Unit 8a, which in hand sample has distinctive olive-gold banding (Chapter 4, Figure 4.15), has several different textural domains in thin section (Figure 5.26). These correspond to at least two chemically distinct mingled magmas: 1) the majority of the clast is composed of a finely vesicular, microlite-rich glass (Figure 5.26 a) ranging from 63.6-64.3 wt% SiO_2, comparable to the other Units 8-10 primary component glasses. 2) a second, more silicic

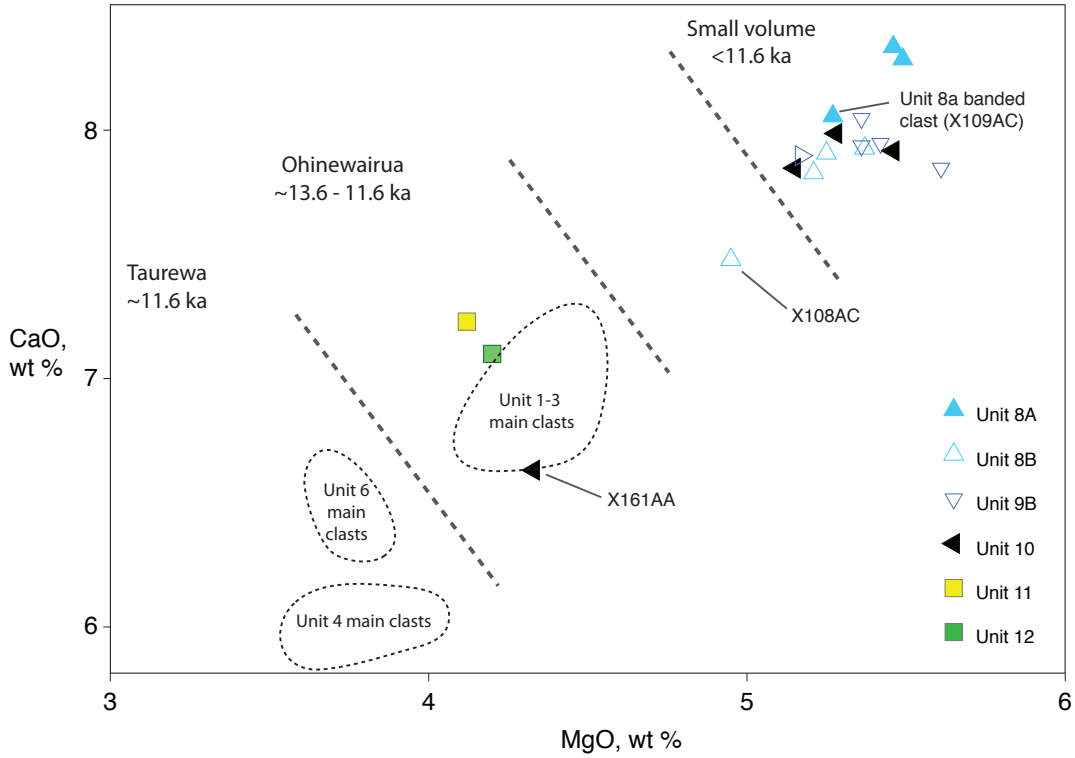

Figure 5.22: Whole-rock major element CaO vs MgO chemistry of clasts from Ruapehu's heterogeneous small volume PDC deposits (Units 8-10, 11 & 12). Fields for Units 1-3, 4 & 6 are shown for comparison.

microlite-free glass is present in highly vesicular bands (Figure 5.26 b), and has similar chemistry to all of the preceding pumice-dominated and variably welded PDC Units 1-6 (analysis 109ACb, 70.5 wt% SiO_2; Figure 5.23). A second highly vesicular domain is also present (Figure 5.26 d), but its chemistry (analysis 109ACc, 62.7 wt% SiO_2) does not sufficiently differ from the primary component glass to definitely allocate it to a third magma type despite the distinct textural differences.

Banded sample X108AC, from PDC Unit 8b, reinforces the observations from Unit 8a. In hand sample, X108AC does not have the distinctive olive-gold banding, but instead has an olive interior with a darker black-brown band. However, the glass analyses show the same trends observed in Unit 8a, with a microlite-rich primary-component (analysis 108ACa, 64.2 wt% SiO_2), and a secondary microlite-poor silicic component (analysis 109ACb, 73.8 wt% SiO_2, Table 5.11). However in this instance the mingled secondary glass is by far the most silicic of any of the Ruapehu analyses; with the closest comparable glass chemistries being those from pumice-dominated Unit 4 and variably welded Unit 6

(Figure 5.23).

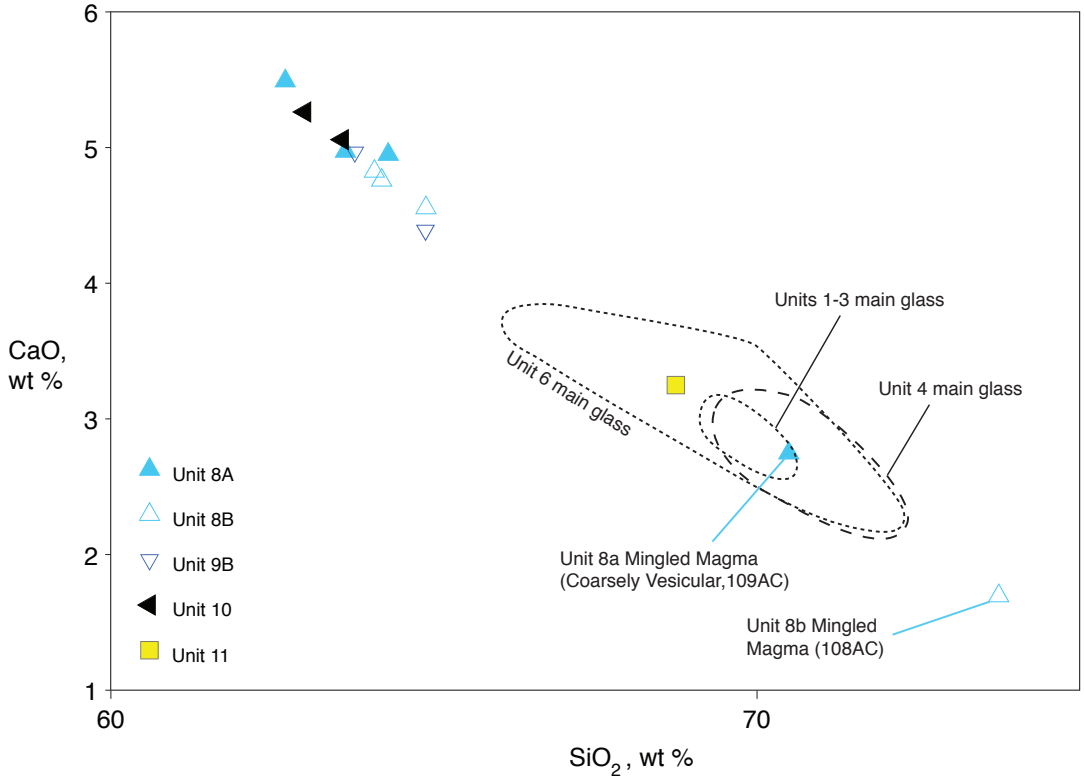

Figure 5.23: SiO_2-CaO glass chemistry of Ruapehu's denser PDC Units 8-10, and 11. Fields for the primary pyroclasts from the pumiceous PDCs 1-3, 4, and variably welded Unit 6 are shown for comparison.

Sample	Unit	Clast Type	Storage P, Mpa	Storage T, Degrees C	Δ T	Log Viscosity, Pas	Melt density, kgm^{-3}	SiO2	TiO2	Al2O3	FeO(T)	MgO	CaO	Na2O	K2O	Total	Fe2O3**	FeO**	H2O**
PDC Unit 8a																			
X109ACa	Unit 8a	Larger banded clast, finely vesicular glass bulk inc. microlites						64.30	0.91	15.84	5.81	1.98	4.95	3.49	2.73	100.00			
X109ACb	Unit 8a	Larger banded clast, coarsely vesicular glass	114	886	7	4.51	2308	70.50	0.77	14.09	3.73	0.85	2.75	3.66	3.67	100.00	1.00	2.69	3.58
X109ACc	Unit 8a	Larger banded clast, second coarsely vesicular glass	56	1041	32		2493	62.70	0.94	16.11	6.33	2.50	5.49	3.63	2.30	100.00	1.14	5.15	2.42
X109ACd	Unit 8a	Larger banded clast, glass in microlite rich zone						63.63	1.15	15.17	7.55	1.56	4.97	3.48	2.51	100.00			
PDC Unit 8b																			
X108ACa	Unit 8b	Larger banded primary clast, glass btwn. microlites						64.19	1.13	15.26	6.76	1.56	4.76	3.60	2.72	100.00			
X108ACb	Unit 8b	Larger banded primary clast, microlite poor domain						73.75	0.68	12.82	2.86	0.47	1.70	3.59	4.13	100.00			
X108AD	Unit 8b	Larger primary clast, glass btwn. microlites						64.88	1.00	15.01	6.25	1.88	4.56	3.68	2.74	100.00			
RUA-S108-A1	Unit 8b	Primary clast, glass btwn. microlites	22	1030	8	4.02	2556	64.08	1.12	15.09	6.91	1.74	4.82	3.50	2.73	100.00	1.26	5.69	1.13
PDC Unit 9b																			
X108BC	Unit 9b	Larger primary clast, glass btwn. microlites					2574*	64.87	1.15	14.67	6.87	1.60	4.39	3.63	2.82	100.00	1.25	5.70	0.62
RUA-S108-B1	Unit 9b	Primary clast, glass btwn. microlites						63.78	1.18	14.87	7.40	1.70	4.97	3.33	2.78	100.00			
PDC Unit 10																			
X161AC	Unit 10	Larger primary clast, glass btwn. microlites	58	986	7	3.63	2493	63.59	1.13	15.69	6.77	1.68	5.06	3.43	2.66	100.00	1.24	5.49	2.42
RUA-S161-A1	Unit 10	Primary clast, glass btwn. microlites	57	1028	29		2500	63.01	1.07	15.71	6.85	2.17	5.26	3.56	2.37	100.00	1.23	5.57	2.42
PDC Unit 11																			
RUA12-225-19A / X225EB	Unit 11	Larger primary clast, glass btwn. microlites	88	914	11	4.33	2364	68.75	0.94	14.21	4.91	0.96	3.25	3.76	3.23	100.00	1.27	3.60	3.14

Table 5.11: Glass chemistry, modelled magma storage pressures and temperatures, and calculated melt densities and viscosities of Ruapehu's heterogenous small volume PDCs. Glass chemistry is 100% anhydrous as this was provided directly from the EDS analyses. Numbers of analyses and standard deviations are provided in Appendix 4. Secondary magmatic components are highlighted in grey. Modelled storage conditions that did not reach the required $\Delta T_m in \leq 10°C$ are highlighted in pink, and will have greater associated errors (Box 5.2). **$Fe2O_3$, FeO and H_2O are calculated by the MELTS thermodynamic model, and wt. %s are recast to include the hydrous phases. They are included for reference only since not all of the analyses were able to be modelled in this way.

Magma storage conditions

SEM and thin section analyses (Appendix 4) show that all of the heterogenous small volume PDCs contain plagioclase (labradorite ± bytownite), clinopyroxene (augite), orthopyroxene (enstatite) and titanomagnetite. Ilmenite was not observed in PDC Units 8-10, but is present in Unit 11. Rhyolite-MELTS modelling of simultaneous crystallisation of plagioclase, orthopyroxene and clinopyroxene in equilibrium with the measured glass chemistries suggests that all of Ruapehu's small volume PDCs with denser juvenile clasts were sourced from water-rich magmas (1.1 - 3.6 wt %, considering only the higher-quality MELTS analyses, Table 5.11) stored, in general, in Ruapehu's shallow magma system (Figure 5.28).

PDC Unit 11, previously interpreted on the basis of its stratigraphic position and chemistry to belong to the end of the Units 1-3 eruptions (Chapter 4), is modelled to have been stored at ~3.3km (88 MPa) at a maximum temperature of 914°C (Table 5.11). This is slightly shallower and hotter than the modelled storage field for Units 1-3 (Figure 5.28), but is sufficiently similar to not disprove the field and chemical evidence that it is part of the same eruptive sequence.

PDC Units 8-10 have the shallowest and hottest storage chambers of all of Ruapehu's PDCs, with pressures <58 MPa (~2.2km) and maximum temperatures of 986-1030°C (Table 5.4.5). This is comparable to the shallowest magmas from historical eruptions at Ruapehu that have estimated storage depths of 2-9km and temperatures ranging from 910-1080°C, with the majority between 950 and 1050°C (Kilgour et al., 2013). In the case of the mingled clasts, many of the glass analyses did not return definitive P-T results which is consistent with non-equilibrium conditions between the secondary melts and assumed crystallising assemblage. However, the silicic, microlite-free mingled component from Sample X108ACb (Unit 8a) returned P-T results of 114 MPa and 886°C. This fits within the storage fields of PDC Units 1-6 (Figure 5.28), and is consistent with the observation that this mingled component has similar chemistry to those units.

Density

Ruapehu's heterogenous small volume PDCs have the highest primary clast densities of all of the observed PDC units (Figures 5.24 and 5.14), averaging >1365 kgm^{-3} in Units 8-10 (Appendix 3.1.2).

Primary pyroclasts in Unit 8 (a & b) are the densest of all of Ruapehu's PDCs (Unit 8a: 805 to 2138 kgm^{-3}, average, $\bar{\rho}$ = 1505 kgm^{-3}; Unit 8b: 1202 to 2250 kgm^{-3}, average, $\bar{\rho}$ = 1458 kgm^{-3}), and have significant variability that evidences heterogeneity in the vesiculating magma (Figure 5.14).

Unit 10 has primary clast densities ranging from 950 to 1845 kgm^{-3} (average, $\bar{\rho}$ = 1366 kgm^{-3}). It is therefore slightly lower density and less variable than underlying Unit 8, but still significantly higher density than Ruapehu's pumiceous and variably welded PDCs (Figure 5.14).

The total (all clasts) densities for Units 8 and 10 show the same trends as the primary clasts (Figure 5.14). In Unit 8b, a large number (13%) of dense 'lithic' clasts are texturally similar to, but denser than, the primary clast type. Some of these even have slightly cauliform surface textures, and we therefore interpret these as cognate lithics (Chapter 4, Figure 4.16). These clasts have even higher densities than the primary clasts ($\bar{\rho}$ = 2254 kgm^{-3} vs. $\bar{\rho}$ = 1505 kgm^{-3}). Therefore, the high cognate (Unit 8a) and non-cognate lithic (Unit 8a; 33% and Unit 8b; 28%) contents in Unit 8 (Chapter 4, Figure 4.16) *significantly increases* Unit 8's bulk (all-clast) density (Figure 5.24). In contrast, monolithologic Unit 10 contains no lithic clasts (Chapter 4, Figure 4.16) so Unit 10's bulk pyroclast density does not change (Figure 5.24). Calculated melt densities in Units 8-11 range from 2524 to 2676 kgm^{-3} (Table 5.11), in agreement with the high bulk densities of the primary pyroclasts.

The calculated viscosities of primary melt (Table 5.11) in PDC Units 8 and 10 range from log 3.63 to log 4.02 Pa s. This is slightly lower than Ruapehu's pumiceous and variably welded PDC Units, probably reflecting the hotter modelled magma storage temperatures

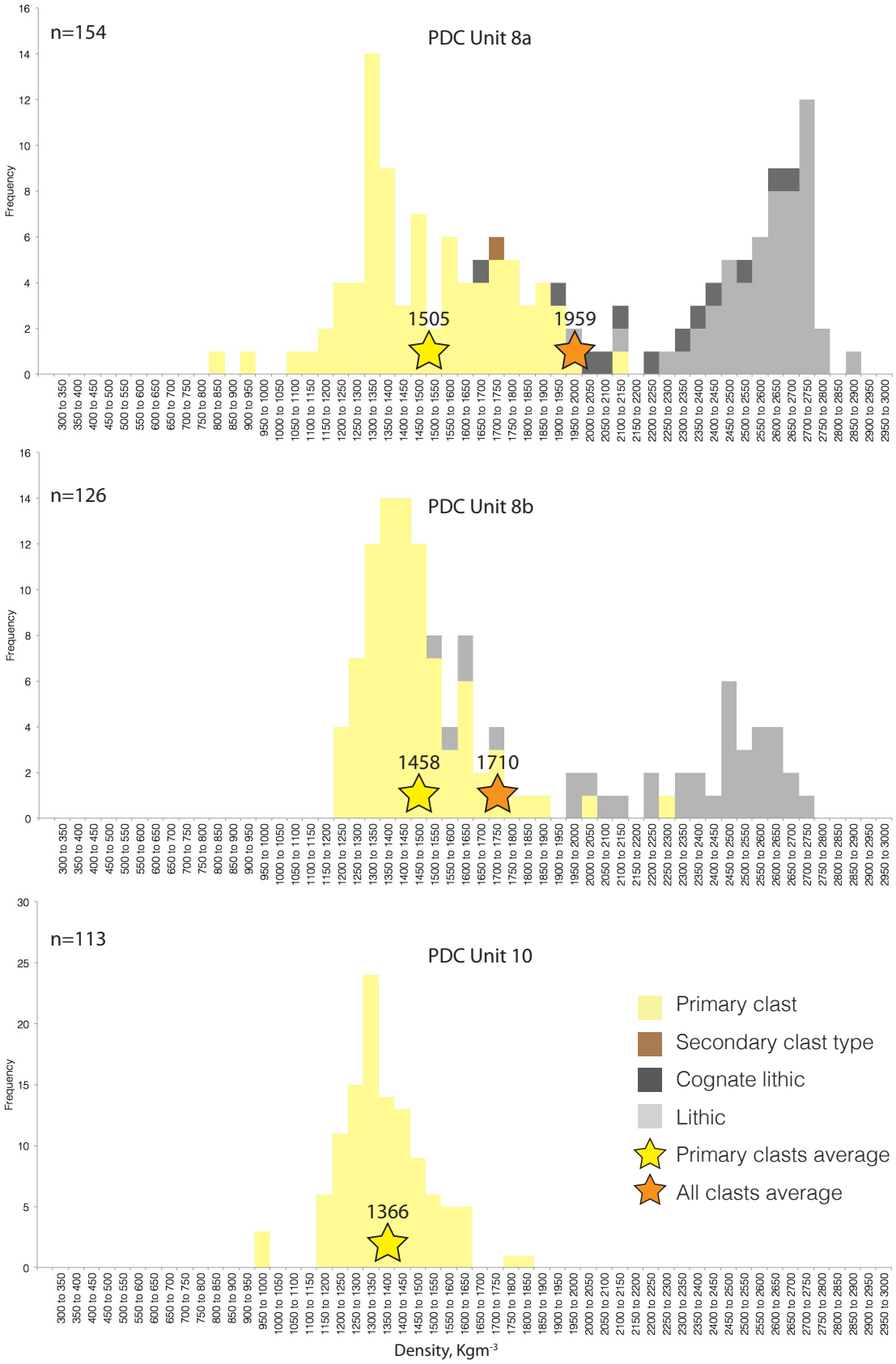

Figure 5.24: Whole-clast densities of clasts from the -5ϕ to -4ϕ sieved size fractions of Ruapehu's heterolithologic small-volume PDC Units 8a, 8b and 10 deposits.

(Table 5.11). The modelled viscosity for the mingled silicic component in sample X109ACb (Table 5.11) is log 4.51 Pa s (comparable with Units 4 and 6), consistent with the chemical and magma storage results that suggest this component shares characteristic with the older pumice-dominated and variably welded units. The modelled viscosity for primary melt in Unit 11 is log 4.33 Pa s (Table 5.11), and is therefore similar to the directly-underlying pumice-dominated Units 1 & 2.

Micro-scale textures, vesicularity and vesicle shapes

Clasts from the small volume PDCs (Units 8-12) have the lowest vesicularities of Ruapehu's PDCs, with average vesicularities ranging from 50-55% in Units 8-10 using Pardo's (2012) DRE density of 3040 kgm^{-3} for pumices from the Okupata-Pourahu fall deposits. However Units 8-10 have higher modelled melt densities than Unit 4 (Pourahu PDC); this means that 3040 kgm^{-3} may be a slight underestimate of the DRE density, in turn suggesting the calculated vesicularities may also slightly underestimate the true values.

Primary clasts from the small-volume PDCs have isolated vesicles with highly irregular vesicle shapes and thick bubble walls containing abundant tabular plagioclase and pyroxene microlites (Figure 5.25) consistent with degassing-induced crystallisation (Wright et al., 2012). Very small vesicles are almost completely absent (Figure 5.25 a-d), and there are large areas of dense vesicle-free groundmass (Figure 5.25 b). Extensive shearing is not evident in any of the samples, but there is prominent aligment of tabular microlites and accompanying subtle elongation of vesicles in many of the samples (Figure 5.25 a & c), sometimes deflecting around larger phenocrysts (Figure 5.25 c). The 3D tomography (Figure 5.25 e & f) highlights the isolated vesicles, and also shows small connected bubble networks with irregular shapes and narrow, pinched connections that suggest vesicle collapse associated with outgassing. PDC Unit 11 (Figure 5.25 d), whose chemistry more closely matches the pumiceous Units 1-3, is texturally similar to Units 8-10 with sparse, isolated and distorted vesicles in a dense microlite-rich groundmass.

Banded samples mostly occur in PDC Unit 8, with the secondary bands generally present as more coarsely vesicular, microlite-poor domains with larger, highly connected

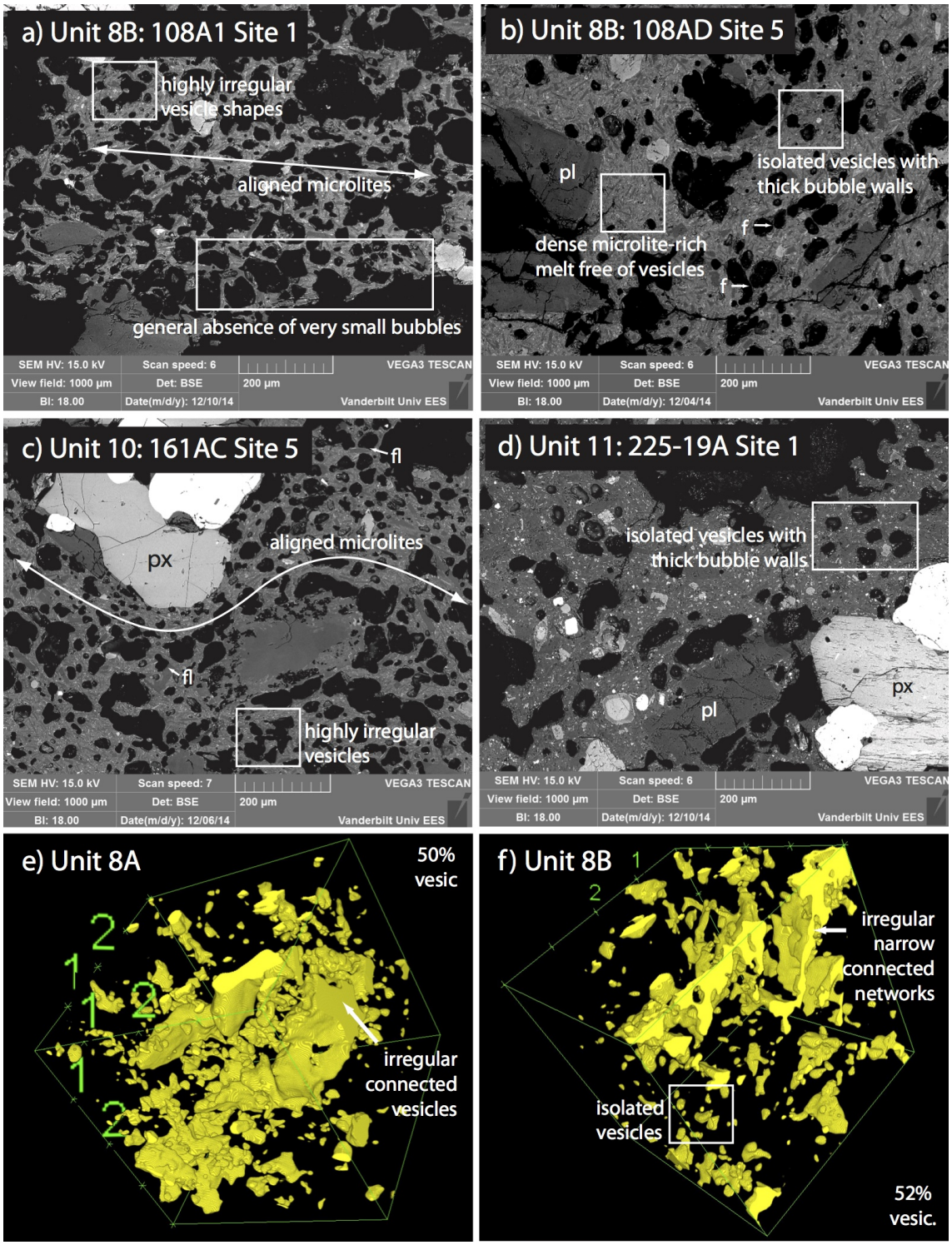

Figure 5.25: Textures in Ruapehu's heterogenous small volume PDCs. a-d) Units 8-11 all have highly irregular, isolated vesicles with thick walls and highly microlitic groundmasses that frequently result in flattened vesicle sides (labelled 'fl' in c). Delicate glass filaments (labelled 'f' in b) are frequently present between vesicles that may otherwise have coalesced. Alignment of tabular microlites (arrows) and slight elongation of vesicles evidence minor shearing during ascent and eruption. (e-f) 3D tomography highlights the isolated vesicles and irregular narrowly connected bubble networks that suggest vesicle deflation during outgassing (Kennedy et al., 2016). Average primary clast vesicularities calcuated from the density data are shown for comparison.

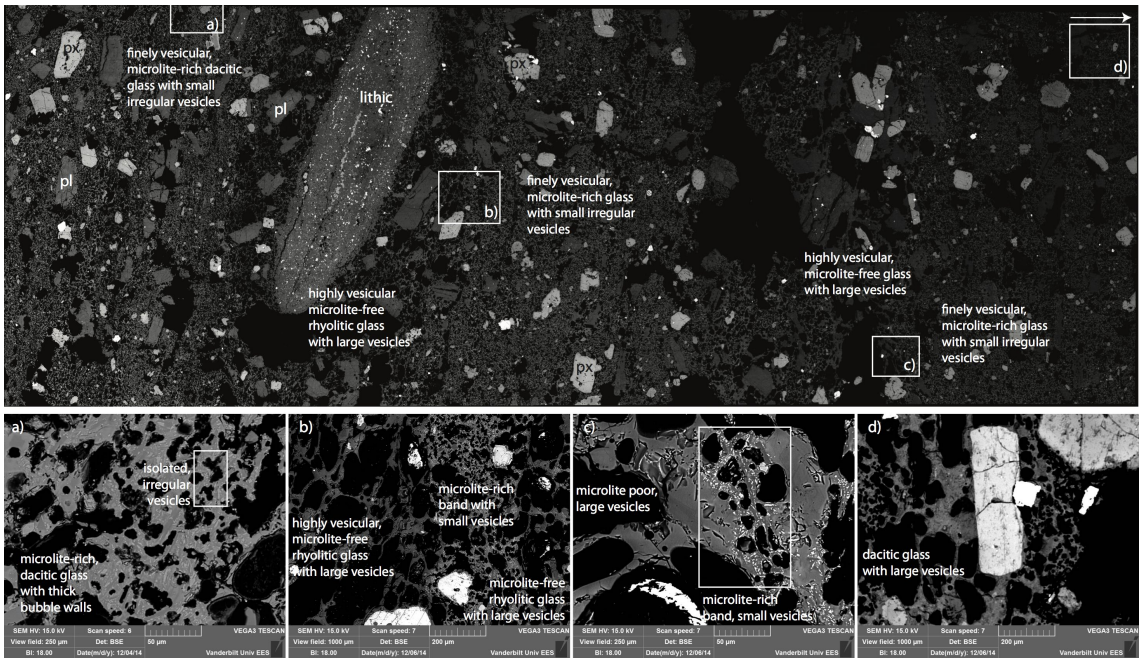

Figure 5.26: Different textural domains within Sample X109AC from PDC Unit 8a. a) Finely vesicular domain with abundant plagioclase and pyroxene microlites and dacitic glass (63.6-64.3 wt% SiO_2), representative of the primary magma in Units 8-10 b) Regions of more highly vesicular, secondary microlite-free glass (left and right sides) that is much more silicic (analysis 109ACb, 70.5 wt% SiO_2). This region surrounds a small xenolith, implying that it may be a glass coating on a recycled lithic clast. However, similar highly vesicular microlite-free secondary glass is observed elsewhere in the sample, for example in c) which shows a zone of intermingled microlite-rich and microlite-poor magmas d) Another region of more vesicular glass that is much less silicic than the other vesicular domains and is chemically most similar to the primary glass (analysis 109ACc, 62.7 wt% SiO_2).

vesicles and thin vesicle walls (e.g. Figure 5.26 b). These vesicular domains are comparable to those in pumiceous PDC units 1-4, and have similar rhyolitic glass chemistry. Sample X109AC, which has the distinctive olive-golden bands shown in Figure 4.15 (Chapter 4), is extremely heterogenous, with intermingled zones of finely vesicular primary magma (Figure 5.26 a) and coarsely vesicular secondary magma (Figure 5.26 b), as well another region of coarsely vesicular glass that nonetheless has similar glass chemistry to the primary melt (Table 5.11 and Figure 5.26 d).

Deposit Features	Chemistry	Magma Storage (MELTS)	Mingling	Densities	Vesicularity
Cauliflower textured pyroclasts; No known correlative fall deposits; Unit 8a has 13% cognate and 28-33% weathered lithics; Unit 10 similar to Ngauruhoe 1975 subplinian and vulcanian PDC deposits. Unit 11 statigraphically above Units 1-3.	Basaltic-andesite to andesite, with dacite glass,	Units 8-10 - Shallowest (<2.2km); Highest T (>1000C); H_2O-rich (0.62-2.42%). Unit 11 storage similar to Units 1-3 but slightly hotter and shallower.	Banding in Unit 8, with a silicic secondary glass similar to Units 1-6 and falling within the modelled Units 1-6 storage fields.	Highest (averages >1365 kgm^{-3} in Units 8-10) and highly variable. High lithic contents in Unit 8 increase all-clasts average density by 454 kgm^{-3}.	Lowest vesicularities (50-55% in Units 8-10); isolated, irregular vesicles with thick microlite-rich bubble walls and patches of vesicle-free groundmass; indicating significant pre-eruptive degassing. Aligned microlites show small amounts of shear.

Table 5.12: Summary of the key observations for Ruapehu's small volume, denser PDC Units 8-12

All of the results show that Ruapehu's heterogenous small-volume PDCs were erupted from generally shallow, water-rich storage zones. The PDCs contain dense primary clasts, and have textures indicating significant pre-eruptive degassing and degassing-induced microlite crystalisation. The key observations are presented in Table 5.12

5.4.6 Interpretation of the small-volume denser PDC textures

The modelled storage conditions, high densities and low vesicularities of the primary pyroclasts, and evidence of bubble collapse and extensive microlite crystallisation, suggests PDC Units 8-12 were generated by eruption of generally shallow (<2.2km for Units 8-10), highly degassed magmas. All of these PDCs are interpreted to represent 'boiling over' or low collapse of subplinian/vulcanian eruption columns for which no correlative tephras are known to be preserved.

Units 8-10:

For Units 8-10, the main factor for PDC generation appears to have been extensive pre-eruptive degassing, resulting in dense pyroclasts (and therefore a denser erupting mixture), as well as low exit velocities due to low exsolved gas contents at the time of fragmentation. As with the other PDC units, incorporation of dense cognate and non-cognate lithics, and

mingling within Ruapehu's heterogenous magma system also appear to have been important in triggering the PDC Unit 8 eruption, while the abundant cauliform pyroclasts in Units 8-12 suggests phreatomagmatic processes may also have been important.

Degassing: Primary clasts in Units 8-10 have high bulk densities, low vesicularities, and isolated, highly irregular vesicles with thick microlite-rich vesicle walls. These textures, together with the absence of very small vesicles and large areas of vesicle-free groundmass (Figure 5.25) all evidence eruption of small batches of hot, shallow (Table 5.11) magmas that have undergone extensive pre-eruptive outgassing through narrow interconnected bubble networks, accompanied with vesicle deflation (Kennedy et al., 2016) and extensive degassing-induced crystallisation (Wright et al., 2012). The dense erupting mixtures are interpreted to have rapidly approached the collapse condition due to both low exit velocities (due to low exsolved gas contents) and high bulk pyroclast densities (Shea et al., 2011), with the resulting PDCs interpreted to result from low column collapse or 'boiling over'-style mechanisms (Figure 5.1). The monolitholigical nature and much coarser grain size of PDC Unit 10 (with clasts up to ~1m diameter) contrasts markedly with underlying Units 8 and 9, and is interpreted to represent reduced fragmentation efficiency and a more stable (i.e. non-eroding) vent, consistent with Unit 10 occuring at the end of the Units 8-10 eruption sequence.

Mingling: The abundance of mingled clasts in Unit 8 (Chapter 4, Figure 4.15), at the base of the Units 8-10 sequence, suggests that magma mingling was important to the onset of these eruptions. Mingled clasts in Units 8a and 8b both show mingling between a more mafic, primary, microlite-rich magma and a secondary microlite-free more silicic melt (Figure 5.26). The mingled component in Unit 8A (Sample X109ACb) has equivalent glass chemistry and modelled storage conditions to the older plinian and variably welded PDC Units 1-6 (Table 5.11), and is interpreted to represent left-over magma from the Ohinewairua (Units 1-3) or Taurewa (Units 4-6) eruptive periods that remained in storage at ~4km depth (Figure 5.28). Since the mingled component in Unit 8b (Sample X108ACb) is the most silicic glass analysed (Table 5.11), this implies it most likely correlates with left over magma from silicic Unit 4 (the most silicic of the pumice-dominated PDCs), which immediately preceded Units 8-10 and was erupted from the same source near South

Crater. In either case, it appears that the secondary silicic component was already present in the Ruapehu system prior to arrival of the Unit 8 magma, and was therefore entrained during ascent. The highly vesicular textures of the secondary component suggests that this magma was remobilised by the hotter primary melt (1041°C vs 886°C, Table 5.11), triggering vesiculation during ascent that *may* have been important in providing the impetus for eruption of the otherwise relatively degassed primary magma. Only a single secondary clast (in Unit 8a, Figure 5.24) and no banded clasts were identified in the -5 to -4ϕ whole-clast samples used for density and componentry measurements, since the banding is here only easily observed in the clast interiors. Therefore, we cannot be certain how the mingling affected the bulk densities of the erupting pyroclasts. However, given that in thin section the secondary bands appear much more vesicular (Figure 5.26), it is reasonable to infer that the magma mingling in Unit 8 this time *reduced* the bulk density of the pyroclasts and so did *not* therefore contribute to PDC generation by increasing the density of the erupting mixture. However, by possibly contributing volatiles that *enabled* eruption of already-denser, degassed primary melt that may not have otherwise erupted, the mingling event is nonetheless interpreted to have influence PDC generation for Unit 8. This again emphasises how the heterogeneous magma system at Ruapehu in general appears to favour conditions for PDC generation.

Phreatomagmatism: The characteristic cauliform clast textures observed in Units 8-12 (Figure 5.21) have traditionally been interpreted as evidence of magma-water interaction (Lorenz, 1973) or catastrophic Arenal-style failure of a summit lava lake (Alvarado and Soto, 2002; Miyabuchi et al., 2006). However, similar textures from mostly dry subplinian/vulcanian eruptions at Ngauruhoe (Figure 5.21 and Nairn and Self, 1978), as well as similarities with some lava autobreccias, suggest these textures occur across a broad variety of eruptive styles and do not only point to phreatomagmatism as previously thought. Nevertheless, other authors (e.g. Donoghue et al., 1997; Donoghue and Neall, 2001; Pardo et al., 2011) have suggested a change towards smaller, more phreatomagmatic eruption styles at Ruapehu during the Holocene, and the ubiquitous cauliflower textures in Units 8-12 may support this. This interpretation is consistent with the interpretation that Units 8-12 reflect slow ascent rates, allowing greater opportunity for interaction with external water. Similarly, the generally blockier primary clasts (average roundness = 4.2 in Unit

8b, 4.5 in Unit 10, Appendix 3.1.2) and high lithic contents of Units 8a and 8b are also consistent with phreatomagmatic fragmentation, while the lack of correlatable fall deposits are consistent with smaller sub-plinian or vulcanian-style eruptions similar to Ruapehu's modern activity. Again, this has implications for PDC generation, since limited input of external water may provide sufficent impetus for eruption of otherwise dense, degassed magma whose high bulk density means the erupting mixture is already close to the column collapse threshold at the time of fragmentation.

Insights from other volcanoes: The microlite textures observed in PDC Units 8-10 are strikingly similar to those observed in ash samples from the 1999-2006 eruptions at Tungurahua volcano, Ecuador (Wright et al., 2012), appearing to have similar microlite number densities and sizes (Figure 5.27). At Tungurahua, Wright et al. (2012) observed a direct correlation between magma supply rate (i.e. decompression rate) and the Tungurahua microlite textures, evidencing syn-ascent microlite crystallisation resulting from degassing-induced crystallisation at very low pressures («50MPa). The similarities with the Ruapehu samples therefore provides insight into the magmatic processes leading to eruption of Ruapehu's small volume PDCs. The Tungurahua eruptives are very slightly more silicic than Units 8-10 (~58 wt % SiO_2 compared to ~54-58 wt % SiO_2 at Ruapehu), but the observed microlite textures are almost identical to Wright et al's (2012) Type III-V examples (Figure 5.27, c-e & g). While direct quantitative comparison is not possible (e.g. the Tungurahua study considered average bulk microlite contents from erupted ash fractions, and not lapilli from PDC deposits), in general the Tungurahua study found that these textures first appear at low magma supply and decompression rates (<3 m^3s^{-1}, and <0.001 MPa s^{-1}), and then become more prevalent at even lower ascent rates (<0.03 m^3s^{-1}, and <0.00001 MPa s^{-1}). They also mostly correlated with vulcanian-style activity interpreted to result from trapping of exsolving bubbles below a vent-capping, variably viscous and crystalline magma (Wright et al., 2012). These observations are fully consistent with the interpretations of Ruapehu's small volume PDCs presented here. We also interpret that the high numbers of dense, apparently cognate lithic clasts in Unit 8a (the oldest of the Units 8-10 eruptions) may represent fragments of a similar degassed vent-capping magma that was explosively disrupted by eruption of Unit 8a.

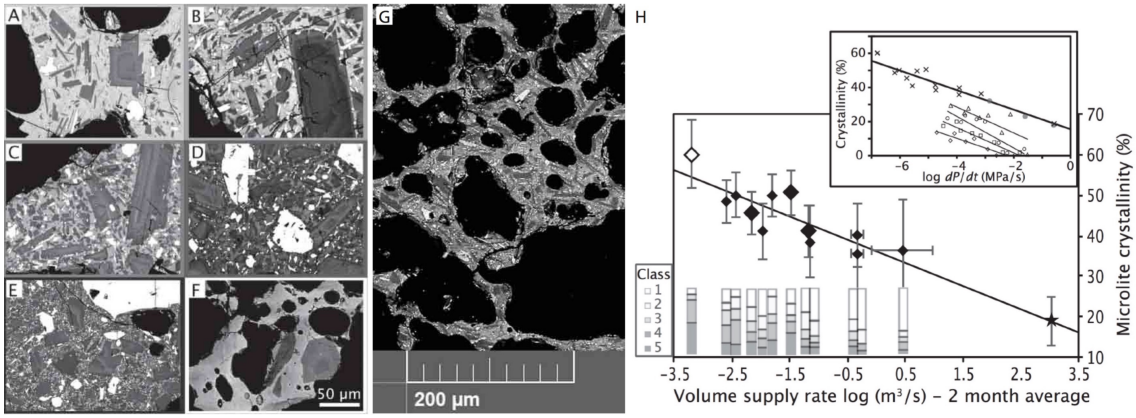

Figure 5.27: Comparison of microlite textures in Ruapehu's small volume PDCs with those from vulcanian/strombolian eruptions at Tungurahu volcano during 1999-2006 (modified from citeWright2012). Wright et al.'s 2012 Type III to IV samples (D-E, 45-57% crystallinity) are broadly similar to the samples from Ruapehu's PDC Units 8-10 (G). The graphs in (H) shows that at Tungurahua the Type III and IV textures become more prevalent for low magma supply rates ~<0.03 m^3s^{-1} (main graph), and correspond to low decompression rates <0.00001 MPa s^{-1} (inset graph, top line = Tungurahua).

The observation that Ruapehu's PDC Unit 10 deposits are texturally similar to the 1975 PDC deposits from Ngauruhoe volcano provides additional insight into the PDC generation and transport mechanisms at Ruapehu. The Ngauruhoe PDCs were produced during a climactic eruption on 19th February 1975 (Lube et al., 2007), consisting of an initial subplinian phase followed by nine individual vulcanian explosions. During the subplinian phase, fountaining in the lower part of the eruption column (see Figure 5.1) resulted in rapid accumulation of near-vent poorly welded agglutinate, and eyewitness accounts suggest that ongoing collapse of these deposits was the dominant PDC generation mechanism (Lube et al., 2007). This process was supplemented by continuous feeding from the collapsing part of the eruption column, and both of these processes can be seen in the image in Figure 5.1. These observations are consistent with our interpretations that Unit 10 (as well as the other small volume units) were mostly generated by low-collapse or boiling over of dense degassed material erupted during subplinian/vulcanian-style activity.

The very coarse grained nature of the Ngauruhoe deposits (65% coarser than -1ϕ) and absence of gas-escape structures is interpreted by Lube et al. (2007) as evidence that PDC transport was dominated by granular flow, with gas-fluidisation playing only a minor role. Ruapehu's Unit 10 deposits are similarly coarse grained (59% coarser than -1ϕ) and can be interpreted similarly. However, Unit 10 was significantly more mobile than the Ngauruhoe

PDCs: The Ngauruhoe deposits had runout distances <2.3 km and began deposition at slopes of 30°(~static angle of repose for granular material), whereas the Ruapehu Units 8-10 all reached more than 4.5 km from source with the majority of their transport occuring over much shallower slopes than the Ngauruhoe PDCs. Reasons for the apparently greater mobility of the Ruapehu units could include differences in the height at which the column collapse occurred, or perhaps that gas fluidisation played a greater role during transport of the Ruapehu PDCs. However, another possibility is that the substantially greater mobility of the Ruapehu units might also be explained by transport over proximal snow or ice (Chapter 4 and Conway et al., 2015) that significantly reduced the surface roughness. Similar mobility increases have previously been described for non-volcanic landslides travelling over glacial ice (Evans and Clague, 1988; Deline et al., 2015), but are investigated for PDCs for the first time in Chapter 6 by combining microphysical ice-contact experiments with high resolution multiphase numerical simulations. Our results suggest that transport over only ~2 km of ice (similar to the conditions for Ruapehu's PDC Unit 6) can significantly increase the runout distance of the granular fluid-based PDC bedload (Chapter 6). Transport over snow or ice is a plausible scenario given Ruapehu's glacial history,the absence of deposits higher up the mountain (possibly reflecting deposition on thick snow or ice that hindered long-term preservation), and the observation that even today Ruapehu has significant snow cover over the length of most of the interpreted PDC transport paths for >4 months each year (see Chapter 4, Section 4.5.3).

Unit 11:

The textural similarities between Units 8-10 and the more silicic (57wt% SiO_2) Unit 11 supports an interpretation that Unit 11 was also generated by low collapse or boiling over of dense, degassed magma from a subplinian/vulcanian eruption column. This suggests that the eruptive style and resulting PDC generation for Ruapehu's small dense PDCs is primarily a function of pre-eruptive magmatic degassing, and is less dependent on magma chemistry. Unit 11 has a modelled magmatic storage depth of 3.1 km (Table 5.11), significantly deeper than Units 8-10 (Figure 5.28). This, together with its major element chemistry and stratigraphic position at the top of the Units 1-3 sequence, is consistent with the interpretation that Unit 11 represented the final stages of eruption at the end

of the plinian Units 1-3 eruptions (Chapter 4). Unit 12, not investigated here in detail, is likely to have been generated in a similar way.

5.5 Discussion

The 12 PDC deposits observed close to the Tukino Ski Area show that Ruapehu has produced hazardous PDCs from a broad range of eruptive styles, magnitudes, and generation mechanisms. The data presented here expand upon the field-based interpretations presented in Chapter 4, and provide insight into the underlying magmatic processes that contributed to PDC formation at this volcano.

Figure 5.28 summarises the modelled pressure and temperature fields of the primary magmatic storage zones that supplied Ruapehu's PDC-forming eruptions. The results show a clear change from older (>11.6 ka), larger eruptions that produced more silicic pumice-dominated PDCs associated with plinian eruptions from deep (>4.1 km) gas-rich magmas; to smaller, younger (<11.6 ka) subplinian/vulcanian eruptions of more mafic magmas from shallow (<2.2km), actively degassing storage zones. This change coincided with a shift in activity away from the pre-existing North Crater system, towards new activity in the still-active South Crater area following the excavation of a new vent during the ~11.6 ka Okupata-Pourahu (Unit 4) eruption (Pardo et al., 2012, 2014).

While large-scale shifts in Ruapehu's magma system were responsible for the changing style of Ruapehu's PDCs, in all cases it appears that underlying heterogeneities in the magmatic system were instrumental in bringing the erupting mixtures closer to the collapse threshold. In particular, the ubiquity of magma mingling, incorporating secondary magmatic components from different storage regions and with different densities and volatile contents, appears to have almost always favoured PDC generation. Firstly, incorporation of a denser secondary component will always move the eruption column towards the collapse threshold by increasing the bulk density of the erupting mixture (Shea et al., 2011), and may also reduce exit velocities by contributing fewer exsolved volatiles to drive the eruption. Secondly, incorporation of less-dense, volatile-rich secondary components can

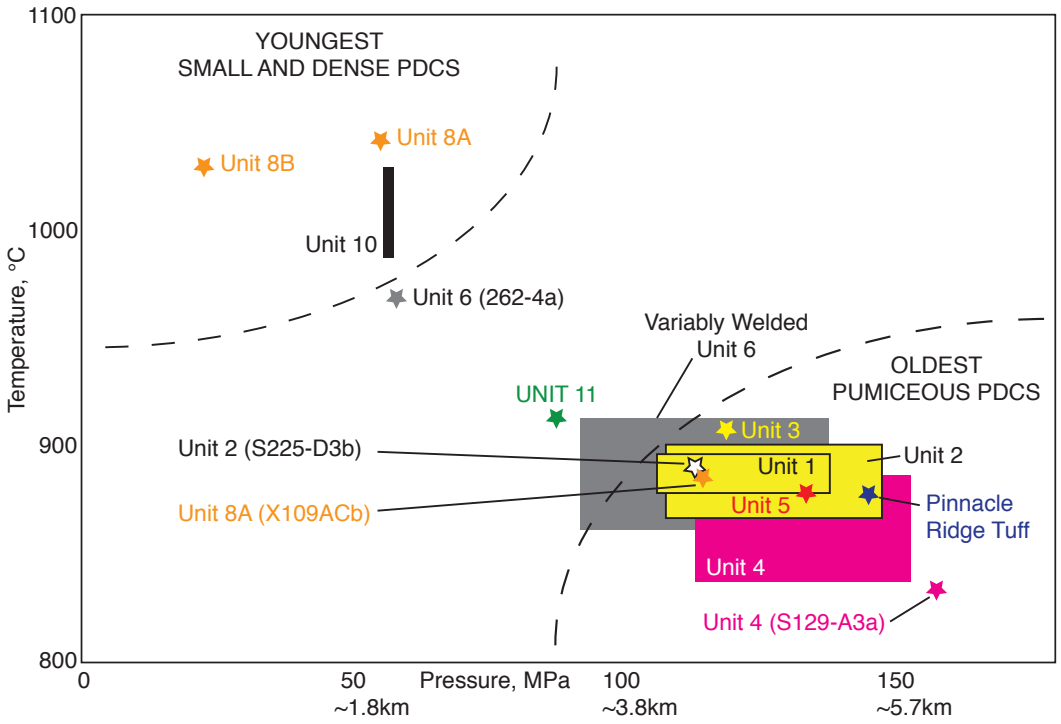

Figure 5.28: Magma storage pressures and temperatures for the Ruapehu PDCs using the new rhyolite-MELTS geobarometer to model simultaneous crystallisation of orthopyroxene, clinopyroxene and plagioclase in equilibrium with measured glass compositions. Model convergence indicates the melts were generally H_2O-rich, with oxygen fugacities equivalent to the Ni-NiO oxygen buffer. Named samples represent secondary glass types from banded samples or discrete secondary clasts.

also promote PDC generation by providing the impetus for eruption of otherwise dense, degassed primary magmas that may otherwise not erupt.

5.5.1 Eruption model

Bringing together all of the observed field, chemical, textural and modelling data, Figure 5.29 presents an integrated model for Ruapehu's PDC-producing eruption sequence over the last ~13.6 ka. The oldest PDCs, the 13.6-11.6 ka Ohinewairua Units 1-3 (Figure 5.29 a) were erupted from a moderately deep magma chamber through a partially sealed pre-existing system at Northern Ruapehu. The eruption sequence appears to have been triggered by magma mingling, with mingled or mixed clasts observed in all units and both more mafic and more silicic secondary magmas observed in PDC Unit 2. The first eruption (Unit 1) resulted in rapid vent widening/opening that introduced large amounts of lithic clasts into the eruption column (Chapter 4, Figure 4.5), densifying the

erupting mixture and leading to column collapse. The amount of mingling increased in pumiceous PDC Unit 2 which extracted slightly deeper magma (Figure 5.28), and this mingling appears to have contributed to column collapse by introducing vesicularity and density hetrogeneities into the erupting mixture. Towards the end of the Ohinewairua sequence, small amounts of remaining magma slowly ascended and efficiently degassed through the now-open system, promoting microlite crystallisation and eruption of gas-poor magma in subplinian/vulcanian eruptions that produced PDC Units 11 and 12 by boiling over/collapse of their denser eruption columns.

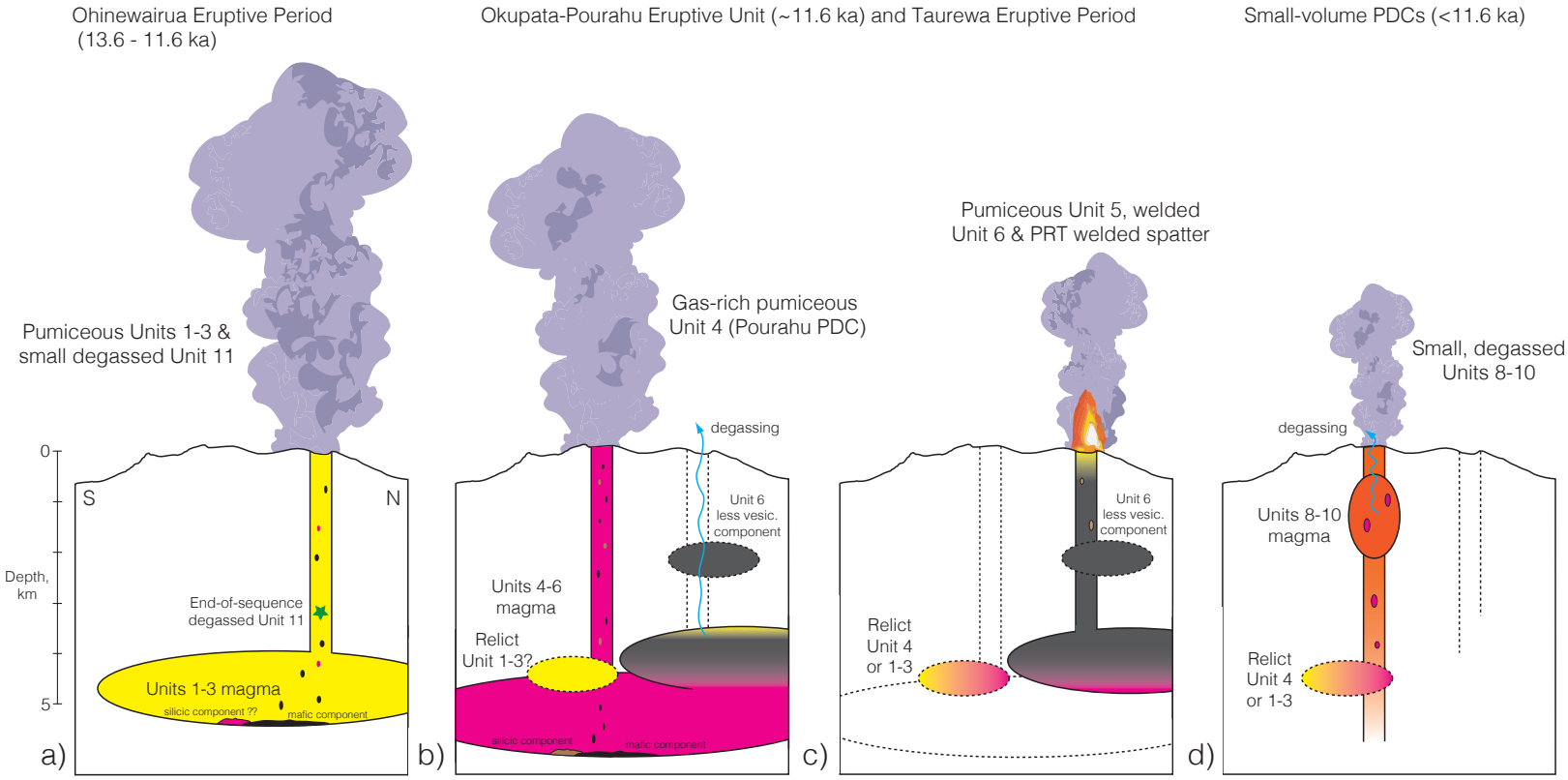

Unit 1: Plinian column collapse (densification due to vent widening)

Units 2-3: Plinian column collapse (densification due to mingling)

Unit 11-12: Sub-plinian/vulcanian column collapse/boiling over (densification and low exit velocities due to degassing; end of Ohinewairua sequence).

Unit 4: Plinian column collapse (densification due to mingling)

Unit 5: Frothier magma cap preceding Unit 6 magma producing pumiceous PDC.

Unit 6: Collapsing spatter (fountaining associated with sub-plinian or smaller eruption due to degassed magma, deposition on steep topographic gradients). PRT is non-collapsing equivalent.

Unit 7: Inferred same mechanism as Unit 6

Unit 8: Sub-plinian/vulcanian column collapse/boiling over (densification due to degassing, mingling may have aided eruptibility)

Units 9-10: Sub-plinian/vulcanian column collapse/boiling (densification due to degassing)

Figure 5.29: Interpreted eruption sequence based on the textural features observed within Ruapehu's PDC deposits. See text for detailed description. Volcano and storage depths to scale, chamber sizes diagrammatic.

The ~11.6ka PDCs from the Taurewa eruptive period (Figure 5.29 b and c) began with accumulation of a large silicic-andesite magma body beneath much of Ruapehu's edifice. Much of this magma accumulated at depths ~4.3-5.8 km, but some ascended through the pre-existing system in northern Ruapehu to shallower chambers at ~3.5-5.2 and 2.2km. The observations of Donoghue et al. (1995a) suggest that eruption of the deeper magma was triggered by mingling of a hot mafic secondary component not observed in the Tukino deposits due to preservation limitations; whereby the Tukino deposits represent the upper parts of a density-stratified PDC that was only preserved where its low-density upper parts overtopped the valley side away from the main flow path (Chapter 4). Mingling with a silicic secondary component, as well as with Donoghue et al.'s (1995a) mafic component caused the volatile-rich primary magma (Table 5.5) to explosively excavate a new vent from the South Crater area and produce the plinian Okupata tephra and pumiceous PDC Unit 4 (Pourahu PDC). The ascending melt may also have undergone limited outgassing through its highly connected vesicle network, resulting in lower exit velocities that may also have contributed to column collapse. At approximately the same time, the hotter, shallower and slightly more degassed magma underneath northern Ruapehu erupted in a brief explosive eruption that produced pumiceous PDC Unit 5, followed by a sustained (possibly subplinian; Hackett and Houghton, 1985) fountaining/spatter-forming eruption that rapidly emplaced hot material across much of Northern Ruapehu. This magma mingled with the compositionally similar melt present in the shallower ~2.2 km chamber during ascent. On shallower topographic gradients the erupted material was preserved in-situ to form welded spatter (Pinnacle Ridge Tuff deposit), while on the steeper slopes beneath Te Heuheu Peak the material repeatedly collapsed to produce PDCs whose combined deposits form Unit 6. Short transport times in both the eruption column and the PDCs, coupled with rapid near-vent accumulation rates, allowed the deposits to retain sufficient heat to form welded spatter in the near-vent pile, and then to weld more completely upon final PDC deposition. Cooling columns that extend across multiple PDC layers show that the accumulation-collapse-PDC cycles occured in quick succession throughout this eruption.

After the Okupata-Pourahu eruption, the now-opened system in southern Ruapehu became the main pathway for smaller, more mafic magma batches to accumulate at shallow depths (<2.2 km, Figure 5.29 d). The first-ascending melts (leading to PDC Unit 8)

entrained and mingled with older silicic magmas interpreted to be relict magmas from Units 1-4 during ascent, and the contribution of volatiles from this silicic melt may have assisted eruption of the otherwise degassed Unit 8 magma. Efficient shallow degassing of the slowly ascending magma columns (Units 8-10) resulted in bubble collapse and extensive pre-eruptive microlite crystallisation, densifying the magma and reducing the available volatiles necessary for high exit velocities and stable eruption columns. The slow ascent rates are also interpreted to have favoured access of external water, providing additional volatiles that may have assisted with shallow fragmentation. The high bulk densities and low exsolved volatile contents (Units 8-10), and incorporation of dense cognate lithic clasts interpreted to represent a pre-existing degassed vent-capping magma (Unit 8), are all interpreted to have resulted in unstable subplinian/vulcanian eruption columns that rapidly collapsed by boiling over/low collapse mechanisms to produce PDC Units 8-10.

5.6 Conclusions

12 newly-described PDC deposits preserved near the Tukino Ski Area in eastern Ruapehu demonstrate that hazardous PDCs have frequently occured at Ruapehu volcano over the past ~13.6 k.a.; despite an absence of granular fluid-based PDCs in historical time. The deposits represent PDCs from most of Ruapehu's explosive eruption styles, including:

1. PDCs generated by collapse of plinian eruption columns, interpreted to result from densification of the erupting mixture by vent widening and addition of denser lithic clasts (Unit 1), as well as addition of denser mingled secondary magmas (Units 2 & 4), and pre- and syn- eruptive degassing/outgassing (Units 1-3).

2. PDCs generated by gravitational collapse of rapidly accumulating proximal spatter and cinders sourced from energetic fountaining/spatter-forming eruptions of partially degassed magmas (Units 6 and 7).

3. PDCs generated by low collapse or 'boiling over' of dense eruption columns resulting from smaller subplinian/vulcanian eruptions of small batches of shallow, degassed, microlite-rich magmas.

Clast textures within the PDC deposits emphasise the heterogeneity of Ruapehu's young magmatic system, with a complex interplay between different magmas, magma storage zones, degassing pathways and vent systems. While these are not uniquely tied to PDC production, the high degrees of rheological heterogeneity (Pardo et al., 2014) in Ruapehu's young magmatic system appear in almost all cases to have favoured eruption instabilities that led to PDCs. This also appears to be independent to the source eruption style. The ongoing heterogeneity of the young Ruapehu system (e.g. Nakagawa et al., 1999; Nakagawa, 2002; Kilgour et al., 2013) is therefore an important consideration when assessing the future PDC hazard at this volcano.

6

Pyroclastic density current dynamics and hazards at icy volcanoes

Introduction to Chapter 6

This chapter is the product of collaborative research with Dr. Joseph Dufek at the Georgia Institute of Technology, and extends the observations presented in **Chapter 4** that many of Ruapehu's prehistoric PDCs may have encountered snow and ice during transport. At Ruapehu this appears to have affected the PDC transport, distributions, and preservation of the deposits. However, despite the prevalence of snow and ice at many tall volcanoes, few studies have investigated how transport over ice affects the large-scale PDC dynamics and associated hazards. Therefore, in this chapter we present a coupled experimental and numerical modelling approach to investigate the large-scale effects of PDC transport over ice for the first time.

The key outcomes are:

1. Recognition that transport over ice can significantly affect PDC dynamics through changes in surface roughness (compared to ice-free terrain) and incorporation of meltwater and steam into the PDC.

2. Development of microphysical experiments to quantify water and steam production when hot pyroclasts from Ruapehu's PDC Unit 6 are in contact with ice, and incorporation of the experimental results into new high-resolution multiphase simulations to investigate the large-scale effects of PDC transport over ice for the first time.

3. Observation that transport over ice for 2 km (i.e. the interpreted ice extent for PDC Unit 6) increases the runout distance of the granular fluid-based PDC bedload and generates meltwater volumes equivalent to ~25% of the PDC bedload volume. Comparisons with Nevado del Ruiz volcano (Columbia) suggest that even this small amount of PDC-ice transport may produce lahars with volumes equivalent to at least 50% of the primary PDC bedload volume. These results are significant for assessing the PDC and associated hazards at Ruapehu and other glaciated volcanoes.

The chapter is presented in the style of an academic paper, though with expanded detail that will be condensed for submission to a peer-reviewed journal. As such, the relevant contextual background and analysis methods are presented in full.

Abstract

Understanding the processes by which pyroclastic density currents (PDCs) are emplaced is crucial for volcanic hazard prediction and assessment. Where PDCs travel over snow or glacial ice, the reduction in surface roughness and generation of steam and meltwater significantly changes the PDC dynamics, including the flow velocities and runout distances. Additionally, meltwater generated during transit and after the flow has come to rest presents an immediate secondary lahar hazard that can impact areas many tens of kilometres beyond the primary PDC (Major and Newhall, 1989). Here, we combine experimental determinations of water and steam production with high-resolution multiphase numerical models to investigate the effects that transport over ice has on PDC dynamics and the associated hazards. Using the example of a PDC deposit at Ruapehu volcano (New Zealand) that travelled over ice for ~2km, the simulations suggest that transport over smooth ice *increases* the runout distance of the concentrated bedload that forms the majority of the PDC deposits. However, incorporation of steam into the PDC also increases the buoyancy and *reduces* the runout distance of the more mobile dilute parts of the PDC, thus reducing the overall distance impacted by the primary PDC hazard. Significant thermal and mechanical interactions take place between the PDC and underlying ice during transport, producing meltwater volumes equivalent to ~25% of the PDC bedload volume over the simulated 2km of ice transport. Using observations from the 1985 Nevado del Ruiz eruption in Colombia, this meltwater may then erode and entrain the volcanic substrate to produce debris flows with volumes equivalent to at least 50% of the original PDC bedload volume. Therefore even small PDCs represent a significant lahar hazard when all or part of their transport occurs over ice.

6.1 Introduction

Sudden melting, scouring and mass failure of summit ice due to volcanic activity can pose severe hazards to populations near glaciated volcanoes (Thouret, 1990; Gardner et al., 1994; Huggel et al., 2007). Pyroclastic density currents (PDCs) emplaced onto snow or ice are a particular concern due to their ability to very rapidly scour, mix and melt large volumes of glacial ice and generate hazardous lahars (Major and Newhall, 1989). A small

plinian eruption at Nevado del Ruiz volcano in 1985 emplaced pyroclastic density currents over ~10-18 km^2 of the summit snowpack, producing large volumes of meltwater that flowed downslope and generated debris flows that killed more than 23,000 people (Pierson et al., 1990; Thouret et al., 2007). Similarly, eruptions at Redoubt volcano in 1990 also generated sizeable lahars when pyroclastic flows from a series of lava dome collapses were emplaced onto snow and ice (Gardner et al., 1994). Both the Nevado del Ruiz and Redoubt eruptions were volumetrically small (Calvache, 1990; Gardner et al., 1994) and showed that the ability of hot rock to efficiently mix with snow or ice is more important than eruption size for lahar generation (Pierson et al., 1990). This is especially significant for high-risk volcanoes like Mt. Rainier (USA) and Cotopaxi (Ecuador) that have large summit ice caps and many thousands of people living within the lahar hazard zones (Wood and Soulard, 2009; Pistolesi et al., 2013). It is also important for high-use volcanoes like Mt. Ruapehu (NZ), which has historically produced hazardous ice-slurry lahars when erupted material and fully dilute PDCs have disrupted the thick winter snowpack (Cronin et al., 1996a; Lube et al., 2009; Kilgour et al., 2010).

Although events like those at Nevado del Ruiz and Redoubt have highlighted the secondary lahar hazard from PDC-ice interactions, few studies have investigated the direct effect an ice substrate has on the primary PDC hazard. Snow or ice reduces the coefficients of static and kinetic friction between erupted material and the surface, and may favour PDC generation by encouraging pyroclasts landing on a slope to either continue their motion downslope immediately or to later collapse once they have accumulated to a critical thickness. PDCs can also be generated when lava flows travelling over snow/ice are explosively disrupted by secondary hydrovolcanic explosions (Belousov et al., 2011). The effect that an ice substrate has on PDC mobility (i.e. runout distance, impact area, and flow velocity) has not been described, not least because the significant variability in PDC types makes it difficult to quantitatively compare and isolate only those effects resulting from ice interaction. However studies of rock avalanches have shown that interaction with glacier ice significantly increases rock avalanche mobility, resulting in higher flow velocities (Sosio et al., 2012) and greater runout distances (Figure 6.1 a; Evans and Clague, 1988; Deline et al., 2015). Smoother and more open glacial terrains also promote lateral and longitudinal spreading of debris, resulting in thinner, more extensive deposits than

those in equivalent non-glacial environments (Deline et al., 2015). Several mechanisms have been proposed to explain this higher mobility of glacial rock avalanches (Evans and Clague, 1988, 1994), including a) transport on low friction surfaces (i.e. ice and snow); b) generation of high basal pore pressures by frictional melting (Sosio et al., 2012); and c) reduction of internal friction by incorporating ice and snow into the flow. Non-glacial PDCs are frequently more mobile than dry rock avalanches of equivalent size (Figure 6.1 b), but it is reasonable to hypothesize that the processes that increase rock avalanche mobility over ice will also apply to PDCs transported over ice. However the additional effects of thermal interactions between hot pyroclasts and ice, resulting in water and steam generation and changes to the PDC mass and energy balances, are not well understood and may offset some of the mobility increases observed for cold rock avalanches. Analogue experiments and modelling using hot water and polyethylene glycol (Thouret et al., 2007) found that melting induced by a turbulent fluid occurred at rates 10-60 times faster than for conductive, non-turbulent melting. Thouret et al. (2007) attributes this to the ability of turbulence to carry away any melted material and maintain a consistant temperature at the fluid and unmelted substrate interface. These observations support the calculations of Pierson et al. (1990) that suggest passive melting of the Nevado del Ruiz icecap by hot pyroclastic material underestimates the true melting by a factor of 40. These observations reinforce that mechanical processes such as those resulting from PDC transport (e.g. dynamic mixing, fluid drag, mass failure) are critical for rapidly generating large volumes of meltwater.

In one of the only studies to directly investigate the interaction between hot pyroclasts and snow/ice, Walder (2000a,b) found that thermal scour, in addition to mechanical scour, may be another important process by which PDCs can erode underlying ice. Experimental observations of hot sand placed on shaved ice (Walder, 2000b) demonstrated that unstable vapour-driven fluidization of the sand permitted efficient thermal scour, leading to generation of a sand-and-water slurry that could also form at the base of natural PDCs and contribute to lahar generation (Figure 6.2). However, although Walder's (2000b) experiments shed light on thermal interactions at the particle-ice interface, these static experiments did not investigate the effects of larger (lapilli or bomb), porous natural volcanic samples, or model the dynamic implications for PDC transport. Here, we use natural samples from

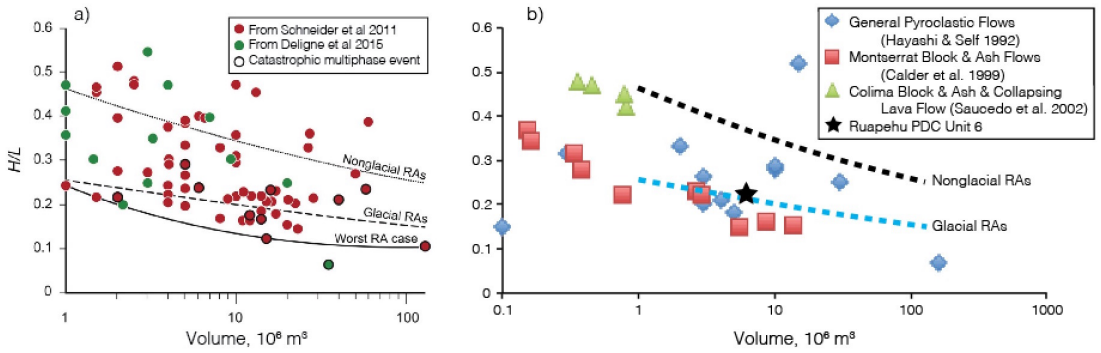

Figure 6.1: Mobility of rock avalanches and pyroclastic density currents, shown by the relationships between deposit volume and the ratio of vertical (H) and horizontal (L) travel distances. a) Rock avalanches emplaced onto glaciers are significantly more mobile than their dry equivalents, b) Nonglacial PDCs are generally more mobile than nonglacial rock avalanches. Lack of deposit data for glacial PDCs, as well as much greater complexity in terms of PDC generation and transport parameters compared to rock avalanches (e.g. eruptive style, clast temperatures, componentry, density, magmatic gas content etc.) means an equivalent comparison is not currently possible for the effects of PDC transport over ice. Ruapehu's ice-transported Unit 6 deposit has comparable mobility to glacial rock avalanches, and is towards the higher-mobility end of the PDCs shown here (Modified from Deline et al., 2015. Regression lines from Schneider et al., 2011, and Evans and Clague, 1988)

an ice-transported PDC deposit at Ruapehu volcano to perform similar microphysical experiments and measure the rates of water and steam generation when hot pyroclasts come into contact with ice. We then use these experimental results to inform high-resolution continuum multiphase models that allow us to investigate the dynamic effects of PDC-ice interactions for the first time.

Ruapehu volcano is a 2797m andesitic-dacitic composite volcano in New Zealand's North Island. It currently supports about 20 small glaciers and glacier remnants at its summit (Williams, 2013), but had an extensive Pleistocene ice cap with outlet glaciers reaching as low as 1300m between ~27-15 ka (McArthur and Shepherd, 1990; Conway et al., 2015). Lava-ice contact features (e.g. Spörli and Rowland, 2006) show that ice was present to ~1700m until 8.8 ± 2.2 ka (C. Conway, pers. comm), consistent with the ~1600m starting elevation of an unusual ~11.6 ka pyroclastic density current deposit (PDC Unit 6) whose textures suggest most of its pre-depositional transport occurred over glacial ice (Chapter 4). The deposit is dominantly monolithologic, reflecting isolation from the volcanic surface, and contains unusually rounded clasts with chilled margins that are in-

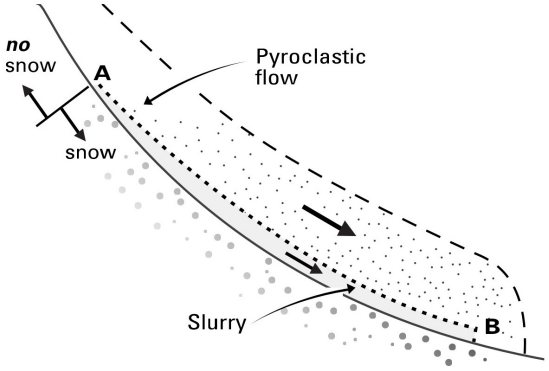

Figure 6.2: Conceptual drawing to illustrate a PDC tavelling over snow (from Walder, 2000b). Walder (2000b) used experimental observations of hot sand placed on shaved ice to propose that convective vapour-driven 'thermal scour' occurs at the particle-snow interface, which draws snow into the base of the PDC to form a pyroclast-water slurry. The model does not consider subsequent incorporation of meltwater or steam into the main PDC.

terpreted to reflect efficient chilling and abrasion by wet ash during transport (Chapter 4). Striations on the deposit's upper surface evidence later glacial advance, but the majority of the deposit is exceptionally well preserved due to its final deposition on ice-free ground and partial deposit welding. It therefore provides a rare (or at least rarely identified) example of a PDC that has been transported over ice for most of its flow path, yet has nonetheless remained preserved in the long-term deposit record.

Using samples from Ruapehu's Unit 6 deposit, we aim to: 1) quantify the rates of water and steam generation when hot porous natural samples contact ice; 2) use this microphysical data as an input for high-resolution multiphase numerical simulations to investigate PDC transport over ice; 3) model the effects that (a) ice smoothness and (b) water and steam production has on PDC runout and dynamics; and 4) assess the volume of meltwater produced when hot PDCs are transported over ice, with implications for the lahar hazard.

6.2 Methods

6.2.1 Microphysical Experiments

Natural samples of lapilli to bomb sized scoria collected from the unwelded base of Ruapehu's ice-contact PDC Unit 6 were dried, weighed, heated to 500-900°C (773-1173K) and held at temperature for up to 4 hours to fully equilibrate. Rates of water and steam generation at each temperature (T) were then measured over 10s by placing the hot clasts on blocks of ice frozen at -15°C (258K). The whole setup was mounted atop a mass balance so that the net loss in mass reflected direct steam production as vapour was lost to the atmosphere (Figure 6.3). Any meltwater generated was collected through a drainage hole in the ice block and weighed separately at the end of each experimental run. As well as producing external meltwater, the hot clasts were observed to ingest significant quantities of water as previously described by Dufek et al. (2007). Therefore, following each 10s experiment the clasts were removed from the ice and immediately weighed to measure the amount of ingested water by mass difference. Once removed from the ice, the ingested water was observed to immediately be expelled as steam, and so the ingested mass was added to the total steam budget. Temperature-dependent heat capacity (C_p) was calculated using the formula in Dufek et al. (2007), and the excess thermal energy available for meltwater production (Q_E) for a clast of known mass (m, kg) and temperature (T, K) was approximated by $Q_E = (m.T.C_{p(T)}) - (m.258.C_{p(258K)})$ since the ice was frozen at 258K. Since only part of each clast made contact with the ice during the 10s runs, only a fraction of each clast's thermal energy was available for melting the ice due to the low thermal conductivity of andesite. Therefore, each clast's excess thermal energy (Q_E) was scaled by the ratio F/V, where F (m^2) is the clast-ice contact footprint and V (m^3) is the total clast volume (Figure 6.4). The contact footprint (F) of each natural sample was obtained by digital image analysis of the imprint of each clast when pressed gently on a bed of flour, and clast volume (V) was measured by water displacement following the methods of Houghton and Wilson (1989), Barker et al. (2012), and Rotella (2013). For the natural lapilli and bomb-sized samples investigated here, the scaling factor F/V (in m^{-1}) was found to be approximately related to the clast volume by the formula $F/V = 0.4234V^{-0.4059}$, thereby permitting the appropriate scaling factor to be calculated for any clast size for use in the subsequent models.

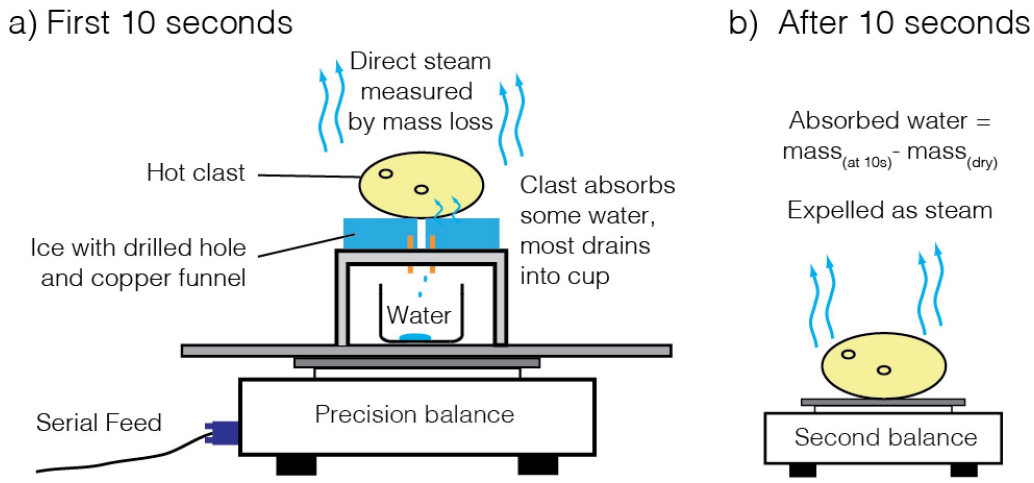

Figure 6.3: Experimental setup for quantifying the amount of steam and meltwater production over 10s when hot pyroclasts from a PDC interact with ice.

6.2.2 Numerical model

The ice contact experiments provide numerical constraints for the average rates of water and steam production over 10s when hot natural samples from Ruapehu's ice-transported PDC were placed on ice (Figure 6.4). We then developed a subgrid continuum multiphase model for water and steam production to extend the laboratory measurements to predictive models of macroscopic PDC behaviour over ice. Here, separate equations for mass, momentum and thermal energy are solved for each mechanically distinct phase, i.e. ice, water, steam, air, and modelled particles (1 or 2 grain sizes). The separate phases are interpenetrating continua with volume fractions equal to unity in a control volume. The model code is an adaptation of the MFIX (multiphase flow with interface exchanges) numerical approach to volcanic flows (Gera et al., 2004), and develops the ideas presented in Dufek and Bergantz (2007) and Dufek et al. (2007). Heat transfer that results in water and steam production is primarily accomplished by transfer of thermal energy from the particle phase to the ice phase, then into the water phase and then into the gas phase. The amount of water and steam production is therefore controlled by the amount of contact the particles have with the ice and subsequently generated meltwater. The subgrid heat transfer and phase change model is guided by the experimental results, and assumes that

(1) all of the subgrid-scale heat transfer occurs near the surface of the ice/meltwater (2) the mass of meltwater produced for a given amount of particle energy is given by the experimental results (3) the mass of steam produced for a given amount of particle energy is given by the relations found in Dufek et al. (2007) for water-to-steam and, to a smaller extent from the experimental results here for ice-to-steam (4) the rate of ice-water phase change is approximated by the average rate calculated from the 10s experimental runs, and (5) the rate of water-steam phase change is given by the relations in Dufek et al. (2007) and the experimental results here.

6.3 Results and Discussion

We used the Ruapehu Unit 6 example as a template for a series of two-dimensional (channelised) and quasi-3D (i.e. two dimensions with prescribed 22.5° out-of-plane spreading) numerical simulations aimed at understanding the sensitivity of PDC dynamics to transport over glacial ice. The model geometry (Figure 6.5) is based on the simplified interpreted flow path of Ruapehu's PDC Unit 6, from its source as a rapidly accumulating spatter pile beneath North Crater down to deposition in a branch of the Mangatoetoenui Valley in eastern Ruapehu (Chapter 4). We emphasise, however, that the simulations primarily aim to investigate the general effects that transport over ice has on PDC dynamics rather than recreating the specific details of Ruapehu's Unit 6. In each simulation the PDC is introduced in a constant flow boundary at a temperature of 1200 K, and then allowed to propagate downslope. The simulations have two grain sizes (1cm and 100μm) to investigate rudimentary sorting dynamics, and were run over three different modelled surfaces to specifically isolate the effects of surface roughness and water and steam generation. The three surfaces are 1) an ice reservoir that is both smooth *and* interacts with the PDC to produce water and steam (hereafter termed "ice"); 2) an ice-free surface with the same smoothness as the ice, but which does not generate water and steam ("smooth ice-free surface"); and 3) an ice-free surface (i.e. no phase changes) with characteristic volcanic surface roughness ("normal ice-free volcanic surfaces"). The "ice" and "smooth ice-free surfaces" are present for only the first 2km of transport, in line with the interpreted prehistoric ice extent for Ruapehu's Unit 6 (Chapter 4 and Conway et al., 2015).

The preliminary simulations highlight a number of flow features that result from the interactions between PDCs and surface ice during transport. Firstly, if all other parameters are equal then the simulations show that the high particle concentration component at the base of the PDCs (i.e. bedload) travels further (~1km further in these 2D simulations) when transported over "ice" (with water and steam generation) compared to transport over "normal ice-free volcanic surfaces" (Figure 6.6). This suggests that the reduced basal friction of the glacial surface increases the runout distance for the bedload fraction. Since the bedload forms the majority of the PDC mass, it is these deposits that are most likely to be preserved in the long-term record. Therefore, the preserved deposits from prehistoric PDCs may show greater runout distances if they were transported over ice, consistent with the observations from glacial rock avalanche deposits. We therefore interpret the surviving bedded deposits from Ruapehu's PDC Unit 6, which on average are ~6.5m thick and reach >30m thick in a palaeovalley (Chapter 4), to represent only the bedload components from multiple small PDCs.

In contrast to the concentrated bedload, the volumetrically-smaller dilute parts of the simulated PDCs travel *less* far when transported over ice (Figure 6.7). In the quasi 3-dimensional simulations, the dilute fractions of the ice-transported PDCs travel ~500m less far than equivalent PDCs transported over "smooth ice-free surfaces." This shows that water and steam generation, not roughness, is the main factor in reducing the runout of the dilute component when the PDC travels over ice. This appears to be a consequence of steam production causing more fine material to ascend in buoyant plumes, therefore hindering forward propagation of the density current. This steam-driven elutriation may also result in better size segregation of the resulting deposits by removing fine material from the advancing PDC. Because the dilute fraction carries a smaller part of the PDC's total mass, these deposits are less likely to be preserved in the long-term record than deposits from the main bedload. However, from a hazards perspective, the shorter runout distances suggests that transport over ice slightly reduces the *direct* hazard from the low-particle concentration, dilute component of the PDC.

The flow fronts of the simulated PDCs are not significantly affected by transport over

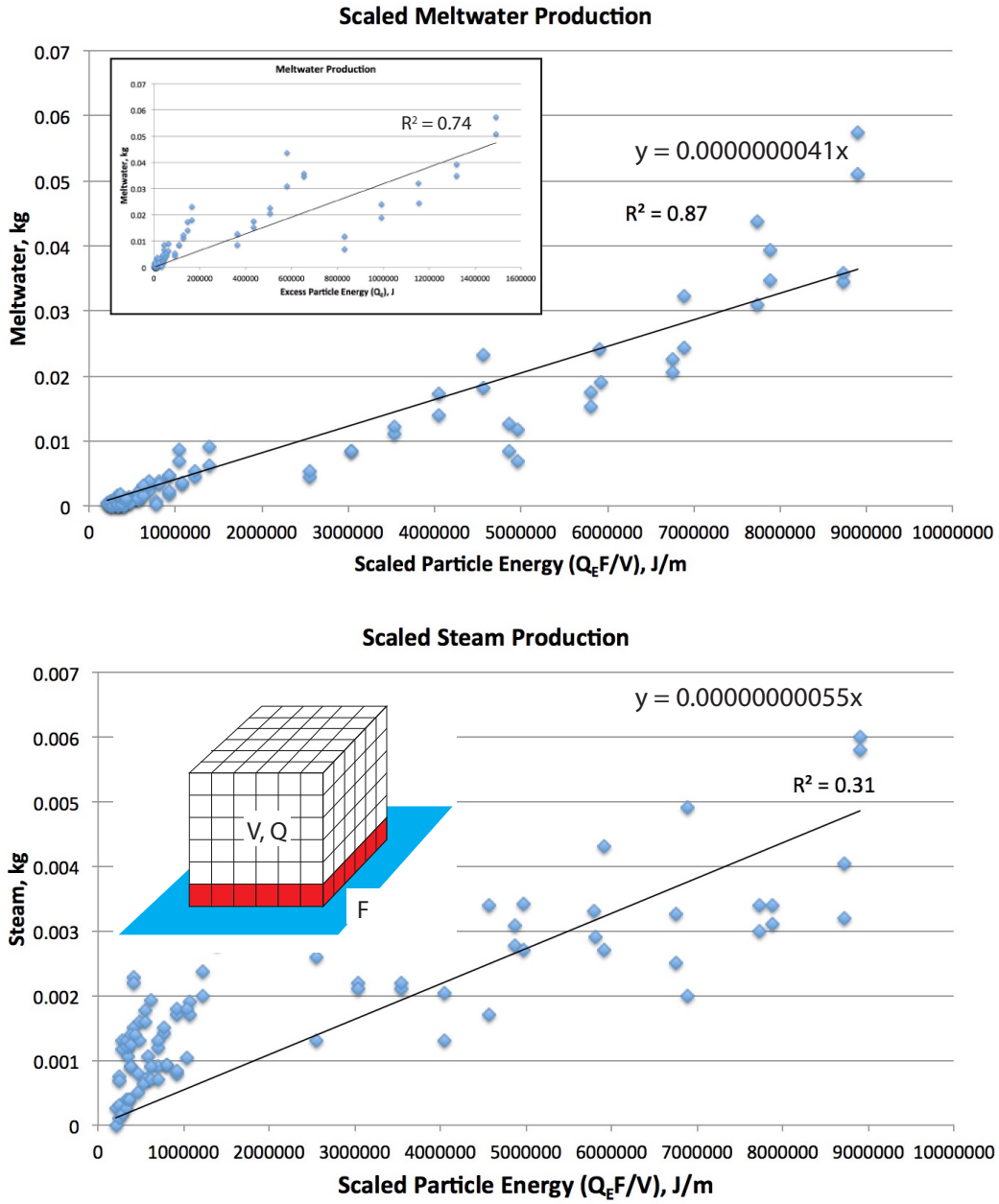

Figure 6.4: Total meltwater and steam production over 10s (mass, kg) positively correlates with the excess thermal energy of the clast (Q_E, J; top inset). Since only a small part of the clast is in contact with the ice, better correlation coefficients are achieved by scaling Q_E by the ratio of its ice-contact area (F) and total volume (V) (bottom inset). The lower correlation coefficient for the steam production results is due to the very small mass of steam produced, with experimental errors therefore introducing significant noise.

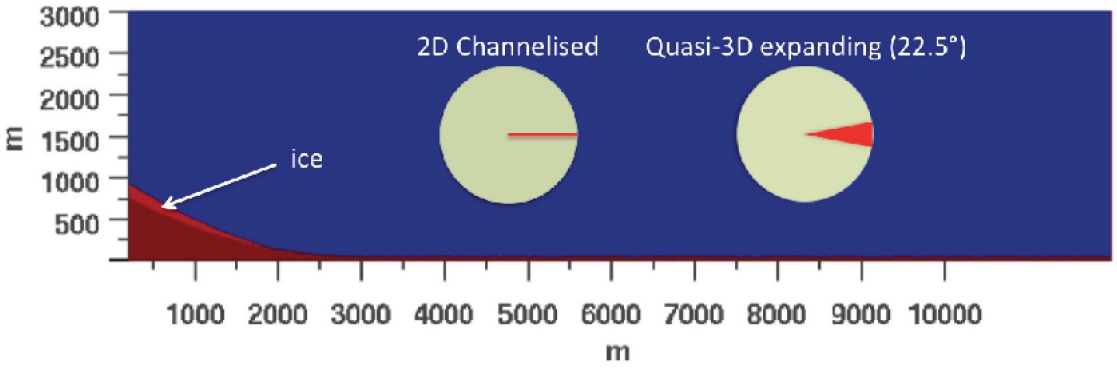

Figure 6.5: Geometry for the model simulations, based on a simplified version of the topography for the interpreted flow path of Ruapehu's PDC Unit 6. The model grid has a 15m horizontal and 10m vertical resolution, following the sensitivity analysis of Dufek and Bergantz (2007) which showed that higher resolutions produced no statistical differences in the modeled flow fields.

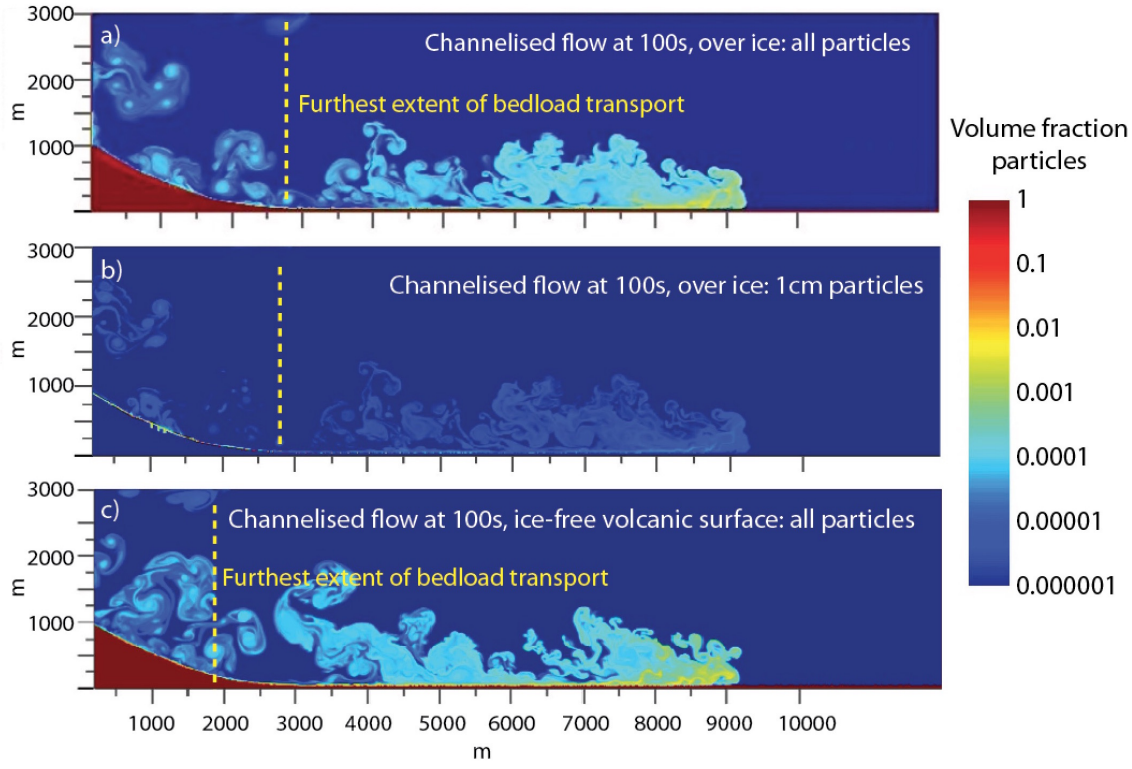

Figure 6.6: PDC particle concentrations after 100s for the 2-dimensional channelised simulations. a) and b) show the same PDC that has initially travelled over ice, and c) shows a PDC with identical starting conditions that has travelled over an ice-free surface (no water or steam generation) with characteristic volcanic roughness. a) The dilute part of the current is still advancing and appears to be slightly more inflated than the ice-free flow in c, possibly due to buoyancy imparted by the generated steam. However the coarser bedload particles (b) forming the majority of the PDC mass and energy have mostly been deposited in the first ~2700m. c) In the ice-free flow, the topographic roughness has encouraged mixing of the dilute component in the upper edifice, but has also reduced the runout distance of the main bedload to ~1800m.

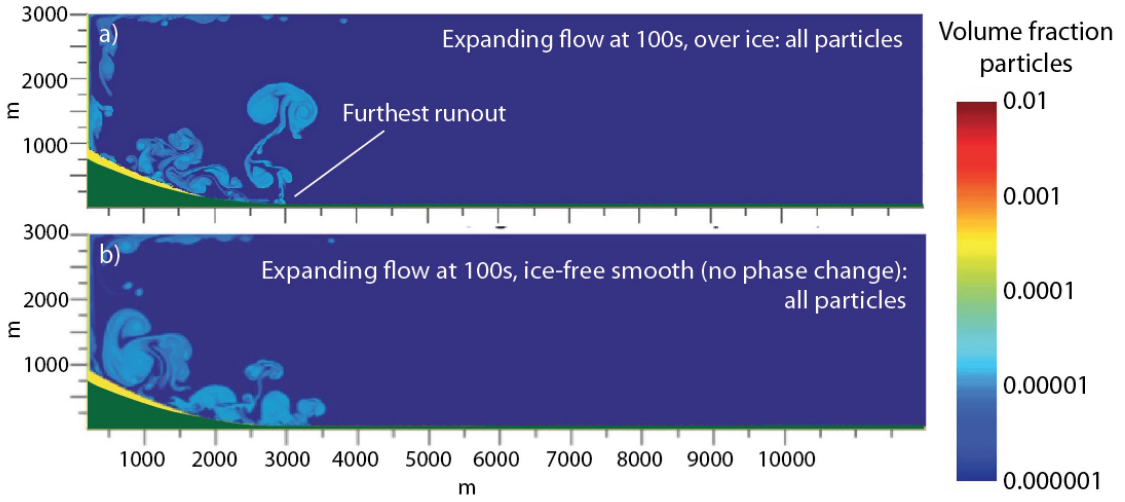

Figure 6.7: PDC particle concentrations after 100s for the quasi 3-dimensional expanding simulations. These simulations have much shorter runout distances than the 2D simulations as a result of the prescribed out-of-plane flow expansion. a) shows a PDC transported over ice (with phase changes) that has reached its furthest runout by 100s, and the front has lifted as a buoyant plume. b) shows a PDC transported over a surface with the same smoothness as ice but with no phase changes ("smooth ice-free"). The dilute parts of the ice-transported PDC travel ~500m less far, and this is interpreted to be due to increased PDC buoyancy as a result of steam generation that causes the material to ascend in buoyant plumes rather than propegating downslope.

ice, and maintain high temperatures and contain lower amounts of steam than the trailing parts of the flows (Figure 6.8 a and b). This is interpreted to result from the PDC fronts outpacing the rates of water and steam production, with most phase changes occurring after the flow front has passed. Consequently, the PDC bodies contain high quantities of meltwater and steam that is most concentrated towards the base of the flows (Figure 6.8 b). The incorporation of significant amounts of water vapour into the PDC supports the hypothesis that wet ash within the PDC might have formed an efficient abrasive that contributed to the unusually rapid rounding of larger lapilli and bombs observed in Ruapehu's Unit 6 deposit (Chapter 4). Here, the steam- or water-saturated ash is hypothesised to have adhered to the surfaces of larger clasts, resulting in sandpaper-like abrasion of clast surfaces during subsequent particle collisions.

Water generation is prolific in the simulations over ice, with the total meltwater volume peaking at 100 seconds at 5 x 10^6 m^3, equivalent to ~35% of the simulated PDC bedload volume (Figure 6.8 c & d). The amount of total meltwater then decreases slightly with time as water incorporated within the PDC is converted to steam, but remains close to the

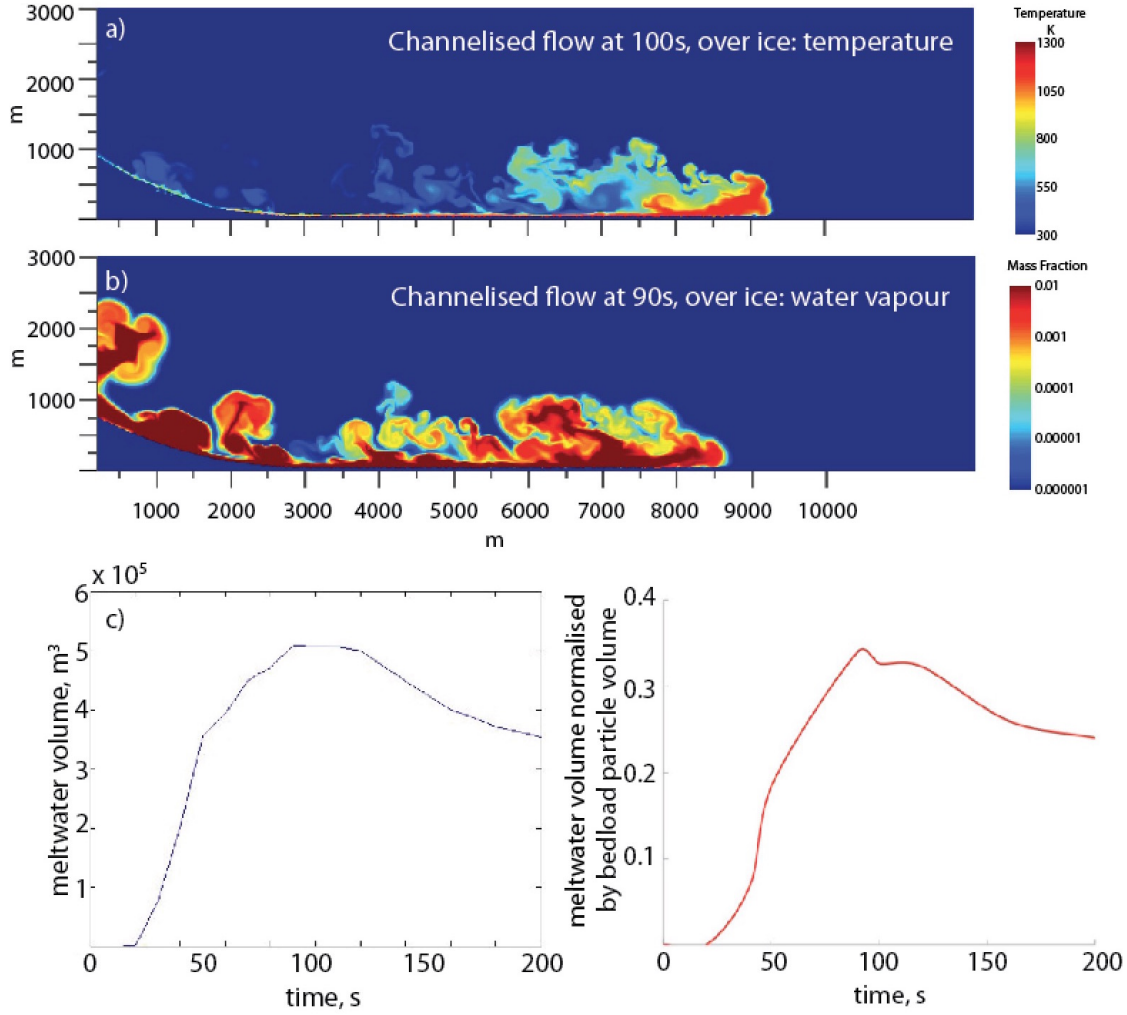

Figure 6.8: Temperature, water vapour, and meltwater production for the 2D simulated PDCs traveling over ice. a) The flow front maintains a higher temperature and b) contains lower amounts of water vapour than the trailing PDC body. Water vapour is incorporated into the entire PDC, but is most concentrated towards the base of the flow. c) Meltwater is only generated in the first 2km as the PDC is transported over ice on the upper edifice. Total meltwater peaks at 100s but then declines as some of that water is subsequently vaporised as the flow continues over ice-free terain. d) Total meltwater produced by the PDC over the 200s simulation is equivalent to ~25% of the PDC bedload particle volume.

equivalent of ~25% of the bedload volume by the end of the simulation. The reason that the total meltwater first peaks then declines in these simulations is interpreted to result from ice-transport only occurring for the first ~2km (where the ice-to-water phase change occurs); whereas after this point the dominant phase change is water to steam as meltwater incorporated within the PDC continues to be vapourised by the hot pyroclasts. Meltwater production would therefore be expected to be much higher if the PDC were transported over ice for its entire flow path. Additionally, the simulated meltwater values are likely to be minimum estimates, since real-world PDCs can be expected to be significantly more efficient at mechanically eroding (in addition to the thermal erosion modelled here), entraining and then melting glacial ice as well as snow cover during transport (e.g. due to irregularities in the glacial surface). Nonetheless, the simulated meltwater results (equivalent to ~25% of the PDC bedload volume) are well supported by the best-constrained historical data from Nevado del Ruiz (Columbia) in 1985. That eruption emplaced approximately 0.09 km^3 of pyroclastic deposits on the volcano's glaciated summit area (Calvache, 1990), removing the equivalent of ~0.0385 - 0.0436 km^3 water from the snow and ice cap (Pierson et al., 1990; Thouret, 1990). Hence, the estimated meltwater volume at Nevado del Ruiz was equivalent to approximately 43-48% of the volume of the pyroclastic deposit. Given that the Nevado del Ruiz deposits were *entirely* emplaced on the summit snow/ice, whereas the simulated PDCs here only transit ice for 2km, the lower meltwater volumes in the simulations are very reasonable. Both examples show that PDCs transported over snow/ice are highly efficient at very rapidly generating large volumes of meltwater; a key process for generating syn-eruptive lahars. At Nevado del-Ruiz, between 25-57% (0.0011-0.0022 km^3, Thouret, 1990) of the total generated meltwater was incorporated into lahars. In-flow bulking then meant the total volume of lahars reaching low-gradient depositional areas was about 0.089 km^3 (Pierson et al., 1990), *equivalent to the original volume of the pyroclastic deposits*. Using these values to *very generally* illustrate the implications of our numerical simulations for PDC transport over just 2km of ice, this suggests a volume of water equivalent to ~6-14% of the PDC bedload volume may then contribute to lahars whose final flow volume may be equivalent to at least 50% of the volume of the original PDC bedload. Since an estimated 0.119 km^3 of PDC deposits were emplaced on Ruapehu's eastern flanks during the past ~13.6 Ka (Chapter 4), we therefore hypothesise that some of the 0.094 km^3 (deposit volume) of laharic and hyperconcentrated flow deposits from

eastern Ruapehu's 14.7 - 5.4 ka Tangatu Formation (Donoghue and Neall, 2001) may have resulted from meltwater generated when PDCs were transported over snow and ice on the volcano's upper flanks.

6.4 Conclusions

Initial results from the microphysical experiments and numerical simulations show that the reduced surface roughness and phase changes that result from PDC transport over ice serve to *increase* the runout distance of the granular fluid-based PDC bedload, but at the same time *decrease* the overall runout of the further-reaching dilute parts of the PDC. Therefore, the primary PDC hazard is changed as a consequence of transport over ice, but from a deposit perspective the main bedload-derived deposits will be more extensive than their ice-free counterparts. This is important from a hazard mapping perspective, and highlights the idea that while ice cover may actually reduce the *total* PDC runout (i.e. including the low particle concentration, dilute component), at the same time hazard mapping based only on prehistoric deposits preserved from the granular fluid-based bedload may not fully represent the original extent reached by more dilute parts of the PDC. The simulations also show that PDCs transported over ice are highly effective at very rapidly generating large volumes of meltwater and steam, and even with only 2km of PDC-ice transport in the Ruapehu-inspired geometry used here, meltwater volumes equivalent to ~25% of the PDC bedload volume were produced in only 200s. After further downstream erosion and bulking, even these small ice-covered transport distances could result in debris flows that have flow volumes equivalent to at least 50% the volume of the primary PDC bedload. These results are not only significant for high-risk volcanoes like Mt. Rainier or Cotopaxi, but are also important for high-use volcanoes like Ruapehu where even relatively small PDCs could present a significant and rapidly-generated secondary lahar hazard that threatens the volcano's skifield and tourist populations and infrastructure.

7

Conclusions

7.1 Summary

Pyroclastic density currents (PDCs) frequently occur at andesitic volcanoes and are a significant threat to life and infrastructure (**Chapter 2**). Although most kinds of volcanic eruption can generate PDCs, granular fluid-based PDCs have not historically been documented at Mount Ruapehu, New Zealand. Furthermore, very few prehistoric PDC deposits have previously been identified here, and only one (Pourahu PDC) has been investigated in detail (Donoghue et al., 1995a, 1999). Therefore, current understanding of Ruapehu's PDC hazard has been limited by a lack of knowledge of the characteristic PDC generation mechanisms, frequencies, sizes and extents at this volcano.

In this thesis, **Chapter 2** first summarised the relevant literature regarding pyroclastic density currents and Ruapehu's volcanic setting (**Objective 1**, Figure 7.1). The remaining chapters (**Chapters 3 - 6**) then identified and investigated 12 young (<13.6 ka) granular fluid-based PDC deposits in eastern Ruapehu to address the existing gaps in knowledge regarding PDCs at this volcano. The original thesis objectives and key findings of this research are summarised in Figure 7.1.

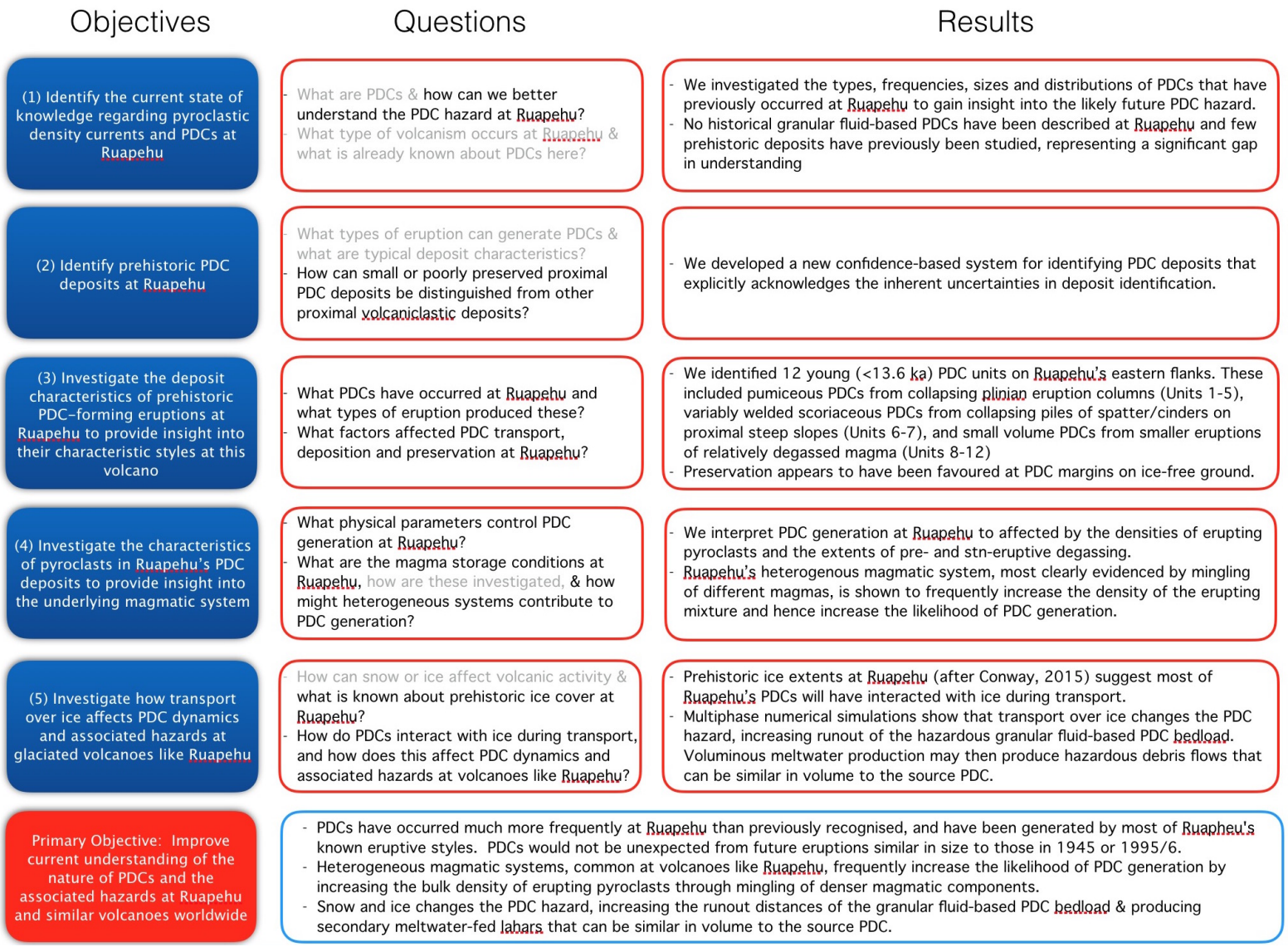

Figure 7.1: Review of the original thesis objectives and summary of main results. The parts of the objectives that were addressed by a review of existing literature (Chapter 2) are in grey, while the main science objectives and results (Chapters 3 - 6) are emphasised here.

7.2 Specific findings of this study

7.2.1 Identifying prehistoric PDC deposits at Ruapehu (Objective 2)

Overcoming the challenges involved in distinguishing small volume proximal PDC deposits from other volcaniclastic deposits is essential for properly characterising a volcano's prehistoric PDC record and hence understanding the likely future PDC hazard (Nakada, 2000). **Chapter 3** approached this problem from a new perspective, departing from traditional list-based identification schemes and instead adopting a confidence rating system that considered the most likely volcaniclastic processes to have formed the observed deposit textures. This provided a formal structure for assessing small, poorly exposed volcaniclastic deposits in the field at Ruapehu (**Objective 2**; Figure 7.1), and resulted in identification of 12 PDC deposits in eastern Ruapehu (Chapter 4), of which 10 (Units 1-3, 5, 7-12) have never previously been identified.

Future work: The confidence-based system developed here can be adapted and expanded for any fragmental deposits for which an element of judgement is needed in the interpretation. Such confidence-based interpretations may also benefit probabilistic hazard assessments by allowing rapid assessment of more deposits, therefore improving understanding of a volcano's past activity. Developing a digital version of the system for use as a field application would allow inclusion of more criteria, and would enable rapid and repeatable in-field deposit assessments.

7.2.2 Characteristic PDC styles at Ruapehu (Objective 3)

The field characteristics of the 12 PDC units identified in eastern Ruapehu are described in **Chapter 4**. These show that hazardous granular fluid-based PDCs have regularly occurred at Ruapehu during the past ~13.6 ka, and were generated from a wide range of eruption styles (**Objective 3**; Figure 7.1). The key results are:

1. Pumice-dominated Units 1-3 evidence collapse of eruption columns associated with Ruapehu's largest known eruptions from North Crater (Ohinewairu eruptive period, 13.6-11.6 ka). These deposits confirm Pardo's (2014) hypothesis that sizeable

PDCs accompanied the Ohinewairua eruptions, based on observations of thin matrix supported layers and disequilibrium bubble textures in the associated plinian fall deposits. Small-volume PDC Units 11 & 12, containing dense cauliflower-textured clasts, show that the Ohinewairua PDC sequence ended with still-hazardous PDCs from smaller eruptions of more degassed magma; resolving detail that is not present in the tephra-fall record.

2. Pumice-dominated Units 4 (Pourahu PDC) and 5 are interpreted to correlate with the ~11.6 ka Okupata-Pourahu eruptive episode, and are interpeted to represent closely spaced eruptions of gas-rich magma from a new vent near South Crater (Unit 4), as well as a smaller short-lived eruption from the pre-existing open system near North Crater (Unit 5).

3. Scoria-dominated variably welded Units 6 (~11.6 ka) & 7 (unknown age) evidence PDCs generated by periodic collapse of accumulating erupted spatter/cinders on steep proximal slopes near North Crater. These eruptions demonstrate that PDCs can occur from eruption styles not normally associated with PDCs, and highlight the significance of topographic slope when assessing the PDC hazard.

4. Heterogeneous small-volume Units 8-10 (<11.6 ka) evidence PDCs from collapse of smaller eruption columns from relatively degassed magmas erupted near South Crater. These eruptions are interpreted to be similar in magnitude to Ruapehu's historical activity, and highlight that granular fluid-based PDCs may represent an important *current* hazard at Ruapehu despite their absence in historical time.

Future work: This study focused *only* on deposits in eastern Ruapehu. Two further young PDC deposits have since been observed at Turoa Ski Area in southern Ruapehu (G. Leonard and D. Townsend, pers. comm.), one of which is texturally similar to, but more extensive than, PDC Unit 12 (observed by J. Cowlyn, May 2015). At least one other candidate PDC deposit is known in south-eastern Ruapehu (J. Procter, pers. comm.), and more units are likely to be preserved in other parts of the edifice. Therefore, expanding this research to the whole volcano, and taking advantage of the rapid field identification system developed in Chapter 3, will enable Ruapehu's PDC hazard to be more fully characterised.

7.2.3 Underlying magmatic processes that contributed to PDCs at Ruapehu (Objective 4)

While the field observations of PDC deposit facies presented in Chapter 4 provide insight into the types of eruption that have previously generated PDCs at Ruapehu, it is the underlying magmatic processes that control Ruapehu's eruption styles and the nature of the erupted pyroclasts. Therefore, in **Chapter 5** we investigated the chemical and physical properties of pyroclasts within the PDCs **Objective 4** (Figure 7.1), and demonstrated that Ruapehu's underlying heterogeneous magmatic system appears to directly contribute to PDC generation at this volcano. The key results are:

1. Pyroclast textures, chemistries, and modelled magmatic storage conditions for Ruapehu's PDC deposits emphasise the high levels of heterogeneity within Ruapehu's young magmatic system. The results suggest that frequent mingling and mixing between different magmas with different storage, ascent and degassing histories strongly influenced Ruapehu's eruptive styles and nature of the PDC hazard.

2. Pumice-dominated PDC Units 1-5 are interpreted to have resulted from collapsing plinian eruption columns due to densification of the erupting mixture by a) vent erosion and addition of denser lithic clasts (Unit 1), b) mingling with denser secondary magmas (Units 2 & 4), and c) limited pre- and syn- eruptive degassing/outgassing (Units 1-3).

3. The fountaining/spatter-forming eruptions thought to have generated variably welded PDC Units 6 & 7 were interpreted in Chapter 4 to have resulted from pre- and syn-eruptive degassing through a pre-existing magmatic system in Northern Ruapehu. The textural results here support this hypothesis, with vesicle textures in Unit 6 evidencing greater amounts of degassing and vesicle collapse that the compositionally-similar Unit 4 pyroclasts erupted from a new (previously closed) vent near South Crater.

4. Shallow storage and slow ascent of the heterogenous small volume PDC Units 8-12 magmas are interpreted to have permitted high levels of pre-eruptive degassing, resulting in dense pyroclasts with isolated, irregular vesicles and high groundmass

microlite contents. Here, PDC generation is interpreted to have resulted from low collapse or 'boiling over' of dense eruption columns from smaller subplinian/vulcanian activity, and this is supported by textural correlations with modern deposits from similar eruptions at Ngauruhoe and Tungurahua volcanoes.

Future work: The results from this chapter consider PDC generation from the perspective of the physical properties of the erupted pyroclasts, emphasising that parameters such as bulk pyroclast densities and magmatic volatile contents *directly control* eruptive parameters like mass eruption rate and exit velocity. This concept allows the contributions of different components (e.g. secondary magmas or heterogeneities within the primary magma) to be investigated. The observation that heterogeneous underlying magmatic systems *almost always* increase the likelihood of PDC generation is an important result; therefore future work at Ruapehu and other volcanoes is needed to fully constrain what this means for the PDC hazard.

7.2.4 The effects of PDC transport over snow and ice (Objective 5)

Snow and ice is a common feature at many tall stratovolcanoes, and is important as it can both directly affect PDC dynamics and also influence the characteristics of preserved volcanic deposits. Thesis **Objective 5** (Figure 7.1) aimed to address these effects. The key results are:

1. The field observations presented in **Chapter 4** show that the limits of prehistoric ice cover at Ruapehu appear to correlate with the distribution of preserved PDC deposits, suggesting preserved PDC deposits may *only* reflect the extents of ice-free terrain at the time of emplacement. Consequently, deposit distributions and volumes may significantly under-represent the original depositional extents of the source PDCs. Similarly, any PDCs that do not reach ice-free surfaces may never have their deposits preserved, meaning the frequency and magnitudes of PDC events interpreted from the geological record may underestimate the hazard.

2. The *lack* of identifiable textural evidence for ice transport in many of Ruapehu's PDC deposits, even when transport over ice is reasonably inferred from the glacial record, shows that volcanological studies must *at least consider* a volcano's glacial history when interpreting prehistoric deposits.

3. Despite its common occurrence, few previous studies have investigated how snow or ice affects PDC dynamics and the associated hazards. In **Chapter 6**, we presented experimental observations of pyroclast-ice interactions combined with high-resolution multiphase numerical simulations to model the large-scale effects of PDC transport over ice for the first time. The models suggest that transport over ice significantly changes PDC dynamics, increasing the runout distance of the hazardous granular fluid-based PDC bedload and generating large amounts of meltwater and steam.

4. Meltwater volumes equivalent to ~25% of the PDC bedload volume were produced over *only 2km of ice transport* in the Ruapehu-inspired simulations. Comparisons with observational data from Nevado del Ruiz (Calvache, 1990; Pierson et al., 1990; Thouret, 1990) suggest that this may result in hazardous debris flows with volumes equivalent to at least 50% of the primary PDC bedload volume *for the model conditions*. At Nevado del Ruiz, where the *entire PDC transport* occurred over ice, the resulting debris flows had volumes equivalent in size to the primary PDCs. These results are significant for high-risk glaciated like Mt. Rainier (USA) and Cotopaxi (Ecuador), as well as high-use volcanoes like Ruapehu where even small PDCs may interact with summit glaciers and winter snowpacks and generate hazardous lahars.

Future work: The models developed in Chapter 6 have important applications for understanding PDC-ice interactions at glaciated volcanoes worldwide. We aim to continue developing these models to assess different initial conditions, and hope to move to full-3D simulations that will permit more accurate model calibration against real-world examples. The calibrated models may then be used to inform hazard assessments at high-risk volcanoes using real-world topography and eruption scenarios.

7.3 Understanding the nature of PDCs and associated hazards at Ruapehu (Primary Objective)

The **Primary Objective** (Figure 7.1) of this thesis was to *"investigate prehistoric pyroclastic density current deposits at Ruapehu, in order to improve current understanding of the nature of PDCs and associated hazards at Ruapehu and similar volcanoes worldwide."*

Overall conclusions:

- ✓ PDCs have occurred much more frequently at Ruapehu that have been previously recognised, and have been generated by most of Ruapheu's known eruptive styles (Chapters 3 and 4). PDCs would *not* be unexpected from future eruptions similar in size to those in 1945 or 1995/6.
- ✓ Heterogeneous magmatic systems, common at many andesitic volcanoes like Ruapehu, often increase the likelihood of PDC generation by increasing the density of erupting pyroclasts through mingling of denser magmatic components (Chapter 5).
- ✓ Snow and ice significantly changes the PDC hazard, increasing runout distances of the hazardous granular fluid-based PDC bedload and producing secondary meltwater-fed lahars whose flow volumes can be comparable to the volume of the source PDC (Chapter 6 and Pierson et al., 1990). Glacial ice also affects understanding of prehistoric PDCs by affecting the distributions, textures, and preservation of PDC deposits in the volcanic record.

References

Allen, S. (2004). "Complex spatter- and pumice-rich pyroclastic deposits from an andesitic caldera-forming eruption: the Siwi pyroclastic sequence, Tanna, Vanuatu". In: *Bulletin of Volcanology* 67.1, pp. 27–41. ISSN: 0258-8900. DOI: 10.1007/s00445-004-0358-6.

Alvarado, G. E. and G. J. Soto (2002). "Pyroclastic flow generated by crater-wall collapse and outpouring of the lava pool of Arenal Volcano, Costa Rica". In: *Bulletin of Volcanology* 63.8, pp. 557–568. ISSN: 0258-8900. DOI: 10.1007/s00445-001-0179-9.

Anderson, Jr., A. T., A. M. Davis, and F. Lu (2000). "Evolution of Bishop Tuff Rhyolitic Magma Based on Melt and Magnetite Inclusions and Zoned Phenocrysts". In: *Journal of Petrology* 41.3, pp. 449–473. DOI: 10.1093/petrology/41.3.449.

Aramaki, S. and S. Akimoto (1957). "Temperature estimation of pyroclastic deposits by natural remanent magnetism". In: *American Journal of Science* 255.9, pp. 619–627. ISSN: 0002-9599. DOI: 10.2475/ajs.255.9.619.

Aspinall, W. P. (2006). "Structured Elicitation of Expert Judgment for Probabilistic Hazard and Risk Assessment in Volcanic Eruptions". In: *Statistics in Volcanology* 1, pp. 1–31.

Aspinall, W. (2010). "A route to more tractable expert advice". In: *Nature* 463.7279, pp. 294–295. ISSN: 0028-0836. DOI: 10.1038/463294a.

Barker, S. J., M. D. Rotella, C. Wilson, I. C. Wright, and R. J. Wysoczanski (2012). "Contrasting pyroclast density spectra from subaerial and submarine silicic eruptions in the Kermadec arc: implications for eruption processes and dredge sampling". In: *Bulletin of Volcanology* 74.6, pp. 1425–1443. ISSN: 0258-8900. DOI: 10.1007/s00445-012-0604-2.

Beck, A. (1950). "Volcanic activity at Mt. Ruapehu from August to December, 1945". In: *New Zealand Journal of Science and Technology* B31, pp. 1–13.

Bégué, F., G. A. Gualda, M. S. Ghiorso, A. S. Pamukcu, B. M. Kennedy, D. M. Gravley, C. D. Deering, and I. Chambefort (2014). "Phase-equilibrium geobarometers for silicic rocks based on rhyolite-MELTS. Part 2: application to Taupo Volcanic Zone rhyolites". In: *Contributions to Mineralogy and Petrology* 168.5, p. 1082. ISSN: 0010-7999. DOI: 10.1007/s00410-014-1082-7.

Behncke, B., S. Calvari, S. Giammanco, M. Neri, and H. Pinkerton (2008). "Pyroclastic density currents resulting from the interaction of basaltic magma with hydrothermally altered rock: an example from the 2006 summit eruptions of Mount Etna, Italy". In: *Bulletin of Volcanology* 70.10, pp. 1249–1268. ISSN: 0258-8900. DOI: 10.1007/s00445-008-0200-7.

Belousov, A., B. Behncke, and M. Belousova (2011). "Generation of pyroclastic flows by explosive interaction of lava flows with ice/water-saturated substrate". In: *Journal of Volcanology and Geothermal Research* 202.1-2, pp. 60–72. ISSN: 03770273. DOI: 10.1016/j.jvolgeores.2011.01.004.

Belousov, A., B. Voight, and M. Belousova (2007). "Directed blasts and blast-generated pyroclastic density currents: a comparison of the Bezymianny 1956, Mount St Helens 1980, and Soufrière Hills, Montserrat 1997 eruptions and deposits". In: *Bulletin of Volcanology* 69.7, pp. 701–740. ISSN: 0258-8900. DOI: 10.1007/s00445-006-0109-y.

Bloomfield, K. and S. Valastro (1977). "Late Quaternary tephrochronology of Nevado de Toluca volcano, central Mexico". In: *Institute of Geological Sciences, Overseas Geology and Mineral Resources* 46.46, pp. 1–15.

Bond, A. and R. Sparks (1976). "The Minoan eruption of Santorini, Greece". In: *Journal of the Geological Society* 132.1, pp. 1–16. ISSN: 0016-7649. DOI: 10.1144/gsjgs.132.1.0001.

Boudon, G., G. Camus, A. Gourgaud, and J. Lajoie (1993). "The 1984 nufffde-ardente deposits of Merapi volcano, Central Java, Indonesia: stratigraphy, textural characteristics, and transport mechanisms". In: *Bulletin of Volcanology* 55.5, pp. 327–342. ISSN: 0258-8900. DOI: 10.1007/BF00301144.

Bragagni, A., R. Avanzinelli, H. Freymuth, and L. Francalanci (2014). "Recycling of crystal mush-derived melts and short magma residence times revealed by U-series disequilibria

at Stromboli volcano". In: *Earth and Planetary Science Letters* 404, pp. 206–219. ISSN: 0012821X. DOI: 10.1016/j.epsl.2014.07.028.

Branney, M. J. and P. Kokelaar (2002). *Pyroclastic density currents and the sedimentation of ignimbrites*. Bath: Geological Society Publishing House, p. 143. ISBN: 1862390975.

Brantley, S. R. and R. B. Waitt (1988). "Interrelations among pyroclastic surge, pyroclastic flow, and lahars in Smith Creek valley during first minutes of 18 May 1980 eruption of Mount St. Helens, USA". In: *Bulletin of Volcanology* 50.5, pp. 304–326. ISSN: 0258-8900. DOI: 10.1007/BF01073588.

Breard, E., G. Lube, S. Cronin, R. Fitzgerald, B. Kennedy, B. Scheu, C. Montanaro, J. White, M. Tost, J. Procter, and A. Moebis (2014). "Using the spatial distribution and lithology of ballistic blocks to interpret eruption sequence and dynamics: August 6 2012 Upper Te Maari eruption, New Zealand". In: *Journal of Volcanology and Geothermal Research* 286, pp. 373–386. ISSN: 03770273. DOI: 10.1016/j.jvolgeores.2014.03.006.

Brown, R. J. and G. D. Andrews (2015). "Deposits of Pyroclastic Density Currents". In: *The Encyclopedia of Volcanoes*. Ed. by H. Sigurdsson, B. Houghton, S. McNutt, H. Rymer, and J. Stix. 2nd. Elsevier Academic Press. Chap. 36, pp. 631–648. ISBN: 9780123859389. DOI: 10.1016/B978-0-12-385938-9.00036-5.

Brown, R. and M. Branney (2004). "Bypassing and diachronous deposition from density currents: Evidence from a giant regressive bed form in the Poris ignimbrite, Tenerife, Canary Islands". In: *Geology* 32.5, p. 445. ISSN: 0091-7613. DOI: 10.1130/G20188.1.

Bryan, C., B. Christenson, and K. Hodgson (1996). "Volcanic eruption at a New Zealand ski resort prompts reevaluation of hazards". In: *Eos, Transactions American Geophysical Union* 77.20, p. 189. ISSN: 0096-3941. DOI: 10.1029/96EO00129.

Burgisser, A. and J. E. Gardner (2004). "Experimental constraints on degassing and permeability in volcanic conduit flow". In: *Bulletin of Volcanology* 67.1, pp. 42–56. ISSN: 0258-8900. DOI: 10.1007/s00445-004-0359-5.

Bursik, M. I. and A. W. Woods (1991). "Buoyant, superbuoyant and collapsing eruption columns". In: *Journal of Volcanology and Geothermal Research* 45.3-4, pp. 347–350. ISSN: 03770273. DOI: 10.1016/0377-0273(91)90069-C.

Calder, E., P. Cole, W. Dade, T. Druitt, R. P. Hoblitt, H. Huppert, L. Ritchie, R. Sparks, and S. Young (1999). "Mobility of pyroclastic flows and surges at the Soufriere Hills Vol-

cano, Montserrat". In: *Geophysical Research Letters* 26.5, pp. 537–540. ISSN: 00948276. DOI: 10.1029/1999GL900051.

Calvache, M. L. V. (1990). "Pyroclastic deposits of the November 13, 1985 eruption of Nevado del Ruiz volcano, Colombia". In: *Journal of Volcanology and Geothermal Research* 41.1–4, pp. 67–78. ISSN: 0377-0273. DOI: http://dx.doi.org/10.1016/0377-0273(90)90083-R.

Carazzo, G., É. Kaminski, and S. Tait (2008). "On the dynamics of volcanic columns: A comparison of field data with a new model of negatively buoyant jets". In: *Journal of Volcanology and Geothermal Research* 178.1, pp. 94–103. ISSN: 03770273. DOI: 10.1016/j.jvolgeores.2008.01.002.

Carey, S., H. Sigurdsson, J. Gardner, and W. Criswell (1990). "Variations in column height and magma discharge during the May 18, 1980 eruption of Mount St. Helens". In: *Journal of Volcanology and Geothermal Research* 43.1-4, pp. 99–112. ISSN: 03770273. DOI: 10.1016/0377-0273(90)90047-J.

Cas, R. and J. Wright (1987). *Volcanic successions: Modern and ancient*. London: Allen & Unwin, p. 528. ISBN: 0-04-552021-6.

Cashman, K. V. (1992). "Groundmass crystallization of Mount St. Helens dacite, 1980?1986: a tool for interpreting shallow magmatic processes". In: *Contributions to Mineralogy and Petrology* 109.4, pp. 431–449. ISSN: 0010-7999. DOI: 10.1007/BF00306547.

Cashman, K. and J. Biggs (2014). "Common processes at unique volcanoes - a volcanological conundrum". In: *Frontiers in Earth Science* 2.November, pp. 1–4. ISSN: 2296-6463. DOI: 10.3389/feart.2014.00028.

Cashman, K. and J. Blundy (2013). "Petrological cannibalism: the chemical and textural consequences of incremental magma body growth". In: *Contributions to Mineralogy and Petrology* 166.3, pp. 703–729. ISSN: 0010-7999. DOI: 10.1007/s00410-013-0895-0.

Chapman, J. (1996). "Geology and Geochemistry of Andesitic Rocks of the Upper Mangatoetoenui Valley, Mount Ruapehu, North Island, New Zealand". BSc Honours Thesis. La Trobe University, Bundoora, New Zealand.

Charbonnier, S., A. Germa, C. Connor, R. Gertisser, K. Preece, J.-C. Komorowski, F. Lavigne, T. Dixon, and L. Connor (2013). "Evaluation of the impact of the 2010 pyroclastic density currents at Merapi volcano from high-resolution satellite imagery, field inves-

tigations and numerical simulations". In: *Journal of Volcanology and Geothermal Research* 261, pp. 295–315. ISSN: 03770273. DOI: 10.1016/j.jvolgeores.2012.12.021.

Christenson, B. and C. Wood (1993). "Evolution of a vent-hosted hydrothermal system beneath Ruapehu Crater Lake, New Zealand". In: *Bulletin of Volcanology* 55.8, pp. 547–565. ISSN: 0258-8900. DOI: 10.1007/BF00301808.

Christopher, T. E., M. C. Humphreys, J. Barclay, K. Genareau, S. M. De Angelis, M. Plail, and A. Donovan (2014). "Petrological and geochemical variation during the Soufriere Hills eruption, 1995 to 2010". In: *Geological Society, London, Memoirs* 39.1, pp. 317–342. ISSN: 0435-4052. DOI: 10.1144/M39.17.

Cioni, R., M. Pistolesi, and M. Rosi (2015). "Plinian and Subplinian Eruptions". In: *The Encyclopedia of Volcanoes*. Elsevier, pp. 519–535. ISBN: 9780123859389. DOI: 10.1016/B978-0-12-385938-9.00029-8.

Cole, J. (1990). "Structural control and origin of volcanism in the Taupo volcanic zone, New Zealand". In: *Bulletin of Volcanology* 52.6, pp. 445–459. ISSN: 0258-8900. DOI: 10.1007/BF00268925.

Cole, J. and I. A. Nairn (1975). *Catalogue of the active volcanoes of the world, including solfatara fields. Part XXII New Zealand*. Rome: International Association of Volcanology and Chemistry of the Earth's Interior, p. 156.

Cole, J. and K. Spinks (2009). "Caldera volcanism and rift structure in the Taupo Volcanic Zone, New Zealand". In: *Geological Society, London, Special Publications* 327.1, pp. 9–29. ISSN: 0305-8719. DOI: 10.1144/SP327.2.

Cole, P., E. Calder, T. Druitt, R. P. Hoblitt, R. Robertson, R. Sparks, and S. Young (1998). "Pyroclastic flows generated by gravitational instability of the 1996-97 Lava Dome of Soufriere Hills Volcano, Montserrat". In: *Geophysical Research Letters* 25.18, pp. 3425–3428. ISSN: 00948276. DOI: 10.1029/98GL01510.

Cole, P., E. Fernandez, E. Duarte, and A. Duncan (2005). "Explosive activity and generation mechanisms of pyroclastic flows at Arenal volcano, Costa Rica between 1987 and 2001". In: *Bulletin of Volcanology* 67.8, pp. 695–716. ISSN: 0258-8900. DOI: 10.1007/s00445-004-0402-6.

Conway, C., D. Townsend, G. S. Leonard, C. Wilson, A. Calvert, and J. A. Gamble (2015). "Lava-ice interaction on a large composite volcano: a case study from Ruapehu, New

Zealand". In: *Bulletin of Volcanology* 77.3, p. 21. ISSN: 0258-8900. DOI: 10.1007/s00445-015-0906-2.

Crandell, D. (1971). "Postglacial lahars from Mount Rainier Volcano, Washington". In: *U. S. Geological Survey Professional Paper* 677, p. 75.

— (1987). *Deposits of pre-1980 pyroclastic flows and lahars from Mount St. Helens Volcano, Washington*. Tech. rep.

Cronin, S. J., K. Hodgson, V. E. Neall, A. S. Palmer, and J. A. Lecointre (1997a). "1995 Ruapehu lahars in relation to the late Holocene lahars of Whangaehu River, New Zealand". In: *New Zealand Journal of Geology and Geophysics* 40.4, pp. 507–520. ISSN: 0028-8306. DOI: 10.1080/00288306.1997.9514780.

Cronin, S. J., G. Lube, D. S. Dayudi, S. Sumarti, S. Subrandiyo, and Surono (2013). "Insights into the October–November 2010 Gunung Merapi eruption (Central Java, Indonesia) from the stratigraphy, volume and characteristics of its pyroclastic deposits". In: *Journal of Volcanology and Geothermal Research* 261.November 2010, pp. 244–259. ISSN: 03770273. DOI: 10.1016/j.jvolgeores.2013.01.005.

Cronin, S. J., V. E. Neall, J. A. Lecointre, and A. S. Palmer (1996a). "Unusual ısnow slurryȷ lahars from Ruapehu volcano, New Zealand, September 1995". In: *Geology* 24.12, p. 1107. ISSN: 0091-7613. DOI: 10.1130/0091-7613(1996)024<1107:USSLFR>2.3.CO;2.

— (1997b). "Changes in Whangaehu river lahar characteristics during the 1995 eruption sequence, Ruapehu volcano, New Zealand". In: *Journal of Volcanology and Geothermal Research* 76.1-2, pp. 47–61. ISSN: 03770273. DOI: 10.1016/S0377-0273(96)00064-9.

Cronin, S. J., V. E. Neall, and A. S. Palmer (1996b). "Geological history of the northeastern ring plain of Ruapehu volcano, New Zealand". In: *Quaternary International* 34-36.95, pp. 21–28. ISSN: 10406182. DOI: 10.1016/1040-6182(95)00066-6.

Dahren, B., V. R. Troll, U. B. Andersson, J. P. Chadwick, M. F. Gardner, K. Jaxybulatov, and I. Koulakov (2011). "Magma plumbing beneath Anak Krakatau volcano, Indonesia: evidence for multiple magma storage regions". In: *Contributions to Mineralogy and Petrology* 163.4, pp. 631–651. ISSN: 0010-7999. DOI: 10.1007/s00410-011-0690-8.

Davidson, J. P., J. M. Hora, J. M. Garrison, and M. A. Dungan (2005). "Crustal forensics in arc magmas". In: *Journal of Volcanology and Geothermal Research* 140.1-3, pp. 157–170. ISSN: 03770273. DOI: 10.1016/j.jvolgeores.2004.07.019.

Deal, B. and A. Grove (1965). "General Relationship for the Thermal Oxidation of Silicon". In: *Journal of Applied Physics* 36.12, p. 3770. ISSN: 00218979. DOI: 10.1063/1.1713945.

Degruyter, W. and C. Bonadonna (2013). "Impact of wind on the condition for column collapse of volcanic plumes". In: *Earth and Planetary Science Letters* 377-378, pp. 218–226. ISSN: 0012821X. DOI: 10.1016/j.epsl.2013.06.041.

Deline, P., K. Hewitt, N. Reznichenko, and D. Shugar (2015). "Rock Avalanches onto Glaciers". In: *Landslide Hazards, Risks and Disasters*. Elsevier, pp. 263–319. ISBN: 9780123964526. DOI: 10.1016/B978-0-12-396452-6.00009-4.

Donoghue, S. (1991). "Late quaternary volcanic stratigraphy of the southeastern sector of the Mount Ruapehu ring plain New Zealand: a thesis presented as partial fulfilment of the requirements for the degree of Doctor of Philosophy in Soil Science". PhD Thesis. Massey University, Palmerston North, New Zealand.

Donoghue, S., J. A. Gamble, A. S. Palmer, and R. B. Stewart (1995a). "Magma mingling in an andesite pyroclastic flow of the Pourahu Member, Ruapehu volcano, New Zealand". In: *Journal of Volcanology and Geothermal Research* 68.1-3, pp. 177–191. ISSN: 03770273. DOI: 10.1016/0377-0273(95)00012-J.

Donoghue, S. and V. E. Neall (2001). "Late Quaternary constructional history of the southeastern Ruapehu ring plain, New Zealand". In: *New Zealand Journal of Geology and Geophysics* 44.3, pp. 439–466. ISSN: 0028-8306. DOI: 10.1080/00288306.2001.9514949.

Donoghue, S., V. E. Neall, and A. S. Palmer (1995b). "Stratigraphy and chronology of late Quaternary andesitic tephra deposits, Tongariro Volcanic Centre, New Zealand". In: *Journal of the Royal Society of New Zealand* 25.2, pp. 115–206. ISSN: 0303-6758. DOI: 10.1080/03014223.1995.9517487.

Donoghue, S., V. E. Neall, A. S. Palmer, and R. B. Stewart (1997). "The volcanic history of Ruapehu during the past 2 millennia based on the record of Tufa Trig tephras". In: *Bulletin of Volcanology* 59.2, pp. 136–146. ISSN: 0258-8900. DOI: 10.1007/s004450050181.

Donoghue, S., A. S. Palmer, E. McClelland, K. Hobson, R. B. Stewart, V. E. Neall, J. A. Lecointre, and R. C. Price (1999). "The Taurewa Eruptive Episode: evidence for climactic eruptions at Ruapehu volcano, New Zealand". In: *Bulletin of Volcanology* 61.4, pp. 223–240. ISSN: 0258-8900. DOI: 10.1007/s004450050273.

Druitt, T. (1998). "Pyroclastic density currents". In: *Geological Society, London, Special Publications* 145.1, pp. 145–182. ISSN: 0305-8719. DOI: 10.1144/GSL.SP.1996.145.01.08.

Dufek, J. and G. Bergantz (2007). "Suspended load and bedload transport of particle-laden gravity currents: The role of particle bed interaction". In: *Theoretical and Computational Fluid Dynamics* 21.2, pp. 119–145. ISSN: 0935-4964. DOI: 10.1007/s00162-007-0041-6.

Dufek, J., M. Manga, and M. Staedter (2007). "Littoral blasts: Pumice-water heat transfer and the conditions for steam explosions when pyroclastic flows enter the ocean". In: *Journal of Geophysical Research* 112.B11, p. 201. ISSN: 0148-0227. DOI: 10.1029/2006JB004910.

Eichelberger, J. C. (1975). "Origin of andesite and dacite: Evidence of mixing at Glass Mountain in California and at other circum-Pacific volcanoes". In: *Geological Society of America Bulletin* 86.10, p. 1381. ISSN: 0016-7606. DOI: 10.1130/0016-7606(1975)86<1381:OOAADE>2.0.CO;2.

— (1995). "Silicic Volcanism: Ascent of Viscous Magmas from Crustal Reservoirs". In: *Annual Review of Earth and Planetary Sciences* 23.1, pp. 41–63. ISSN: 0084-6597. DOI: 10.1146/annurev.ea.23.050195.000353.

Evans, S. G. and J. Clague (1988). "Catastrophic rock avalanches in glacial environments". In: *Landslides-Glissements de terrains: Proceedings, 5th International Symposium of Landslides, Lausanne*. Vol. 2, pp. 1153–1159.

— (1994). "Recent climatic change and catastrophic geomorphic processes in mountain environments". In: *Geomorphology* 10.1-4, pp. 107–128. ISSN: 0169555X. DOI: 10.1016/0169-555X(94)90011-6.

Fink, J. H. and S. W. Kieffer (1993). "Estimate of pyroclastic flow velocities resulting from explosive decompression of lava domes". In: *Nature* 363.6430, pp. 612–615. ISSN: 0028-0836. DOI: 10.1038/363612a0.

Fisher, R. V. (1961). "Proposed classification of volcaniclastic sediments and rocks". In: *Geological Society of America Bulletin* 72.9, p. 1409. ISSN: 0016-7606. DOI: 10.1130/0016-7606(1961)72[1409:PCOVSA]2.0.CO;2.

— (1966). “Rocks composed of volcanic fragments and their classification”. In: *Earth-Science Reviews* 1.4, pp. 287–298. ISSN: 00128252. DOI: 10.1016/0012-8252(66)90010-9. arXiv: arXiv:1011.1669v3.

Fisher, R. V. and G. Heiken (1982). “Mt. Pelée, Martinique: May 8 and 20, 1902, pyroclastic flows and surges”. In: *Journal of Volcanology and Geothermal Research* 13.3-4, pp. 339–371. ISSN: 03770273. DOI: 10.1016/0377-0273(82)90056-7.

Fisher, R. V. and H.-U. Schmincke (1984). *Pyroclastic Rocks*. Berlin, Heidelberg, New York, Tokyo: Springer-Verlag, p. 472. ISBN: 3-540-12756-9.

Fitzgerald, R., K. Tsunematsu, B. Kennedy, E. Breard, G. Lube, T. Wilson, A. Jolly, J. Pawson, M. Rosenberg, and S. Cronin (2014). “The application of a calibrated 3D ballistic trajectory model to ballistic hazard assessments at Upper Te Maari, Tongariro”. In: *Journal of Volcanology and Geothermal Research* 286, pp. 248–262. ISSN: 03770273. DOI: 10.1016/j.jvolgeores.2014.04.006.

Freundt, A., C. Wilson, and S. Carey (2000). “Ignimbrites and block-and-ash flow deposits”. In: *Encyclopedia of Volcanoes*. Ed. by H. Sigurdsson, B. Houghton, S. McNutt, H. Rymer, and J. Stix. San Diego: Academic Press, pp. 581–599. ISBN: 978-0-12-643140-7.

Frey, H. M. and R. A. Lange (2011). “Phenocryst complexity in andesites and dacites from the Tequila volcanic field, Mexico: resolving the effects of degassing vs. magma mixing”. In: *Contributions to Mineralogy and Petrology* 162.2, pp. 415–445. ISSN: 0010-7999. DOI: 10.1007/s00410-010-0604-1.

Frost, B. R. and D. H. Lindsley (1992). “Equilibria among Fe-Ti oxides, pyroxenes, olivine, and quartz: Part II. Application”. In: *American Mineralogist* 77. ISSN: 0003004X.

Gamble, J. A., R. C. Price, I. E. Smith, W. C. McIntosh, and N. W. Dunbar (2003). “40Ar/39Ar geochronology of magmatic activity, magma flux and hazards at Ruapehu volcano, Taupo Volcanic Zone, New Zealand”. In: *Journal of Volcanology and Geothermal Research* 120.3-4, pp. 271–287. ISSN: 03770273. DOI: 10.1016/S0377-0273(02)00407-9.

Gamble, J. A., C. Wood, R. C. Price, I. E. Smith, R. B. Stewart, and T. Waight (1999). “A fifty year perspective of magmatic evolution on Ruapehu Volcano, New Zealand: verification of open system behaviour in an arc volcano”. In: *Earth and Planetary*

Science Letters 170.3, pp. 301–314. ISSN: 0012821X. DOI: 10.1016/S0012-821X(99)00106-5.

Gardner, C. A., C. A. Neal, R. B. Waitt, and R. J. Janda (1994). "Proximal pyroclastic deposits from the 1989–1990 eruption of Redoubt Volcano, Alaska — stratigraphy, distribution, and physical characteristics". In: *Journal of Volcanology and Geothermal Research* 62.1-4, pp. 213–250. ISSN: 03770273. DOI: 10.1016/0377-0273(94)90035-3.

Gera, D., M. Syamlal, and T. J. O'Brien (2004). "Hydrodynamics of particle segregation in fluidized beds". In: *International Journal of Multiphase Flow* 30.4, pp. 419–428. ISSN: 03019322. DOI: 10.1016/j.ijmultiphaseflow.2004.01.003.

Ghiorso, M. S., M. M. Hirschmann, P. W. Reiners, and V. C. Kress (2002). "The pMELTS: A revision of MELTS for improved calculation of phase relations and major element partitioning related to partial melting of the mantle to 3 GPa". In: *Geochemistry, Geophysics, Geosystems* 3.5, pp. 1–35. ISSN: 15252027. DOI: 10.1029/2001GC000217.

Giordano, D., J. K. Russell, and D. Dingwell (2008). "Viscosity of magmatic liquids: A model". In: *Earth and Planetary Science Letters* 271.1-4, pp. 123–134. ISSN: 0012821X. DOI: 10.1016/j.epsl.2008.03.038.

Graham, I. and W. Hackett (1987). "Petrology of Calc-alkaline Lavas from Ruapehu Volcano and Related Vents, Taupo Volcanic Zone, New Zealand". In: *Journal of Petrology* 28.3, pp. 531–567. ISSN: 0022-3530. DOI: 10.1093/petrology/28.3.531.

Gualda, G. A. and M. S. Ghiorso (2014). "Phase-equilibrium geobarometers for silicic rocks based on rhyolite-MELTS. Part 1: Principles, procedures, and evaluation of the method". In: *Contributions to Mineralogy and Petrology* 168.1, p. 1033. ISSN: 0010-7999. DOI: 10.1007/s00410-014-1033-3.

Gualda, G. A., M. S. Ghiorso, R. V. Lemons, and T. L. Carley (2012). "Rhyolite-MELTS: a Modified Calibration of MELTS Optimized for Silica-rich, Fluid-bearing Magmatic Systems". In: *Journal of Petrology* 53.5, pp. 875–890. ISSN: 0022-3530. DOI: 10.1093/petrology/egr080.

Gudmundsson, M. T., T. Thordarson, Á. Höskuldsson, G. Larsen, H. Björnsson, F. J. Prata, B. Oddsson, E. Magnússon, T. Högnadóttir, G. N. Petersen, C. L. Hayward, J. a. Stevenson, and I. Jónsdóttir (2012). "Ash generation and distribution from the April-May 2010 eruption of Eyjafjallajökull, Iceland". In: *Scientific Reports* 2.May 2010, pp. 1–12. ISSN: 2045-2322. DOI: 10.1038/srep00572.

Hackett, W. R. and B. F. Houghton (1985). “Pinnacle Ridge Member, Whakapapa Formation: a welded airfall deposit from Ruapehu volcano, Taupo Volcanic Zone”. In: *New Zealand Geological Survey Record* 8, pp. 24–29.

Hackett, W. (1985). “Geology and petrology of Ruapehu volcano and related vents”. PhD Thesis. Victoria University, Wellington.

Hackett, W. and B. Houghton (1989). “A facies model for a quaternary andesitic composite volcano: Ruapehu, New Zealand”. In: *Bulletin of Volcanology* 51.1, pp. 51–68. ISSN: 0258-8900. DOI: 10.1007/BF01086761.

Healy, J., E. Lloyd, and D. Rishworth (1978). “The eruption of Ruapehu, New Zealand, on 22 June 1969”. In:

Hoblitt, R. P. and K. S. Kellogg (1979). “Emplacement temperatures of unsorted and unstratified deposits of volcanic rock debris as determined by paleomagnetic techniques”. In: *Geological Society of America Bulletin* 90.7, p. 633. ISSN: 0016-7606. DOI: 10.1130/0016-7606(1979)90<633:ETOUAU>2.0.CO;2.

Hodgson, K., J. A. Lecointre, and V. E. Neall (2007). “Onetapu Formation: The last 2000 yr of laharic activity at Ruapehu volcano, New Zealand”. In: *New Zealand Journal of Geology and Geophysics* 50.2, pp. 81–99. ISSN: 0028-8306. DOI: 10.1080/00288300709509823.

Hodgson, K. and V. R. Manville (1999). “Sedimentology and flow behavior of a rain-triggered lahar, Mangatoetoenui Stream, Ruapehu volcano, New Zealand”. In: *Geological Society of America Bulletin* 111.5, pp. 743–754. ISSN: 00167606. DOI: 10.1130/0016-7606(1999)111<0743:SAFBOA>2.3.CO;2.

Houghton, B., J. Latter, and W. Hackett (1987). “Volcanic hazard assessment for Ruapehu composite volcano, taupo volcanic zone, New Zealand”. In: *Bulletin of Volcanology* 49.6, pp. 737–751. ISSN: 0258-8900. DOI: 10.1007/BF01079825.

Houghton, B. and C. Wilson (1989). “A vesicularity index for pyroclastic deposits”. In: *Bulletin of Volcanology* 51.6, pp. 451–462. ISSN: 0258-8900. DOI: 10.1007/BF01078811.

Houghton, B., C. Wilson, M. McWilliams, M. Lanphere, S. Weaver, R. Briggs, and M. Pringle (1995). “Chronology and dynamics of a large silicic magmatic system: Central Taupo Volcanic Zone, New Zealand”. In: *Geology* 23.1, p. 13. ISSN: 0091-7613. DOI: 10.1130/0091-7613(1995)023<0013:CADOAL>2.3.CO;2.

Housh, T. B. and J. F. Luhr (1991). *Plagioclase-melt equilibria in hydrous systems.*

Huggel, C., J. Caplan-Auerbach, C. F. Waythomas, and R. L. Wessels (2007). "Monitoring and modeling ice-rock avalanches from ice-capped volcanoes: A case study of frequent large avalanches on Iliamna Volcano, Alaska". In: *Journal of Volcanology and Geothermal Research* 168.1-4, pp. 114–136. ISSN: 03770273. DOI: 10.1016/j.jvolgeores.2007.08.009.

Humphreys, M. C., J. Blundy, and R. Sparks (2006). "Magma Evolution and Open-System Processes at Shiveluch Volcano: Insights from Phenocryst Zoning". In: *Journal of Petrology* 47.12, pp. 2303–2334. ISSN: 0022-3530. DOI: 10.1093/petrology/egl045.

Jenkins, S., J.-C. Komorowski, P. Baxter, R. Spence, A. Picquout, F. Lavigne, and Surono (2013). "The Merapi 2010 eruption: An interdisciplinary impact assessment methodology for studying pyroclastic density current dynamics". In: *Journal of Volcanology and Geothermal Research* 261, pp. 316–329. ISSN: 03770273. DOI: 10.1016/j.jvolgeores.2013.02.012.

Johnson, A. (1970). *Physical Processes in Geology: A Method for Interpretation of Natural Phenomena; Intrusions in Igneous Rocks, Fractures, and Folds, Flow of Debris and Ice*. Freeman, Cooper, p. 577. ISBN: 0877353190.

Johnston, D. M., B. Houghton, V. E. Neall, K. Ronan, and D. Paton (2000). "Impacts of the 1945 and 1995-1996 Ruapehu eruptions, New Zealand: An example of increasing societal vulnerability". In: *Geological Society of America Bulletin* 112.5, pp. 720–726. ISSN: 0016-7606. DOI: 10.1130/0016-7606(2000)112<720:IOTARE>2.0.CO;2.

Johnston, D. M. and V. E. Neall (1995). *Ruapehu Awakens: The 1945 Eruption of Ruapehu*. 1. Palmerston North: The Science Centre and Manawatu Museum Scientific Monograph No. 1, p. 28. ISBN: 0473032236.

Jolly, A., S. Sherburn, P. Jousset, and G. N. Kilgour (2010). "Eruption source processes derived from seismic and acoustic observations of the 25 September 2007 Ruapehu eruption—North Island, New Zealand". In: *Journal of Volcanology and Geothermal Research* 191.1-2, pp. 33–45. ISSN: 03770273. DOI: 10.1016/j.jvolgeores.2010.01.009.

Julio-Miranda, P., H. Delgado-Granados, C. Huggel, and A. Kääb (2008). "Impact of the eruptive activity on glacier evolution at Popocatépetl Volcano (México) during 1994–2004". In: *Journal of Volcanology and Geothermal* 170.1-2, pp. 86–98. ISSN: 03770273. DOI: 10.1016/j.jvolgeores.2007.09.011.

Kennedy, B. M., O. Spieler, B. Scheu, U. Kueppers, J. Taddeucci, and D. Dingwell (2005). "Conduit implosion during Vulcanian eruptions". In: *Geology* 33.7, p. 581. ISSN: 0091-7613. DOI: 10.1130/G21488.1.

Kennedy, B. M., F. B. Wadsworth, J. Vasseur, C. Ian Schipper, A. Mark Jellinek, F. W. von Aulock, K.-U. Hess, J. Kelly Russell, Y. Lavallée, A. R. Nichols, and D. B. Dingwell (2016). "Surface tension driven processes densify and retain permeability in magma and lava". In: *Earth and Planetary Science Letters* 433, pp. 116–124. ISSN: 0012821X. DOI: 10.1016/j.epsl.2015.10.031.

Keys, H. J. (2007). "Lahars of Ruapehu Volcano, New Zealand: risk mitigation". In: *Annals of Glaciology* 45.1, pp. 155–162. ISSN: 02603055. DOI: 10.3189/172756407782282390.

Kilgour, G. N., J. Blundy, K. Cashman, and H. M. Mader (2013). "Small volume andesite magmas and melt–mush interactions at Ruapehu, New Zealand: evidence from melt inclusions". In: *Contributions to Mineralogy and Petrology* 166.2, pp. 371–392. ISSN: 0010-7999. DOI: 10.1007/s00410-013-0880-7.

Kilgour, G. N., V. Manville, F. Della Pasqua, A. Graettinger, K. Hodgson, and G. Jolly (2010). "The 25 September 2007 eruption of Mount Ruapehu, New Zealand: Directed ballistics, surtseyan jets, and ice-slurry lahars". In: *Journal of Volcanology and Geothermal Research* 191.1-2, pp. 1–14. ISSN: 03770273. DOI: 10.1016/j.jvolgeores.2009.10.015.

Komorowski, J.-C., S. Jenkins, P. Baxter, A. Picquout, F. Lavigne, S. Charbonnier, R. Gertisser, K. Preece, N. Cholik, A. Budi-Santoso, and Surono (2013). "Paroxysmal dome explosion during the Merapi 2010 eruption: Processes and facies relationships of associated high-energy pyroclastic density currents". In: *Journal of Volcanology and Geothermal Research* 261.November 2010, pp. 260–294. ISSN: 03770273. DOI: 10.1016/j.jvolgeores.2013.01.007.

Koyaguchi, T., Y. J. Suzuki, and T. Kozono (2010). "Effects of the crater on eruption column dynamics". In: *Journal of Geophysical Research* 115.B7, B07205. ISSN: 0148-0227. DOI: 10.1029/2009JB007146.

Krumbein, W. (1941). "Measurement and Geological Significance of Shape and Roundness of Sedimentary Particles". In: *Journal of Sedimentary Research* 11.2, pp. 64–72.

Latter, J. (1981). "Volcanic earthquakes, and their relationship to eruptions at Ruapehu and Ngauruhoe volcanoes". In: *Journal of Volcanology and Geothermal Research* 9.4, pp. 293–309. ISSN: 03770273. DOI: 10.1016/0377-0273(81)90041-X.

Lecointre, J. A., K. Hodgson, V. E. Neall, and S. J. Cronin (2004). "Lahar-Triggering Mechanisms and Hazard at Ruapehu Volcano, New Zealand". In: *Natural Hazards* 31.1, pp. 85–109. ISSN: 0921-030X. DOI: 10.1023/B:NHAZ.0000020256.16645.eb.

Lecointre, J. A., V. E. Neall, and A. S. Palmer (1998). "Quaternary lahar stratigraphy of the western Ruapehu ring plain, New Zealand". In: *New Zealand Journal of Geology and Geophysics* 41.3, pp. 225–245. ISSN: 0028-8306. DOI: 10.1080/00288306.1998.9514807.

Leonard, G. S., D. M. Johnston, D. Paton, A. Christianson, J. Becker, and H. J. Keys (2008). "Developing effective warning systems: Ongoing research at Ruapehu volcano, New Zealand". In: *Journal of Volcanology and Geothermal Research* 172.3-4, pp. 199–215. ISSN: 03770273. DOI: 10.1016/j.jvolgeores.2007.12.008.

Lescinsky, D. T. and J. Fink (2000). "Lava and ice interaction at stratovolcanoes: Use of characteristic features to determine past glacial extents and future volcanic hazards". In: *Journal of geophysical research* 105.B10, pp. 23711–23.

Lescinsky, D. T. and T. W. Sisson (1998). "Ridge-forming, ice-bounded lava flows at Mount Rainier, Washington". In: *Geology* 26.4, p. 351. ISSN: 0091-7613. DOI: 10.1130/0091-7613(1998)026<0351:RFIBLF>2.3.CO;2.

Lodge, R. W. and D. T. Lescinsky (2009). "Fracture patterns at lava–ice contacts on Kokostick Butte, OR, and Mazama Ridge, Mount Rainier, WA: Implications for flow emplacement and cooling histories". In: *Journal of Volcanology and Geothermal* 185.4, pp. 298–310. ISSN: 03770273. DOI: 10.1016/j.jvolgeores.2008.10.010.

Lorenz, V. (1973). "On the formation of maars". In: *Bulletin Volcanologique* 37.2, pp. 183–204. ISSN: 0258-8900. DOI: 10.1007/BF02597130.

Lube, G., E. C. Breard, S. J. Cronin, J. N. Procter, M. Brenna, A. Moebis, N. Pardo, R. B. Stewart, A. Jolly, and N. Fournier (2014). "Dynamics of surges generated by hydrothermal blasts during the 6 August 2012 Te Maari eruption, Mt. Tongariro, New Zealand". In: *Journal of Volcanology and Geothermal Research* 286, pp. 348–366. ISSN: 03770273. DOI: 10.1016/j.jvolgeores.2014.05.010.

Lube, G., S. J. Cronin, T. Platz, A. Freundt, J. N. Procter, C. Henderson, and M. F. Sheridan (2007). "Flow and deposition of pyroclastic granular flows: A type example from the 1975 Ngauruhoe eruption, New Zealand". In: *Journal of Volcanology and Geothermal Research* 161.3, pp. 165–186. ISSN: 03770273. DOI: 10.1016/j.jvolgeores.2006.12.003.

Lube, G., S. J. Cronin, and J. N. Procter (2009). "Explaining the extreme mobility of volcanic ice-slurry flows, Ruapehu volcano, New Zealand". In: *Geology* 37.1, pp. 15–18. ISSN: 0091-7613. DOI: 10.1130/G25352A.1.

Major, J. J. and C. G. Newhall (1989). "Snow and ice perturbation during historical volcanic eruptions and the formation of lahars and floods". In: *Bulletin of Volcanology* 52.1, pp. 1–27. ISSN: 0258-8900. DOI: 10.1007/BF00641384.

Manville, V. (2004). "Palaeohydraulic analysis of the 1953 Tangiwai lahar; New Zealand's worst volcanic disaster". In: *Acta Vulcanologica* 16, pp. 137–152.

Manville, V. R., K. A. Hodgson, B. F. Houghton, H. J. Keys, and J. White (2000). "Tephra, snow and water: complex sedimentary responses at an active snow-capped stratovolcano, Ruapehu, New Zealand". In: *Bulletin of Volcanology* 62.4-5, pp. 278–293. ISSN: 0258-8900. DOI: 10.1007/s004450000096.

Marzocchi, W., L. Sandri, P. Gasparini, C. Newhall, and E. Boschi (2004). "Quantifying probabilities of volcanic events: The example of volcanic hazard at Mount Vesuvius". In: *Journal of Geophysical Research: Solid Earth* 109.B11, n/a–n/a. ISSN: 01480227. DOI: 10.1029/2004JB003155.

Massey, C. I., V. R. Manville, G. H. Hancox, H. J. Keys, C. Lawrence, and M. McSaveney (2010). "Out-burst flood (lahar) triggered by retrogressive landsliding, 18 March 2007 at Mt Ruapehu, New Zealand—a successful early warning". In: *Landslides* 7.3, pp. 303–315. ISSN: 1612-510X. DOI: 10.1007/s10346-009-0180-5.

McArthur, J. and M. Shepherd (1990). "Late Quaternary glaciation of Mt Ruapehu, North Island, New Zealand". In: *Journal of the Royal Society of New Zealand* 20.3, pp. 287–296. ISSN: 0303-6758. DOI: 10.1080/03036758.1990.10416823.

McClelland, E. and P. S. Erwin (2003). "Was a dacite dome implicated in the 9,500 b.p. collapse of Mt Ruapehu? A palaeomagnetic investigation". In: *Bulletin of Volcanology* 65.4, pp. 294–305. ISSN: 0258-8900. DOI: 10.1007/s00445-002-0261-y.

McGarvie, D. W. (2009). "Rhyolitic volcano–ice interactions in Iceland". In: *Journal of Volcanology and Geothermal* 185.4, pp. 367–389. ISSN: 03770273. DOI: 10.1016/j.jvolgeores.2008.11.019.

McPhie, J., M. Doyle, and R. L. Allen (1993). *Volcanic textures: A guide to the interpretation of textures in volcanic rocks*. Vol. 64. CODES-University of Tasmania., p. 198. ISBN: 0-85901-522-X.

Mendoza-Rosas, A. T. and S. De la Cruz-Reyna (2008). "A statistical method linking geological and historical eruption time series for volcanic hazard estimations: Applications to active polygenetic volcanoes". In: *Journal of Volcanology and Geothermal Research* 176.2, pp. 277–290. ISSN: 03770273. DOI: 10.1016/j.jvolgeores.2008.04.005.

Miyabuchi, Y., K. Watanabe, and Y. Egawa (2006). "Bomb-rich basaltic pyroclastic flow deposit from Nakadake, Aso Volcano, southwestern Japan". In: *Journal of Volcanology and Geothermal Research* 155.1-2, pp. 90–103. ISSN: 03770273. DOI: 10.1016/j.jvolgeores.2006.02.007.

Moebis, A., S. J. Cronin, V. E. Neall, and I. E. Smith (2011). "Unravelling a complex volcanic history from fine-grained, intricate Holocene ash00a0sequences at the Tongariro Volcanic Centre, New Zealand". In: *Quaternary International* 246.1-2, pp. 352–363. ISSN: 10406182. DOI: 10.1016/j.quaint.2011.05.035.

Moore, G. (2008). "Interpreting H2O and CO2 Contents in Melt Inclusions: Constraints from Solubility Experiments and Modeling". In: *Reviews in Mineralogy and Geochemistry* 69.1, pp. 333–362. ISSN: 1529-6466. DOI: 10.2138/rmg.2008.69.9.

Mullineaux, D. and D. Crandell (1962). "Recent Lahars from Mount St. Helens, Washington". In: *Geological Society of America Bulletin* 73.7, p. 855. ISSN: 0016-7606. DOI: 10.1130/0016-7606(1962)73[855:RLFMSH]2.0.CO;2.

Murphy, M. and R. Sparks (2000). "Remobilization of Andesite Magma by Intrusion of Mafic Magma at the Soufriere Hills Volcano, Montserrat, West Indies". In: *Journal of ...* 41.1, pp. 21–42.

Murphy, M., R. Sparks, J. Barclay, M. Carroll, A.-M. Lejeune, T. Brewer, R. Macdonald, S. Black, and S. Young (1998). "The role of magma mixing in triggering the current eruption at the Soufriere Hills Volcano, Montserrat, West Indies". In: *Geophysical Research Letters* 25.18, pp. 3433–3436. ISSN: 00948276. DOI: 10.1029/98GL00713.

Nairn, I. A. and S. Self (1978). "Explosive eruptions and pyroclastic avalanches from Ngauruhoe in February 1975". In: *Journal of Volcanology and Geothermal Research* 3.1-2, pp. 39–60. ISSN: 03770273. DOI: 10.1016/0377-0273(78)90003-3.

Nairn, I. A., C. Wood, and C. Hewson (1979). "Phreatic eruptions of Ruapehu: April 1975". In: *New Zealand Journal of Geology and Geophysics* 22.2, pp. 155–170. ISSN: 0028-8306. DOI: 10.1080/00288306.1979.10424215.

Nakada, S. (2000). "Hazards from pyroclastic flows and surges". In: *Encyclopedia of Volcanoes*. Ed. by H. Sigurdsson, B. Houghton, S. McNutt, H. Rymer, and J. Stix. San Diego: Academic Press, pp. 945–995. ISBN: 0855385146.

Nakagawa, M. (2002). "Mixed Magmas, Mush Chambers and Eruption Triggers: Evidence from Zoned Clinopyroxene Phenocrysts in Andesitic Scoria from the 1995 Eruptions of Ruapehu Volcano, New Zealand". In: *Journal of Petrology* 43.12, pp. 2279–2303. ISSN: 14602415. DOI: 10.1093/petrology/43.12.2279.

Nakagawa, M., K. Wada, T. Thordarson, C. Wood, and J. A. Gamble (1999). "Petrologic investigations of the 1995 and 1996 eruptions of Ruapehu volcano, New Zealand: formation of discrete and small magma pockets and their intermittent discharge". In: *Bulletin of Volcanology* 61.1-2, pp. 15–31. ISSN: 0258-8900. DOI: 10.1007/s004450050259.

Nakamura, M. (1995). "Continuous mixing of crystal mush and replenished magma in the ongoing Unzen eruption". In: *Geology* 23.9, p. 807. ISSN: 0091-7613. DOI: 10.1130/0091-7613(1995)023<0807:CMOCMA>2.3.CO;2.

Newman, S. and J. B. Lowenstern (2002). "VolatileCalc: a silicate melt–H2O–CO2 solution model written in Visual Basic for excel". In: *Computers & Geosciences* 28.5, pp. 597–604. ISSN: 00983004. DOI: 10.1016/S0098-3004(01)00081-4.

Nimis, P. (1999). "Clinopyroxene geobarometry of magmatic rocks. Part 2. Structural geobarometers for basic to acid, tholeiitic and mildly alkaline magmatic systems". In: *Contributions to Mineralogy and Petrology* 135.1, pp. 62–74. ISSN: 0010-7999. DOI: 10.1007/s004100050498.

Nimis, P. and P. Ulmer (1998). "Clinopyroxene geobarometry of magmatic rocks Part 1: An expanded structural geobarometer for anhydrous and hydrous, basic and ultrabasic systems". In: *Contributions to Mineralogy and Petrology* 133.1-2, pp. 122–135. ISSN: 0010-7999. DOI: 10.1007/s004100050442.

Norrish, K. and B. Chappell (1967). "X-ray fluorescence spectrography". In: *Physical methods of determinative mineralogy*. Ed. by J. Zussman. Academic Press. Chap. 4, pp. 201–272.

Norrish, K. and J. Hutton (1969). "An accurate X-ray spectrographic method for the analysis of a wide range of geological samples". In: *Geochimica et Cosmochimica Acta* 33.4, pp. 431–453. ISSN: 00167037. DOI: 10.1016/0016-7037(69)90126-4.

Ogden, D. E., G. A. Glatzmaier, and K. H. Wohletz (2008a). "Effects of vent overpressure on buoyant eruption columns: Implications for plume stability". In: *Earth and Planetary Science Letters* 268.3-4, pp. 283–292. ISSN: 0012821X. DOI: 10.1016/j.epsl.2008.01.014.

Ogden, D. E., K. H. Wohletz, G. A. Glatzmaier, and E. E. Brodsky (2008b). "Numerical simulations of volcanic jets: Importance of vent overpressure". In: *Journal of Geophysical Research* 113.B2, B02204. ISSN: 0148-0227. DOI: 10.1029/2007JB005133.

Oliver, R. (1945). "Further activity of Mount Ruapehu, May–July, 1945". In: *New Zealand Journal of Science and Technology* B26, pp. 24–33.

O'Shea, B. E. (1954). "Ruapehu and the Tangiwai Disaster". In: *New Zealand Journal of Science and Technology* B-36, pp. 174–189.

Palmer, B. A. (1991). "Holocene lahar deposits in the Whakapapa catchment, northwestern ring plain, Ruapehu volcano (North Island, New Zealand)". In: *New Zealand Journal of Geology and Geophysics* 34.2, pp. 177–190. ISSN: 0028-8306. DOI: 10.1080/00288306.1991.9514455.

Palmer, B. A. and V. E. Neall (1989). "The Murimotu Formation—9500 year old deposits of a debris avalanche and associated lahars, Mount Ruapehu, North Island, New Zealand". In: *New Zealand Journal of Geology and Geophysics* 32.4, pp. 477–486. ISSN: 0028-8306. DOI: 10.1080/00288306.1989.10427555.

Palmer, B. A., A. M. Purves, and S. Donoghue (1993). "Controls on accumulation of a volcaniclastic fan, Ruapehu composite volcano, New Zealand". In: *Bulletin of Volcanology* 55.3, pp. 176–189. ISSN: 0258-8900. DOI: 10.1007/BF00301515.

Papale, P., R. Moretti, and D. Barbato (2006). "The compositional dependence of the saturation surface of H2O+CO2 fluids in silicate melts". In: *Chemical Geology* 229.1-3, pp. 78–95. ISSN: 00092541. DOI: 10.1016/j.chemgeo.2006.01.013.

Pardo Villaveces, N. (2012). "Andesitic Plinian Eruptions at Mt. Ruapehu (New Zealand): From Lithofacies to Eruption Dynamics". PhD Thesis. Massey University, Palmerston North, New Zealand.

Pardo, N., S. J. Cronin, A. S. Palmer, and K. Németh (2011). "Reconstructing the largest explosive eruptions of Mt. Ruapehu, New Zealand: lithostratigraphic tools to understand subplinian–plinian eruptions at andesitic volcanoes". In: *Bulletin of Volcanology* 74.3, pp. 617–640. ISSN: 0258-8900. DOI: 10.1007/s00445-011-0555-z.

Pardo, N., S. J. Cronin, A. S. Palmer, J. N. Procter, and I. E. Smith (2012). "Andesitic Plinian eruptions at Mt. Ruapehu: quantifying the uppermost limits of eruptive parameters". In: *Bulletin of Volcanology* 74.5, pp. 1161–1185. ISSN: 0258-8900. DOI: 10.1007/s00445-012-0588-y.

Pardo, N., S. J. Cronin, H. M. Wright, C. I. Schipper, I. Smith, and B. Stewart (2014). "Pyroclast textural variation as an indicator of eruption column steadiness in andesitic Plinian eruptions at Mt. Ruapehu". In: *Bulletin of Volcanology* 76.5, p. 822. ISSN: 0258-8900. DOI: 10.1007/s00445-014-0822-x.

Parsons, W. H. (1969). "Criteria for the Recognition of Volcanic Breccias: Review". In: *The Geological Society of America Memoir*. Vol. 115, pp. 263–304. DOI: 10.1130/MEM115-p263.

Patel, A., M. Manga, R. J. Carey, and W. Degruyter (2013). "Effects of thermal quenching on mechanical properties of pyroclasts". In: *Journal of Volcanology and Geothermal Research* 258, pp. 24–30. ISSN: 03770273. DOI: 10.1016/j.jvolgeores.2013.04.001.

Pierson, T. C. and R. J. Janda (1994). "Volcanic mixed avalanches: A distinct eruption-triggered mass-flow process at snow-clad volcanoes". In: *Geological Society of America Bulletin* 106.10, pp. 1351–1358. ISSN: 00167606. DOI: 10.1130/0016-7606(1994)106<1351:VMAADE>2.3.CO;2.

Pierson, T. C., R. J. Janda, J.-C. Thouret, and C. A. Borrero (1990). "Perturbation and melting of snow and ice by the 13 November 1985 eruption of Nevado del Ruiz, Colombia, and consequent mobilization, flow and deposition of lahars". In: *Journal of Volcanology and Geothermal Research* 41.1-4, pp. 17–66. ISSN: 03770273. DOI: 10.1016/0377-0273(90)90082-Q.

Pistolesi, M., R. Cioni, M. Rosi, K. Cashman, A. Rossotti, and E. Aguilera (2013). "Evidence for lahar-triggering mechanisms in complex stratigraphic sequences: the post-

twelfth century eruptive activity of Cotopaxi Volcano, Ecuador". In: *Bulletin of Volcanology* 75.3, p. 698. ISSN: 0258-8900. DOI: 10.1007/s00445-013-0698-1.

Platz, T., S. J. Cronin, J. N. Procter, V. E. Neall, and S. F. Foley (2012). "Non-explosive, dome-forming eruptions at Mt. Taranaki, New Zealand". In: *Geomorphology* 136.1, pp. 15–30. ISSN: 0169555X. DOI: 10.1016/j.geomorph.2011.06.016.

Powers, M. C. (1953). "A New Roundness Scale for Sedimentary Particles". In: *Journal of Sedimentary Research* 23.2, pp. 117–119.

Procter, J. N., S. J. Cronin, I. Fuller, G. Lube, and V. R. Manville (2010). "Quantifying the geomorphic impacts of a lake-breakout lahar, Mount Ruapehu, New Zealand". In: *Geology* 38.1, pp. 67–70. ISSN: 0091-7613. DOI: 10.1130/G30129.1.

Putirka, K. (2005). "Igneous thermometers and barometers based on plagioclase + liquid equilibria: Tests of some existing models and new calibrations". In: *American Mineralogist* 90.2-3, pp. 336–346. ISSN: 0003-004X. DOI: 10.2138/am.2005.1449.

— (2008). "Thermometers and Barometers for Volcanic Systems". In: *Reviews in Mineralogy and Geochemistry* 69.1, pp. 61–120. ISSN: 1529-6466. DOI: 10.2138/rmg.2008.69.3.

Putirka, K. D., H. Mikaelian, F. Ryerson, and H. Shaw (2003). "New clinopyroxene-liquid thermobarometers for mafic, evolved, and volatile-bearing lava compositions, with applications to lavas from Tibet and the Snake River Plain, Idaho". In: *American Mineralogist* 88.10, pp. 1542–1554. ISSN: 0003004X. DOI: 10.2138/am.2005.431.

Reed, J. (1945). "Activity at Ruapehu, March–April, 1945". In: *New Zealand Journal of Science and Technology* B26, pp. 17–23.

Richardson, J. M. and M. S. Brook (2010). "Ablation of debris-covered ice: some effects of the 25 September 2007 Mt Ruapehu eruption". In: *Journal of the Royal Society of New Zealand* 40.2, pp. 45–55. ISSN: 0303-6758. DOI: 10.1080/03036758.2010.494714.

Roche, O., Y. Nino, A. Mangeney, B. Brand, N. Pollock, and G. a. Valentine (2013). "Dynamic pore-pressure variations induce substrate erosion by pyroclastic flows". In: *Geology* 41.10, pp. 1107–1110. ISSN: 0091-7613. DOI: 10.1130/G34668.1.

Roman, D. C., K. Cashman, C. A. Gardner, P. J. Wallace, and J. J. Donovan (2006). "Storage and interaction of compositionally heterogeneous magmas from the 1986 eruption of Augustine Volcano, Alaska". In: *Bulletin of Volcanology* 68.3, pp. 240–254. ISSN: 0258-8900. DOI: 10.1007/s00445-005-0003-z.

Rosi, M., M. Paladio-Melosantos, A. Di Muro, R. Leoni, and T. Bacolcol (2001). "Fall vs flow activity during the 1991 climactic eruption of Pinatubo Volcano (Philippines)". In: *Bulletin of Volcanology* 62.8, pp. 549–566. ISSN: 0258-8900. DOI: 10.1007/s004450000118.

Rotella, M. D. (2013). "Physical Processes in Subaerial and Submarine Explosive Volcanism: Case Studies from the Kermadec Arc, SW Pacific by". PhD Thesis. Victoria University, Wellington, New Zealand.

Rust, A. and K. Cashman (2011). "Permeability controls on expansion and size distributions of pyroclasts". In: *Journal of Geophysical Research* 116.B11, B11202. ISSN: 0148-0227. DOI: 10.1029/2011JB008494.

Saucedo, R., J. Macías, and M. Bursik (2004). "Pyroclastic flow deposits of the 1991 eruption of Volcfffdn de Colima, Mexico". In: *Bulletin of Volcanology* 66.4, pp. 291–306. ISSN: 0258-8900. DOI: 10.1007/s00445-003-0311-0.

Schneider, D., C. Huggel, W. Haeberli, and R. Kaitna (2011). "Unraveling driving factors for large rock-ice avalanche mobility". In: *Earth Surface Processes and Landforms* 36.14, pp. 1948–1966. ISSN: 01979337. DOI: 10.1002/esp.2218.

Shane, P., L. R. Doyle, and I. A. Nairn (2008). "Heterogeneous andesite–dacite ejecta in 26–16.6 ka pyroclastic deposits of Tongariro Volcano, New Zealand: the product of multiple magma-mixing events". In: *Bulletin of Volcanology* 70.4, pp. 517–536. ISSN: 0258-8900. DOI: 10.1007/s00445-007-0152-3.

Shea, T., L. Gurioli, B. Houghton, R. Cioni, and K. Cashman (2011). "Column collapse and generation of pyroclastic density currents during the A.D. 79 eruption of Vesuvius: The role of pyroclast density". In: *Geology* 39.7, pp. 695–698. ISSN: 0091-7613. DOI: 10.1130/G32092.1.

Sheridan, M. F. (1979). "Emplacement of pyroclastic flows: A review". In: *Geological Society of America Special Papers*. Vol. 180, pp. 125–136. DOI: 10.1130/SPE180-p125.

Smellie, J. (2006). "The relative importance of supraglacial versus subglacial meltwater escape in basaltic subglacial tuya eruptions: An important unresolved conundrum". In: *Earth-Science Reviews* 74.3-4, pp. 241–268. ISSN: 00128252. DOI: 10.1016/j.earscirev.2005.09.004.

Smith, G. A., M. J. Grubensky, and J. W. Geissman (1999). "Nature and origin of cone-forming volcanic breccias in the Te Herenga Formation, Ruapehu, New Zealand". In: *Bulletin of Volcanology* 61.1-2, pp. 64–82. ISSN: 0258-8900. DOI: 10.1007/s004450050263.

Smith, V. C., J. Blundy, and J. L. Arce (2009). "A Temporal Record of Magma Accumulation and Evolution beneath Nevado de Toluca, Mexico, Preserved in Plagioclase Phenocrysts". In: *Journal of Petrology* 50.3, pp. 405–426. ISSN: 0022-3530. DOI: 10.1093/petrology/egp005.

Snyder, D. (1997). "The mixing and mingling of magmas". In: *Endeavour* 21.1, pp. 19–22. ISSN: 01609327. DOI: 10.1016/S0160-9327(96)10032-6.

Sosio, R., G. B. Crosta, J. H. Chen, and O. Hungr (2012). "Modelling rock avalanche propagation onto glaciers". In: *Quaternary Science Reviews* 47, pp. 23–40. ISSN: 02773791. DOI: 10.1016/j.quascirev.2012.05.010.

Sparks, R. (1997). "Causes and consequences of pressurisation in lava dome eruptions". In: *Earth and Planetary Science Letters* 150.3-4, pp. 177–189. ISSN: 0012821X. DOI: 10.1016/S0012-821X(97)00109-X.

Sparks, R. and L. Marshall (1986). "Thermal and mechanical constraints on mixing between mafic and silicic magmas". In: *Journal of Volcanology and Geothermal Research* 29.1-4, pp. 99–124. ISSN: 03770273. DOI: 10.1016/0377-0273(86)90041-7.

Sparks, R. and G. P. Walker (1977). "The significance of vitric-enriched air-fall ashes associated with crystal-enriched ignimbrites". In: *Journal of Volcanology and Geothermal Research* 2.4, pp. 329–341. ISSN: 03770273. DOI: 10.1016/0377-0273(77)90019-1.

Sparks, R. and L. Wilson (1976). "A model for the formation of ignimbrite by gravitational column collapse". In: *Journal of the Geological Society* 132.4, pp. 441–451. ISSN: 0016-7649. DOI: 10.1144/gsjgs.132.4.0441.

Sparks, S. R., H. Sigurdsson, and L. Wilson (1977). "Magma mixing: a mechanism for triggering acid explosive eruptions". In: *Nature* 267.5609, pp. 315–318. ISSN: 0028-0836. DOI: 10.1038/267315a0.

Spera, F. (2000). "Physical properties of Magma". In: *Encyclopedia of Volcanoes*. Ed. by H. Sigurdsson, B. F. Houghton, S. McNutt, H. Rymer, and J. Stix. San Diego: Academic Press, pp. 171–190.

Spörli, K. and J. Rowland (2006). "'Column on column′ structures as indicators of lava/ice interaction, Ruapehu andesite volcano, New Zealand". In: *Journal of Volcanology and Geothermal Research* 157.4, pp. 294–310. ISSN: 03770273. DOI: 10.1016/j.jvolgeores.2006.04.004.

Stevenson, J. A., D. W. McGarvie, J. L. Smellie, and J. S. Gilbert (2006). "Subglacial and ice-contact volcanism at the Öræfajökull stratovolcano, Iceland". In: *Bulletin of Volcanology* 68.7-8, pp. 737–752. ISSN: 0258-8900. DOI: 10.1007/s00445-005-0047-0.

Stevenson, J. A., J. L. Smellie, D. W. McGarvie, J. S. Gilbert, and B. I. Cameron (2009). "Subglacial intermediate volcanism at Kerlingarfjöll, Iceland: Magma–water interactions beneath thick ice". In: *Journal of Volcanology and Geothermal* 185.4, pp. 337–351. ISSN: 03770273. DOI: 10.1016/j.jvolgeores.2008.12.016.

Stewart, R. B. (2010). "Andesites as Magmatic Liquids or Liquid-crystal Mixtures; Insights from Egmont and Ruapehu Volcanoes, New Zealand Research Article". In: *Open Geosciences* 2.3, pp. 329–338. ISSN: 2391-5447. DOI: 10.2478/v10085-010-0022-7.

Stinton, A. J. and M. F. Sheridan (2008). "Implications of long-term changes in valley geomorphology on the behavior of small-volume pyroclastic flows". In: *Journal of Volcanology and Geothermal Research* 176.1, pp. 134–140. ISSN: 03770273. DOI: 10.1016/j.jvolgeores.2008.01.010.

Sulpizio, R. (2005). "Three empirical methods for the calculation of distal volume of tephra-fall deposits". In: *Journal of Volcanology and Geothermal Research* 145.3-4, pp. 315–336. ISSN: 03770273. DOI: 10.1016/j.jvolgeores.2005.03.001.

Suzuki, Y. J. and T. Koyaguchi (2012). "3-D numerical simulations of eruption column collapse: Effects of vent size on pressure-balanced jet/plumes". In: *Journal of Volcanology and Geothermal Research* 221-222, pp. 1–13. ISSN: 03770273. DOI: 10.1016/j.jvolgeores.2012.01.013.

Tanguy, J.-C., C. Ribèire, A. Scarth, and W. Tjetjep (1998). "Victims from volcanic eruptions: a revised database". In: *Bulletin of Volcanology* 60.2, pp. 137–144. ISSN: 0258-8900. DOI: 10.1007/s004450050222.

Thouret, J., J. Ramírez, B. Gibert-Malengreau, C. Vargas, J. Naranjo, J. Vandemeulebrouck, F. Valla, and M. Funk (2007). "Volcano–glacier interactions on composite cones and lahar generation: Nevado del Ruiz, Colombia, case study". In: *Annals of Glaciology* 45.1, pp. 115–127. ISSN: 02603055. DOI: 10.3189/172756407782282589.

Thouret, J.-C. (1990). "Effects of the November 13, 1985 eruption on the snow pack and ice cap of Nevado del Ruiz volcano, Colombia". In: *Journal of Volcanology and Geothermal Research* 41.1-4, pp. 177–201. ISSN: 03770273. DOI: 10.1016/0377-0273(90)90088-W.

Topping, W. (1973). "Tephrostratigraphy and chronology of late quaternary eruptives from the Tongariro Volcanic Centre, New Zealand". In: *New Zealand Journal of Geology and Geophysics* 16.3, pp. 397–423. ISSN: 0028-8306. DOI: 10.1080/00288306.1973.10431368.

Valentine, G. A. and R. V. Fisher (1993). "Glowing Avalanches: New Research on Volcanic Density Currents". In: *Science* 259.5098, pp. 1130–1131. ISSN: 0036-8075. DOI: 10.1126/science.259.5098.1130.

— (2000). "Pyroclastic surges and blasts". In: *Encyclopedia of Volcanoes*. Ed. by H. Sigurdsson, B. Houghton, S. McNutt, H. Rymer, and J. Stix. San Diego: Academic Press, pp. 581–589. ISBN: 0855385146.

Voight, B. and D. Elsworth (2000). "Instability and collapse of hazardous gas-pressurized lava domes". In: *Geophysical Research Letters* 27.1, pp. 1–4. ISSN: 00948276. DOI: 10.1029/1999GL008389.

Wadsworth, F. B., B. M. Kennedy, M. J. Branney, F. W. von Aulock, Y. Lavallée, and A. Menendez (2015). "Exhumed conduit records magma ascent and drain-back during a Strombolian eruption at Tongariro volcano, New Zealand". In: *Bulletin of Volcanology* 77.9, p. 71. ISSN: 0258-8900. DOI: 10.1007/s00445-015-0962-7.

Waight, T., R. C. Price, R. B. Stewart, I. E. Smith, and J. A. Gamble (1999). "Stratigraphy and geochemistry of the Turoa area, with implications for andesite petrogenesis at Mt Ruapehu, Taupo Volcanic Zone, New Zealand". In: *New Zealand Journal of Geology and Geophysics* 42.4, pp. 513–532. ISSN: 0028-8306. DOI: 10.1080/00288306.1999.9514858.

Waitt, R. B. (1981). "Devastating pyroclastic density flow and attendant air fall of May 18 - stratigraphy and sedimentology of deposits". In: *The 1980 Eruptions of Mount St. Helens, Washington: U.S. Geological Survey Professional Paper 1250*. Ed. by P. Lipman and D. Mullineaux, pp. 439–458.

Walder, J. S. (2000a). "Pyroclast/snow interactions and thermally driven slurry formation. Part 1: Theory for monodisperse grain beds". In: *Bulletin of Volcanology* 62.2, pp. 105–118. ISSN: 0258-8900. DOI: 10.1007/s004459900069.

— (2000b). "Pyroclast/snow interactions and thermally driven slurry formation. Part 2: Experiments and theoretical extension to polydisperse tephra". In: *Bulletin of Volcanology* 62.2, pp. 119–129. ISSN: 0258-8900. DOI: 10.1007/s004459900070.

Walker, G. P. (1971). "Grain-Size Characteristics of Pyroclastic Deposits". In: *The Journal of Geology* 79.6, pp. 696–714. ISSN: 0022-1376.

— (1983). "Ignimbrite types and ignimbrite problems". In: *Journal of Volcanology and Geothermal Research* 17.1-4, pp. 65–88. ISSN: 03770273. DOI: 10.1016/0377-0273(83)90062-8.

Walker, G. P. and R. Croasdale (1971). "Characteristics of some basaltic pyroclastics". In: *Bulletin Volcanologique* 35.2, pp. 303–317. ISSN: 0258-8900. DOI: 10.1007/BF02596957.

Wentworth, C. and H. Williams (1932). "The classification and terminology of the pyroclastic rocks". In: *Bulletin of the National Research Council* 89.Report of the Commission on Sedimentation, pp. 19–53.

White, J. and B. Houghton (2006). "Primary volcaniclastic rocks". In: *Geology* 34.8, p. 677. ISSN: 0091-7613. DOI: 10.1130/G22346.1.

Williams, K. (2013). *Volcanoes of the South Wind: A Volcanic Guide to Tongariro National Park*. Glenfield, Auckland, New Zealand: Random House. ISBN: 978 1 77553 530 0.

Wilson, C. (1980). "The role of fluidization in the emplacement of pyroclastic flows: An experimental approach". In: *Journal of Volcanology and Geothermal Research* 8.2-4, pp. 231–249. ISSN: 03770273. DOI: 10.1016/0377-0273(80)90106-7.

Wilson, C., B. Houghton, M. McWilliams, M. Lanphere, S. Weaver, and R. Briggs (1995). "Volcanic and structural evolution of Taupo Volcanic Zone, New Zealand: a review". In: *Journal of Volcanology and Geothermal Research* 68.1-3, pp. 1–28. ISSN: 03770273. DOI: 10.1016/0377-0273(95)00006-G.

Wilson, L. and J. W. Head III (2002). "Heat transfer and melting in subglacial basaltic volcanic eruptions: implications for volcanic deposit morphology and meltwater volumes". In: *Volcano-Ice Interaction on Earth and Mars*. Ed. by J. L. Smellie and M. Chapman. London: The Geological Society, p. 8719.

Wilson, L., R. Sparks, and G. P. Walker (1980). "Explosive volcanic eruptions – IV. The control of magma properties and conduit geometry on eruption column behaviour". In: *Geophysical Journal International* 63.1, pp. 117–148. ISSN: 0956-540X. DOI: 10.1111/j.1365-246X.1980.tb02613.x.

Witham, C. (2005). "Volcanic disasters and incidents: A new database". In: *Journal of Volcanology and Geothermal Research* 148.3-4, pp. 191–233. ISSN: 03770273. DOI: 10.1016/j.jvolgeores.2005.04.017.

Wood, N. and C. Soulard (2009). "Variations in population exposure and sensitivity to lahar hazards from Mount Rainier, Washington". In: *Journal of Volcanology and Geothermal Research* 188.4, pp. 367–378. ISSN: 03770273. DOI: 10.1016/j.jvolgeores.2009.09.019.

Wright, H., K. Cashman, P. A. Mothes, M. L. Hall, A. G. Ruiz, and J.-L. Le Pennec (2012). "Estimating rates of decompression from textures of erupted ash particles produced by 1999-2006 eruptions of Tungurahua volcano, Ecuador". In: *Geology* 40.7, pp. 619–622. ISSN: 0091-7613. DOI: 10.1130/G32948.1.

Yamamoto, T., A. Takada, Y. Ishizuka, N. Miyaji, and Y. Tajima (2005). "Basaltic pyroclastic flows of Fuji volcano, Japan: characteristics of the deposits and their origin". In: *Bulletin of Volcanology* 67.7, pp. 622–633. ISSN: 0258-8900. DOI: 10.1007/s00445-004-0398-y.

Yamamoto, T., S. Takarada, and S. Suto (1993). "Pyroclastic flows from the 1991 eruption of Unzen volcano, Japan". In: *Bulletin of Volcanology* 55.3, pp. 166–175. ISSN: 0258-8900. DOI: 10.1007/BF00301514.